Geosynthetics '99

"Specifying Geosynthetics and Developing Design Details"

GEOSYNTHETICS 99 CONFERENCE
Boston, Massachusetts USA

Conference Proceedings

April 28-30, 1999

Organized by:

IFAI
Industrial Fabrics Association International

NAGS
North American Geosynthetics Society

GMA
Geosynthetic Materials Association

under the auspices of
IGS
International Geosynthetics Society

SPONSORED BY

Table of Contents

Interface Friction Testing II

Volume 2

Leak Detection

Student Papers

Estimation of Dynamic Frictional Properties of Geonet Interfaces

Anirban De

Senior Staff Engineer, GeoSyntec Consultants, Walnut Creek, USA

Thomas F. Zimmie

Professor, Department of Civil Engineering, Rensselaer Polytechnic Institute, Troy, USA.

ABSTRACT:

This paper presents experimental results from monotonic (commonly called static) and dynamic shear tests on geonet/geotextile and geonet/geomembrane interfaces. Both smooth and textured geomembranes have been considered. The testing methods covered include tilt table, direct shear tests on specimens of two different sizes, cyclic direct shear tests and shaking table tests under normal as well as high gravity.

The influence of different parameters on the shear strength properties are discussed. It was found that the shear behavior of geonet interfaces is strongly influenced by the orientation of the strands that form the net with respect to the direction of shearing motion. In addition, the behavior of geotextile/ geonet and smooth geomembrane/ geonet interfaces were found to depend on normal stress and the number of cycles of loading, respectively.

Based on the results presented in the paper, and a review of existing material on the subject, recommendations are presented regarding suitable testing procedures and conditions for estimating shear strength properties of geonet interfaces.

Keywords: landfill liner, landfill cover, geonets, interface friction, static-cyclic shear tests

1 INTRODUCTION

Geonets, either in the form of a single layer, or part of a geocomposite layer, are included as drainage components in the liner and cover systems of modern landfills. They are usually placed in contact with a geotextile or a geomembrane surface, where they form interfaces that have relatively low frictional properties. Therefore, the shear strength property of geonet/geotextile or geonet/geomembrane interface represents a critical parameter in the stability analyses of most modern landfills. Since the geonet interfaces may occur in both the liner and the cover systems, it is essential to characterize their frictional behaviors under a very wide range of normal stresses. Dynamic frictional properties may be included as design parameters for seismic stability anlayses for landfills in regions of high seismicity.

2 GEOSYNTHETICS

Ten geosynthetic interfaces were used in the experiments described in this paper. These interfaces were composed of four different materials, and, between them, represent seven different surfaces or orientations. The ten different interfaces are described in Table 1. The trade names of the geosynthetics used, as well as those of the manufacturers, have been used in the table to assist in identification of the materials. In the remaining portions of this paper, the interfaces will be referred to by interface numbers (also presented in Table 1) and geosynthetic types. The geosynthetics used were:

- continuous filament, non-woven needle-punched geotextile, with mass per unit area of 270 g/m^2 (8 oz/yd^2);
- medium density polyethylene (MDPE) geonet, 5.2 mm (205 mils) thick;
- high density polyethylene (HDPE) smooth geomembrane, 1.5 mm (60 mils) thick; and
- high density polyethylene (HDPE) textured geomembrane, 2.0 mm (80 mils) thick.

The frictional properties of the geonet were found to be highly dependent on the orientation of the strands with respect to the direction of shear displacement. Accordingly, three different orientations of the geonet were considered. The orientations were termed "transverse", "longitudinal" and "aligned", and are shown in Figure 1. The orientation in which the one of the strands is along the direction of the force is termed aligned. The case where the strands are at 60° with the direction of the force is termed transverse. When the direction of the strands makes an angle of 30° with the force direction, the orientation is termed longitudinal. The influence of the orientation of geonet on its frictional properties has also been observed by other researchers, viz. Geotek (1987) and Mitchell et al. (1990). The three orientations were treated as three different surfaces.

The textured geomembrane was found to have two surfaces with unequal texturing (observed through physical inspection). One surface was found to contain larger asperities and provided slightly greater surface roughness than the other. Accordingly, the two surfaces were treated as two different materials, and were included in the combinations presented in Table 1.

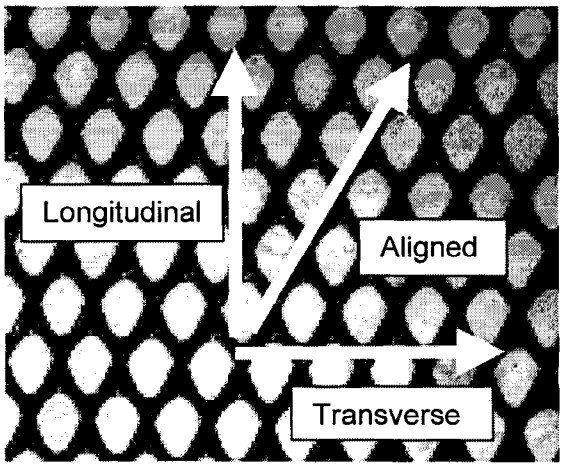

Figure 1. The orientation of the geonet mesh

Table 1. Description of geosynthetic interfaces

Interface number	Geosynthetic A	Geosynthetic B
I	Geotextile: Polyfelt TS700	Geonet (transverse): Tensar NS 1405
II	Geotextile: Polyfelt TS700	Geonet (longitudinal): Tensar NS 1405
III	Geotextile: Polyfelt TS700	Geonet (aligned): Tensar NS 1405
IV	Smooth Geomembrane: Gundline HD 60 mils	Geonet (transverse): Tensar NS 1405
V	Smooth Geomembrane: Gundline HD 60 mils	Geonet (longitudinal): Tensar NS 1405
VI	Smooth Geomembrane: Gundline HD 60 mils	Geonet (aligned): Tensar NS 1405
VII	Textured Geomembrane: Gundline HDT 80 mils (smoother surface)	Geonet (transverse): Tensar NS 1405
VIII	Textured Geomembrane: Gundline HDT 80 mils (rougher surface)	Geonet (transverse): Tensar NS 1405
IX	Textured Geomembrane: Gundline HDT 80 mils (smoother surface)	Geonet (longitudinal): Tensar NS 1405
X	Textured Geomembrane: Gundline HDT 80 mils (rougher surface)	Geonet (longitudinal): Tensar NS 1405

3 EXPERIMENTAL APPROACH

3.1 Monotonic (Static) Friction Tests

The monotonic tests were performed using the following apparatus: :

- a tilt table setup;
- a small-scale direct shear device (specimen size = 50 cm^2); and
- a large-scale direct shear device (specimen size = 900 cm^2).

3.1.1 *Tilt Table Setup*

The tilt table setup is a simple device to estimate angles of static friction. The experimental setup is shown in Figure 2. One layer of geosynthetic is attached to the table, while the other layer is attached to the bottom of a solid block that rests on the table. The table is gradually tilted about a fixed base until the block just begins to move. The angle of inclination of the table at the point where sliding initiates is equal to the angle of static friction for the interface. The normal stress is applied by means of the block, and hence, the tilt table setup is capable of delivering relatively small magnitudes of normal stress.

3.1.2 *Small-scale Direct Shear Device*

A Norwegian Geotechnical Institute (NGI) direct simple shear device was used to perform tests on geosynthetic interfaces. Circular specimens with a cross-sectional area of 50 cm^2 were tested. The specimen assembly used in the small-scale direct shear device is shown in Figure 3. The vertical load

was applied through a system of weights and a lever. The shearing force was applied either by using a hydraulic actuator controlled by an MTS™ unit, or a gear assembly driven by electric motor.

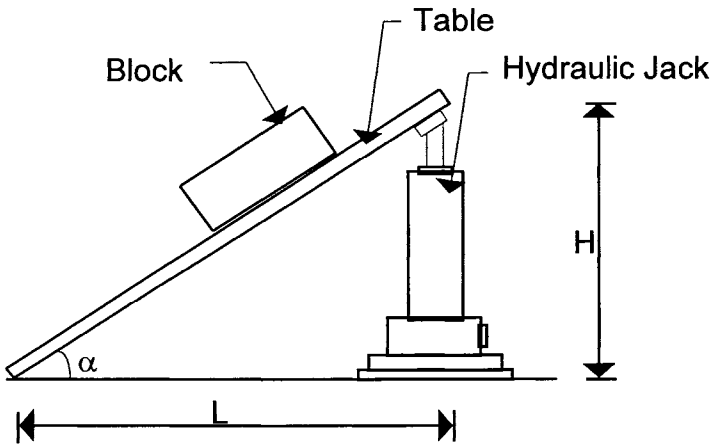

Figure 2. Setup for Tilt Table Experiments

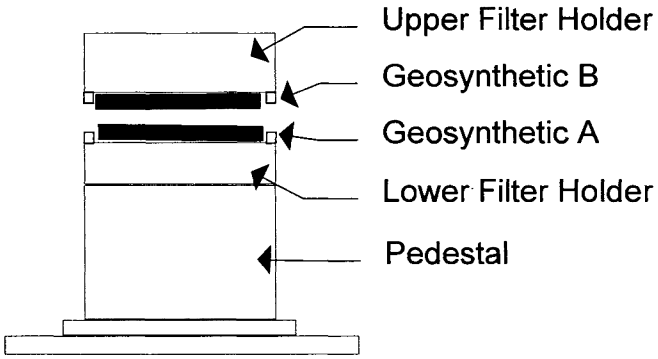

Figure 3. Specimen assembly for geosynthetic specimens – Small-scale device

3.1.3 *Large-scale Direct Shear Device*

A direct shear device, developed at Rensselaer Polytechnic Institute as part of this research work, was used for these experiments. Specimens measuring 30 cm × 30 cm were mounted on aluminum plates and tested in accordance with ASTM D 5321-92 (ASTM, 1992). The specimen assembly for this device is shown in Figure 4. The vertical load is applied through a pneumatic piston. As in the case of the small-scale device, the shearing force is applied either by using a hydraulic actuator controlled by an MTS™ unit, or a gear assembly driven by an electric motor.

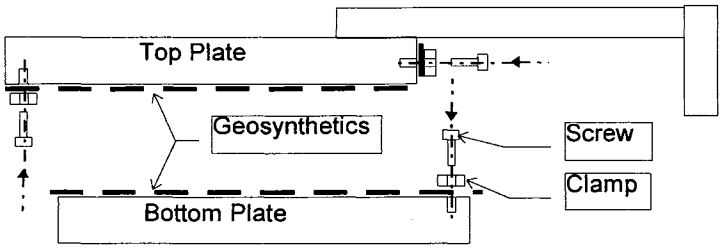

Figure 4. Specimen assembly for geosynthetic specimens – Large-scale device

3.2 Dynamic Friction Tests

3.2.1 *Cyclic Direct Shear Tests*

Cyclic direct shear tests were conducted on the large-scale devices by applying displacement-controlled sinusoidal loading. Important parameters in the case of cyclic direct shear tests are normal stress, frequency of excitation and the amplitude of maximum displacement.

3.2.2 *Shaking Table Tests*

A schematic diagram of the shaking table device is presented in Figure 5. In a shaking table test, one geosynthetic is attached to the table surface and the other to a solid block placed on top of the table. Sinusoidal excitation applied to the table in a horizontal direction is transferred to the block by means of the shearing resistance of the geosynthetic/geosynthetic interface that forms the contact. As the amplitude of base acceleration is increased, eventually a level is reached when the shearing resistance of the interface is not sufficient to transfer the impulse, and relative movement between the two geosynthetics is observed. The magnitude of acceleration at which this slip initiates provides the coefficient of dynamic friction for the interface. Important parameters with relation to shaking table tests are the applied normal stress, frequency of vibration, and the size of the test specimen interface.

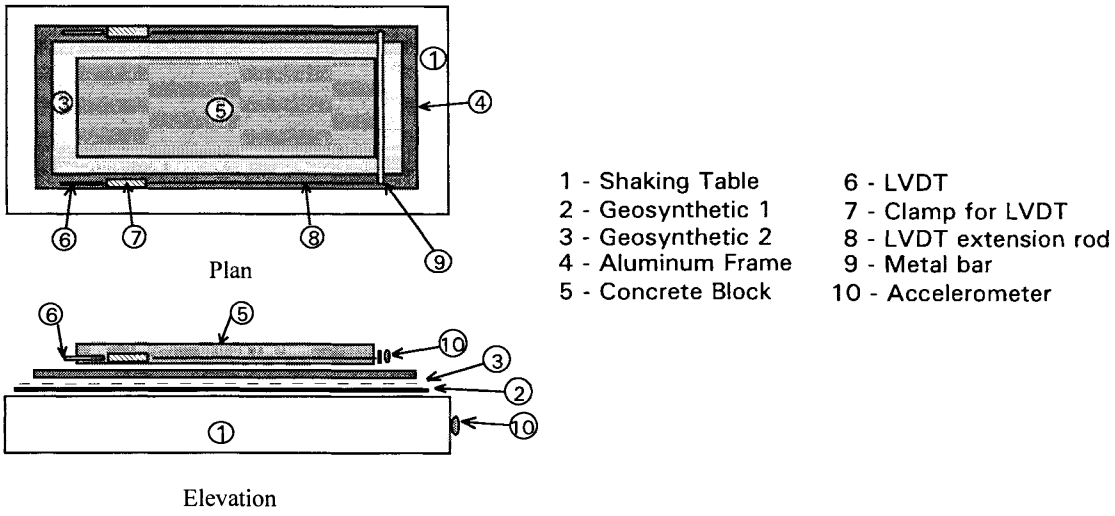

Figure 5. Setup for Shaking Table Experiments

3.2.3 *Shaking Table Tests Using a Geotechnical Centrifuge*

The centrifuge is utilized in geotechnical studies to perform experiments on models of structures that are subjected to the same stress levels as prototypes. In the case of dynamic friction testing, it is possible to produce normal stresses on the interfaces that are within the range of stresses produced on geosynthetic interfaces in field applications, such as landfill liners and base isolators.

4 EXPERIMENTAL RESULTS

4.1 Monotonic Tests

Monotonic tests were performed using the tilt table and the small- and large-scale direct shear devices. All tests were stroke-controlled, i.e. a constant rate of strain was applied in each test. The rates of displacement were 0.125 and 1.27 mm/min on the small-scale and large-scale devices, respectively.

4.1.1 *Geotextile over Geonet (Interfaces I, II, and III)*

Two orientations of the geonet, transverse and longitudinal (i.e. interfaces I and II) were tested on the small-scale device; while all three orientations were tested on the tilt table and the large-scale device.

Figure 6 shows the plots of peak shear stress versus normal stress from small-scale direct shear tests on two of the geotextile over geonet interfaces (transverse and longitudinal orientations). Both plots appear to indicate a linear relationship, corresponding to a peak friction angle of 27° in the case of the geonet in the transverse orientation and 18° in the case of the longitudinal geonet orientation.

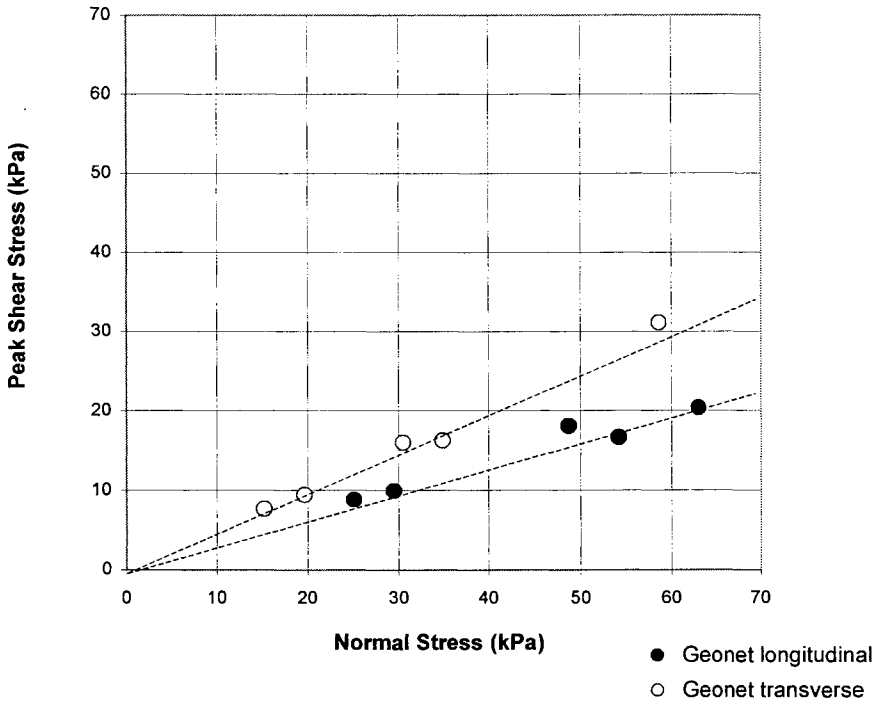

Figure 6. Shear versus Normal Stress from Direct Shear Tests: Geotextile over geonet (interfaces I and II) from Small-scale Tests

Figure 7 shows the plots of peak shear stress versus normal stress from large-scale direct shear tests on geotextile over geonet (interfaces I, II and III). The shear versus normal stress behavior for the transverse and the longitudinal orientations was not linear and depended on normal stress. The behavior of the aligned orientation appeared to be linear. Because of the stress dependent nature of the friction angles for the longitudinal and transverse orientations, the peak friction angle can only be calculated within ranges. For the transverse orientation the calculated friction angles ranged from 15° to 22°, for the range of normal stress from 20.7 to 41.4 kPa, with the smallest value associated with the highest normal stress and the largest value associated with the lowest normal stress. In the case of the longitudinal orientation, the value of the friction angle was between 14° (for normal stress of 41.4 kPa) and 17° (corresponding to 20.7 kPa normal stress). The behavior of the aligned orientation was approximately linear, and the peak friction angle was approximately equal to 11°.

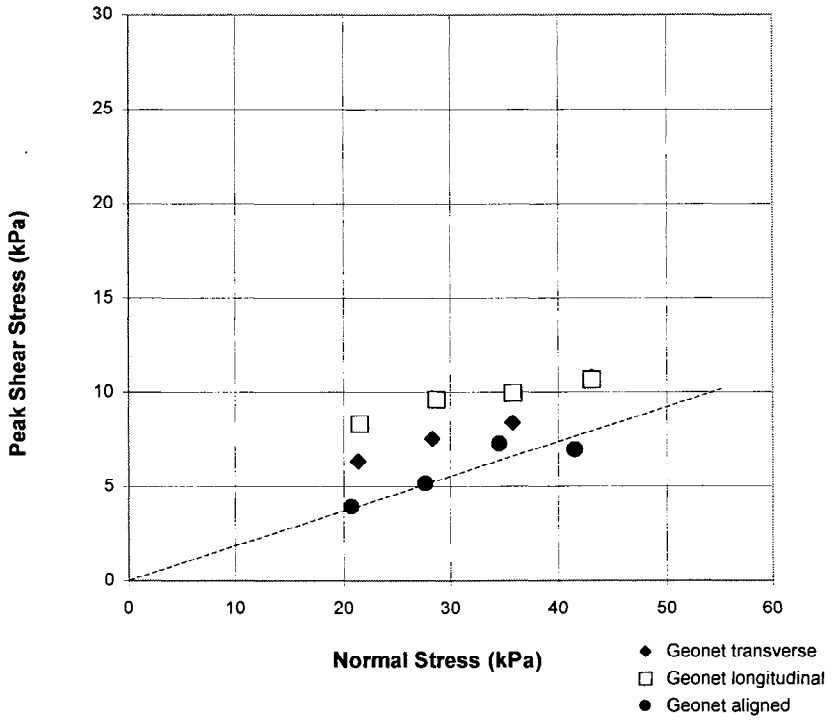

Figure 7. Shear versus Normal Stress from Direct Shear Tests: Geotextile over geonet (interfaces I, II and III) from Large-scale tests

The peak friction angle measured from the tilt table tests on the three orientations were 25°, 14° and 11°, for transverse, longitudinal and aligned orientations, respectively.

The geonet orientation could have a significant influence on the liner interface behavior, after sliding is initiated in the field. In the case of sliding along a geonet oriented transversely to the direction of movement, the resistance to motion offered by the geonet strands is relatively large, and the amount of relative displacement occurring after the shear strength of the interface has been mobilized will be relatively small. However, in the aligned orientation, sliding is initiated in a direction parallel to the direction of the strands, and the relatively low residual shear strength can lead to larger displacements.

4.1.2 *Smooth Geomembrane over Geonet (Interfaces IV, V, and VI)*

Two orientations of the geonet, transverse and longitudinal (i.e. interfaces IV and V) were tested on the small-scale device; while all three orientations were tested on the tilt table and the large-scale device. Figure 8 shows plots of peak shear stress versus normal stress for smooth geomembrane over geonet interfaces tested on the small-scale device. The peak static friction angle for this interface measured on the small-scale device was found to be approximately 11°.

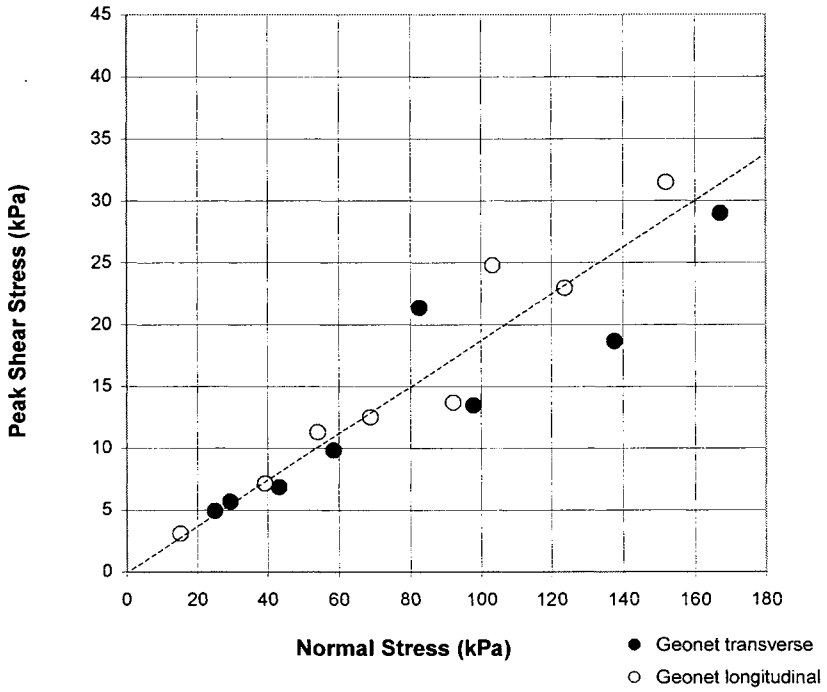

Figure 8. Shear versus Normal Stress from Direct Shear Tests: Smooth geomembrane over geonet (interfaces IV and V) from Small-scale tests

Figure 9 shows plots of peak shear stress versus normal stress for smooth geomembrane over geonet interfaces tested on the large-scale device. In this case, the peak friction angle appears to show some dependence on the orientation of geonet. The behavior of interfaces with the geonet in the transverse and longitudinal orientations, appears to be very similar, with a peak friction angle equal to approximately 11°. In the case of the geonet in aligned orientation, the peak friction angle was about 8°.

The peak friction angle measured from tilt table tests were 10°, 10° and 8°, respectively, for transverse, longitudinal and aligned orientations of the geonet.

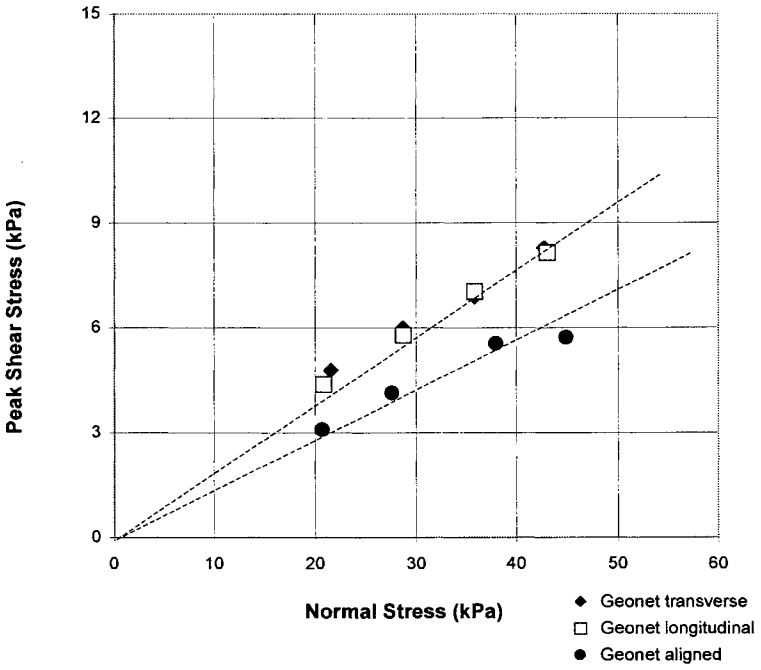

Figure 9. Shear versus Normal Stress from Direct Shear Tests: Smooth geomembrane over geonet (interfaces IV, V and VI) from Large-scale tests

4.1.3 *Textured Geomembrane over Geonet (Interfaces VII, VIII, IX and X)*

As mentioned previously, the two surfaces of the textured geomembrane were found to be slightly different and therefore they were considered separately for the purpose of testing. The two surfaces were designated "smoother" and "rougher" for identification purposes. The textured geomembrane specimens were tested against geonet in two orientations, transverse and longitudinal. Hence, four different interfaces were obtained through a combination of two textured surfaces and two geonet orientations.

The peak shear stress versus normal stress relationships for the textured geomembrane over geonet interfaces, measured in the small-scale device, appeared to be approximately linear. The peak friction angle varied from 31°, in the case of the rougher side of the textured geomembrane over the transverse orientation of the geonet to 19°, in the case of the smoother geomembrane surface over longitudinal geonet orientation.

Plots of peak shear stress versus normal stress for the same interfaces, tested in the large-scale device are presented in Figure 10. The peak static shear stress for the textured geomembrane over geonet interface appears to be independent of the geomembrane texturing or the geonet orientation. The peak friction angle for all four interfaces appear to lie within a range shown in the figure. The upper and lower bounds of this band of friction angles are 14° and 10°, respectively.

The peak friction angles measured from tilt table tests on the same interface varied from 16°, in the case of the rougher geomembrane surface over the geonet in the transverse orientation to 9°, in the case of the smoother geomembrane surface over the geonet in the longitudinal orientation.

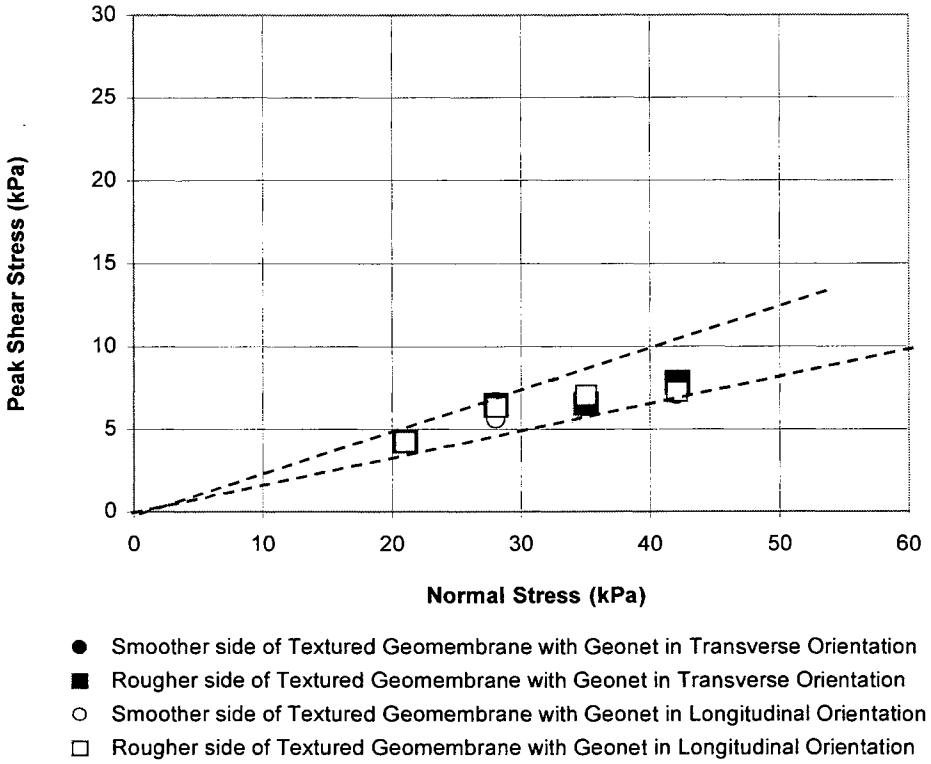

Figure 10. Shear versus Normal Stress from Direct Shear Tests: Textured geomembrane over geonet (interfaces VII, VIII and IX) from Large-scale tests

4.1.4 *Summary*

Table 2 provides a summary of the results of monotonic direct shear tests on the ten interfaces. The static friction angles for some interfaces, such as interfaces I and II, appear to depend on normal stress,. Therefore, it is important to perform interface tests at stress ranges representative of field conditions. While a general agreement exists between the peak static friction angles measured in the large-scale device and the tilt table, the results from the small-scale device appear to be more inconsistent. The small-scale device provided consistent results only in the case of the smooth geomembrane over geonet interfaces. For textured geomembrane interfaces, the results from an approximate method, such as a tilt table appear to be more consistent than results from a small-scale shear device.

On the basis of these results it is recommended that direct shear tests for geonet specimens be performed on large-scale devices, as outlined in ASTM D 5321-92 (ASTM, 1992). This is especially true of interfaces that also include geotextile or textured geomembrane. This is consistent with the observation of Koerner (1994), where the use of 300 mm (12 in.) shear boxes was recommended for tests involving geonets, geogrids and other geocomposites. It appears that specimen size influences the measured friction angles in the case of geosynthetics with pronounced asperities on the surface (such as textured geomembranes and geonets). This may be due to the reduced area of interface contact for such geosynthetics. De (1996) observed this trend in friction tests on a wider range of geosynthetics.

Table 2. Summary of results from monotonic direct shear tests

Interface Number	Peak static friction angles		
	Tilt table	Small-scale	Large-scale
I	25°	27°	15° (at high σ) to 22° (at low σ)
II	14°	18°	14° (at high σ) to 17° (at low σ)
III	11°	not tested	11°
IV	10°	11°	11°
V	10°	11°	11°
VI	8°	not tested	8°
VII	13°	24°	10° to 14°
VIII	16°	31°	10° to 14°
IX	9°	19°	10° to 14°
X	11°	22°	10° to 14°

4.2 Dynamic Tests

Dynamic tests consisted of cyclic direct shear tests and shaking table tests, from which the dynamic friction angles can be determined. The shaking table tests were performed both under normal, one-g condition, as well as under high-g conditions, on board a 100 g-ton geotechnical centrifuge to simulate higher normal stress conditions. These tests are appropriate for interfaces subjected to high overburden stress, such as for landfill bottom liners and structural base isolators. Details regarding the dynamic tests are presented in De (1996) and De and Zimmie (1998a and b). Only an account of the results will be presented here. As explained in section 4.1.4 above, the results from monotonic shear tests on the small-scale device were found to provide inconsistent results. Therefore, dynamic tests were not performed on that device.

4.2.1 *Geotextile over Geonet (Interfaces I, II, and III)*

The peak dynamic friction angles of geotextile/geonet interfaces were found to be a function of the orientation of the geonet. The results did not show any variation with the number of cycles of shear loading. The tests on geotextile over geonet in the transverse orientation (interface I) depended strongly on normal stress, with the highest peak friction angle (24°) obtained from tests at the lowest normal stress (20.7 kPa) and the lowest peak friction angle (17°) obtained from tests at the highest normal stress (41.4 kPa). The results from tests on interfaces II and III did not show any strong dependence on normal stress or the number of cycles. The dynamic friction angle for the longitudinal orientation (interface II) was measured to be 15° and that for the aligned orientation (interface III) to be between 10° and 11°.

Shaking table tests were performed at one-g and higher g's on interfaces I and II. The dynamic friction angle measured from one-g shaking table tests were 24° for interface I and 19° for interface II. The dynamic friction angles measured from high-g shaking tests on the centrifuge were found to depend on the g-level. In the case of interface I (geonet in transverse direction), the dynamic friction angles were 8° and 7° at 30-g and 40-g, respectively. In the case of interface II (geonet in longitudinal direction), the dynamic friction angles were 11° and 10°. Shaking table tests were not performed on interface III.

4.2.2 *Smooth Geomembrane over Geonet (Interfaces IV, V, and VI)*

The results from cyclic shear tests on smooth geomembrane/ geonet interfaces, previously presented in De and Zimmie (1998b) are included here. These results have shown that dynamic friction angle of interface IV depends significantly on the number of cycles of loading. For the first cycle, the dynamic friction angle was approximately 11°, for all normal stress levels. The dynamic friction angle increased rapidly in the first five to ten cycles. The dynamic friction angle at the end of 50 cycles showed a strong dependence on normal stress. After 50 cycles, the dynamic friction angle was 18° for tests at 20.7 kPa and 14° for tests at 41.4 kPa.

Similar trends of increasing dynamic friction angle with number of cycles, were observed in tests on interfaces V and VI (geonet in the longitudinal and aligned orientations). However, the dependence on normal stress was not as pronounced. The reason for this behavior is not clearly understood. For interface V (longitudinal orientation), the dynamic friction angle in the first cycle was 10°. At the end of 50 cycles, the dynamic friction angle was between 16° and 18° (the higher angle corresponding to a lower normal stress). In each of the three cases, the dynamic friction angle in the first cycle of loading was very close to the value of friction angle observed in monotonic tests.

For interface VI (aligned orientation), the dynamic friction angle at the end of the first cycle was 9°. The dynamic friction angle showed no variation with normal stress and the final value at the end of 50 cycles was 18°. The increase in the dynamic friction angle with the number of cycles for geomembrane/geonet interfaces has also been noted by Pasqualini et al. (1995).

Shaking table tests were performed on interfaces IV and V at one- and high-g. Dynamic friction angles measured in one-g shaking table tests were 12° for either interface. From shaking table tests on interface IV at 20-, 30- and 40-g, dynamic friction angles of 7° to 8° were measured. In the case of interface V, a dynamic friction angle of 11° was measured in tests at the same three high-g levels. Since this is very similar to the dynamic friction angle from shaking table tests at one-g, it appears that the shear behavior of this interface is not strongly dependent on g-levels, i.e. normal stress. This same observation can be made from the results of cyclic direct shear tests on the same interface. Shaking table tests were not performed on interface VI.

4.2.3 *Textured Geomembrane over Geonet (Interfaces VII, VIII, IX and X)*

Shaking table tests at one-g were performed on interfaces between textured geomembrane and geonet. The dynamic friction angles were measured to be 12° and 14° for geonet in the transverse orientation over the smoother and the rougher surfaces of the textured geomembrane (interfaces VII and VIII), respectively. In the case of geonet oriented in the longitudinal orientation, the dynamic friction angle was measured to be 11° for both the rougher and the smoother surface of the textured geomembrane (interfaces IX and X). Cyclic direct shear tests and centrifuge tests were not performed on these interfaces.

4.2.4 *Summary*

Table 3 provides a summary of the results of dynamic shear tests on the ten interfaces. The behavior of interfaces involving geonets is highly dependent on the orientation of the geonet strands

with respect to the direction of shear displacement. In general, the lowest friction angle is measured for strands aligned in the direction of displacement.

The cyclic behavior of geotextile/ geonet interface with the geonet in the transverse orientation (interface I) was dependent on the magnitude of normal stress and the higher stress related to a lower friction angle. The behavior of the aligned orientation (interface III) was independent of normal stress.

The dynamic shear behavior of smooth geomembrane/ geonet interfaces (interfaces IV, V and VI) appeared to depend both on the normal stress and the number of cycles of loading. The friction angle was found to increase with the number of cycles of loading.

The behavior of textured geomembrane/ geonet interfaces (interfaces VII, VIII, IX and X) were not found to depend strongly on the geonet orientation. The two surfaces of the textured geomembrane did not show significantly different dynamic friction behavior.

Table 3. Summary of results from dynamic shear tests

Interface Number	**Peak dynamic friction angles**		
	Large-scale direct shear	**One-g centrifuge**	**High-g centrifuge**
I	24° (for low σ to 17° for high σ)	24°	7° to 8°
II	15°	19°	10° to 11°
III	10° to 11°	not tested	not tested
IV	Increases from 11° to 18° (for low σ) or 14° for high σ)	12°	7° to 8°
V	Increases from 10° to 18° (for low σ) or 16° for high σ)	12°	11°
VI	Increases from 9° to 18° (for low or high σ)	not tested	not tested
VII	not tested	12°	not tested
VIII	not tested	14°	not tested
IX	not tested	11°	not tested
X	not tested	11°	not tested

5 CONCLUSIONS

Monotonic (static) and dynamic frictional behavior of ten geosynthetic interfaces have been presented in this paper. The results from monotonic tests indicate that use of large-scale specimens (such as recommended in ASTM D 5321) are appropriate for tests on interfaces that include geonets. Tests on a small-scale device and a tilt table provided results comparable to a large-scale device only in the case of smooth geomembrane/ geonet interfaces.

In general, the peak static and dynamic friction angles were found to be similar. However, several factors, such as normal stress, number of cycles of loading and frequency of excitation complicate the

behaviors. On the basis of the results several important conclusions can be made: The behavior of most interfaces involving geonet is strongly dependent on the orientation of the geonet strands. The behavior of geotextile/ geonet interfaces is dependent on normal stress. The dynamic behavior of smooth geomembrane/ geonet interfaces is dependent on the number of cycles of loading, and to a lesser extent, on normal stress.

On the basis of these observations, it is recommended that experiments be carried out using normal stresses and frequencies (for dynamic friction angle) expected in the field. In the case of interfaces where the friction angle is dependent on normal stress (such as interfaces I and II for monotonic, and IV, V and VI for dynamic), the tests should be performed at stress ranges representative of field conditions. In the case of interfaces where the dynamic friction angle increases with the number of cycles of loading (interfaces IV, V and VI), the range of cycles of loading for which design is intended should be identified. In seismic design, usually the first 5 to 30 cycles are significant. In such cases it is more appropriate to obtain dynamic friction angles from cyclic direct shear tests. For applications where a larger number of cycles of loading are of interest, as in the case of machine foundations, results from shaking table tests are more applicable.

REFERENCE

ASTM, 1992, "Standard Test Method for Determining the Coefficient of Soil and Geosynthetic or Geosynthetic and Geosynthetic Friction by the Direct Shear Method", ASTM Standard Designation D 5321 - 92, *1992 Annual Books of ASTM Standards*, Sec. 4, Vol. 4.08, American Society for Testing and Materials, Philadelphia, Pennsylvania.

De, A., 1996, "Study of Interfacial Friction of Landfill Geosynthetics: Static and Dynamic", Ph.D. Thesis, Rensselaer Polytechnic Institute, Troy, New York, USA, 245 p.

De, A. and Zimmie, T. F, 1998a, "Estimation of Dynamic Interfacial Properties of Geosynthetics", *Geosynthetics International*, Vol. 5, Nos. 1-2, pp. 17-39.

De, A. and Zimmie, T. F., 1998b, "Frictional Behavior of Landfill Liner Interfaces with Geonets", *Proceedings, Sixth International Conference on Geosynthetics*, Vol. 1, pp. 443-446.

Geotek, 1987, "*Direct Shear Testing of Friction Liner Material*", Report for Gundle Lining Systems, Project 21266, March, 1987, 10 p.

Koerner, R. M. (1994), "Designing with Geosynthetics", Third Edition, Prentice Hall, Englewood Cliffs, New Jersey.

Mitchell, J. K., Seed, R. B., and Seed. H. B., 1990, "Kettleman Hills Waste Landfill Slope Failure. I: Liner-System Properties," *Journal of Geotechnical Engineering*, ASCE, Vol. 116, No. 4, pp. 647-668.

Pasqualini, E., Sani, D. and Roccato, M., 1995, "Factors Influencing Geomembrane Interface Friction", *Green '93*, Sarsby, Editor, A. A. Balkema, Rotterdam, The Netherlands, pp. 349 - 356.

THE EVOLUTION OF SAND STRUCTURE ADJACENT TO GEOMEMBRANES

J. DAVID FROST
THE GEORGIA INSTITUTE OF TECHNOLOGY, USA
SEOK-WON LEE
THE GEORGIA INSTITUTE OF TECHNOLOGY, USA
PATRICK E. CARGILL
THE GEORGIA INSTITUTE OF TECHNOLOGY, USA

KEYWORDS: Geomembranes, Friction, Soil Mechanics, Interface, Structure

ABSTRACT

This paper summarizes the results of a study which has quantified the evolution of the structure of sands adjacent to geomembranes of varying roughness at different stages of shearing. The results show that the structure evolution, and hence shear mechanisms for sub-rounded uniform sands adjacent to geomembranes, are directly influenced by the surface roughness of the geomembranes. For smooth geomembranes, the shear mechanism predominantly involves sliding of sand particles and only affects the sand structure within two particle diameters of the geomembrane. For slightly textured geomembranes, the effects of interlocking and dilation of sand particles extends the zone of evolution to four particles diameters from the interface. For moderately/heavily textured geomembranes, the interlocking and dilation of sand particles is fully developed and results in large dilation in the interfacial zone, which extends up to six particle diameters from the interface. By understanding how the structure of the sand adjacent to geomembranes of different roughness changes during shearing, it may be possible to identify alternative geomembrane roughening procedures and patterns that can lead to more efficient interface designs.

INTRODUCTION

Geomembranes are commonly designed to be in contact with soils or other geosynthetics. A textured geomembrane with roughened top and/or bottom surfaces is used to increase the shear resistance mobilized at the interface with other materials, as compared to what is mobilized with interfaces involving smooth geomembranes. However, textured geomembranes are currently selected for use based on experimental tests of possible materials and personal experience. Interface friction angles are used to assess the global stability of the liner system.

Quantitative measurements of surface roughness have shown it to be a controlling parameter in the measured strength of interfaces (Kishida and Uesugi, 1987; Paikowsky et al., 1995; Dove and Frost, 1996; Dove et al., 1997; Lee et al., 1998). The load deformation response has been shown to be a function of the fundamental properties of both materials at the interface (sand

particle size, distribution, shape, and angularity and planar surface hardness and roughness), and the state of the sand at the interface (density, and normal stress).

This paper presents the results of a study which complements the findings of these earlier investigations by providing quantitative evidence of the evolution of the structure of sands of varying angularity adjacent to geomembranes with different surface topography. The term evolution is used to describe how the microstructure of the soil changes during shearing as a result of relative movements between particles. The results show how the thickness and state of the interfacial zone varies as a function of the properties of the interface materials and provides important insight into the shear mechanisms contributing to the observed global response of sand/geomembrane interfaces.

EXPERIMENTAL PROGRAM

A series of direct shear interface tests were performed, in which the structure of specimens sheared to different stages along a predefined stress - horizontal displacement curve were preserved using epoxy impregnation. Coupons sectioned from the specimens were ground and polished so that facets of the soil structure could be accurately quantified from digital images captured using brightfield microscopy methods (Jang, 1997; Jang et al., 1998).

Sand Properties

The majority of the tests reported in this paper were conducted using Ottawa 20/30 sand. A few additional tests to study the effects of angularity were performed using a commercial blasting sand produced by Rollo Silica of Georgia. The Ottawa 20/30 sand particles were rounded to subrounded, whereas the blasting sand particles were composed of angular crushed quartz particles. Table 1 summarizes the index and strength properties of both materials tested in this study. In addition, the properties of Ottawa F-70 sand as reported by Dove et al. (1997) are listed.

Table 1. Soil Index Properties

Soil	D_{50} (mm)	C_u	C_c	G_s	e_{max} (mm)	e_{min} (mm)	ϕ'_p (2)	ϕ'_r (2)
Ottawa 20/30	0.72	1.19	0.98	2.65	0.742	0.502	38.5	27.9
Blasting sand	0.74	1.83	0.84	2.65	0.951	0.698	47.7	42.9
Ottawa F-70(1)	0.20	1.70	1.17	2.65	0.740	0.500	37.4	31.0

Note: (1) Data from Dove et al. (1997)
(2) Normal Stress ≈ 300kPa

Geomembrane Characteristics

One smooth and two textured HDPE geomembranes, considered to be representative of the range of textures currently used in practice, were utilized in this study. The samples included National Seal Co. Dura Seal HD, which is a smooth-surfaced geomembrane, GSE Lining

Technology, Inc. Friction Flex which has a slightly textured surface, and Poly-Flex Inc. Textured HDPE, which has a moderately/heavily textured surface.

The average and standard deviation of surface roughness values (R_S), determined using the Optical Profile Microscopy (OPM) method (Dove and Frost, 1996) for these geomembranes, are summarized in Table 2. The last column of Table 2 gives the corresponding texture descriptor proposed by Dove and Frost (1996) and is based on the average value of R_S.

Table 2. Results of Surface Roughness Determinations

Geomembrane	Average R_S	Standard Deviation	Texture Descriptor
NSC Dura Seal	1.09	0.01	Smooth
GSE Friction Flex	1.25	0.03	Slightly Textured
Poly-Flex Textured	1.71	0.12	Moderately/Heavily Textured

Interface Shear Test Equipment

Interface shear tests were performed using a large displacement direct shear device (Figure 1). This device was used to permit large displacements and hence quasi-residual conditions to be achieved in the tests. The shear tests were conducted at a constant displacement rate of 0.01 inches per minute or less. Normal stresses of 100 and 300 kPa were applied.

The geomembrane specimens, measuring approximately 220 mm (8.7 inches) wide by 300 mm (11.8 inches) long, were placed on the testing platform of the interface shear apparatus, with the machine direction of the geomembrane parallel to the shear direction (Figure 1). The geomembrane was secured by fastening 25 mm (1 inch) wide metal brackets along the rear and two side edges of the specimen. The shear box was constructed out of a 102 mm (4 inch) square block of teflon. The diameter of the soil specimen was 63.5 mm (2.5 inches) and the nominal height of the soil specimen was 38.1 mm (1.5 inches). Although this is not the standard recommended box size for tests on geosynthetics as outlined in ASTM D5321, for the purpose of the research study described herein, this is not considered to be of significant concern. It has been shown that values obtained with a given box size are internally consistent (O'Rourke et al., 1990; Takasumi et al., 1991). Since all data used in the present study was determined using the same 63.5 mm (2.5 inches) box, the relative values of peak and residual friction angles for the various sand/ geomembrane combinations can expected to be quite consistent and allow for evaluation of mechanisms. In addition, the decision to use a smaller box in the present study was influenced by the desire to minimize the amount of resin used. The low viscosity, low volume change resin used in this study would cost about $500 for each 30 x 30 cm (12 x 12 inch) box specimen as opposed to the actual $15 for the specimens size used. Normal load was applied using dead weights attached to an aluminum yoke. A LabView data acquisition system was used to record the test results. The horizontal displacement transducer and the two vertical displacement transducers recorded global test variables.

Air pluviation was used in this study to create uniform sand specimens. Using a pre-selected combination of discs (different number of holes and hole diameters) and fall height, the target relative density of 80 percent was consistently obtained. Details of the pluviation procedure are described in Dove et al. (1997).

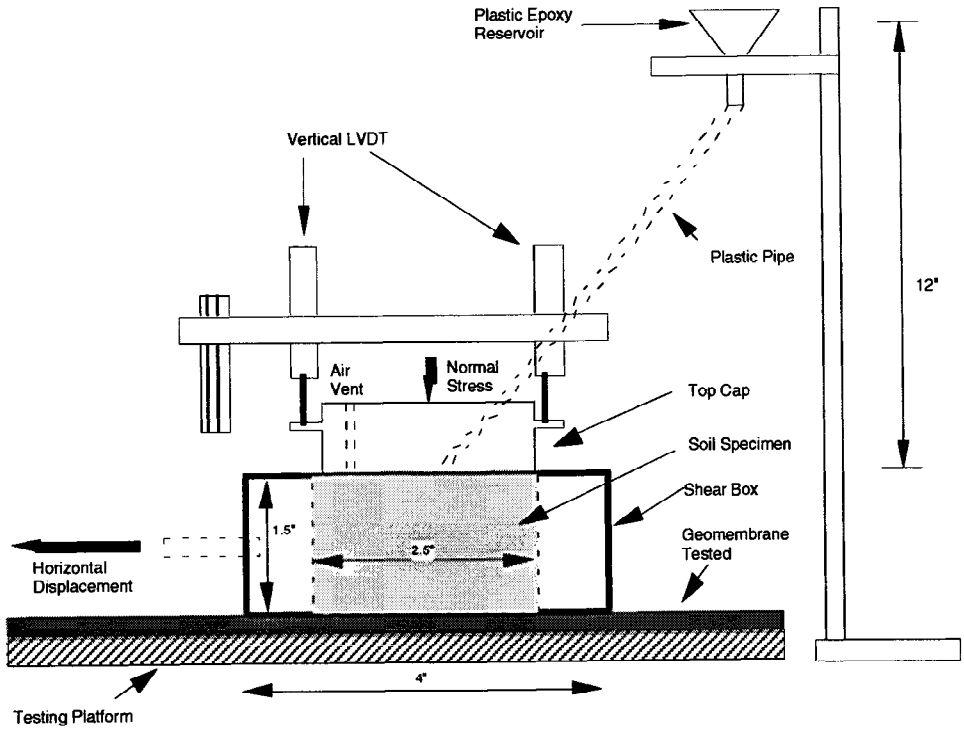

Figure 1. Schematic of Soil/Geomembrane Interface Shear Test System

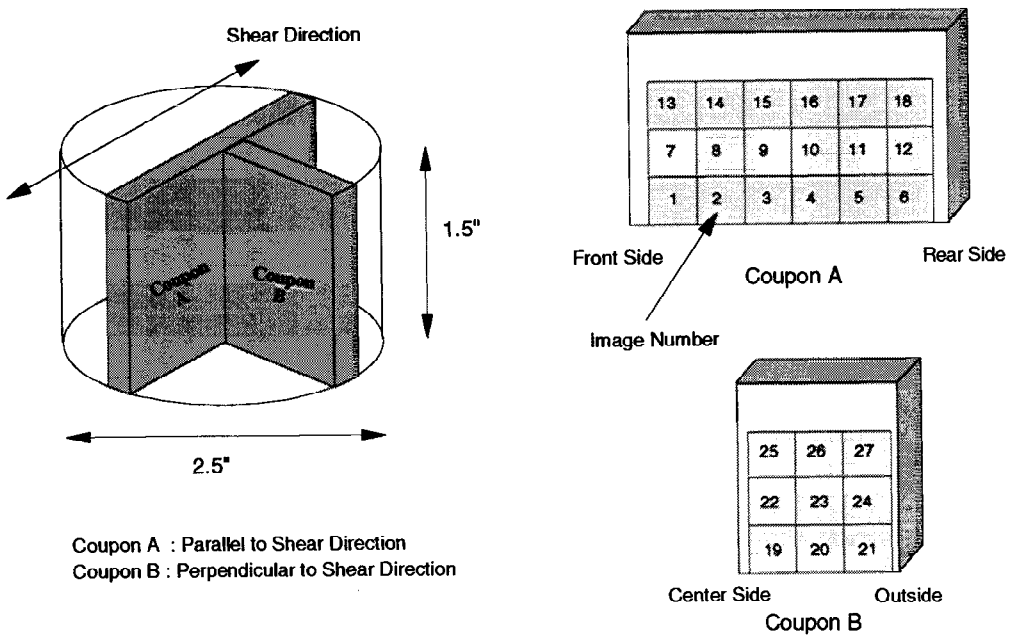

Figure 2. Typical Locations of Coupons and Images

Soil Specimen Preservation and Coupon Surface Preparation

After the sand specimens were sheared to their target displacement and stress states, they were impregnated with EPO-TEK 301 epoxy resin (Figure 1). Only elevation head was applied during impregnation of the sand specimen. Once the resin impregnated specimens had cured and were removed from the teflon shear box, coupons were cut using the pattern indicated in Figure 2. Coupon A was cut parallel to the shear direction, and coupon B was cut perpendicular to the shear direction.

The coupon surfaces from which images were to be captured, were then subjected to an extensive sequence of grinding and polishing stages referred to as the modified BUEHLER DIALOG method (Jang et al., 1998) to produce surfaces which would yield unbiased high quality images requiring minimal processing. Once the coupon surfaces were prepared, the complete coupon was placed on the stage of an optical microscope and images of areas approximately 9.2 mm by 8.6 mm were obtained with a CCD (Charge Coupled Device) camera mounted directly on top of the microscope using brightfield illumination (Jang et al., 1998).

For each specimen, 18 images from coupon A and 9 images from coupon B were captured. Each image included somewhere in the range of 110 sand particles. The 27 images from each specimen were divided into three layers for analysis. Layer I included images 1 to 6 from the shear direction coupon (coupon A), and 19 to 21 from the coupon perpendicular to the shear direction (coupon B) and represented conditions in the area from the interface to 9.2 mm above it. Layer II included images 7 to 12 and 22 to 24, while layer III included images 13 to 18 and 25 to 27 (Figure 2). The layer II and layer III images occupied the areas 9.2 to 18.4 mm, and 18.4 to 27.6 mm above the interface, respectively.

Gray scale images were captured which were then converted to a binary image by setting a threshold in the gray scale. A typical binary image is shown in Figure 3. Sand structure analyses were performed on the captured binary images using a Cambridge Instruments, Leica Quantimet Q-570 image analysis system. Sand structure analyses included determination of the void ratio variation as a function of the shear displacement and the distance from the interface. This was accomplished by computing the void ratio of areas D_{50} high in each image.

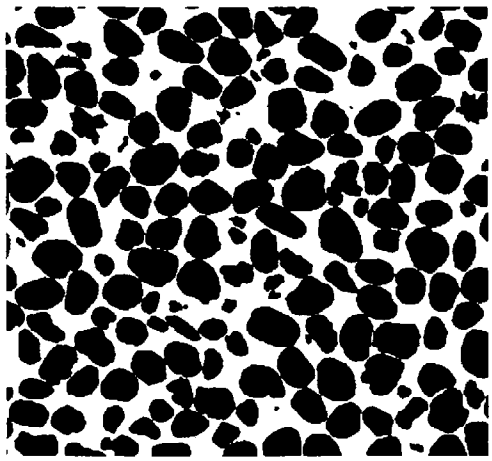

Figure 3. Typical Binary Image of Ottawa 20-30 Sand

INTERFACE STRENGTH TEST RESULTS

The interface shear test results performed as part of this study confirm the previously reported important effect that surface roughness has on the shear behavior of sand/geomembrane interfaces (Dove et al., 1997). For example, the results presented in Figure 4 are for tests performed in this study as well as those from Dove et al. (1997). The tests show that, for various sand/geomembrane combinations under a normal stress of 300 kPa, as the roughness increases, the peak and residual interface friction increases significantly with changes in roughness up to an R_S value of about 1.35. At higher roughness values, the interface friction remains approximately constant and equal to the soil friction angle, reflecting the fact that failure is occurring in the soil near the geomembrane. Similar trends have been observed for different normal stress levels (Dove et al., 1997).

The results also show the importance of particle angularity on the interface strength for sand/smooth geomembrane interfaces. While the peak friction angles mobilized with the blasting sand are very similar to those for Ottawa 20/30 sand in contact with the smooth geomembranes, the residual friction angles for blasting sand are significantly higher (3 degree) than those for Ottawa 20/30. This is due to differences in the plowing effects resulting from the displacement of a harder material (sand) relative to a softer material (geomembrane) such that the harder material scratches and removes the soft material in its path (Dove, 1996). The angular soil particles indent the softer geomembrane more deeply making more scratches as described below. It is noted that the plowing effect is less significant for the textured geomembranes where other shear mechanisms dominate the shear strength, as opposed to interfaces involving smooth geomembranes where sliding is the main shear mechanism.

This plowing effect on the smooth geomembranes is evident from the variations in surface roughness measured at various stages of shearing, as shown in Figure 5. The interface shear tests were terminated at horizontal displacements of about 0.1, 10, 40 and 80 mm and the surface roughness perpendicular to the shear direction was measured using a stylus profilometer.

The roughness parameter, R_a, shown in Figure 5 is an arithmetic mean of the departures of the profile from the mean line. At peak, the roughness values for Ottawa 20/30 and blasting sand are similar although the Ottawa 20/30 shows marginally larger values (see expanded view in Figure 5). This is due to the difference of angularity of the sand particles. Even though angular particles indent more deeply, the rounded to subrounded Ottawa 20/30 initially indents a larger area than angular blasting sand. At residual state, the blasting sand produces more scratches as reflected in the significantly higher roughness value. The increasing slope of the plots also infer that blasting sand starts to scratch the geomembrane at the peak stress, and then continuously makes deeper scratches. This plowing effect also increases as the normal stress is increased.

EFFECT OF GEOMEMBRANE SURFACE ROUGHNESS ON THE EVOLUTION OF SAND STRUCTURE

An initial set of tests using geomembranes of various textures and Ottawa 20/30 sand were conducted to evaluate the effect of geomembrane surface roughness on the evolution of sand

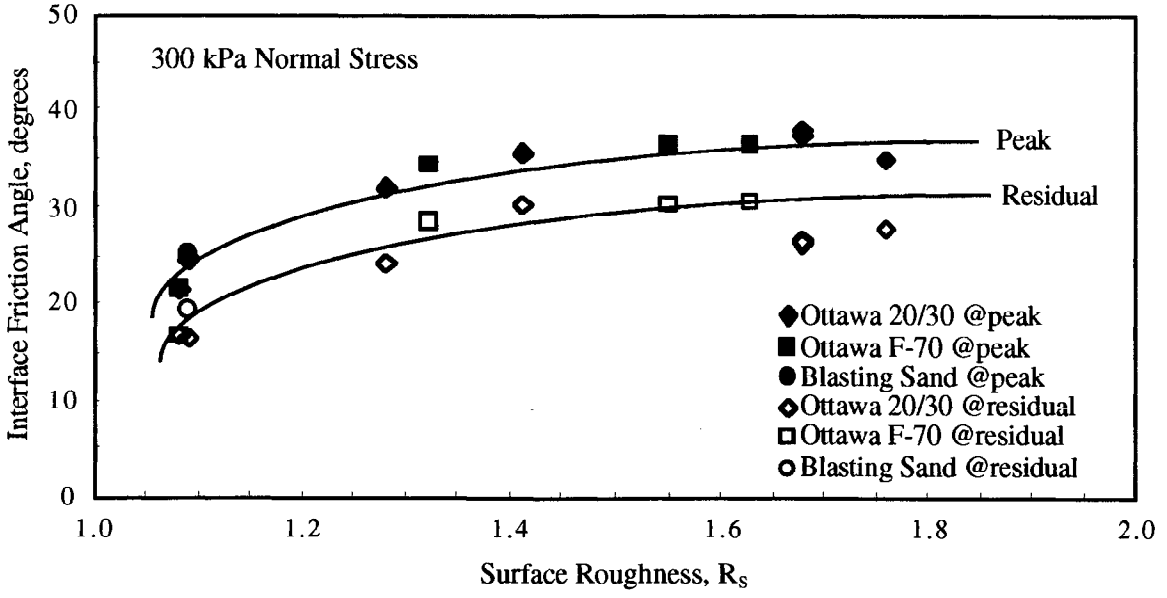

Figure 4. Peak and Residual Interface Friction Angles with Roughness

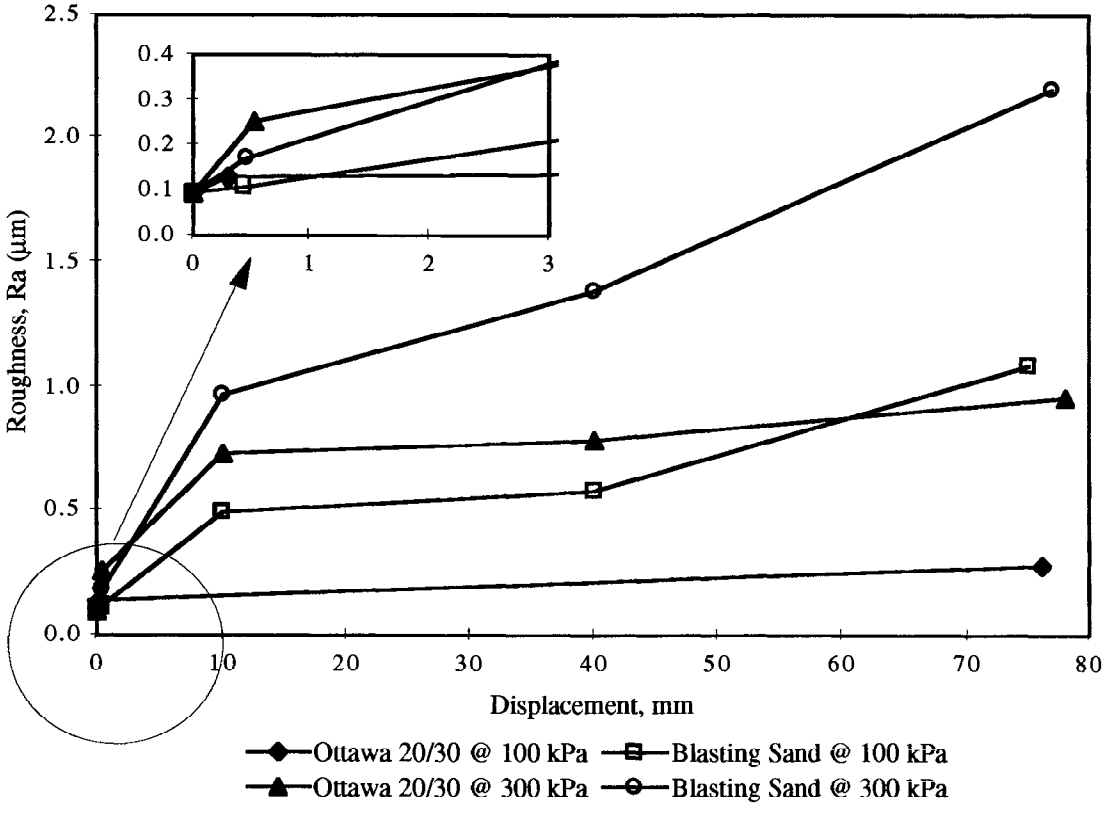

Figure 5. Increase in Surface Roughness Due to Plowing

structure during shearing. Specimens at different stages of shearing along the predefined stress-displacement curve were preserved using epoxy impregnation. Variations in void ratio as a function of distance from the interface were quantified using image analysis.

Smooth Geomembrane

To study the shear behavior of smooth geomembrane/Ottawa 20/30 sand interfaces, six specimens under normal stresses of 100 kPa were sheared along the same predefined stress-displacement curve. The shearing of these specimens was terminated at the stress and displacement states shown in Table 3 before the specimens were preserved by epoxy impregnation. Figure 6 shows the evolution of the void ratio as a function of distance from the interface. For clarity, only the initial, peak, and residual values are plotted.

In the initial pre-shearing state, the air pluviation resulted in the layer I (lower 9.2 mm) being slightly more dense than layers II and III. However in the immediate interfacial zone (within two particle diameters from the interface), the void ratio was slightly higher as would be expected at the interface between any particulate material and any planar surface. At pre-peak displacements, the void ratio in the interfacial zone remained relatively constant indicating no relative movement between particles. At peak stress displacements, sand particles in the interfacial zone start to move relative to each other. Even though the void ratio in the layer I is seen to increase at peak stress (resulting in a relatively higher void ratio compared to the layers II and III), the sand structure collapses in the interfacial zone as sand particles fill the voids by sliding, and consequently, the void ratio in this interfacial zone decreases slightly to the average void ratio. As the shearing continues, the contraction started in the interfacial zone expands throughout the layer I. This trend continues throughout the whole shearing test. It should be noted that the void ratio changes described on the smooth geomembranes are relatively small compared to those measured with the textured geomembranes as discussed later.

From the above observations, the following mechanism is postulated. Shearing primarily affects a zone two particle diameters from the interface, and no significant dilation or contraction is observed throughout the shear test. This means that the peak stress is induced by the initial sliding of the soil particles in the interfacial zone. Beyond the peak displacement, the shearing is mobilized by the sliding of soils and by the very slight plowing of particles into the geomembrane, which produces the scratches on the surface. Once the residual state is achieved, the soil structure remains unchanged throughout the remainder of the shear test.

Slightly Textured Geomembrane

GSE Friction Flex geomembrane was used to study the interaction between slightly textured geomembranes and Ottawa 20/30. Three specimens under normal stresses of 100 kPa were sheared along the same predefined stress-displacement curve (Table 4). Figure 7 shows the evolution of the void ratio as a function of distance from the interface.

In the initial state, the same trend of a slightly more dense layer I, but with a slightly more loose interfacial zone within two particle diameters from the interface, was observed. At peak stress, the soil particles started to move relative to each other in the interfacial zone. Unlike the smooth geomembrane tests where the sliding induced a decrease in void ratio in the interfacial zone, the void ratio in the interfacial zone increased slightly. This means that at peak stress,

Table 3. Evolution of Specimens' Properties

Specimen	SMOT22	SMOT31	SMOT41	SMOT51	SMOT61	SMOT71
Initial Void Ratio, e_i	0.550	0.551	0.551	0.550	0.549	0.552
Final Void Ratio, e_f	0.544	0.546	0.548	0.545	0.543	0.552
Shear Stress, kPa	0.0	36.5	45.3	37	30.3	26.4
Displacement, mm	0.0	0.1	0.15	1.14	10.06	76

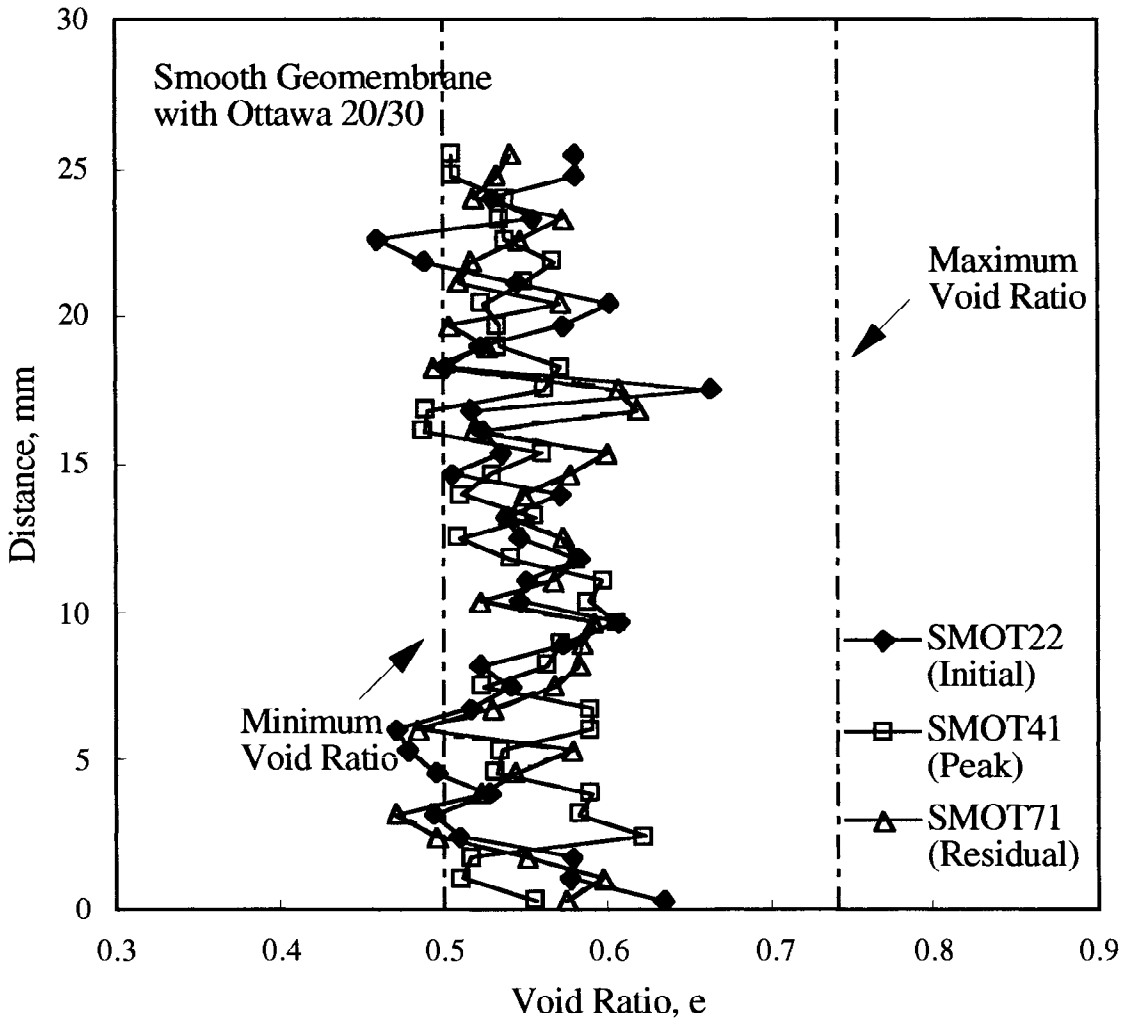

Figure 6. Evolution of Void Ratio as Function of Distance from Interface

Table 4. Evolution of Specimens' Properties

Specimen	GDOT21	GDOT41	GDOT61
Initial Void Ratio, e_i	0.547	0.547	0.548
Final Void Ratio, e_f	0.542	0.545	0.567
Shear Stress, kPa	0.0	77.1	51.2
Horizontal Displacement, mm	0.0	1.09	10.1

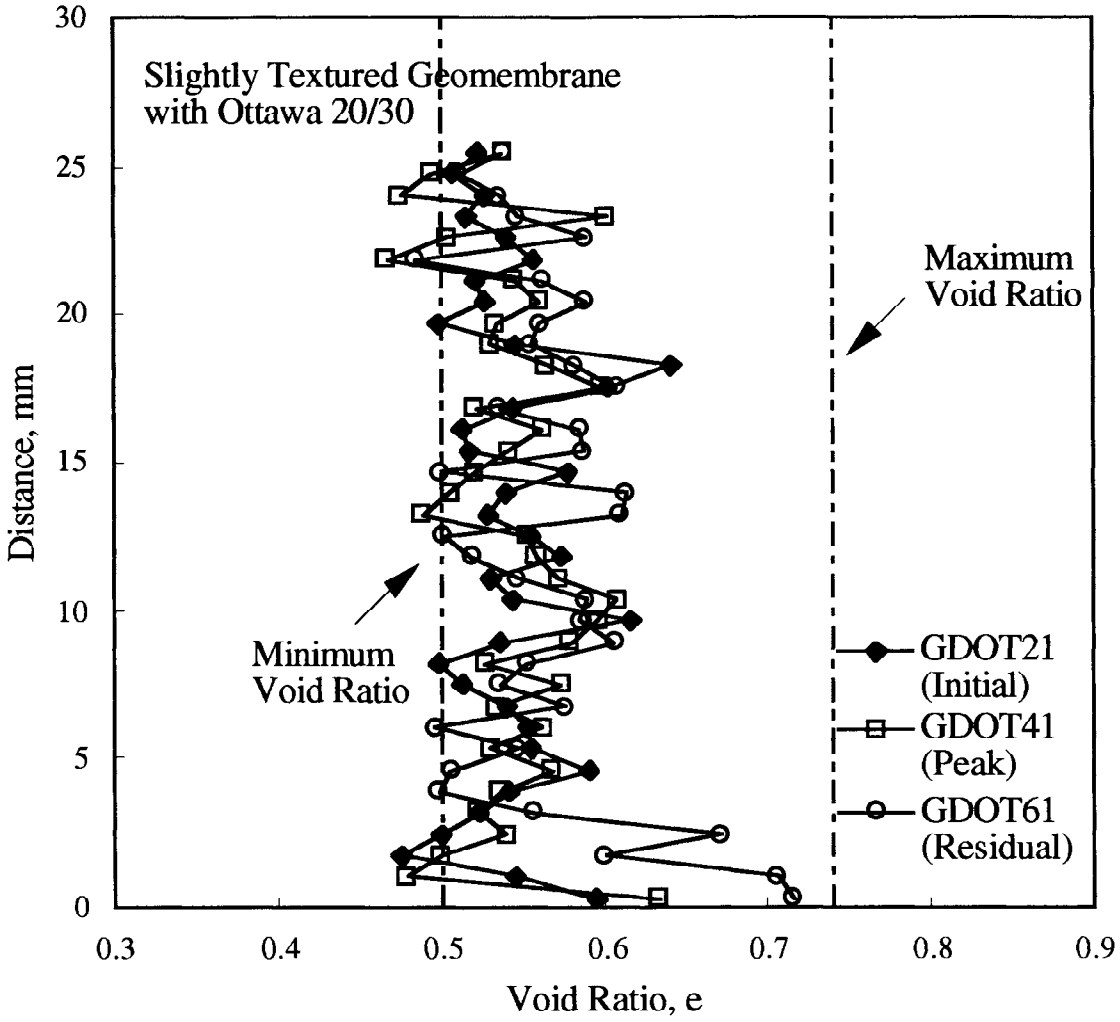

Figure 7. Evolution of Void Ratio as Function of Distance from Interface

while some sliding of the soil particles on the geomembrane may occur, interlocking between the roughened surface of the geomembrane and the sand particles induces a higher void ratio in the interfacial zone. The shear zone is contained within a distance of about two particle diameters from the interface at the peak stress. As the shearing continues beyond peak displacement, the movement of the soil particles increases the porosity and extent of the interfacial zone, with dilation being observed at a distance of up to four particle diameters from the interface. The shearing zone remains about four particles wide even at larger displacements.

Since the void ratio in the interfacial zone increases in the post-peak region, it is inferred that interlocking between the sand and the geomembrane is the principal shearing mechanism although some sliding of sand particles on the geomembrane surface may also be occurring. Moreover, at the start of the residual state, the effect of interlocking between the geomembrane and the sand and more importantly, particle dilation expands the shear zone and induces a higher void ratio in a zone equal to four particle diameters from the interface.

Moderately/Heavily Textured Geomembrane

Poly-Flex Textured geomembrane was used in a similar set of tests to represent the shearing between a moderately/heavily textured geomembrane and Ottawa 20/30. Six specimens under normal stresses of 100 kPa were sheared along the same predefined stress-displacement curve (Table 5). Figure 8 shows the evolution of the void ratio as a function of distance from the interface. For clarity, only the initial, peak, and residual values are plotted.

In the initial state, the void ratio distribution shows the same trend as with the other geomembranes. Below peak displacements, some minimal soil particle reorientation occurs. The results from specimens PFOT41 and PFOT42 which are for displacements just before and just after peak stress respectively, show large relative movement occurring near the peak stress. Just before the peak stress, the void ratio distribution in the interfacial zone, is similar with the initial state. However just after the peak stress, the void ratio substantially increases. This indicates that at the peak stress, relative movements of soil particles are initiated. Soil particles start to slide on the geomembrane and interlock with the geomembrane textured surface. More importantly, dilation of soil particles occurs. As shearing continues, the interlocking and dilation progress further, and consequently, yield a higher void ratio in the interfacial zone which extends up to six particle diameters from the interface.

From the above observations, the following interface mechanism can be postulated for the moderately/heavily textured geomembrane and Ottawa 20/30. Below peak stress, the shearing induces minor reorientation in layer I. At the peak stress, the sand particles near the interfacial zone start to slide, interlock with the geomembrane surface, and cause dilation between sand particles. Consequently, this yields a higher void ratio in the interfacial zone. The peak stress is principally developed by dilation of the soil itself. This means that for the moderately/heavily textured geomembrane, the shear strength is mobilized within the soil.

In conclusion, it is observed that the shear mechanism is significantly changed by the surface roughness of the geomembrane. For the smooth geomembrane (R_S = 1.09), the shearing extends only two particle diameters from the interface, and the shear stress is developed by sliding and slight plowing of sand particles. For the slightly textured geomembrane (R_S = 1.25), the effect of interlocking between the sand particles and geomembrane results in dilation of sand particles along with some sliding, with the shearing extending up to four particle

Table 5. Evolution of Specimens' Properties

Specimen	PFOT21	PFOT31	PFOT41	PFOT42	PFOT51	PFOT61
Initial Void Ratio, e_i	0.548	0.550	0.548	0.551	0.550	0.548
Final Void Ratio, e_f	0.540	0.551	0.559	0.563	0.566	0.571
Shear Stress, kPa	0.0	52.5	83.6	83.7	70.7	56.6
Displacement, mm	0.0	0.30	1.19	1.52	2.90	10.3

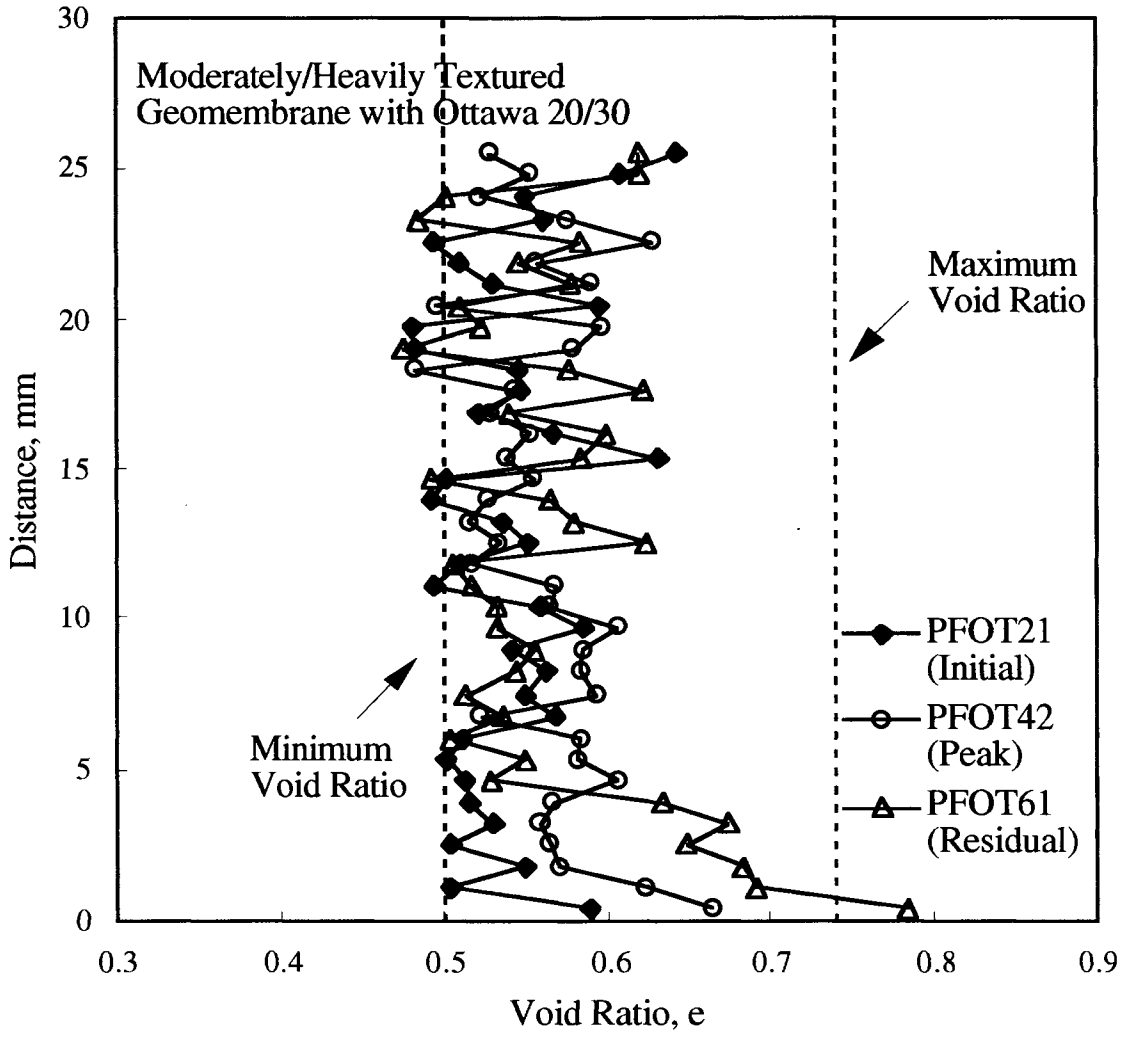

Figure 8 Evolution of Void Ratio as Function of Distance from Interface

diameters from the interface. For the moderately/heavily textured geomembrane (R_S = 1.71), the interlocking and dilation of sand particles is developed fully, resulting in a large void ratio in the interfacial zone, which extends six particle diameters from the interface.

EFFECT OF SAND PARTICLE ANGULARITY ON EVOLUTION OF STRUCTURE

The preceding discussion has shown how interface shear mechanisms vary as a function of geomembrane roughness for a sub-rounded uniform sand. To evaluate the effect of particle angularity on the evolution of sand structure, some additional tests were performed using angular blasting sand and smooth and moderately/heavily textured geomembranes. Specimens at different stages of shearing along a predefined stress-displacement curve were preserved using epoxy impregnation.

Smooth Geomembrane

Four specimens were sheared along the same predefined stress-displacement curve. At the initial state, the blasting sand showed a similar structure to that observed with Ottawa 20/30 (dense layer I and a loose interfacial zone within two particle diameters from the interface). At peak stress, when the soil particles started to move, a small increase of void ratio in the interfacial zone was observed which was in contrast to the observations from the tests on Ottawa 20/30 sand in contact with a smooth geomembrane. It was also found that the blasting sand showed a slightly higher interface strength than the Ottawa 20/30 on the smooth geomembrane. These differences between blasting sand and Ottawa 20/30 on the smooth geomembrane are consistent with the plowing effect described earlier.

From the above observations, the following mechanism can be postulated. The angular blasting sand induces more plowing on the smooth geomembrane than the rounded to sub-rounded Ottawa 20/30. Penetration of angular particles into the smooth geomembrane induces slight interlocking of sand particles near the interface at the peak stress, resulting in a higher void ratio in the interfacial zone. This is in contrast to the Ottawa 20/30 test results which show the decrease in void ratio in the interfacial zone. Beyond the peak stress, the particle movement in the interfacial zone resembles that of the Ottawa 20/30 sand where the void ratio was decreased to the average void ratio by sliding of the sand particles. However, the residual strength for angular blasting sand is higher since it results from deeper scratches.

Moderately/Heavily Textured Geomembrane

Poly-Flex Textured geomembrane was used to study the interaction between moderately/heavily textured geomembranes and angular blasting sand. Three specimens were sheared along the same predefined stress-displacement curve. In general, all the shearing process trends were very similar to those observed with Ottawa 20/30 with the moderately/heavily textured geomembrane. However, more dilation was observed for the blasting sand at both peak and residual states near the interfacial zone. This implies that even though the angular soil shows a similar trend to the Ottawa 20/30, it produces more dilation because of the angularity of soil particles.

In conclusion, it is observed that, for the smooth geomembrane, increased angularity of sand particles induces larger plowing effects so that a higher void ratio is observed at peak stress in the interfacial zone. However, the angularity of the soil particles does not produce a significant

effect on the moderately/heavily textured geomembrane, other than inducing more dilation throughout the shear test.

CONCLUSIONS

This paper has quantitatively illustrated the influence of geomembrane roughness and sand particle angularity on sand/geomembrane interface shear mechanisms. By studying the evolution of the structure of sand adjacent to the geomembranes, it is shown how the shear mechanism is changed by the geomembrane surface roughness. The following conclusions are based on the data and interpretation presented in this paper:

1. For a smooth geomembrane (R_S = 1.09), shearing affects only two particles diameters from the interface, and the shear stress is developed by sliding and slight plowing of sand particles.
2. For a slightly textured geomembrane (R_S = 1.25), the effect of interlocking and dilation of sand particles is observed, where the shearing affects up to four particles diameters from the interface.
3. For a moderately/heavily textured geomembrane (R_S = 1.71), the interlocking and dilation of sand particles are fully developed resulting in a larger void ratio at the interfacial zone. The shearing affects up to six particles diameters from the interface.
4. Increased angularity of sand particles induces higher plowing effects on the smooth geomembrane resulting in higher residual strengths than rounded to subrounded Ottawa 20/30 sand.
5. Soil particle angularity does not produce a significant effect on interfaces mechanisms for moderately/heavily textured geomembrane, with the exception that more dilation is induced throughout the shear test.
6. The surfacial scarring on smooth geomembranes during shearing by the soil particles is found to be directly related to both the normal stress and the angularity of the soil particles at the interface.

The results of this study provide important quantitative evidence of how changes in the property (surface roughness) of one material at an interface influences microstructural changes in the other material at the interface and hence the observed global response. This new insight provides the basis for a more rational selection, for a given sand, of an optimal geomembrane. It is expected that similar insight can be obtained from comparable tests on other combinations of interface materials. For design purposes, tests should be performed using apparatus which satisfies the guidelines outlined in ASTM D5321.

ACKNOWLEDGMENTS

This research is being supported by NSF Grant Number CMS 9700186. This support is gratefully acknowledged. The assistance of J. E. Dove in making the profilometer measurements is appreciated.

REFERENCES

Dove, J. E. (1996) "Particle-geomembrane interface strength behavior as influenced by surface topography", Ph.D. Thesis, School of Civil and Environmental Engineering, Georgia Institute of Technology, 323 p.

Dove, J.E., and Frost, J.D. (1996) "A method for estimating geomembrane surface roughness", Geosynthetics International, Vol. 3, No. 3, pp. 369-392.

Dove, J. E., Frost, J. D., Han, J., and Bachus, R. C. (1997) "The influence of geomembrane surface roughness on interface strength", Proceedings of Geosynthetics '97, Vol. 2, pp.863-876.

Jang, D. J., (1997), "Quantification of sand structure and its evolution during shearing using image analysis", Ph.D. Dissertation, School of Civil and Environmental Engineering, Georgia Institute of Technology, 259 p.

Jang, D. J., Frost, J. D., and Park, J. Y. (1998) "Preparation of epoxy impregnated sand coupons for image analysis", Accepted for publication in ASTM Geotechnical Testing Journal.

Kishida, H., and Uesugi, M. (1987) "Tests of the interface between sand and steel in the simple shear apparatus", Geotechnique, Vol. 37, No. 1, pp.45-52.

Lee, S. W., Frost, J. D., and Righter, G. K. (1998) "The influence of geomembrane surface roughness on geomembrane-geotextile interface strength", Proceedings of Sixth International Conference on Geosynthetics, Vol. 1, pp. 433-438.

O'Rourke, T. D., Druschel, S. J., and Netravali, A. N., (1990) "Shear strength characteristics of sand-polymer interfaces", ASCE Journal of Geotechnical Engineering, Vol. 116, No. 3, pp. 451-469.

Paikowsky, S. G., Player, C. P., and Connors, P. J. (1995) "Dual interface apparatus for testing unrestricted friction of soil along solid surfaces", ASTM Geotechnical Testing Journal, Vol. 18, No. 2, pp. 168-193.

Takasumi, D. L., Green, K. R., and Holtz, R. D., (1991) "Soil-geosynthetics interface strength characteristics: A review of state-of-the-art testing procedures". Proceedings of Geosynthetics '87, Vol. 2, pp. 616- 627.

GEOMETRIC AND SPATIAL PARAMETERS FOR ANALYSIS OF GEOMEMBRANE/SOIL INTERFACE BEHAVIOR

J.E. DOVE
GEORGIA INSTITUTE OF TECHNOLOGY, USA
J.C. HARPRING
GEORGIA INSTITUTE OF TECHNOLOGY, USA

ABSTRACT

The results of a study that employs a new, practical surface characterization and analysis method to predict the behavior of sand/geomembrane interfaces is presented. Average geometric and spatial parameters were obtained from stylus profilometer traces of five different production geomembranes. It is shown that average roughness, average slope, average spacing, and average wavelength parameters can be used to relate geomembrane texture and grain size of dense Ottawa 20/30 to interface performance. The stress-dilatancy response observed in interface shear tests is correlated to average slope parameters. Stylus profilometry has distinct practical advantages over other surface analysis methods as it: (1) rapidly and non-destructively characterizes surfaces, (2) measures actual physical surface features, and (3) offers a standardized surface analysis technique used in other engineering disciplines.

INTRODUCTION

Advances in understanding the behavior of earth and manufactured material interface behavior can be made from use of surface characterization methods. The purpose of characterizing surfaces is to provide "index" parameters that relate physical attributes of the surface to mechanical performance. While mechanical property characterization of geosynthetics and soil has rapidly developed over time, use of quantitative engineering data on manufactured surfaces has been hampered by slow development of surface analysis techniques and roughness parameters that relate the physical processes involved. The goals of this paper are to present results from a research effort to develop geomembrane surface design methods, and demonstrate the relationship of surface texture parameters with physical processes governing soil/geomembrane interface shear.

Major contributions using surface analysis for geotechnical applications came from Yoshimi and Kishida (1982) and Kishida and Uesugi (1987) who studied the friction behavior between sand and relatively smooth steel surfaces. Using stylus profilometer traces, they evaluated Relative Roughness, R_n, which is defined as the maximum peak-to-valley height within a profiling distance equal to the soil particle D_{50}, divided by D_{50}. This normalized

parameter provides a roughness measure that scales with grain size. However, their approach used short profile lengths that are not representative of textured surfaces and required traces at a large number of points. More recently, Dove and Frost, 1996 presented an optical profilometry method that utilized a Surface Roughness Parameter, R_s, derived from stereology. R_s was shown to correlate with peak and residual efficiency of Ottawa 20/30 sand/geomembrane interface combinations (Dove et al. 1997). However, R_s is limited by its inability to provide dimensional and directional surface information and it is relatively time consuming to determine.

Because of the practical limitations of the above methods, a new stylus profilometry technique has been developed. Stylus profilometry is a standard measurement method that has been used in mechanical engineering applications since the early 1940's. By employing devices that enable measurement of the large relief of many textured geomembranes, real geometric dimensions can be obtained for typical applications and suites of materials.

EXPERIMENTAL STUDY

Surface Analysis. A Taylor-Hobson Form Taylsurf Series S3F stylus profilometer was used to perform the surface characterization. Surface profiles are produced with a 2 μm diameter diamond stylus attached to a 30 mm long arm which gives a total working height range of 2.0 mm (80 mil). The arm is connected to a pickup device which has a vertical resolution of about 0.03 μm. A motor drive unit pulls the pickup and stylus over the surface in a precise horizontal plane at a rate of 1 mm per minute. The drive unit has a maximum profiling length of 50 mm. Figure 1 is a photograph of the device situated on a vibration isolation table. All profiling functions, data acquisition and analysis are through a computer system.

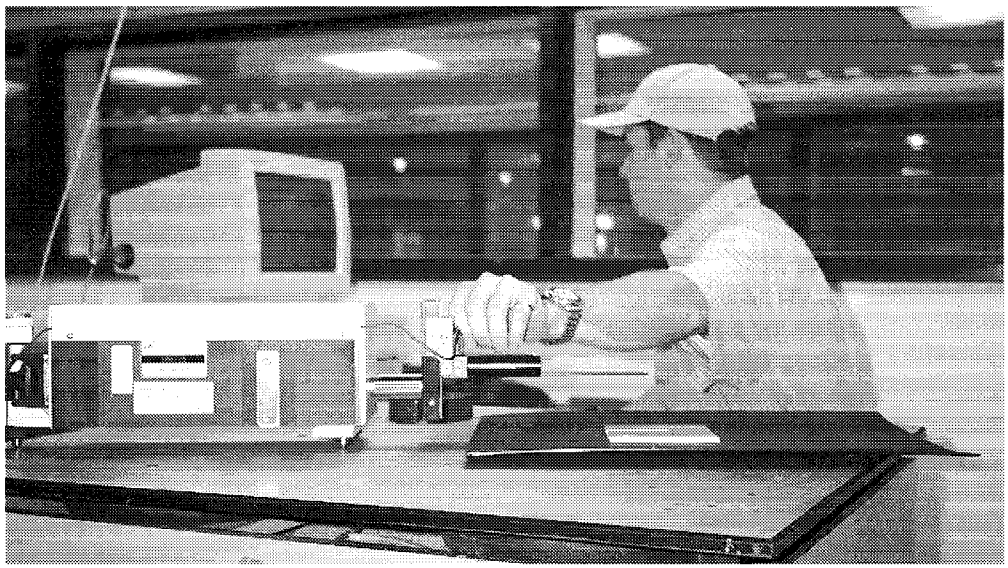

Figure 1. Stylus Profilometer System

There are two independent properties of surface asperities: wavelength (or spacing) and height. More than 30 different standardized parameters exist which can be used to quantify these properties (Dove, 1996). To fully characterize a surface and to understand the

mechanisms responsible for observed behavior, it is necessary to determine how these parameters relate to the physical process of interest. This paper presents results using the following parameters: average roughness, R_a; maximum peak-to-valley height, R_t; average slope, Δ_a; RMS slope, Δ_q; average wavelength, λ_q; and, average peak spacing, S. These parameters quantify a particular dimension of the surface and allow analysis of the influence on behavior. Each are briefly discussed below; a full theoretical treatment is beyond the scope of the present paper and will be presented elsewhere.

Parameters. The roughness parameters are obtained from the profilometer computer data acquisition system which analyses each profile using pre-programmed routines. Average roughness, R_a, is the most universally used parameter worldwide (Dagnall, 1986). It is a measure of asperity height and is defined as (Rank Taylor Hobson, Ltd):

$$R_a = \frac{1}{L}\int_0^L |z(x)|dx \tag{1}$$

where: L = profile length (mm) and,
z(x) = profile height at an instantaneous horizontal position (x).

R_a is the average of the absolute value of vertical height on a profile. Figure 2 shows profilometer output of a idealized profile. All information above the centerline is considered positive and below is negative. Conceptually, computation of R_a involves rotating all the negative values to the positive axis and averaging the resulting heights.

The peak-to-valley height, R_t, is the maximum relief of the profile. The maximum and minimum points do not necessarily lie adjacent to one another on the profile. For the ideal surface of Figure 2, the maximum peak-to-valley height is $4R_a$. For other regular surfaces, the average asperity height ranges from $3.14R_a$ to $5.7R_a$. In concept, R_t is analogous to the Asperity Measurement as determined manually using GRI Method GM12 which measures asperity height using a depth gage that extends from a flat base plate resting on the tops of the asperities down to the lowest points near the core of the geomembrane sheet. The asperity height is the average of ten measurements made over the roll width.

Average slope, Δ_a, is the arithmetic mean slope (in degrees from horizontal) of the profile, defined as (Rank Taylor Hobson, Ltd):

$$\Delta_a = \frac{1}{L}\int_0^L \left|\frac{d(y)}{d(x)}\right| dx. \tag{2}$$

The root mean square (RMS) average slope, Δ_q, is the standard deviation value of average slope, Δ_a. Practically, it gives greater weight to the larger angles than Δ_a. Both slope parameters combine height variations, spatial variations, and asperity shape. They are computed for the idealized profile of Figure 2.

Two parameters which relate spatial configuration of the asperities making up the texture pattern were used. The average wavelength, λ_q, is the root mean square of the

wavelength content of the surface. Average spacing, S, is the mean local peak-to-peak spacing between asperities, as shown on the idealized profile of Figure 2. The average mean line spacing, S_m, is the distance between the intersection of the mean line and the profile, as shown by the distance between the solid circles on Figure 2.

General Profiling Background. Roughness and waviness are the two basic waveform components of a surface profile. Waviness is the large wavelength, large amplitude component due to material variations. Roughness consists of small wavelength, small amplitude waves superimposed on the waviness (Dove et al, 1996). The point at which roughness becomes waviness depends on the length scales determined important to a particular application. Filters may be used to eliminate either roughness or waviness from a profile. However, filtering surface data naturally alters the true height and spatial relationship between asperities.

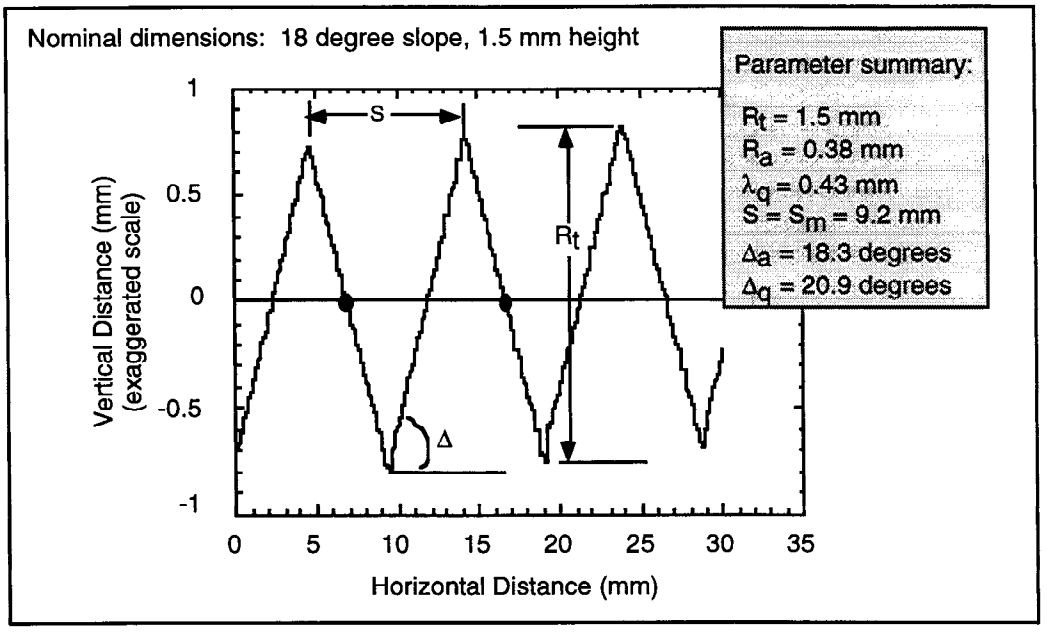

Figure 2. Profile of a Machined Model Surface

This study employs unfiltered profiles because geomembrane texturing has components of roughness and waviness that are important at the length scales of interest. Unfiltered profiles capture actual height and spatial relationships while accepting a minor amount of waviness due to surface form.

Geomembrane Profile Length. An analysis was conducted to determine the optimum number of profiles and profile lengths for the geomembranes used in this study. This analysis consisted of making a series of 5 profiles 10, 20, 30, 40 and 50 mm in length for each geomembrane. A set of the five increasing profile lengths were made at the same profile location with subsequent sets made at five adjacent parallel positions. Cumulative parameter averages at each length and number were computed and plotted in a stability diagram, such as presented in Dove and Frost, 1996.

Materials. The soil material used in this study was Ottawa 20/30 testing sand from U.S. Silica Company of Ottawa, Illinois. The median grain size (D_{50}) is 0.65 mm. Maximum and minimum void ratio were determined by ASTM D4254-91, Methods B and 2A as 0.72 and 0.51, respectively. Ottawa sand was used in this study since a database of existing soil and interface tests on similar geomembranes could be used to aid in understanding the observed behavior.

One smooth (GM-1) and four textured (GM-2 to GM-5) readily available geomembrane surfaces were used. The samples were produced using various proprietary methods. Figure 3 provides profiles of each textured geomembrane surface.

Interface Strength Testing. Interface strength tests were performed using a Geotest, Inc. 300 mm square shear device in accordance with ASTM D5321. The device has two normal load ranges which yield working normal stresses of 20 to 1,500 kPa and has 100 mm of horizontal travel.

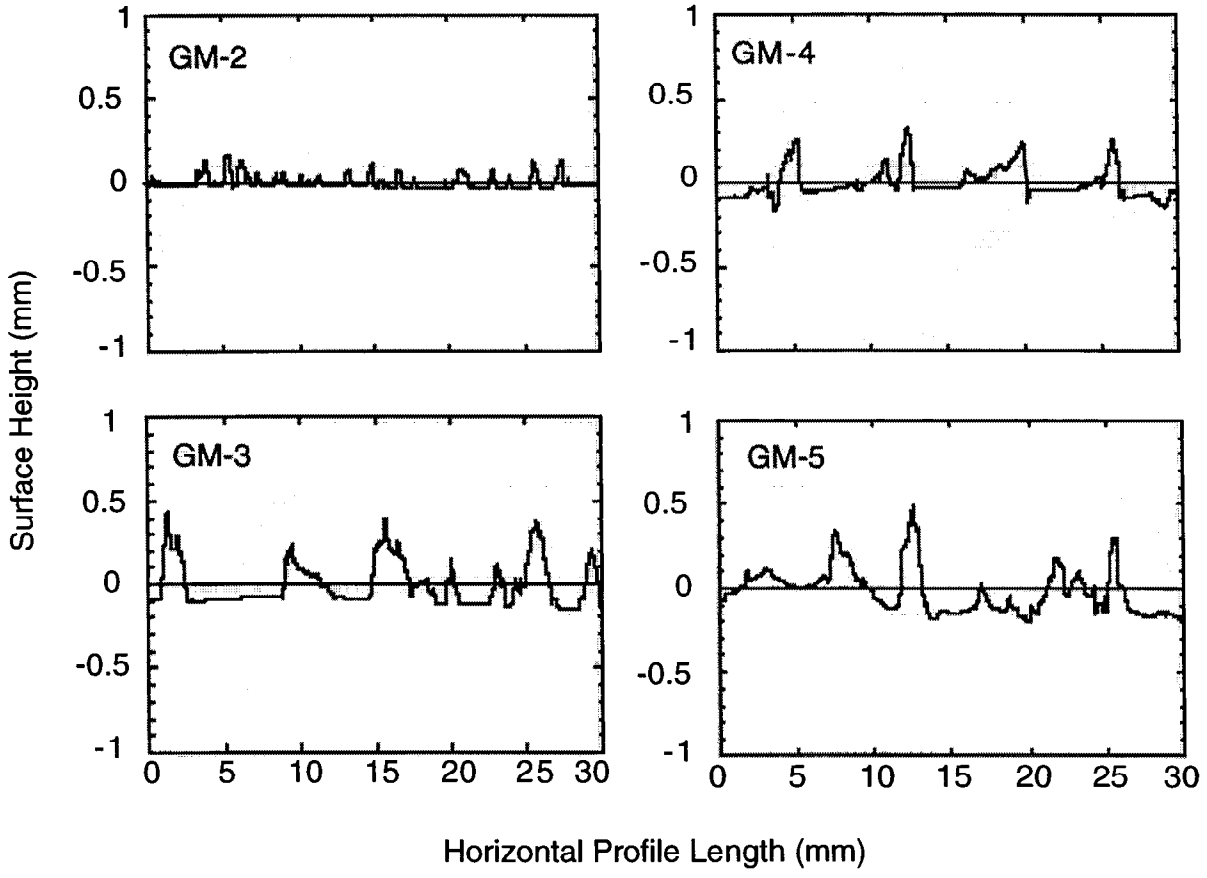

Figure 3. Profiles of Geomembranes used
(Note: vertical scales are exaggerated)

Geomembrane samples were cut from roll stock and prior to mounting in the shear box, each surface was profiled in the midportion of the shear area using the stylus device. The specimens were then clamped onto the lower shear box at the leading edge and along the sides

with the direction of shear in the machine direction. In the interface testing configuration, the bottom shear box is covered with a sintered brass plate to further prevent geomembrane movement. Soil was then placed in three, 25 mm thick lifts and tamped to a pre-determined height to yield a relative density of 80 percent. All tests were performed in a dry condition at 50 kPa, 100 kPa, and 300 kPa normal stress and at a shear rate of 1 mm per minute. Tests were allowed to proceed until a steady-state strength condition was reached. Soil height change during shear was recorded. Two interface shear tests were performed on new samples of each geomembrane at each normal stress. The results presented herein are the average of these two tests.

Soil strength tests were performed in the same shear device on dry specimens at 50 kPa, 100 kPa, and 300 kPa normal stress and 80 percent relative density. The average value of two tests conducted at each normal stress is reported.

RESULTS

Surface Analysis. Table 1 presents a summary of the average geometric and spatial parameter values for each of the five geomembranes. The parameter values for GM-1 (smooth) were determined from the average of 3 profiles, 10 mm in length. Values for all textured samples were from 4 profiles, 40 mm in length. All profiles were taken parallel to the machine direction. These profiling criteria were developed to meet the following objectives: 1) limit the amount of waviness; 2) capture at least one repeat length of the texturing; and, 3) better define the mean value. For smooth geomembranes there is no definable repeat length and a 10 mm long profile adequately represents the surface at the length scales used in this study.

Table 1. Results of Geomembrane Profiling

Geomembrane	Average Parameter Value					
	R_a (mm)	R_t (mm)	λq (mm)	S (mm)	Δ_q (degrees)	Δ_a (degrees)
GM-1 (smooth)	0.002	0.02	0.17	0.03	5.7	4.0
GM-2 (textured)	0.078	0.54	0.83	0.47	37.2	24.4
GM-3 (textured)	0.055	0.38	1.37	0.50	18.2	9.7
GM-4 (textured)	0.155	0.84	1.92	0.62	32.1	18.4
GM-5 (textured)	0.087	0.69	1.70	0.71	23.8	12.1

These values are considered preliminary as they are from a set of 24 profiles on each geomembrane prepared for this study. An exhaustive study of variation within and across rolls of geomembrane was not performed. However, based on experience gained in characterizing these and other materials, the values are not expected to vary significantly.

The average roughness, R_a, for all geomembranes is less than 0.2 mm. As expected for the smooth surface of GM-1, average wavelength, λ_q, is large in comparison to the height parameter, R_a. As texturing increases, the wavelengths become smaller in proportion to height.

The maximum peak-to-valley height, R_t as determined by the profilometer is the distance between the highest peak and deepest valley occurring at any point along four 40 mm long profiles (160 mm total length). R_t for all geomembranes is less than 1.0 mm with the textured

surfaces ranging from $5.4R_a$ to $7.9R_a$ with an average of $6.7R_a$. For comparison, asperity values were determined for GM-3, GM-4 and GM-5 using GRI Method GM12. These values are 0.48 mm, 1.1 mm and 0.72 mm, respectively. As observed from Table 1, R_t is slightly smaller than the GRI asperity height probably from limited dial gage resolution on the asperity height device.

The peak-to-peak spacing, S, provides information necessary to determine critical particle length scales. For the textured materials, S ranges from 0.47 mm to 0.71 mm with an average of 0.57 mm which is in the medium sand range. The smaller the particle size relative to the asperity spacing is believed to cause fully roughened behavior, or full mobilization of soil shear strength (Yoshimi and Kishida 1982; Kishida and Uesugi 1987).

Sand/Geomembrane Interface Strength. Average peak stress ratios (ratio of peak shear stress to applied normal stress) for Ottawa sand are 0.86, 0.79, and 0.71 at 50 kPa, 100 kPa, and 300 kPa respectively. These values were used in computing peak interface efficiency factors presented below. Results of interface strength tests are shown on Figures 4, 5, and 6 where the peak secant interface efficiency is plotted against the six surface parameters. Table 2 provides a summary of the parameter values required to achieve full peak interface efficiency, E, and those values normalized by the D_{50} of Ottawa sand.

The parameters R_a and R_t show that asperity height directly controls interface strength. For the Ottawa 20/30 sand used in this study, peak interface efficiency is achieved for R_a of about 0.10 to 0.15 mm which corresponds to an R_t value of about 0.65 mm. Similar results are observed with R_t where a peak efficiency is attained at a value of about 0.6 mm to 0.8 mm. These dimensions correspond to the D_{50} of Ottawa 20/30 sand of 0.65 mm. Therefore, to achieve full efficiency, the asperity heights must be as large as the median particle diameter.

The spatial parameters λ_q and S quantify the physical relationship between grain size, surface texture and interface strength for production geomembrane materials. Average wavelength for the textured materials ranges from 0.83 mm to 1.92 mm. It may be seen that full interface efficiency is achieved for λ_q between 1.5 mm and 1.8 mm. This suggests that a particle D_{50} of approximately one-half the average wavelength will fully mobilize soil strength for the geomembranes used in this study. An average spacing, S, of approximately 0.6 to 0.7 mm is required to achieve full efficiency. This indicates an average asperity spacing of at least the particle D_{50} is required for full efficiency. However, preliminary results from ongoing research indicates that there may be an upper limit to the spacing to achieve full efficiency, after which the interface strength decreases (i.e., the surface becomes effectively smoother).

Table 2. Relation of Surface Geometry to Sand/Geomembrane Interface Strength

	Average Parameter Value					
	R_a (mm)	R_t (mm)	λq (mm)	S (mm)	Δ_q (degrees)	Δ_a (degrees)
Value for E=1.0	0.1 to 0.15	0.6 to 0.8	1.5 to 1.8	0.6 to 0.7	30 to 35	23 to 25
Parameter/D_{50}	0.1 to 0.2	0.9 to 1.2	2.3 to 2.8	0.9 to 1.1	-	-

The average slope parameters, Δ_a and Δ_q, are the average of all incremental slope angles on the surface. The relationship between the slope parameters and efficiency shown on Figures 4, 5, and 6 indicate that asperity slope plays a key role in controlling interface behavior.

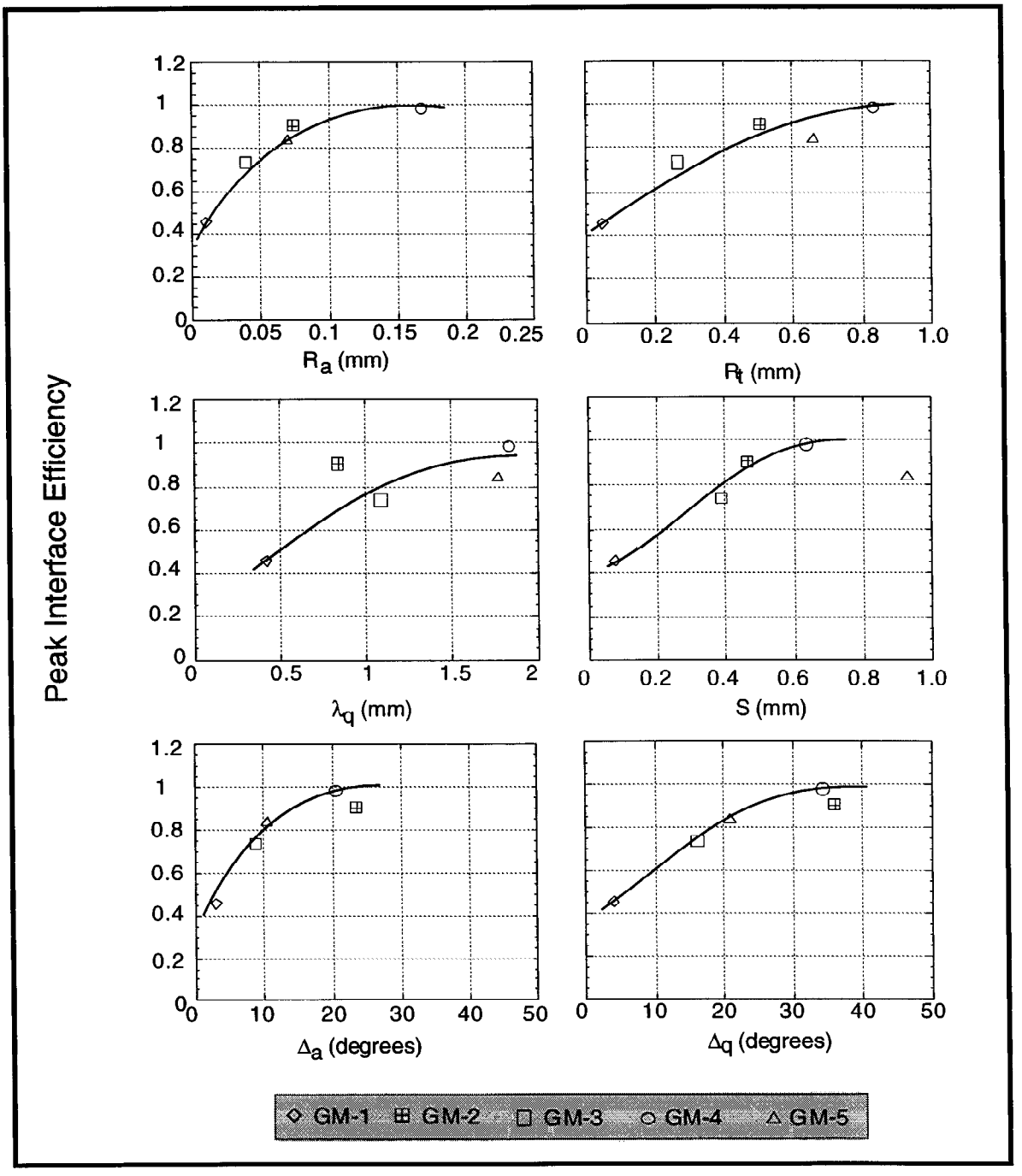

Figure 4. Results of Surface and Strength Analysis, 50 kPa Normal Stress

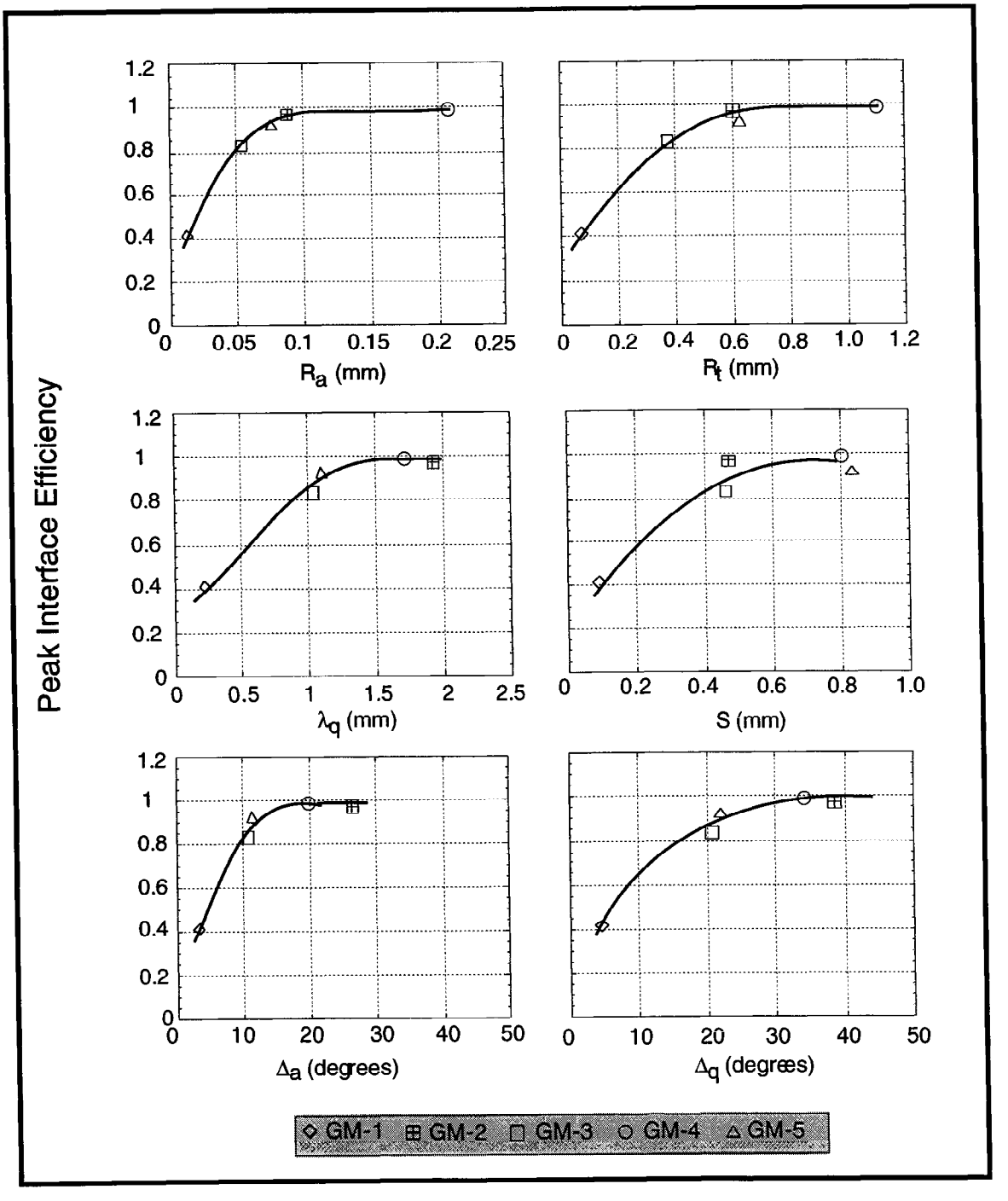

Figure 5. Results of Surface and Strength Analysis, 100 kPa Normal Stress

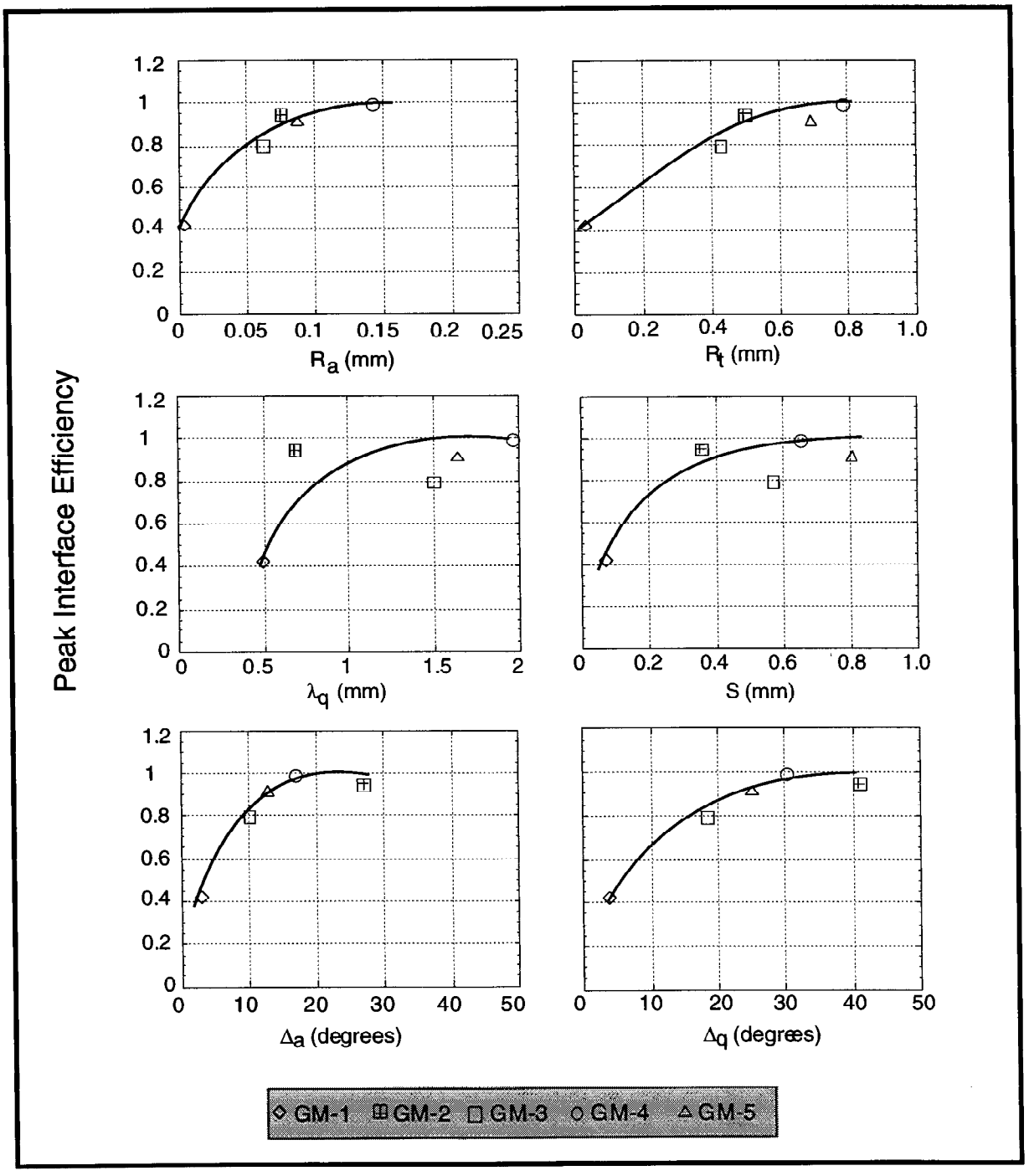

Figure 6. Results of Surface and Strength Analysis, 300 kPa Normal Stress

Peak efficiency is achieved at Δ_a values between about 23 degrees to 26 degrees, and at Δ_q values of between 30 to 35 degrees. GM-2 deviates from the data trend somewhat in that it has fairly large average slopes but has an interface efficiency of between 0.85 to 1.0. This behavior is this geomembrane has a granular surface texture with no apparent directionality whereas the other materials have a patterned texture (not embossed) with directionality in the machine direction. This illustrates the importance of texture pattern.

Physical Relationships. It is instructive to analyze the roughness parameter/strength behavior relationship in terms of fundamental soil mechanics principles. Figure 7 depicts the "sawtooth" model of Coulomb friction. This model depicts soil shear as analogous to the teeth of two sawblades moving relative to each other (Bolton, 1989) or the movement of a block up an plane inclined at an angle β (Rowe, 1962). In the context of the parameters introduced in this paper, β is analogous to the average slope, Δ, shown on Figure 7.

Since the two surfaces are in plane shear, they must move both horizontally and vertically with respect to one another. The instantaneous angle of relative movement between the top and bottom of the shearing mass is the dilatancy angle, φ. The total resistance is the sum of friction between the materials comprising the teeth, ϕ, and the energy required to move the teeth up and over one another against the confinement of the normal stress. If the asperities serve as the lower surface of a fixed slope, the minimum energy state (Rowe, 1969) requires the soil grains to either move along the asperities or move over one another above the interface, assuming no grain crushing.

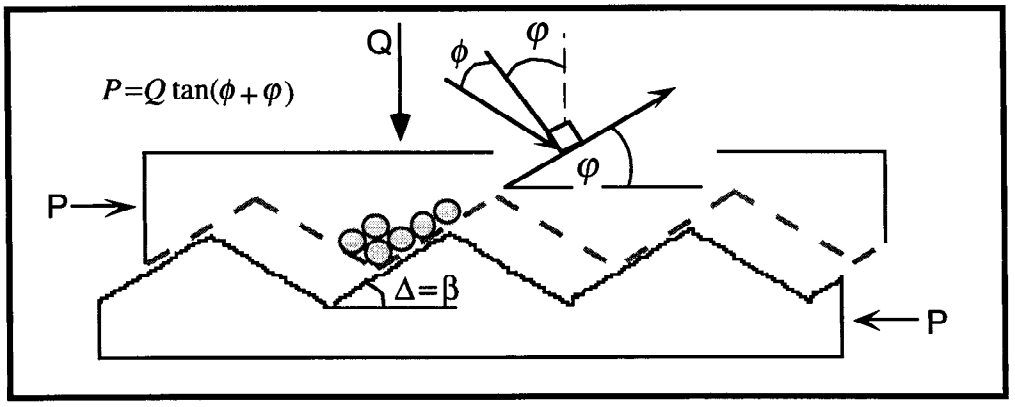

Figure 7. Sawtooth Model of Dilatancy and Friction
(after Rowe, 1962 and Bolton, 1986)

Figure 8 shows the relationship between average asperity slope and dilation angle for tests at 100 kPa normal stress. The dilation angle can be measured in a interface shear test as the slope of the volume (height) change versus horizontal displacement plot at the point corresponding to the peak on the stress-displacement diagram. Peak stress occurs at the maximum rate of dilation. Smooth surfaces do not promote dilation regardless of the soil density. The shear mechanism for Ottawa 20/30 sand/smooth geomembrane was determined by Dove, 1996 to be elastic-plastic sliding below a normal stress 50 kPa and the combination of sliding and plowing above 50 kPa. However, as the slope angle, or roughness, increases, soil

grains must move in relation to the asperities and to one another resulting in increasing dilation and mobilization of soil strength.

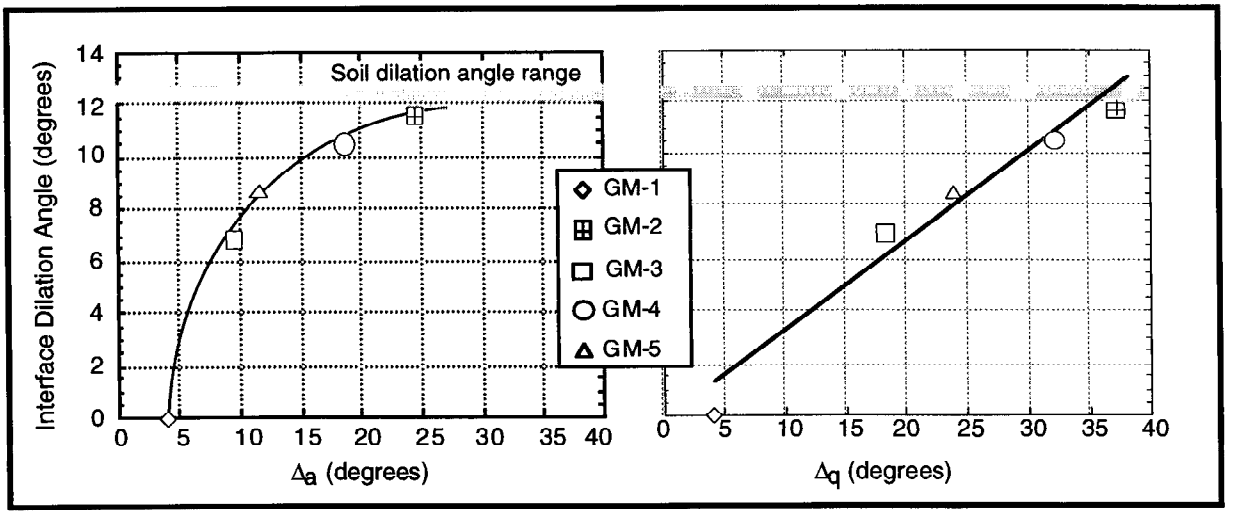

Figure 8. Interface Dilation Angles, 100 kPa Normal Stress

Just as the interface efficiency parameter indicates the percentage of soil strength mobilized, interface dilation increases with increasing average slope up to a limiting value of the soil dilation angle. In reference to Figure 8, critical slopes of 30 to 37 degrees cause full mobilization of soil dilation as predicted by Δ_a and Δ_q. For asperity slopes less than 30 degrees, the soil grains have a component of movement along the surface and the mobilized strength and volume change are less than achieved in soil alone. However, at angles equal to or greater than 30 degrees, the grains expend less energy by shearing within the soil mass resulting in full soil strength mobilization. This further confirms that surface geometry controls system behavior at a fundamental level. The RMS average slope, Δ_q, appears linearly related to dilation possibly because it minimizes the influence of horizontal areas on the surface which do not promote volume change. Figure 8 shows that interface dilation angle for Ottawa 20/30 sand is about $0.3\Delta_q$. Similar relationships are observed for other normal stresses.

The relationship between average slope and dilation of soil indicates traditional steady-state soil mechanics concepts may apply to interface problems. The peak friction angle of soil is related to the dilation angle by the following simple expression:

$$\phi_p = \phi_{ss} + \varphi \tag{3}$$

where: ϕ_p is the peak friction angle,

ϕ_{ss} is the steady-state friction angle, and,

φ is the dilation angle (equal to $0.3\Delta_q$ for 100 kPa example of Figure 8).

Using the surface and interface shear data, the peak interface friction angle was predicted using Equation 3. Figure 9 shows the relationship between the asperity slope and

peak friction for dense Ottawa 20/30 sand/geomembranes at 100 kPa normal stress. There is excellent agreement between predicted and measured peak interface friction angles for these geomembranes.

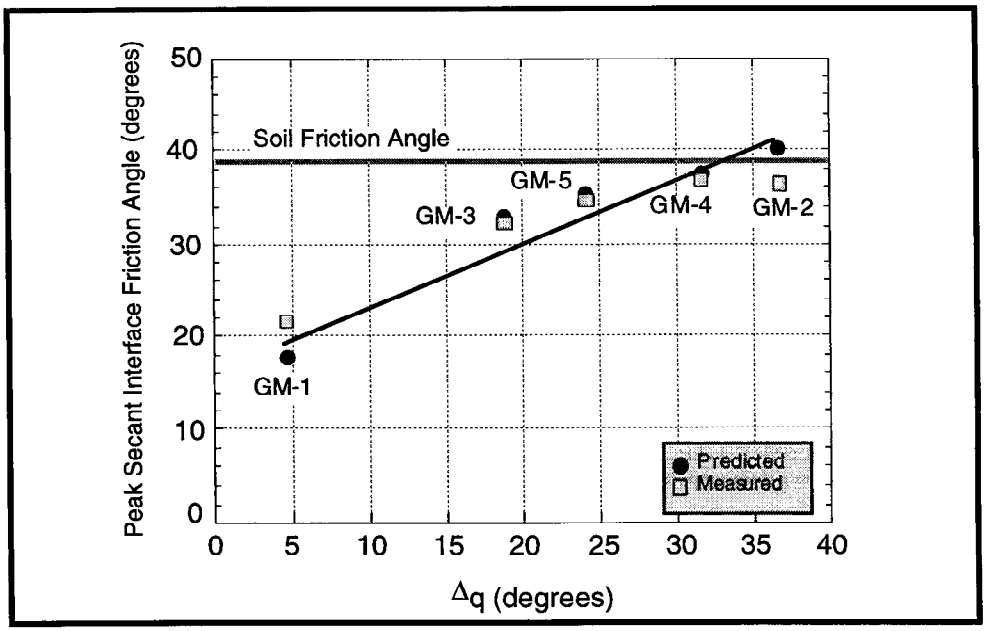

Figure 9. Measured and Predicted Peak Interface Friction Angles, 100 kPa Normal Stress

PRACTICAL APPLICATIONS

The practical applications for surface characterization in geosynthetics engineering are significant. As stated earlier, the profession has used soil characterization for many years. With an ability to quantify surface texture, engineers can extend the same concept to surfaces and interfaces. This could take the form of predicting interface strengths, design of a surface/soil combination for a particular application (see Luellen et al., In Press), or field/manufacturing quality control. A design methodology for soil/geomembrane interfaces is under development and will be presented elsewhere.

There are other important variables not discussed herein that are the subjects on ongoing research. Particle shape and roughness play a key role in interface behavior and are being examined at a fundamental level to incorporate into a design methodology. Research is also underway to better establish relationships between surface geometry, texture patterns and interface behavior.

CONCLUSIONS

This paper has presented a new way to examine the surfaces of geomembranes and to analyze the resulting interface shear behavior. The surface characterization tool used herein, stylus profilometry, has been shown to yield parameters which relate to the physical process of granular material/interface shear. The results show that geometric attributes of height, spatial distribution, and slope control Ottawa 20/30 sand/geomembrane interface behavior. Asperity heights and spacing on the order of the median grain diameter are shown to be required for full

mobilization of interface strength. Asperity geometry controls the ability of soil grains to move at the interface and influence the stress-dilatancy relationships found to determine soil and interface strengths. Because of the relationship to physical processes, this method is believed to be equally applicable to other granular and fine-grained materials, and to the pullout mode.

ACKNOWLEDGMENTS

This material is based on work supported by the National Science Foundation under Grant No. CMS-9800291 and by the Georgia Institute of Technology. This support is gratefully acknowledged. The authors thank GSE Lining Technology, Inc. of Houston, Texas; National Seal Co. of Aurora, Illinois; and Poly-flex, Inc, of Grand Prarie, Texas for providing the geomembrane material used in the study.

REFERENCES

Bolton, M.D., (1986). "The Strength and Dilatancy of Sands", Geotechnique, Vol. 36, No. 1, pp. 65-78.

Dagnall, M.A., (1986). "Exploring Surface Texture", Rank Taylor Hobson Ltd., Leicester, UK, 178 p.

Dove, J.E., (1996). "Particle-Geomembrane Interface Behavior as Influenced by Surface Topography", Ph.D. Dissertation, Georgia Institute of Technology, Atlanta, GA, 323 p.

Dove, J.E., Frost, J.D. and Dove, P.M., (1996). "Geomembrane Microtopography by Atomic Force Microscopy", Geosynthetics International, Vol. 3, No. 2, pp. 227-245.

Dove, J.E. and Frost, J.D., (1996). "A Method for Estimating Geomembrane Surface Roughness", Geosynthetics International, Vol. 3, No. 3, pp. 369-392.

Dove, J.E., Frost, J.D., Han, J., and Bachus, R.C., (1997). "The Influence of Geomembrane Surface Roughness on Interface Strength", Proceedings of Geosynthetics '97, North American Geosynthetics Society, Long Beach, California, pp. 863-876.

Kishida, H. and Uesugi, M. (1987). "Tests of the Interface Between Sand and Steel in the Simple Shear Apparatus", Geotechnique, Vol. 37. No. 1, pp. 45-52.

Luellen, J.R., Dove, J.E. and Swan, R.H. "Development of Two New Engineered Interfaces for a Landfill Containment System", Geotechnical Fabrics Report, IFAI, In press.

Rank Taylor Hobson, Ltd., (1997). "Operator and Technical Guide", 300 pp.

Rowe, P. W. (1962). "The Stress-Dilatancy Relation for Static Equilibrium of an Assembly of Particles in Contact". Proceedings of the Royal Society, A, Vol. 269, pp. 500-527.

Rowe, P. W. (1969). "The Relation Between the Shear Strength of Sands in Triaxial Compression, Plane Strain and Direct Shear". Geotechnique Vol. 19, No. 1, pp. 75-86.

Yoshimi, Y. and Kishida, T. (1982). "A Ring Torsion Apparatus for Evaluating Friction Between Soil and Metal Surfaces." Geotechnical Testing Journal, Vol. 4, No. 4. pp. 145-152.

INNOVATIVE DESIGN AND CONSTRUCTION OF LANDFILL SIDE-SLOPE LINERS IN HIGH SEISMIC RISK AREAS, A CASE STUDY

DAMON BROWN
EBA WASTECHNOLOGIES, SANTA ROSA, CALIFORNIA USA
RICK THIEL
THIEL ENGINEERING, OREGON HOUSE, CALIFORNIA USA
CHRIS BRUMMER
EBA WASTECHNOLOGIES, SANTA ROSA, CALIFORNIA USA
STEVE HUVANE
EBA WASTECHNOLOGIES, SANTA ROSA, CALIFORNIA USA

ABSTRACT

Design and construction of a side-slope composite liner system for the expansion of the Toland Road Landfill in Ventura County, California required the innovative use of enhanced geosynthetic materials to achieve desired slope stability performance objectives. Extensive laboratory testing of numerous geosynthetic materials led to the development of a preferential slip plane above the geomembrane liner using materials which fell within a narrow shear strength envelope determined from the minimum friction angle required for slope stability and the lowest friction angle beneath the geomembrane. Discussions with two major geosynthetic clay liner (GCL) manufacturers and with the selected geomembrane manufacturer led to the development of customized GCL products with increased internal strength and geomembrane products with more aggressive texturing on one side. In order to demonstrate their ability to comply with construction specifications, project bidders were required to perform material performance testing prior to contract execution.

INTRODUCTION

The Toland Road Landfill is located within a high seismic risk area of Southern California in a narrow canyon with steep walls on three sides. Subgrade conditions consist of the moderately indurated Pliocene-Pleistocene age Pico formation, a commonly jointed and fractured marine claystone. Lined side-slopes for the Phase IIA Expansion at the Toland Road Landfill are 1.5H:1V and range in height from 80 to 190 feet (24.4 to 57.9 m) with 25-foot (7.6 m) wide benches every 50 vertical feet (15.2 m). The Phase IIA Expansion is shown in Figure 1. For this project, the State of California required the lined expansion to resist the effects of a Maximum Credible Earthquake (MCE). Therefore, the liner is designed to withstand anticipated peak ground accelerations of up to 0.8g.

The liner system design incorporates a preferential slip plane above the geomembrane in order to provide a high level of confidence that the liner system will maintain its long-term integrity during potential slippage. Meeting this criteria is particularly important at the Toland Road Landfill because the steep side-slopes are prone to relative movement between the waste and the subgrade due to either refuse settlement down-drag forces or seismically induced strong ground motions.

SLOPE STABILITY AND SEISMIC RESPONSE ANALYSIS

The stability and seismic response of the liner system was evaluated for both interim fill conditions and the proposed final landfill configuration. Numerous two-dimensional and pseudo three-dimensional slope stability analyses were performed for the design and further verified using a more sophisticated multi-planar wedge, three-dimensional analysis. The pseudo three-dimensional analysis was performed using the weighted average of several parallel two-dimensional sections. Results of the three-dimensional analysis indicate that three-dimensional effects increase the calculated factor of safety by 13 to 21 percent for the unique geometry analyzed. Based on conventional 3H:1V fill slopes with intermediate benches for the interim fill plan and an acceptable static factor of safety and permanent seismic displacement, a minimum acceptable friction angle of 13 degrees was established for the liner system.

DESIGN GOALS AND CRITERIA

Fundamental design goals for the Toland Road Landfill project include providing a durable and dependable containment liner system for the landfill to meet the intent of state and federal regulations. The following specific issues were addressed to provide a high level of confidence that the liner system will receive acceptable stress levels and maintain its long-term integrity.

Design Goal No. 1 - Provide Protective Cushioning for the Geomembrane

Primary containment for landfill leachate is provided by the geomembrane. The integrity of the geomembrane is affected by the firmness and smoothness of the underlying subgrade. Although the subgrade is very firm due to the nature of the underlying material, it was difficult to provide a smooth surface due to the steepness of bedrock side-slopes. Therefore, it is desirable to provide protective cushioning between the geomembrane and the prepared subgrade. Testing at the Geosynthetics Research Institute (GRI) in the United States (Koerner et al., 1996; Narejo et al., 1996; and Wilson-Fahmy et al., 1996), has shown that GCLs are among the best cushion materials available for geomembranes. In addition, the use of a GCL on the underside of a geomembrane provides additional containment benefits by creating a composite liner system. For these reasons, a GCL was chosen to provide the necessary cushioning.

A design methodology for estimating the degree of cushioning provided by a GCL has been discussed by Koerner et al. (1996), Narejo et al. (1996), and Wilson-Fahmy et al. (1996). The methodology accounts for the normal stress conditions, type of cushioning, angularity of the

subgrade protrusions, isolated stones, arching conditions in the waste, creep, chemical and biological degradation, and a global factor of safety. Taking these factors into account for a GCL cushion, a maximum protrusion size of one inch (25 mm) was specified for subgrade preparation before deployment of the GCL. This is the same value generally recommended by the GCL manufacturers and which was being proposed (during design) in the draft ASTM standard for GCL installation. For ridges and other non-point subgrade irregularities, the value is allowed to be increased to 1.5 inches (38 mm). Construction according to these specifications provides a factor of safety of at least 6 against geomembrane damage. These conclusions resulted in design criteria which were incorporated into the construction specifications.

Design Goal No. 2 - Require Potential Slippage to Occur Above the Geomembrane

The design required careful consideration of the interface strengths between each layer of the liner system. Extensive laboratory testing of numerous geosynthetic materials was conducted to develop a preferential slip plane that has a suitably high post-peak shear strength to achieve slope stability requirements, yet has a lower shear strength than the weakest interface below the geomembrane. There are three potential failure planes below the geomembrane (other than failure in the native soil, which is not anticipated):

1) Interface between GCL and textured geomembrane
2) Internal strength of the GCL
3) Interface between the GCL and the subgrade

Direct shear test parameters and materials were specified by the designers. Geosynthetic testing was performed utilizing a 12-inch by 12-inch (30 cm by 30 cm) shear box in accordance with ASTM Method D5321. Prior to all testing, the GCL was hydrated under zero confining load for 24 hours, followed by consolidation under one-half the specified normal load for an additional 24 hours, with the remainder of the normal load applied just prior to testing. The geonet/geotextile/geomembrane interfaces were sprayed with water immediately prior to testing during unconstrained direct shear tests of the entire liner system. All direct shear tests were conducted at normal stresses of 2,000 psf (96 kPa), 6,000 psf (290 kPa), and 10,000 psf (480 kPa) in order to simulate anticipated normal loads. A shear rate of 0.04 inches/min (1 mm/min) was specified for all direct shear tests.

Based on the authors' experiences with other projects, the peak interface friction angle between a textured HDPE geomembrane and the non-fixated side of a non-woven (NW) needle-punched (NP) GCL is typically greater than 20 degrees for the range of normal loads anticipated at the Toland Road Landfill. For this project, a friction angle greater than 26 degrees for the textured geomembrane/NW side of a NW-NP GCL interface was measured by the geosynthetic supplier.

The friction angle for the peak internal shear strength of NW-NP GCLs is approximately 26 degrees for the range of normal loads anticipated at the Toland Road Landfill (see Design Goal No.

3 below). Laboratory interface testing of the GCL against relatively undisturbed samples of subgrade bedrock material indicated an interface friction angle of 18 degrees (both peak and post-peak) when the side of the GCL which receives the secondary fixation is placed against the subgrade. This orientation also resulted in a more favorable (higher) GCL/geomembrane interface friction angle. Based on these results, the peak and post-peak friction angle of the weakest interface above the geomembrane should be less than 18 degrees.

The selected LCRS system included a geonet composite consisting of a 6-oz/yd^2 (200 g/m^2) NW-NP geotextile heat bonded to the top of an HDPE geonet. A 4-oz/yd^2 (135 g/m^2) geotextile shear sheet was placed between the bottom of the geonet composite and the top (less aggressively textured side) of the geomembrane to provide a preferential slip plane above the geomembrane. Laboratory testing of the interface between the geotextile shear sheet and the geonet portion of the geonet composite conducted for this project indicated a peak interface friction angle of 14 degrees, and post-peak friction angle of 13 degrees. This is the minimum post-peak friction angle allowed under conditions of the slope stability analysis, as previously described. This value is also less than the maximum allowable value of 18 degrees. Several unconstrained direct shear tests of the entire liner system were performed as part of conformance testing. With this method of testing, shear failure is free to occur at the weakest interface within the liner system test cross section. Results of shear testing consistently exhibited failure on the preferred interface between the NW geotextile shear sheet and the geonet composite.

Peak stress within the geomembrane will not occur until mobilization of the shear sheet by refuse settlement down-drag forces or seismically induced strong ground motions. The amount of shear stress imposed upon the geomembrane will be limited to that which can be carried by the weakest interface, or the geotextile shear sheet. In theory, the geomembrane at the top of the slope should remain loose and relatively stress-free, even following significant waste-mass displacement along the geotextile shear sheet (assuming waste has already been placed and post-installation downslope creep caused by diurnal expansion and contraction of the geomembrane is not occurring). This concept may present a useful way of monitoring the stress performance of the design after installation.

Design Goal No. 3 - Provide Adequate Long-Term Creep Shear Strength Within the GCL

The NP fibers of the GCL act as structural members and provide internal shear strength. Hence, there is a design concern regarding the long-term creep potential in case the fibers "untangle" or pull out. Long-term shearing behavior of GCLs has been evaluated by Siebken et al. (1996) and Trauger et al. (1996). Both investigators performed creep tests by hydrating the samples prior to loading, followed by the application of constant shear stress for a period of over 7,000 hours. Friction angles reported from these tests ranged from 19 to 27 degrees.

In order to provide GCL materials representative of those used in the long-term creep tests, peel tests (ASTM D 4632) of the same material tested by the investigators were performed with results

ranging from 37 to 49 lbs (6.5 to 8.6 kN). (Note that peel test results are per 4-inches (100 mm) of specimen width.) The minimum acceptable peel test value used for manufacturing quality control is 15 lbs (2.6 kN). However, actual test results typically vary between 15 and 50 lbs (2.6 to 8.8 kN), depending on the quality of the needling board at any given time.

Based on this information, construction specifications required a GCL product with a minimum average roll value (MARV) peel strength of 35 lbs (6.1 kN). The required peel value of 35 lbs (6.1 kN) allowed a correlation with the friction angles obtained from the long-term creep tests.

Design Criteria and Material Specifications

Design Criteria for the Toland Road Landfill project were developed from results of seismic slope stability analyses and extensive geosynthetic laboratory testing in order to meet established design goals and assist in the selection and specification of customized geosynthetic materials. Pretesting was performed during design to determine materials which would be specified for individual liner components (i.e., double-NW GCL, aggressive geomembrane texturing, and hard HDPE geonet instead of a lower density PE). The selected liner system (Figure 2) is a single composite liner incorporating a high performance GCL and a geotextile shear sheet which acts as a critical transitional interface above the geomembrane. A summary of design criteria is presented in Table 1.

Collaboration with geosynthetic manufacturers resulted in development of superior performing products which met or exceeded design specifications. Discussions with two major GCL manufacturers led to the development of custom GCL products with increased peel strengths in order to meet long-term creep performance objectives. The selected GCL consisted of bentonite at the approximate dry weight of 0.90 lbs/ft^2 (4.4 kg/m^2) carried between two NW geotextiles with nominal weights of 6 oz/yd^2 (200 g/m^2) that were needle-punched together and secondarily fixed on one side.

Discussions with the selected geomembrane manufacturer allowed adjustments to be made during production to obtain a more aggressive texturing on the bottom of the sheet. This resulted in a geomembrane/GCL interface shear strength that exceeded design criteria. The selected geomembrane consisted of double-sided textured 60-mil HDPE.

LINER INSTALLATION

The Phase IIA Expansion was successfully constructed in the summer of 1997. Excavation, supply of geosynthetic materials, and liner installation were bid separately by the owner. Separating the supply and installation bids allowed for the selection of a single supplier for all geosynthetic materials, simplifying rigorous testing and consolidating responsibility for material compatibility. In addition, this allowed time for the owner and engineer to perform conformance testing prior to shipment of geosynthetic materials to the site.

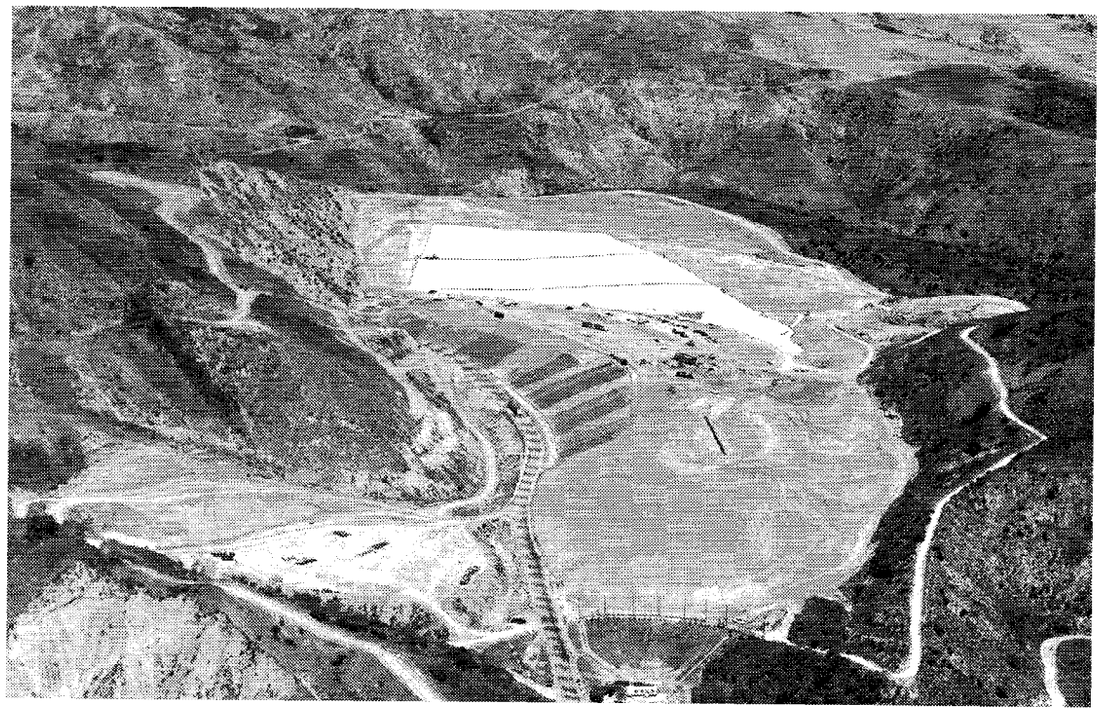

Figure 1. Oblique aerial view of the Phase IIA Expansion, Toland Road Landfill.

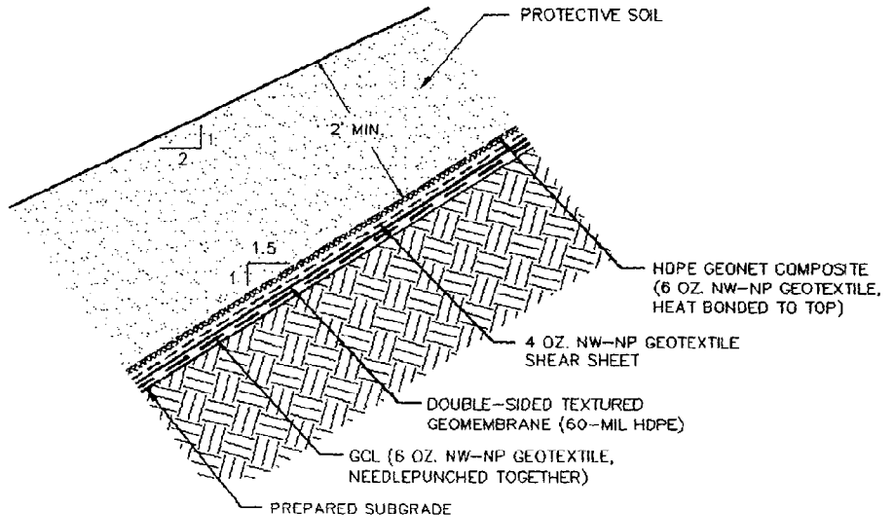

Figure 2. Typical section illustrating components of the liner system.

Table 1. Design Criteria

Interface	Peak Shear Strength Requirements	Shear Strength Requirements after a minimum of 3 inches of displacement
GCL - internal	25 degrees min. (provides a correlation with long-term creep tests)	N/A
GCL /subgrade interface	18 degrees min.; Subgrade protrusions < 1 in., irregularities < 1.5 in.	18 degrees min. (post-peak value required since some sliding of this interface may occur during construction)
GCL/textured geomembrane interface	24 degrees min. (exceeds actual requirement of 18 degrees to allow for installation damage and product variability)	N/A (post-peak value not required since design is based on peak strength being maintained, while accounting for some potential installation damage)
geotextile shear sheet/textured geomembrane interface	22 degrees min. (exceeds actual requirement of 18 degrees to allow for installation damage and product variability)	N/A (post-peak value not required since design is based on peak strength being maintained, while accounting for some potential installation damage)
geotextile shear sheet/geonet composite interface	16 degrees max., 13 degrees min. (max. value set to meet Design Goal No. 2; min. value set to meet slope stability requirements)	16 degrees max., 13 degrees min. (post-peak values required since this is the interface that will slip during waste settlement or seismic events)

Because it was critical for each element of the liner system to perform as designed, the selected supplier was required to demonstrate that the various interface shear strength specifications could be met by submitting interface shear test results of representative materials prior to contract execution. Bidding the supply portion of the contract separately allowed the owner and engineer to coordinate directly with the geosynthetic supplier and eliminated the possibility of the general contractor or installer from bidding material which did not meet the performance requirements.

The highly jointed and fractured nature of native materials made it difficult for the contractor to provide subgrade conditions which met the construction specifications. Final slope preparation involved manual raking by laborers and smoothing using a backhoe and bar attachment. On portions of the slope, landslide and unconsolidated material required excavation and replacement with compacted fill keyed into the subgrade.

During installation of the GCL, the subgrade surface was continuously inspected to verify the removal of materials that could damage or adversely affect the integrity of the liner system. GCL panels were deployed from the top of slopes and unrolled down the entire length of the slope, across intermediate benches, beneath the LCRS header along the toe, and anchored at the limit of the adjacent unlined portion of the landfill.

Geomembrane panels were deployed in a continuous sheet from the uppermost bench to the bottom of the slope with the more aggressively textured side facing down, utilizing a thin HDPE slip sheet to avoid snagging and weakening the NW fibers of the GCL. Once a geomembrane panel was positioned, the slip sheet was removed. Only as much GCL that could be covered in the same day by the geomembrane was deployed. The need for cross-slope seams and anchor trenches on intermediate benches was eliminated by specifying 520 foot (158 m) long roll lengths. Initially, this resulted in bridging of geomembrane panels along the back of benches which was remedied by increasing the number of sandbags placed on the geomembrane immediately following liner placement, most notably in the afternoon during peak thermal elongation. Areas which had already bridged were cut out and replaced with an extrusion-welded cap strip. Geomembrane installation is shown in Figure 3.

As in the case of the geomembrane, the geotextile shear sheet was installed utilizing a slip sheet to allow positioning of panels and to prevent dragging of the shear sheet over the geomembrane which could damage the NW fibers (Figure 4). The preferential slip plane was completed with installation of the geonet composite, with the HDPE drainage net side facing down against the geotextile shear sheet. As with the deployment of other liner system components, the geonet composite was unrolled from the uppermost bench, but did not utilize a slip sheet and was slid down the slope directly over the geotextile shear sheet.

Remaining components of the LCRS, including leachate collection pipe, granular leachate collection layer, and geotextile filter, were subsequently installed along the back of benches and at the toe of the slope following construction quality assurance (CQA) approval of the underlying composite liner. A 10-foot (3 m) high temporary operational and leachate containment berm was constructed at the toe of the expansion between lined slopes and existing unlined waste fill areas. A prefabricated HDPE boot provided temporary penetration for the LCRS header until construction of the adjacent expansion phase.

A temporary plastic cover manufactured from laminated scrim-reinforced polyethylene sheeting and anchored with roped sandbags placed on 10-foot centers was installed over portions of the liner which would not immediately receive waste. The purpose of the temporary plastic cover was to protect the geonet composite from ultraviolet degradation and prevent stormwater runoff from entering the LCRS. The cover is peeled back as operations proceed and anchored within the operations layer to create a lined interim V-ditch.

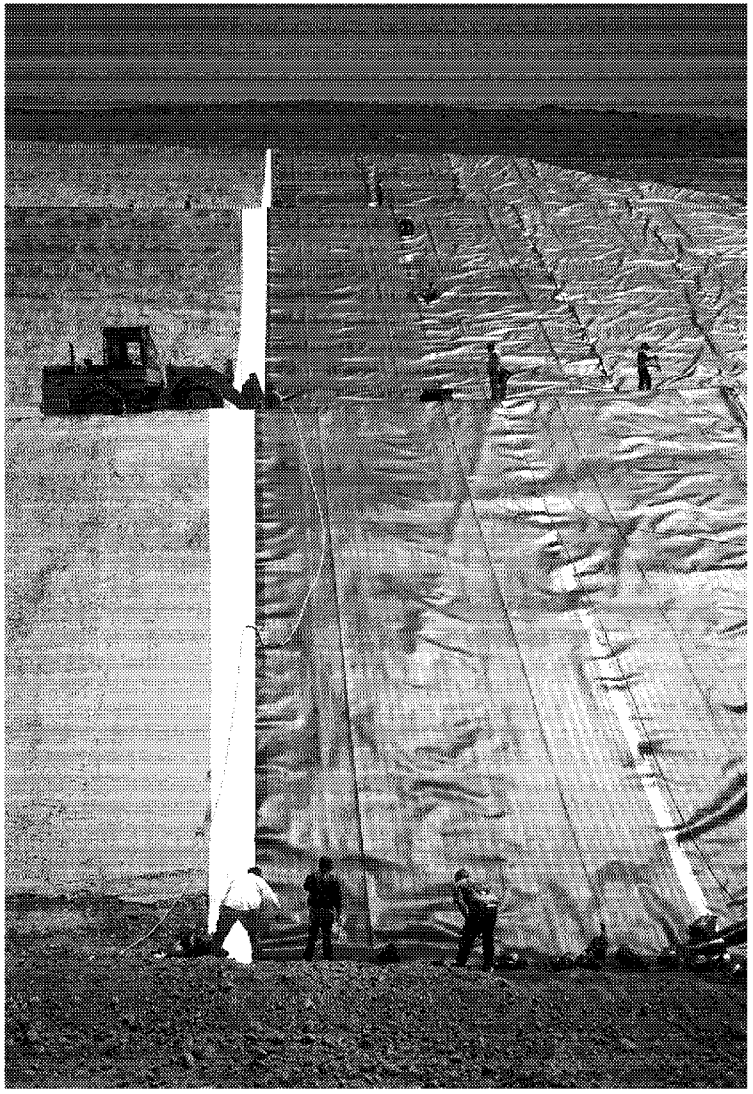

Figure 3 (left). Geomembrane installation over GCL showing 1.5H:1V slopes and intermediate benches.

Figure 4 (below). Geotextile shear sheet installation over geomembrane on 1.5H:1V slope. Photo taken from intermediate bench at the top of slope.

CONCLUSIONS

This case study has presented the innovative specification and use of customized geosynthetic materials to meet slope stability requirements and achieve design goals for a composite liner system installed on steep side-slopes in a high seismic risk area. Working closely with geosynthetic manufacturers, customized products with enhanced properties can be produced to suit the needs of the designer for projects which require superior performing products. The authors recommend visiting the geosynthetic manufacturing plant during production to perform quality assurance inspection, collect conformance test samples, and personally observe production of actual materials to be used in construction.

A preferential slip plane may be incorporated into a composite liner system in order to restrict sliding to a specific interface located above the geomembrane. Extensive laboratory interface testing during the design phase of numerous geosynthetic materials under various conditions is necessary to identify the appropriate combination of materials which will satisfy both slope stability and containment goals. In this case study, a slip plane design utilizing a NW geotextile shear sheet is based on a narrow shear strength envelope determined by the minimum friction angle required for slope stability and the lowest interface friction angle beneath the geomembrane. The weight of the shear sheet was not specified, allowing the supplier a degree of flexibility in meeting the performance specifications.

The stability of the design needs to be evaluated to determine not only how the proposed liner system will perform during interim fill conditions, but how it will integrate with future expansions and impact the long-term performance of the proposed final configuration. In this case study, a pseudo three-dimensional analysis was performed using the weighted average of several parallel two-dimensional sections and further verified using a more rigorous three-dimensional analysis. Results of the three-dimensional analysis indicate that the more simplified pseudo three-dimensional analysis is conservative and has merit in the analysis of landfill liner systems.

Because a composite liner has to act as a single system, careful consideration must be given to development of construction specifications. The authors believe that requiring suppliers of geosynthetic materials to provide performance testing as a condition of contract should be considered. In addition, the contractor needs to demonstrate an ability to comply with specification requirements and can be required to conduct performance testing.

Bidding the supply of geosynthetic materials separate from the installation offered numerous advantages. For this case study, the selected supplier was able to supply all geosynthetic materials, allowing the owner and engineer to coordinate directly with the manufacturer and eliminating the possibility of general contractors incorrectly evaluating results of specialized and complicated testing which may have resulted in the disqualification of several otherwise responsive bidders.

ACKNOWLEDGMENTS

The authors wish to thank Rob Swan of GeoSyntec Consultants for providing geosynthetic testing, Jonathan Bray and Timothy Stark for separate reviews of the seismic stability, CETCO and National Seal Company for providing GCL materials used in preliminary testing, Greg Sharrun of Columbia Geosystems Ltd. for providing geomembrane materials used in testing, and the cooperation of John Conaway and the Ventura Regional Sanitation District for allowing the use of their case history in this paper.

REFERENCES

Koerner, R.M., Wilson-Fahmy, R.F., and Narejo, D., and 1996, Puncture Protection of Geomembranes Part III: Examples, Geosynthetics International, Vol. 3, No. 5, 1996, pp. 655-675.

Narejo, D., and Koerner, R.M., and Wilson-Fahmy, R.F., 1996, Puncture Protection of Geomembranes Part I: Theory, Geosynthetics International, Vol. 3, No. 5, 1996, pp. 605-628.

Siebken, J.R., Swan, R.H., and Yuan, Z., 1996, Short-Term and Creep Shear Characteristics of a Needlepunched Thermally Locked Geosynthetic Clay Liner, in Testing and Acceptance Criteria for Geosynthetic Clay Liners, ASTM STP 1308, Larry Well (ed.), American Society for Testing and Materials, Philadelphia.

Trauger, R.J., Swan, Jr., R.H., and Yuan, Z., 1996, Long-Term Shear Strength Behavior of a Needlepunched Geosynthetic Clay Liner, in Testing and Acceptance Criteria for Geosynthetic Clay Liners, ASTM STP 1308, Larry W. Well, (ed.), American Society for Testing and Materials, Philadelphia.

Wilson-Fahmy, R.F., Narejo, D., and Koerner, R.M., 1996, Puncture Protection of Geomembranes Part II: Experimental, Geosynthetics International, Vol. 3, No. 5, 1996, pp. 629-653.

LEAK TESTING OF GEOMEMBRANES AS A QUALITY ASSURANCE TOOL

STEPHEN G. LEHRKE
FOTH & VAN DYKE, USA
NANDAKUMARAN PARUVAKAT
FOTH & VAN DYKE, USA
GERALD W. SEVICK
FOTH & VAN DYKE, USA
KENNETH P. BLACK
NICOLET MINERALS COMPANY, USA

ABSTRACT

Current design practices for geomembranes in composite liners assume that a certain number of pinholes and installation defects will exist even with the employment of the best of Quality Assurance/Quality Control (QA/QC) practices. The performance of the geomembrane is assessed accounting for the defects. Therefore, if it can be ascertained that post construction defects do not exceed those used in the design, the construction is verified to be meeting the intent of the design. This paper envisages the use of leak location surveys as a tool to assess whether the post construction defects exceed the design assumptions. The paper also proposes the use of sequential test statistics and sequential probability ratio test to reduce the extent of leak detection survey required before a pass-fail determination can be made with a high degree of confidence. An example of the proposed statistical approach is also included.

INTRODUCTION

The Crandon Project, proposed by Nicolet Minerals Company (NMC) to mine and process zinc and copper ore in Crandon, Wisconsin, will utilize lined containment facilities for disposal of mine tailings in an upland area. Composite liners and caps consisting of a geomembrane overlying low-permeability layers of a geosynthetic clay liner and processed glacial till are being proposed for the Tailings Management Areas (TMA).

A composite barrier is better than the components of the barrier used singly because the components complement each other, thereby decreasing the effects of individual weaknesses. During the past decade or so, design methods have been developed to predict percolation through composite liners (Giroud and Bonaparte, 1989; Giroud, 1997). These methods essentially consist of empirical relationships developed based on laboratory test results and take into account the materials, the defects in the geomembrane (both number of defects and their sizes), the hydraulic properties of the materials, hydraulic head on the barrier, and descriptions of installation quality. Thus, in order to use the currently available methods to estimate percolation through composite liners, one has to use the empirical correlations between the level of Quality Assurance/Quality Control (QA/QC) effort during the installation of the geomembrane and the potential for the number

of geomembrane defects and their sizes. Since it is desirable to have the least amount of percolation through the composite liner, the number and size of defects need to be minimized. Consequently, the level of QA/QC efforts has to be raised. Quality Assurance procedures need to be employed both for manufacturing and installation of the geomembranes. The best geomembrane Construction Quality Assurance (CQA) practice is believed to consist of the following, based on the requirements listed by Daniel and Koerner (1993):

- A licensed QA engineer to have overall responsibility for CQA.
- Certified CQA personnel to make construction observations and perform field tests to verify conformance with permitted design drawings and specifications.
- Independent geosynthetic testing laboratories to conduct tests on the materials and seams.
- A written CQA plan to be prepared.
- CQA personnel to have specified qualifications.
- Pre-construction, progress and conflict resolution meetings to be conducted between involved personnel.
- Appropriateness of geomembrane received at the project site to be observed and verified.
- Conformance tests (sampling, testing and verification) to be completed.
- The acceptability of prepared subgrade to be observed and verified.
- Geomembrane deployment meeting accepted practices, including geomembrane quality to be observed.
- Panel seaming, meeting accepted practices, including acceptability of crew and machine based on trial seam welding and tests, proper overlaps, proper seam preparation with clean, dry surfaces to be observed.
- Conduct of non-destructive tests on seams to be observed.
- Conduct of destructive test sampling to be observed and acceptability of seams based on laboratory test results to be informed to the installation crew.
- Repair of defects to be observed.
- Soil cover placement to be observed.
- Complete documentation, including record drawings, meeting minutes, daily reports, deviations from design, laboratory and field test results to be prepared.

By conducting such a detailed CQA program, the owner can derive a much larger confidence in the quality of geomembrane installation in terms of reduced defects and thus reduced percolation through the barrier. Interpretation of the performance of geomembrane liners and actual monitoring of installed facilities have resulted in quantification of the CQA effort in terms of the number of post-installation defects. Fewer number of defects will result from better CQA efforts.

While preparing a Feasibility Report on the TMA for the regulatory agencies to complete an "Environmental Impact Statement" on the project, NMC initiated a study to evaluate the state-of-the-art CQA procedures for geomembrane installation. This paper is a result of that study.

ELECTRIC LEAK LOCATION SURVEYS

Laine and Darilek (1993) have described the use of electrical leak location method for determining existence of geomembrane defects when it is covered with a protective soil. They concluded that this method is successful in a wide variety of applications. Since successful leak location is possible after cover soil placement (i.e., after practically all construction activities are completed), this opens up an excellent possibility of replacing all or most of the steps of CQA described earlier.

USE OF LEAK TESTING FOR CQA

Testing the integrity of a geomembrane liner by the leak location survey is a time-consuming process. Current methods involve testing the entire area of the liner by taking measurements at discrete points. Since a liner will generally cover a very large area, the amount of "sampling" necessary to cover the entire liner is extensive. However, a decision concerning the integrity of the liner may still be made from a reduced number of samples given that an appropriate statistical plan is utilized.

Sequential Test Statistics

For a geomembrane liner, CQA can be completed by dividing the liner into a large number of segments and randomly testing only a certain number of segments selected using a statistical sampling plan. A liner segment area, for example, may be one-fifth hectare (one-half acre) in size. After testing is complete, the average number of leaks found per segment area is compared to design specifications for the entire liner. A statistical test is used to determine whether the average number of leaks found is within design specifications given the variability which was observed between the tested segments.

There are two types of error associated with a statistical test. A Type I error, commonly denoted by "α", occurs when a true hypothesis is rejected as being false and a Type II error, commonly denoted by "β", occurs when a false hypothesis is accepted as being true. For example, a null hypothesis (H_0) could be that the average number of leaks in an installed liner meets design specifications. If after testing the liner this hypothesis is falsely rejected, a Type I error has occurred. On the other hand, if after testing the liner this hypothesis is falsely accepted, a Type II error has occurred. In this situation, committing a Type I error implies that extra resources would be spent unnecessarily repairing the liner, while committing a Type II error implies that a faulty liner would be left in place.

With a statistical sampling plan it is possible to sample less than the entire liner for leaks and still come to a conclusion regarding liner integrity. However, to maintain confidence in the installation QA/QC process, the α and β must be held to very low levels. In order to decrease both α and β simultaneously, the sample size must be increased. This is intuitive since by increasing the number of collected samples, the amount of known information is increased and the amount of unknown information is decreased, thereby allowing a decision to be made with more confidence.

It is possible to prespecify the maximum allowable error rates for α and β. These criteria can then be used to calculate the required sample size. The sample size necessary to meet the specified α and β will be large if it is of interest to detect slight differences between the hypothesized mean (design specifications) and the true mean (actual liner quality). The required sample size will decrease if it is of interest to detect only larger differences between the hypothesized mean and the true mean. Thus, if the possibility of actual liner quality being either well below or well above design specifications exists, we can conceivably reduce the number of required samples and thus, the CQA effort. However if actual liner quality is very close to design specifications, a larger number of samples would be required.

Sequential sampling is a sampling scheme in which samples are taken one at a time and subsequently evaluated to determine whether enough information is available to make a decision, or whether more sampling is required. The sequential probability ratio test (SPRT) is a statistical test based on this type of sampling. The SPRT was developed by a Statistical Research Group set up at Columbia University in New York in 1942 for the United States Defense Department (Ghosh and Sen, 1991). Procedures of sequential sampling and the SPRT are discussed in Hoel, Port and Stone (1971) and Wetherill and Glazebrook (1986). A comparison of three sequential statistical testing procedures on material loss detection from a nuclear facility is given in Markin and Shipley (1982).

This type of sampling applied to geomembrane liner CQA procedures has several distinct advantages. First, it is possible to determine with a high degree of confidence whether the liner meets or fails to meet design specifications without testing the entire liner. Second, if the true liner integrity is well below or well above design specifications, it will be quickly determined and save extraneous testing costs. Finally, the sampling plan and decision process is relatively easy to implement in the field.

APPLICATION

For geomembrane installation projects, less than ten defects per hectare, (four defects per acre or two defects per half-acre) will be considered acceptable since this is the normal practice for quantifying a liner with good CQA practices during installation. Five defects per hectare (one defect per half-acre) can be considered superior installation.

An SPRT was designed to test the hypotheses of the true mean number of defects to be 1, 1.5 or 2 per half-acre. This would indicate whether liner quality is superior, acceptable, or unacceptable. The formulation of an SPRT under three simple hypotheses is discussed in Wetherill and Glazebrook (1986). In this situation, the three simple hypotheses may be stated as follows:

$$H_{-1}: \theta = 1$$
$$H_0: \theta = 1.5$$
$$H_1: \theta = 2$$

Decision boundaries representing the three hypotheses above were derived as follows:

DERIVATION OF DECISION BOUNDARIES

The sequential probability ratio test is based on the likelihood ratio

$$\frac{L_{1n}}{L_{0n}} = \frac{\prod_{i=1}^{n} f(x_i|\theta_1)}{\prod_{i=1}^{n} f(x_i|\theta_0)}.$$

where L_{1n} and L_{0n} are the likelihood functions of the variable x under the hypothesis of θ_1 and θ_0, respectively.

Hoel, Port and Stone (1971) discuss the construction of the likelihood ratio, and give an example of the SPRT using the standard normal distribution. The number of defects in a geomembrane liner is a discrete random variable, and the occurrence of such defects is expected to be infrequent. Therefore the number of defects per tested liner segment is expected to follow a Poisson distribution. Hoel, Port and Stone (1971, pg. 62) give the likelihood ratio of the Poisson distribution as

$$\frac{L_1}{L_0} = \frac{\prod_{i=1}^{n} e^{-\mu_1} \frac{\mu_1^{x_i}}{x_i!}}{\prod_{i=1}^{n} e^{-\mu_0} \frac{\mu_0^{x_i}}{x_i!}}$$

where x_i is the number of liner defects in segment I, μ_0 is the mean number of defects under the null hypothesis, and μ_1 is the mean number of defects under the alternative hypothesis. The likelihood ratio can be reduced as follows:

$$= \left[\frac{e^{-n\mu_1} \mu_1^{\sum_{i=1}^{n} x_i}}{\prod_{i=1}^{n} x_i!} \right] \cdot \left[\frac{\prod_{i=1}^{n} x_i!}{e^{-n\mu_0} \mu_0^{\sum_{i=1}^{n} x_i}} \right]$$

$$= \frac{e^{-n\mu_1}\mu_1^{\sum_{i=1}^{n} x_i}}{e^{-n\mu_0}\mu_0^{\sum_{i=1}^{n} x_i}}$$

$$= e^{n(\mu_0-\mu_1)}\left(\frac{\mu_1}{\mu_0}\right)^{\sum_{i=1}^{n} x_i}$$

As given in Hoel, Port and Stone (1971, pg. 75), to test the hypothesis $H_0:\gamma=\gamma_0$ against $H_1:\gamma=\gamma_1$, calculate the likelihood ratio L_{1n}/L_{0n} and proceed as follows:

I) if $L_{1n}/L_{0n} \leq \beta/(1-\alpha)$, accept H_0;

ii) if $L_{1n}/L_{0n} \geq (1-\beta)/\alpha$, accept H_1;

iii) if $\beta/(1-\alpha) < L_{1n}/L_{0n} < (1-\beta)/\alpha$, take an additional sample.

For defects in the liner we are testing three simple hypotheses which may be stated as follows:

$$H_{-1}:\mu_{-1}=1$$
$$H_0:\mu_0=1.5$$
$$H_1:\mu_1=2$$

One test is needed to test H_0 against H_{-1}. A second test is needed to test H_0 against H_1. If for the first test the following probabilities hold:

$$\Pr\{\text{accept } H_{-1} | H_0 \text{ true}\}=\alpha/2$$
$$\text{and } \Pr\{\text{accept } H_0 | H_{-1} \text{ true}\}=\beta$$

and for the second test the following probabilities hold:

$$\Pr\{\text{accept } H_1 | H_0 \text{ true}\}=\alpha/2$$
$$\text{and } \Pr\{\text{accept } H_0 | H_1 \text{ true}\}=\beta$$

then Wetherill and Glazebrook (1986 pg. 39) demonstrate that the overall test will reject H_0 when it is true with probability α and accept H_0 when it is false with probability β.

To construct the lower decision boundary for the test of H_{-1} vs. H_0, equation I) is rewritten as:

if $L_{0n}/L_{-1n} \le \beta/(1-\alpha/2)$, accept H_{-1}.

$$e^{n(\mu_{-1}-\mu_0)}\left(\frac{\mu_0}{\mu_{-1}}\right)^{\sum x_i} \le \frac{\beta}{1-\alpha/2}$$

$$\Rightarrow \ln\left(e^{n(\mu_{-1}-\mu_0)}\left(\frac{\mu_0}{\mu_{-1}}\right)^{\sum x_i}\right) \le \ln\left(\frac{\beta}{1-\alpha/2}\right)$$

$$\Rightarrow n(\mu_{-1}-\mu_0) + \sum x_i \ln\left(\frac{\mu_0}{\mu_{-1}}\right) \le \ln\left(\frac{\beta}{1-\alpha/2}\right)$$

Since $\mu_0 > \mu_{-1}$,

$$\Rightarrow \sum_{i=1}^{n} x_i \le \frac{\ln\left(\frac{\beta}{1-\alpha/2}\right)}{\ln\left(\frac{\mu_0}{\mu_{-1}}\right)} + \frac{n(\mu_0-\mu_{-1})}{\ln\left(\frac{\mu_0}{\mu_{-1}}\right)}$$

Therefore, the lower boundary for the first test may be written as

$$\frac{\ln\left(\frac{\beta}{1-\alpha/2}\right)}{\ln\left(\frac{\mu_0}{\mu_{-1}}\right)} + \frac{(\mu_0-\mu_{-1})}{\ln\left(\frac{\mu_0}{\mu_{-1}}\right)} \cdot n.$$

Defining both α and β to be 0.05 yields the following:

$$\frac{\ln\left(\frac{0.05}{1-0.05/2}\right)}{\ln\left(\frac{1.5}{1}\right)} + \frac{(1.5-1)}{\ln\left(\frac{1.5}{1}\right)} \cdot n$$

$$= -7.326 + 1.233n$$

To construct the upper decision boundary for the test of H_{-1} vs. H_0, equation ii) is rewritten as:

$$\text{if } L_{0n}/L_{-1n} \geq (1-\beta)/(\alpha/2), \text{ accept } H_0.$$

$$e^{n(\mu_{-1}-\mu_0)}\left(\frac{\mu_0}{\mu_{-1}}\right)^{\sum x_i} \geq \frac{1-\beta}{\alpha/2}$$

$$\Rightarrow \ln\left(e^{n(\mu_{-1}-\mu_0)}\left(\frac{\mu_0}{\mu_{-1}}\right)^{\sum x_i}\right) \geq \ln\left(\frac{1-\beta}{\alpha/2}\right)$$

$$\Rightarrow n(\mu_{-1}-\mu_0) + \sum x_i \ln\left(\frac{\mu_0}{\mu_{-1}}\right) \geq \ln\left(\frac{1-\beta}{\alpha/2}\right)$$

Since $\mu_0 > \mu_{-1}$,

$$\Rightarrow \sum_{i=1}^{n} x_i \geq \frac{\ln\left(\frac{1-\beta}{\alpha/2}\right)}{\ln\left(\frac{\mu_0}{\mu_{-1}}\right)} + \frac{n(\mu_0-\mu_{-1})}{\ln\left(\frac{\mu_0}{\mu_{-1}}\right)}$$

Therefore, the upper boundary for the first test may be written as

$$\frac{\ln\left(\frac{1-\beta}{\alpha/2}\right)}{\ln\left(\frac{\mu_0}{\mu_{-1}}\right)} + \frac{(\mu_0-\mu_{-1})}{\ln\left(\frac{\mu_0}{\mu_{-1}}\right)} \cdot n.$$

Again defining both α and β to be 0.05 yields the following:

$$\frac{\ln\left(\frac{1-0.05}{0.05/2}\right)}{\ln\left(\frac{1.5}{1}\right)} + \frac{(1.5-1)}{\ln\left(\frac{1.5}{1}\right)} \cdot n$$

$$= 8.971 + 1.233 \cdot n.$$

The lower and upper decision boundaries for the second test are constructed similarly, again using equations I) and ii) as is with the exception of replacing α with $\alpha/2$.

If the upper decision boundary of the test for H_0 against H_{-1} is crossed, H_0 is immediately accepted if the lower boundary for the test of H_0 against H_1 is crossed. In essence, by crossing the upper boundary of H_0 vs. H_{-1}, H_{-1} can no longer be accepted. Then by crossing the lower boundary for the test of H_0 against H_1, H_1 can no longer be accepted.

Likewise, if the lower decision boundary of the test for H_0 against H_1 is crossed, H_0 is immediately accepted if the upper boundary for the test of H_0 against H_{-1} is crossed. By crossing the lower boundary of H_0 vs. H_1, H_1 can no longer be accepted. By crossing the upper boundary for the test of H_0 against H_{-1}, H_{-1} can no longer be accepted.

The sequential test decision boundary under the H_{-1}, i.e. the number of defects in the liner average 1 per half-acre, is given by line AB in Figure 1. The decision boundary under H_1, i.e. the number of defects in the liner average 2 per half-acre, is given by line CD. Lastly, decision boundaries under the H_0, i.e. the number of defects in the liner average 1.5 per acre, are given by lines AF and CE.

The chart in Figure 1 is used by sequentially testing random one-half acre areas of the liner. The cumulative number of defects found are plotted after testing has been completed for each segment. If the cumulative number of defects falls below AB, H_{-1} is accepted. If the cumulative number of defects rises above CD, H_1 is accepted. If the cumulative number of defects either rises above CE and then falls below AF, or falls below AF and then rises above CE, H_0 is accepted. Random sampling continues until one of the above decision boundaries has been crossed.

The decision boundaries in Figure 1 were constructed to maintain maximum Type I and Type II error rates of 0.05. Therefore, only a five percent chance exists of falsely accepting H_0 in favor of H_{-1} or H_1, and only a five percent chance exists of falsely accepting H_{-1} or H_1 in favor of H_0.

EXAMPLE

A simulation of the sampling process was performed using a Poisson random number generator. Simulations were completed using a Poisson distribution with means of 0.5, 1.5, and 2.5. Figures 2, 3 and 4 respectively illustrate the results of each simulation.

In the simulation of 0.5 defects per half-acre on average (Figure 2), the cumulative defects passed below the lower decision boundary for H_{-1} after the 19th sample. Therefore, it would be correctly concluded that the true average number of defects per half-acre was less than or equal to one, indicating superior liner quality.

In the simulation using an average of 1.5 defects per half-acre (Figure 3), the cumulative defects passed below the lower decision boundary for H_1, then above the upper decision boundary for H_{-1} after the 91st sample. Although a larger sample size was required to reach a decision than with the first simulation, the correct decision was still made that the true average number of defects was between one and two. This indicates acceptable liner quality.

In the simulation of 2.5 defects per half-acre on average (Figure 4), the cumulative defects passed above the upper decision boundary for H_1 after the 14th sample. Therefore, it would be correctly concluded that the true average number of defects per half-acre was greater than or equal to two, indicating unacceptable liner quality.

DISCUSSION

Electrical Leak Location surveys have so far remained a research tool rather than a common-place CQA tool. This paper suggests that there is a potential for saving money without sacrificing the performance of the end product. First, the owner of the project could conceivably do away with the expensive CQA activities by an independent CQA firm. Secondly, if electrical leak location survey is used, repairs need only be undertaken if the end product is deemed unsatisfactory, i.e., defects exceed those accounted for in the design. The two above potential avenues for savings will not result in any reduction in the performance of the as-built liner. The use of sequential test statistics and SPRT will also enable the owner of the facility to draw accurate conclusions regarding the installation quality without having to leak test the whole installation. In this regard, it is possible to subdivide the liner into small segments of say 0.2, 0.1 or 0.06 hectares (1/2, 1/4 or 1/6 acres) or grids of 45m x 45m (150' x 150'), 30m x 30m (100' x 100') or 25m x 25m (80' x 80') and then randomly test these segments for leaks. The greatest advantage to result from the conduct of CQA in this fashion is that destructive tests can be eliminated. There is unanimity of opinion in the industry that destructive testing of seams is the least desirable part of current CQA practices.

As demonstrated in the example, a correct decision regarding whether to reject or accept the installation can be made after testing a total of a few acres of liner. This approach will potentially save money in large liner installations (estimated at 15 acres or larger) by not having to test the complete installation.

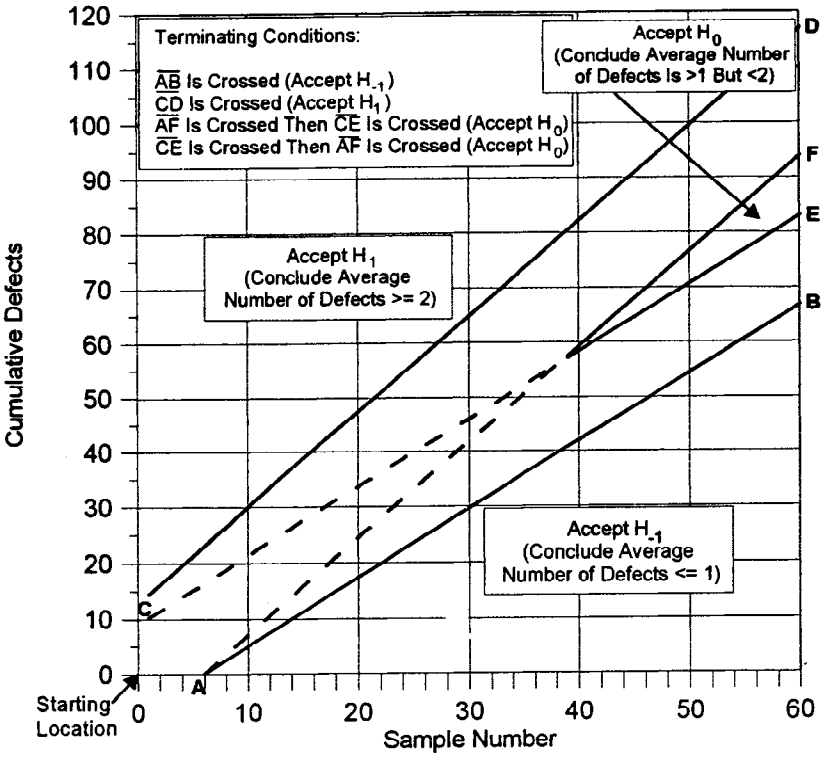

Figure 1 Geomembrane Liner Sequential Test Decision Boundaries
Average Defects per Half-Acre

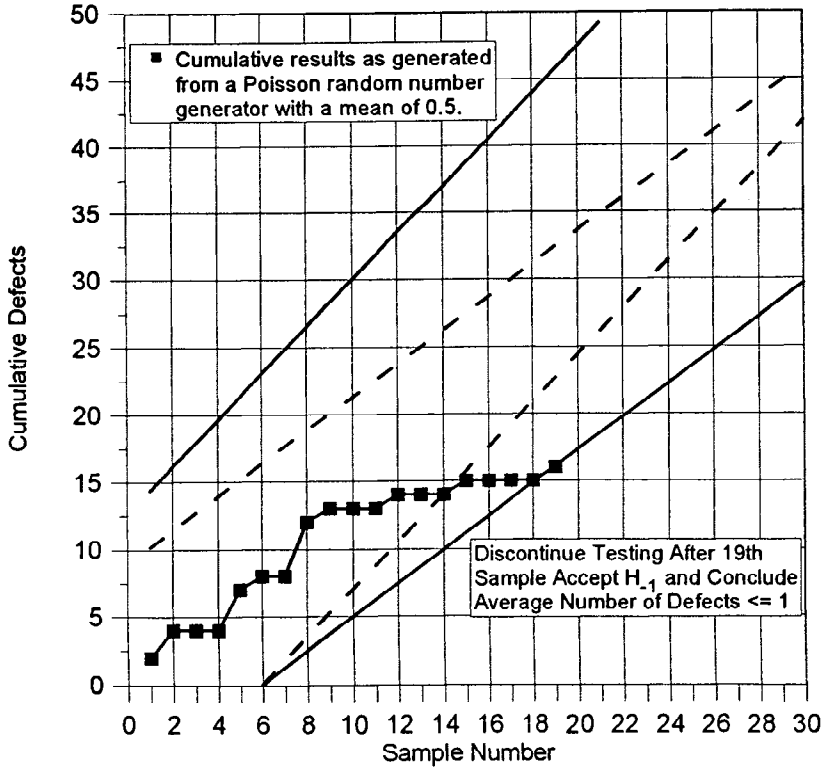

Figure 2 Sequential Test Simulation (Average of 0.5 Defects per Half-Acre)

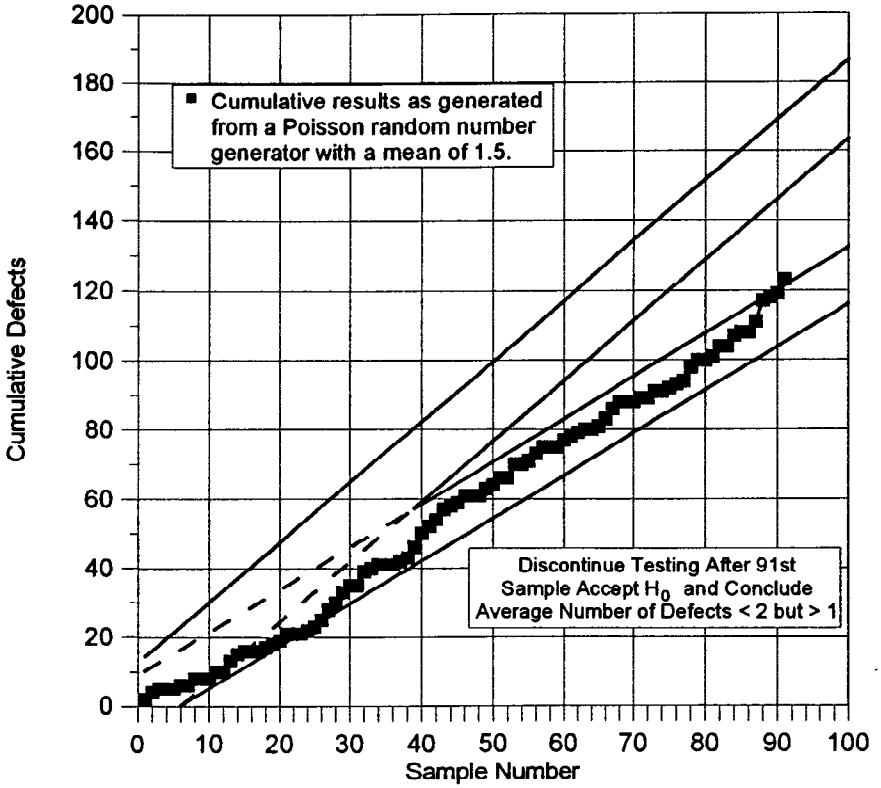

Figure 3 Sequential Test Simulation (Average of 1.5 Defects per Half-Acre)

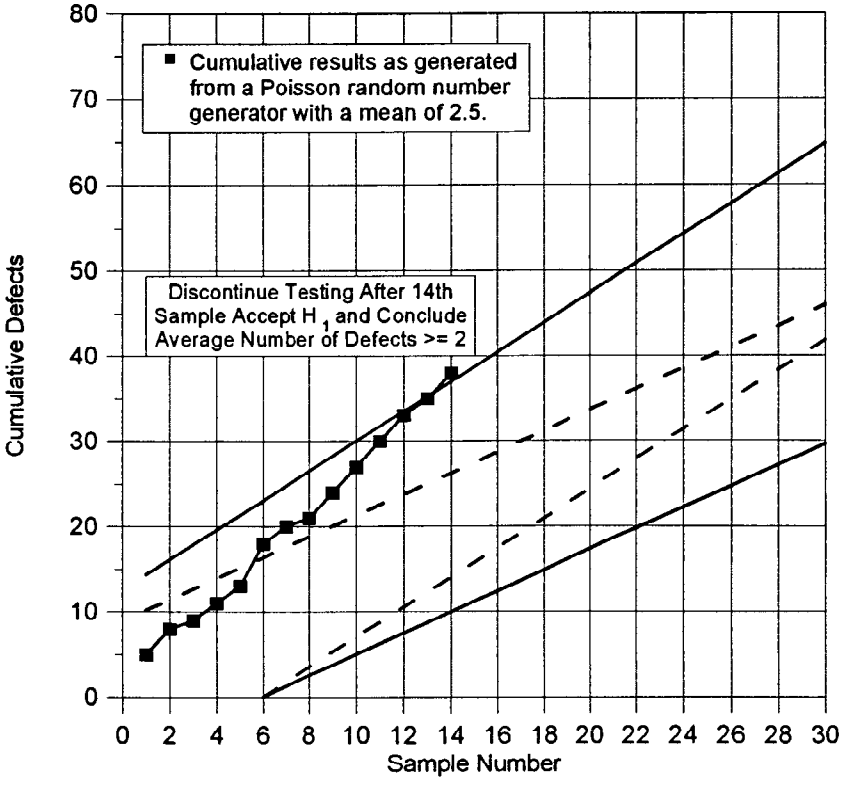

Figure 4 Sequential Test Simulation (Average of 2.5 Defects per Half-Acre)

The main disadvantage of the proposed approach is its inability to measure the dimensions of the defect unless the cover soil is removed to uncover the defect. This inspection may therefore be included as a requirement for successful CQA effort. Such as inspection will be able to identify the unacceptability of large sized holes at the acceptable number of defects or even less. For example, one large bulldozer gash at the toe of slope in an otherwise excellent installation is indeed unacceptable, but can be identified only by an inspection as stated here. Also, such an unacceptable defect may escape discovery during the statistical sampling procedure. It is, however, believed that good Construction Quality Control (CQC) procedures employed by the installers will not permit the occurrence of large bulldozer gashes.

Another disadvantage of this system is believed to be the potential to develop leaks in-service. In other words, in the absence of a close observation during installation, potential for future deterioration due to nicks, improper grinding, absence of slack and other situations leading to liner stressing cannot be identified.

An underlying principle for the proposed CQA approach is that the installation crew will continue to employ good CQC procedures. The human factor of potential for a slack in these activities in the absence of CQA monitors is difficult to quantify. Thus, there could be an unknown risk for the overall quality to deteriorate. This aspect can only be understood if long-term monitoring data are available for facilities built with the proposed method used for CQA.

In the absence of data on long-term monitoring, NMC decided to use electrical leak location survey in addition to, rather than instead of, conventional CQA methods. NMC also decided to conduct leak location surveys for the complete installation and repair any leaks found.

CONCLUSION

Sequential testing is an excellent method for use in geomembrane liner CQA programs. It can be used to accurately predict whether the average number of defects per segment area falls above or below design standards. In addition, the associated error rates (α and β) of making an incorrect decision based on sample results can be set to any level, making them as small as required.

The sampling plan is advantageous over other types of statistical plans in that the number of collected samples does not need to be predefined. Sampling continues until enough information has been collected to decide whether the constructed liner either meets or fails to meet the design specifications.

This sampling plan is generally more applicable to larger sites, installing liners over 15 acres. For these sites there is a considerable cost advantage to avoid the testing of the entire liner.

Performance of liners for which leak testing is used as the only CQA tool will greatly increase the confidence in this method.

REFERENCES

Daniel, D.E. and Koerner, R.M. (1993) "Quality Assurance and Quality Control for Waste Containment Facilities", U.S. EPA Technical Guidance Document EPA/600/R-93/182.

Ghosh, B.K. and Sen, P.K., (1991) "Handbook of Sequential Analysis", Marcel Dekker, Inc., New York.

Giroud, J.P. (1997) "Equations for Calculating the Rate of Liquid Migration Through Composite Liners Due to Geomembrane Defects", Geosynthetics International, Vol. 4, Nos. 3-4.

Giroud, J.P. and Bonaparte R. (1989) "Leakage Through Liners Constructed with Geomembranes - Part II, Composite Liners", Geotextiles and Geomembranes, Vol. 8, No. 2.

Hoel, P.G., Port, S.C. and Stone, C.J. (1971) "Introduction to Statistical Theory" Houghton Mifflin Company, Boston.

Laine D.L. and Darilek G.T. (1993), "Locating Leaks in Geomembrane Liners of Landfills Covered With a Protective Soil", Geosynthetics 93, IFAI.

Markin, J.T., and Shipley, J.P. (1982) "Timely Detection of Materials Loss", Nuclear Materials Management/1982 INMM Proceedings, 11:60-63.

Wetherill, G.B., and Glazebrook, K.D. (1986) "Sequential Methods in Statistics" Chapman and Hall, New York.

LEAK LOCATION IN EXPOSED GEOMEMBRANE LINERS USING AN ELECTRICAL LEAK DETECTION TECHNIQUE

ROLLIN, A.L.,
MARCOTTE, M.,
JACQUELIN, T.
CHAPUT L.
SOLMERS INTERNATIONAL, LONGUEUIL, CANADA

ABSTRACT : An electrical leak detection technique recently developed was used to investigate leaks in exposed geomembrane liners at eleven (11) sites in Canada and France. These surveys covering more than 240 000 m^2 of installed HDPE, PP and bituminous geomembranes liners were performed during their installation on sites including CQA programs. The results obtained demonstrate that essentially three types of leak have been found and that the reported damage densities are less than suggested by other authors basically because these surveys were performed during the liners' installation. Despite the fact that rigorous CQA programs were implemented, the number of leaks found during these electrical leak detection surveys was still greater than expected and considered in the design phase. It stresses the need to improve existing CQA programs, to use high-quality of sub-grade, to insure accuracy of installation and to strengthen inspection of seams especially HDPE fillet extrusion welds performed during repair patches. The higher leak density found in smaller installations suggests that greater CQA must be implemented for small impoundment facilities such as for the leachate collection ponds too often neglected. This electrical leak detection system has demonstrated its viability and usefulness and should be included in all CQA program.

INTRODUCTION

Different kinds of damages may occur in the geomembrane during the construction of a impoundment facility or a landfill cell, depending on the quality of the subgrade and protective/drainage layer materials, on the accuracy of the installation and the quality and thickness of the geomembrane.

Experience demonstrates that even in sites built according to a strict Construction Quality Program (CQA), damages prior to the placement of the protective/drainage soil layer are frequently found during specialized surveys and gross damages occur during placement of the over-cushion layer (Colucci 1995, Laine et al 1993, Rollin 1998). Short-term detection is then

essential in order to verify that the synthetic liner performs the role of flow barrier. Quality control can be carried out by on-site inspection and specified tests during construction phase.

An electrical leak location system has been used to locate leaks in exposed geomembrane liners installed in basins, ponds and landfill cells. More than 240 000 m^2 of uncovered High Density Polyethylene (HDPE), flexible reinforced Polypropylene (PP) and prefabricated bituminous (PBGM) geomembranes have been surveyed in eleven (11) sites located Canada and France during the 1994-1998 period (Solmers 1998). In this paper, results obtained from these surveys are presented, analyzed and related to the quality of the sub-grade, the accuracy of installation and the size of the inspected facilities.

GEO-ELECTRICAL LEAK DETECTION FOR EXPOSED GEOMEMBRANE

A geo-electrical technique was developed by Solmers to rapidly locate leak defects in 100% of uncovered geomembrane during the installation phase of the liner for impoundment facilities and for landfill composite lining system. It can also be used to search for leaks in membrane-lined concrete and steel tanks. It requires an electrically conductive layer below the liner (soil, moist concrete, steel) and above the liner (water puddle maintained by a squeegee) [Rollin 1998].

The principle behind the technique is to insert a 24 VDC voltage onto each side of a geomembrane liner and then detect areas where electrical currents flow through leaks in the liner as shown schematically in Figure 1. The geomembrane must be an insulator, which is the case with conventional PE, PP, PVC, CSPE and bituminous geomembranes. Electrical potential is applied between a water puddle and the conductive layer below the liner as shown schematically in Figure 2. Whenever water is leaking through the geomembrane, an electrical current is immediately detected by an audio signal or by measuring a current of magnitude to the size of the leak. The main advantage of this technique is the possibility to detect leaks in liner seams and sheets as work progressed during the construction phase. The geo-electrical survey rate of approximately 300 to 500 m^2/h per operator does not affect the installation work schedule and allows a rapid quality control of the installer's work.

Water is usually supplied by a water network or by gravity from a tank truck parked at the top edge of the pond or cell. The low voltage and current used with this technique do not involve any risk for the operator or anyone on the site as shown in Figure 3.

The presence of wrinkles and waves, steep slopes and lack of contact between the liner and the conductive soil at the bottom of slopes can slow down significantly the survey speed. This technique cannot be used during stormy weather, when liners are installed on a non-homogeneous conductive layer and whenever isolation is not secured. To insure isolation at pipe penetration, flange bolts, steel drains and batten strips on concrete, insulation must be secured prior to a survey to avoid conduction of electricity through the liner thus masking the leaks.

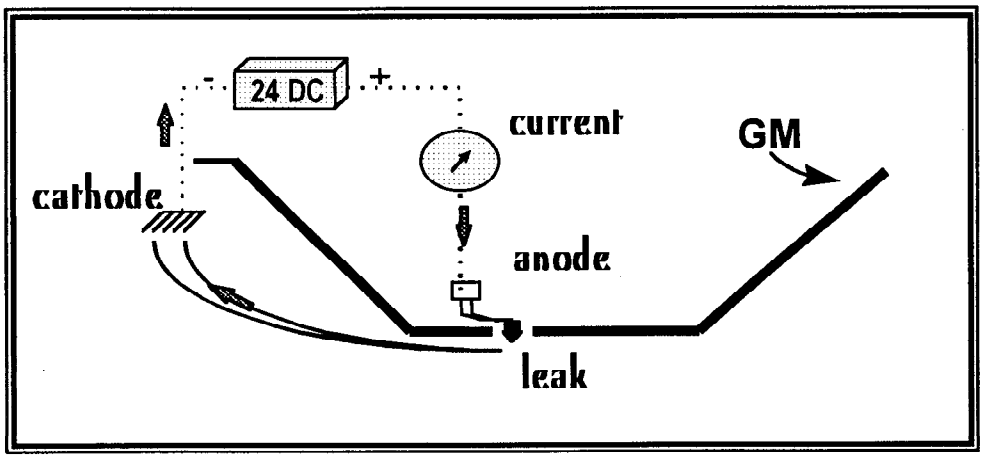

Figure 1. Schematic of electrical leak detection method

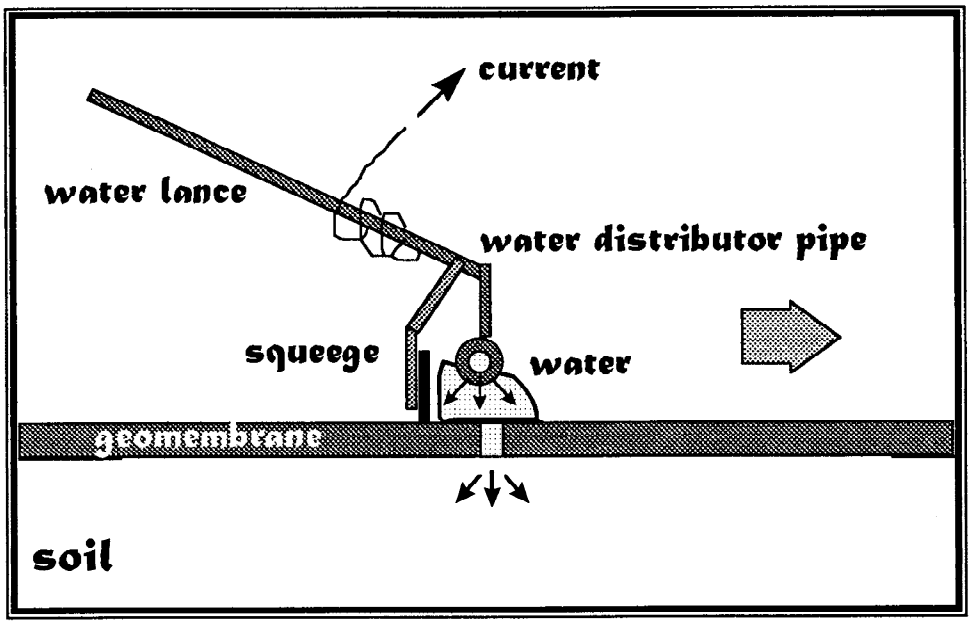

Figure 2. Schematic of electrical leak detection apparatus

RESULTS

Uncovered geomembranes have been prospected at eleven (11) sites using the described geo-electrical leak detection technique corresponding to a total surveyed area of 240 908 m^2 as described in Table 1.

Figure 3. Geo-electrical leaks survey on uncovered geomembrane

Table 1. General information on prospected sites.

Site ID	Type of facility	Site Location	Date	Prospected Area (m^2)
1	Domestic Waste Landfill	France	1995	18 500
2	Domestic Waste Landfill	France	1996	14 926
3	Hazardous Waste Landfill	France	1994	13 480
4	Hazardous Waste Landfill	France	1995	11 652
5	Hazardous Waste Landfill	France	1997	8 200
6	Hazardous Waste Landfill	France	1998	9 284
7	Waste Water Treatment Ponds (1)	Canada	1995	67 100
8	Waste Water Treatment Ponds (2)	Canada	1995	66 150
9	Black Liqueur Retention Pound	Canada	1997	11 460
10	Domestic Waste Landfill	France	1998	18 135
11	Process Water Retention Pounds	Canada	1995	2 021
		Total area:		**240 908**

Three domestic waste landfills, four hazardous waste landfills, two water treatment ponds and two industrial effluents retention ponds were surveyed. Two of the larger sites surveyed (sites no. 7 and 8) were lined with a pre-fabricated bituminous geomembrane while most of the sites surveyed (except for site no 9 lined with a PP membrane) were lined with HDPE membranes covering area ranging from 10000 to 20000 m^2. Only one small site (no. 11) lined by approximately 2000 m^2 of HDPE membrane was surveyed.

Number and density of detected leaks

The number and typology of leaks detected during the surveys are presented in Table 2. Types of leaks being related to the quality of sub-grade material, quality of the cover material, accuracy in their installation and the quality of the liner installation (Colucci 1995), the leaks detected during these surveys have been divided into three categories:

Holes : perforation made by puncture (being round shaped with protuding rims)
Razor cuts : linear leaks with neat close edges usually made by a knife
Welding failure : lack of seaming resulting in holes, channelling and overheating areas

Holes can be related mainly to the quality of the sub-grade and human activities while knife cuts and seam failures are related to the membrane installation quality.

Table 2. Number and typology of located leaks.

Site ID	Prospected	Detected Leaks				Leak Density
	Area (m^2)	Holes	Knife cuts	Seam failures	TOTAL	(leaks per hectare)
1	18 500	0	0	5	5	2.70
2	14 926	4	0	2	6	4.02
3	13 480	1	1	1	3	2.23
4	11 652	1	2	2	5	4.29
5	8 200	0	0	0	0	0.00
6	9 284	0	1	0	1	1.08
7	67 100	3	0	2	5	0.75
8	66 150	1	1	7	9	1.36
9	11 460	2	2	2	6	5.24
10	18 135	0	3	3	6	3.31
11	2 021	0	0	3	3	14.84
TOTAL	240 908	12	10	27	49	
		24.5%	20.4%	55.1%		average 2.03

More than 50% of the detected leaks were located in seams, of which 100% were fillet extrusion seams for HDPE, after they were checked using vacuum box testing programs. Holes accounted for 25% of the leaks while approximately 20% were knife cuts.

The average leak density of all sites was found to be 2 leaks per hectare and of 3.25 leaks per hectare for sites lined with HDPE and PP geomembranes. The average values obtained are relatively lower than others (Colucci 1995, Laine 1989, 1991, 1993, Peggs 1991,1993, Rollin 1998), averaging from 22 to 14 leaks per hectare. The reason for smaller leak density is perhaps related to the surveys being performed during the liner installation with the implantation of stringent CQA programs.

As also observed in other surveys (Colucci & Lavagnolo, 1995 and Laine & Miklas, 1988), the density of leaks generally decreases as the lined impoundment facility dimension increases as shown in Figure 4. For comparision, Colucci data have been plotted on the same graph.

The reasons for greater leak density to liners installed in smaller installations have been summarized by Colucci (1995): smaller installations have proportionally more complex features (corners, sumps, penetrations) and higher percentage of hand seaming; larger installations tend to have better construction quality program and generally receive less traffic.

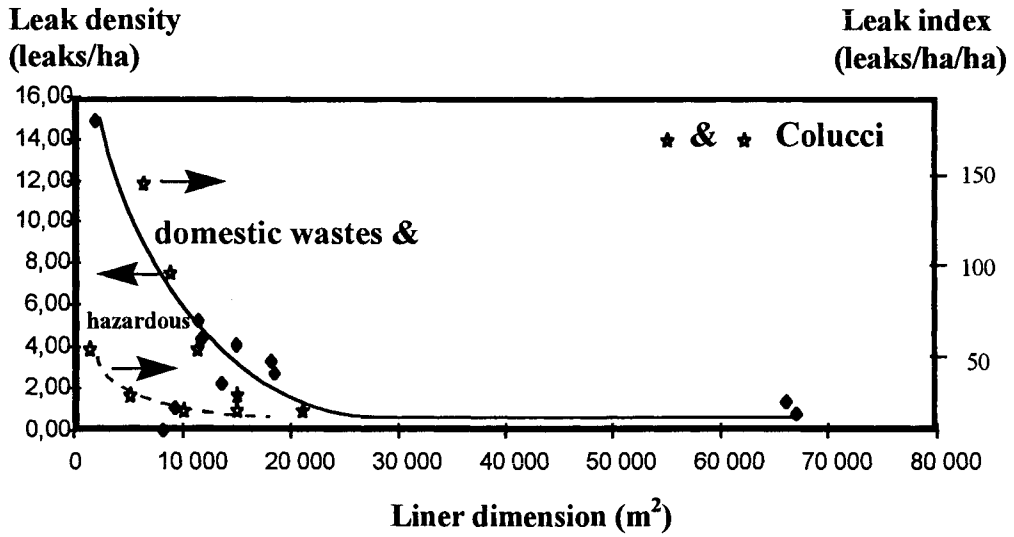

Figure 4. Leak density vs. lined area

Leak size

The detected leak size distribution classified per leak type is presented in Table 3. The smallest leaks, size smaller than 2 mm^2, represent 43% of all detected leaks and are associated

mainly with seam failures while the largest leaks, size greater than 10 mm^2, representing 22.4% of total leaks are more related to holes and razor cuts. Most of smaller leaks were not visible to the naked eye and not detected during the seam non-destructive testing program.

Table 3. Number of leaks vs. leak size.

Leaks Typology	Leak sizes			TOTAL	(%)
	< 2 mm^2	2 to 10 mm^2	> 10 mm^2		
Holes	3	6	3	12	**24.5**
Knife cuts	0	4	6	10	**20.4**
Welding Failures	18	7	2	27	**55.1**
TOTAL	21	17	11	49	100
(%)	**42.9**	**34.7**	**22.4**	100	

A knife cut along the edge of a 2 mm thick double wedge seam is shown in Figure 5. A white paper sheet has been inserted in the cut to observe the cut length.

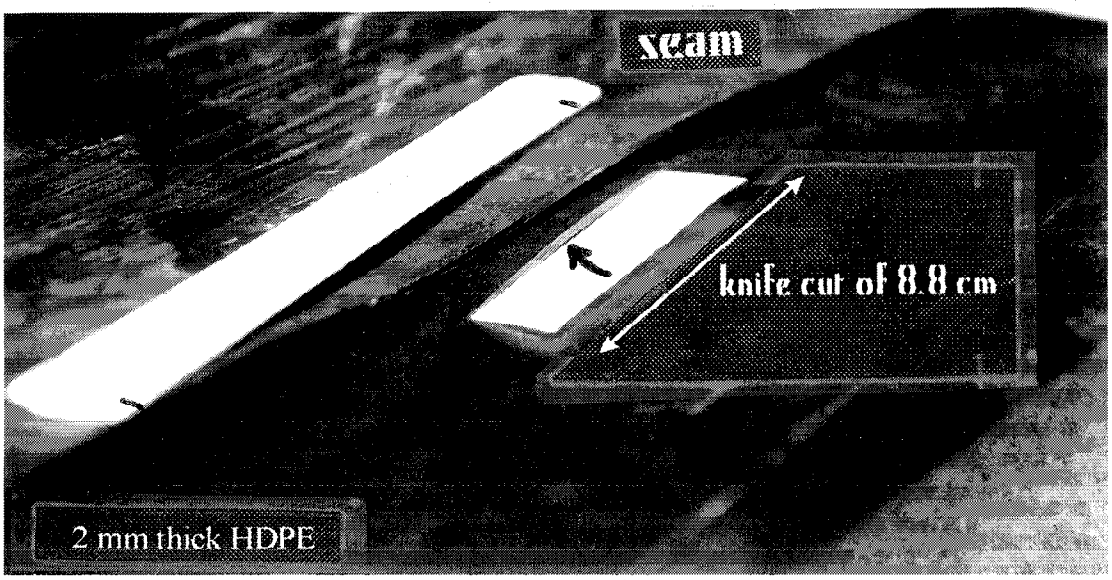

Figure 5. Photograph of a razor cut leak on HDPE liner.

RESULTS ANALYSIS

The number of leaks found in a liner is influenced by many different parameters : the area lined, the quality of the materials under-laying and covering the geomembrane, the accuracy of the installer work and the implantation of a rigorous CQA program. A non-negligible parameter is related to the psychological effect on the installer personal resulting from of a leak survey team presence during the installation of the liner. An attempt was made to relate the quality level assigned for some parameters for each site prospected and data are presented in Table 4.

Table 4. Leak density corresponding to site quality parameters.

Site ID	Leaks survey during (D) / after (A) installation	Quality of material beneath the GM	Installer experience	Rigorous CQA on site	Type of geomembrane	GM thickness (mm)	Leaks Density (per hectare)
1	D	high	high	yes	HDPE	2	2.70
2	D	high	high	yes	HDPE	2	4.02
3	D	high	high	yes	HDPE	2	2.23
4	D	high	high	yes	HDPE	2	4.29
5	D	high	high	yes	HDPE	2	0.00
6	D	high	high	yes	HDPE	2	1.08
7	D	high	low	yes	bituminous	3	0.75
8	D	high	low	yes	bituminous	3	1.36
9	A	high	high	yes	PP	1.14	5.24
10	D	high	high	yes	HDPE	2	3.31
11	A	fair	high	no	HDPE	2	14.84

Quality level assignation of materials under-laying a liner

The level of quality assigned to the materials under-laying a liner can be categorized in the following manner:

high : - clay or granular material, 0 - 5 mm diam., or
- clay or granular material, 0 - 25 mm diam., with a good geotextile for protection

fair: - clay or granular material, 0 - 25 mm diam., without a geotextile for protection

low : - material with particle size superior to 25 mm, without a geotextile for protection

Average leak density of approximately 40 leaks per hectare for low quality sub-grade layers has been reported by Colucci 1995 and Rollin 1998 as compared to 8 leaks per hectare for high-quality materials. The number of leaks per hectare found at site no. 11 is by far the largest leak density recorded and damages occurred because of the sub-grade poor quality coupled with a non-rigorous CQA program.

One can question the impact of the quality of materials beneath the membrane on the number of holes detected, which represent 24,5 % of all detected leaks (Table-2). It is believed that, most of those holes have been created by equipments and tools used during the liner installation (generator, grips, etc.) and by falling rocks from the surrounding slopes. The lower leaks density values generated by these surveys can be explained because good sub-grade quality materials were used and that non-woven geotextiles were installed between the material and the liner.

Experience level assignation of installer

Since 75% of all detected leaks are related to knife cuts and faulty seams, a level of installer's years of experience in liner installation was assigned for each site:

high : more than 6 years
medium : between 2 and 6 years
low : less than 2 years

Many razor cut leaks were detected at repair areas where welders have often to cut small pieces of liner used as repair patches. For all HDPE and PP lined facilities, the installer had vast experience even though results indicate that the majority of leaks are related to installation practice. This worrying fact stresses the need to improve current installation quality assurance programs and that greater cares must be exercised during the liner installation phase. More specifically inspection of fillet extrusion welds at repair patches, in vicinity of pipe penetration and sumps must be exercised with greater care. Moreover, a leak detection survey at the time of the liner installation is having a beneficial psychological impact on the work quality.

Quality assurance on site

As already mentioned, survey no 11, with the largest leak density, was performed on a site constructed without known CQA program. This supports reported cases (Laine 1989, Peggs 1991) where significant number of leaks was recorded in association with poor CQA.

In some cases, large numbers of leaks have been observed after vacuum box tests were performed indicating that some leaks may be easier to detect with the geo-electrical method. More site investigations are needed to clarify the performance of this technique and the viability for substitution to non-destructive on site testing of seams.

A state of the art CQA program should follow-up all installer's activities, be implemented by qualified inspectors during the full installation period and be supported by an electrical leak detection survey.

Expected leakage rates through detected leaks (Global Improvement)

The detection and repair of leaks improve the global quality of the liner by insuring minimum leakage of contaminated liquid into the ground. To support the usefulness of the leak detection technique, an analysis of the leakage rate forecasted from the leaks detected at the containment pond (site no. 9) lined with a PP geomembrane with an average hydraulic charge of 2.5 m of black liquor is presented below.

A total of six (6) leaks of 15 mm^2 equivalent average size (one of those perforations was a razor cut of 150 mm long) were detected. Using equation proposed by Brown 1987, Giroud et al 1989 and 1997 for a design incorporating a sand layer installed beneath the geomembrane (sand permeability ks = E-3 m/s)

$$Q = C_B\, a \sqrt{2\, g\, h}$$

Where a, surface area of hole = 1.5 E-5m^2
h, liquid depth on top of membrane = 2.5m
g, gravitational = 9.8m/s^2
C_B = a dimensionless coefficient related to the shape of the edge of the aperture; for sharp edge, C_B = 0.6

the total estimated leakage rate would have been 29 000 1/d-ha (11 921 m^3 per year), ex-filtration of almost 12 millions liters of contaminated liquid per year. This volume of liquid would have been equivalent to 19% of the total reservoir's capacity.

CONCLUSION

Despite the fact that good CQA programs were implemented on ten surveyed sites, leaks created during the installation phase were detected on uncovered geomembrane. These leaks are usually small but can have a relevant effect, especially for containment basins where an important hydraulic charge is maintained. Engineers should aim to target their design with larger leakage rates.

The higher number of leaks found in smaller installations suggest that greater CQA programs should be implemented for small impoundment facilities such as leachate collection ponds, too often neglected. Moreover, more rigorous inspection procedures should be implemented whenever HDPE fillet extrusion seams are performed at repair patches and in the vicinity of pipe penetration. Designers and installers should always minimize fillet extrusion seams.

Finally, the geo-electrical leak detection method has demonstrated its validity and usefulness to detect leaks in 100% of uncovered geomembranes and should be included in a construction assurance program. This technique should even be considered as a viable substitute to some current non-destructive testing techniques of seams. However, the application of a geo-electrical leak detection technique during construction should not minimize the importance of other CQA activities such as the inspection of the sub-grade material quality and the accuracy of installation of the cover drainage/protective layer.

BIBLIOGRAPHY

1. Brown K.W., Thomas J.C., Lytton R.L., Jayawickrama P. and Bahrt S.C. [1987], "*Quantification of Leak Rates Through Holes in Landfill Liners*", EPA Project EPA/600/S2-87/062, November

2. Colucci P. amd Lavagnolo M.C. [1995], "*Three Years Field Experience in Electrical Control of Synthetic Landfill Liners*", Proceedings of Sardinia'95, CISA, Cagliari, pp 437-451, October

3. Colucci P., Crozier F. and Laine D.L. [1996], "*Geomembrane Liner Testing Using the GLLS: A High-Voltage Electrical Leak Location System*", Proceedings of the First European Geosynthetics Conf., Maastricht, pp 749-750

4. Giroud J.P. and Bonaparte R. [1989], "*Leakage through Liners Constructed with Geomembranes, Part I: Geomembrane liners*", Geotextiles and Geomembranes, vol 8, no 1, pp 27-67

5. Giroud J.P. and Bonaparte R. [1989], "*Leakage through Liners Constructed with Geomembranes, Part II: Composite Liners*", Geotextiles and Geomembranes, vol 8, no 2, pp 71-112

6. Giroud J.P., Gross B.A., Bonaparte R. and McKelvey J.A. [1997], "*Leachate Flow in Leakage Collection Layers Due to Defects in Geomembrane Liners*", Geosynthetics International, vol 4, nos 3-4

7. Laine D.L. and Miklas M.P. [1989], "*Detection and Location of Leaks in Geomembrane Liners Using an Electrical Method: Case Histories*", Proceedings of the 10th National Conf., Superfund'89, Washington, November

8. Laine D.L. [1991], "*Analysis of Pinhole Seam Leaks Located in Geomembrane Liners Using the Electrical Leak Location Method: Case Histories*", Proceedings Geosynthetics'91, IFAI, Atlanta, pp 239-253 , February

9. Laine D.L. and Darilek G.T. [1993], "*Locating Leaks in Geomembrane Liners of Landfills Covered with a Protective Soil*", Proceedings of Geosynthetics'93, IFAI, Vancouver, vol 3, pp 1403-1412, April

10. Peggs I.D. [1993], "*Practical Geoelectric Leak Surveys with Hand-Held, Remote and Water Lance Probes*", Proceedings of Geosynthetics'93, IFAI, pp 1523-1532, Vancouver

11. Rollin A. and Jacquelin T. [1998], "*Geomembrane Failures: Lessons Learned from Geo-Electrical Leaks Surveys*", Lessons Learned from Geomembrane Failures, editor JPG, to be published

MOBILE GEOELECTRIC LINER INTEGRITY SURVEYS: PLANNING AHEAD

IAN D. PEGGS
I-CORP INTERNATIONAL, INC., USA

ABSTRACT

For a successful geoelectric liner survey the electrically conductive medium above the geomembrane must be electrically isolated from any leaking liquid or the medium under the geomembrane except through the leaks. Unavoidable liner penetrations should be made with plastic nonconductive components rather than metal or concrete. Such penetrations may have to be blocked with inflatable rubber plugs during a survey. Metal batten strips should be avoided or covered with a nonconductive mastic. Cover soils on side slopes should not be placed in contact with surrounding subgrade soils. Provision should be made to insert an electrode between the geomembranes of double lining systems.

It is necessary to have an electrically conductive medium in complete (intimate) contact with the underside of the geomembrane being tested. This may necessitate a geonet leakage collection layer being filled with water. Or, electrically conductive sheet may be beneficial in this respect. In effect, the objective is to be able to pass electric current from one side of the geomembrane to the other only through the leaks being sought.

The design features, construction procedures, and testing conditions necessary for the performance of a successful geoelectric liner integrity survey are described.

INTRODUCTION

There are increasing requirements for electrical integrity surveys to be performed on installed geomembrane liners as the final stage of construction quality assurance (CQA). In some jurisdictions this is a legislated requirement. More frequently electrical leak location surveys are required to locate a known leak for compliance with facility permit requirements. Integrity surveys are those performed for the final phase of CQA. Leak surveys are those

performed to locate a known leak. Such surveys can best be performed by an in-situ monitoring system, for then the liner is designed for such a specific function. However, until it is a regulated requirement, most installations will not be built with in-situ systems, thereby requiring the use of a portable/mobile system when necessary. This may require considerable site preparation in order to effectively perform an electrical survey. It would, clearly, be much easier to design a lining system that is suited to the rapid performance of electrical leak surveys. Such features for uncovered, liquid-covered, and soil-covered liners will be described, but it will be apparent that once the basic principle of integrity/leak surveys is understood the requirements for any lining system will be evident.

PRINCIPLE

The basic principle of electrical integrity/leak surveys is simple. An electric potential is applied between the medium on top of the liner and the medium under the liner such that current will only flow through the leaks. If current does not flow leaks do not exist. If current flows through metal pipe penetrations, concrete pads, metal batten strips, or around the edge of the liner (through rainwater or soil), the ability to locate small leaks will be severely compromised. Thus, it is essential to have an electrically conductive medium in intimate contact with the underside of the geomembrane, or there must be a discrete continuous electrically conductive pathway from the leak to the medium in which the underside electrode is placed.

The electrical resistance or potential gradients in the overlying medium are then measured to locate the high gradient, or low resistance, associated with the leak. Actual measurement techniques have been described (Peggs 1996, Laine & Darilek, Laine et al.) so will not be repeated here.

LIQUID-COVERED LINERS

Leak surveys were initially developed (Boryta et al., Darilek et al.) for pond liners. The liquid covering the liner must be electrically conductive. In single lining systems, where the liner is placed on a soil subgrade, the soil should also be electrically conductive. There should be no overflow of contained liquid on to the surrounding soil that would allow current to flow around the liner's edge. If the liner is wet from rain, the efficiency of a survey is compromised, since the current that is needed to flow through the leak flows along the surface of the geomembrane and off the edge into the soil. The more current that flows through the leak, the easier it is to identify and pinpoint.

Metal pipe penetrations should be avoided for the same reason. Pipes should be plastic. Exposed metal pipe, and blind flanges, could be painted. Even then, if piping underground transitions from plastic to metal, or if there is a metal valve in the line in contact with the ground, current will flow through the penetration. During testing such penetrations have to be sealed with a welded cap or an inflatable rubber plug. A plug that is expanded by squeezing with a metal bolt

that penetrates the plug is, therefore, not desirable. Clearly it is preferable that the liner under the liquid have no penetrations at all.

Similarly, metal pipes that are exposed in concrete pads to which the liner is battened preclude the ability to locate small leaks adjacent to those areas - the precise areas that are highly likely to contain leaks. It will be difficult to locate a leak underneath a metal batten strip when the steel bolts are set in concrete. Concrete pads should be covered with a boot to the pipe. Skirts should not be battened to the liner. The liner could be welded to an anchor strip set in the concrete and the skirt welded to the liner. Aerators and floating pumps should have all lines completely disconnected - shutting off power may not be adequate since such lines could ground the device. Even stainless steel tethering lines should be disconnected or substituted by rope or polyester lines which are kept out of the water.

Remove all sandbags and other debris from the floor of the lagoon before it is filled. Keep drums, irrigation pipe, and other items from entering the water. Tripping over these unexpected obstructions is a problem when performing wading surveys, but at least their identity can be felt and explanations provided for noisy signals that occur close to items of different electrical conductivity. However, they are much more problematic when performing remote drag probe surveys in deep water, when their identity is not known. They may provide background noise similar to a leak indication, and the probe may get hung-up on them. Ballast tubes may not be a major problem if their orientation is known and they are all in the same direction.

When performing wading surveys it always helps to know the locations and depths of trenches, sumps, and other topographical profiles. It is occasionally found that higher ridges of sand placed over drainage pipes are more loose than the sand placed over the liner due to migration of sand within the drainage stone.

If a single liner is covered by a ballasting soil layer, a final integrity survey should be performed after the soil has been placed, but before the cover soil is finally placed into electrical contact with the surrounding subgrade soil. If this is not done it will be necessary to dig an isolating trench (Figure 1) around the periphery of the liner in order to perform a post-installation survey. Alternatively, the design could include an isolating barrier - a channel, or a flap welded to the top of the liner.

Soil ballast and sludges on top of a geomembrane are not a problem if they are relatively level, solid, and electrically homogeneous:

- "Level" makes them easy to traverse and helps prevent the drag probe electrodes from coming into contact with them. A noisy signal is generated each time the probe electrode contacts an

object or medium with a different electrical conductivity to the background (liquid) medium.

- "Solid" also makes them stable and prevents the probe from becoming submersed in them.

- "Electrically homogeneous" minimizes background noise and the need to survey back and forth to confirm whether a signal is background noise or an actual leak. Regions of petroleum and metallic sludges are bad in this respect, as are stirred-up bacteria concentrations in wastewater treatment ponds.

Figure 1. Trench dug to isolate cover stone from subgrade soil

A double lining system, in which it can be assured that there is no inward leakage of water between the two liners at the anchor trench, removes many set-up problems, but adds a few new ones. Clearly the system between the two liners can be potentially totally isolated from the liquid above the primary liner and the subgrade soils. However, to be assured of this, it must be possible to remove all electrical lines to pumps and transducers between the liners. These lines must not be available for the passage of current to ground. If such a line does go to ground, and water in a pipe penetration also goes to ground through a gate valve, the two systems are not isolated. The sensitivity of the survey will be compromised.

It may be necessary to fill the space between the two geomembranes with water in order to assure a continuous conductive pathway between the hole and the liquid in which the current return electrode is placed. This is particularly important when the leak is

very small and may not be leaking a continuous stream. A primary geomembrane with an electrically conductive bottom surface precludes the need to flood the secondary system. In most instances flooding can be achieved simply by not pumping the leaking liquid, thus allowing it to fill above the level of the leak. Clearly, care must be taken not to lift the primary geomembrane when the drainage layer is saturated. Whether or not the leakage collection system is full can influence the background/noise signal of the survey at different locations. The primary geomembrane is not a complete insulator, therefore a base signal is generated by the very small current flowing across it, and this will change depending on whether there is liquid or air in contact with its underside surface.

Metal grids at sumps and outlet pipes need to be avoided - they can be a major nuisance, again in an area where a hole is likely. They should be avoided or removed if at all possible. Similarly concrete ramps, with geomembrane battened to their edges, are also a problem.

For a single liner, it helps to have some moist ground around the lagoon in which to place the current return (ground) electrode, although a chain link fence is also very effective. However, good contact has been made with dry desert sands by using a conventional copper ground rod.

When leaks have been identified, except for the application of electrofusion patches, it is necessary to remove liquid from the pond to make repairs. If there is leaked liquid under the liner that is not drawn down at the same time this may induce a new set of stresses in the primary geomembrane and, consequently a new series of leaks. This may also happen when the pond is refilled. This application of post-survey stresses can be a significant problem where there is a poor quality booted pipe penetration close to the outlet sump, as often occurs. New leaks can be generated each emptying/filling cycle, much like chasing crack leaks by welding and rewelding in the same location. Therefore unnecessary booted penetrations close to sumps should be avoided. Boots should be molded, rather than field fabricated, wherever possible.

SOIL AND WASTE COVERED LINERS

Many of the same requirements apply for soil-covered liners as for ballasted pond liners, especially that the soil cover shall be electrically isolated from the conductive medium directly under the primary geomembrane and around the periphery of the cell. Thus, the soil cover should not extend beyond the periphery of the cell if an integrity survey is required to be performed as the final stage of CQA. Clearly, this only applies in the case of a single liner.

When a sacrificial/protective piece of geomembrane is placed on top of a barrier geomembrane, such as below a leachate drainage pipe or in a sump area, it prevents the exact location of a hole in the barrier geomembrane and may even preclude the detection of a hole altogether. Where such a layer is required on top of the geomembrane, it would be better to use a geotextile, which still allows detection

and location of holes in an area of the liner that is highly susceptible to damage.

There must be leaking liquid (or moist soil) within the hole, to provide electrical conductivity across the geomembrane, and the soil above the geomembrane must also be moist. Stone and sand drainage layers in hot environments will need constant moistening to maintain optimum conductivity. Holes that have been dug on the cover layer for previous liner repair work should be refilled to the same density and moisture content as the remainder of the cover, otherwise they can provide anomalous signals that look like leaks (Figure 2).

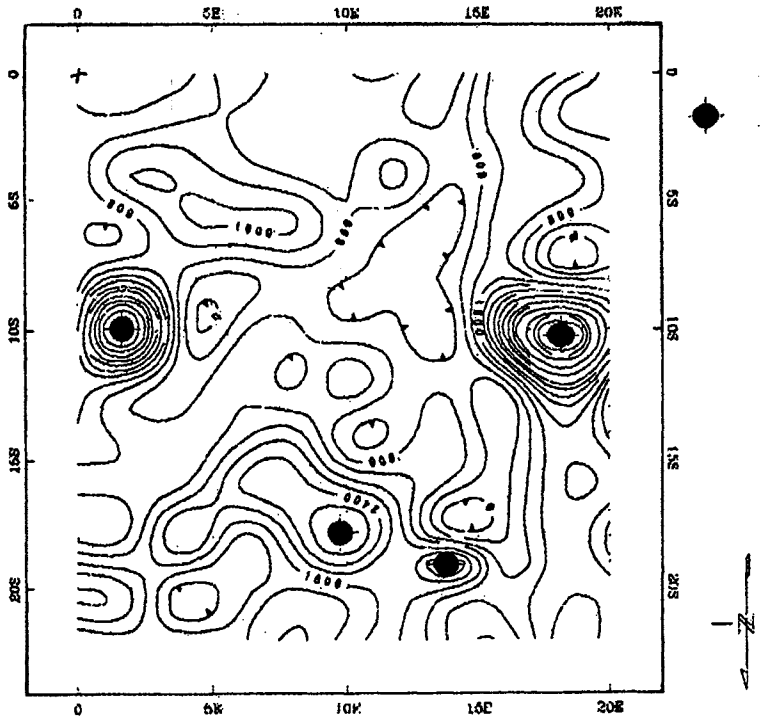

Figure 2. Isopotential contours.
Two leak indications at right are from calibration holes;
the two on the left are from previous excavations.

Vegetation should be removed from soil cover, as should hard dry crusts. Partially buried debris should be removed from the surface, particularly metallic debris.

Waste should be as homogeneous as possible and with relatively smooth surfaces. Haul roads should be removed or it should be recognized that the minimum size of detectable holes under the thicker haul road cover will be increased. Unfortunately, the placement of soil for the haul road, and movement of traffic over the road, make it a likely location for a leak.

A GCL component of a composite liner does not normally interfere with the ability to perform a leak survey, except when the GCL is of the bentonite/geomembrane type with the geomembrane placed down. In this case the current flow path into the subgrade is limited to the GCL seam area and the periphery of the entire GCL - the thin geomembrane prevents current flow through the center of the GCL panels into the subgrade. The efficiency of the survey is somewhat reduced.

At the conclusion of a survey, when removing soil cover to confirm the presence of a leak through the geomembrane of a composite liner, it must be remembered that, since the geomembrane has been forced into intimate contact with the clay layer to perform its required function of preventing liquid transmission along the interface, neither will air flow along the interface to feed a vacuum box. Thus, the electrical survey will identify a hole in the geomembrane that the vacuum box may not.

UNCOVERED LINERS

Water lance surveys (Peggs, 1993) will only function on a single geomembrane placed on a soil (or GCL) subgrade, or on the conductive primary geomembrane of a double geomembrane lining system. Again, the geomembrane must be directly underlain by an electrically conductive medium. In most cases, the floor of a pond will be surveyed by wading, then water will be pumped from the floor of the pond to the water lance for a survey on the side slopes. This saves time and water. However, if a gravity feed is required there must be a road around the periphery of the lagoon to allow access of a water tank. The water tank, preferably plastic, must be electrically isolated from the ground. Therefore, it must not leak. Deployment of liner should be such that water from the lance will not run off an unprotected edge onto subgrade soil. A dam of GCL and sandbags can prevent this. Note that it is quite difficult to maintain unassisted footing on smooth wet geomembrane with slopes exceeding 3H:1V. Sludge residues can make even flat surfaces very slippery.

SUMMARY

The requirement to perform geoelectric liner integrity surveys as the final stage of liner CQA is increasing. The need to perform investigative leak location surveys to isolate leaks that threaten the closure of a waste containment facility is also increasing, due to an apparent decrease in the knowledge, or lack of workmanship, of many of those newly involved with lining systems. A little additional forethought in the design and construction logistics of lining systems can significantly reduce the time and costs associated with performing such surveys, should the need become a regulated requirement (as it undoubtedly will), or should there be a need for an investigative analysis of a problem leak. The primary principle to note is that the electrically conductive medium above the liner must be isolated from the electrically conductive medium below the liner except at the leaks being identified.

REFERENCES

Boryta et al., (1985) United States Patent Number 4,543,525.

Darilek G.T, Laine D.L., Parra, J.O., (1989) "Electrical Leak Location Method for Geomembrane Liners: Development and Applications", Proceedings of Geosynthetics '89, IFAI, Roseville, MN, pp 456-466.

Laine D.L, and Darilek G.T. (1993) "Locating Leaks in Geomembrane Liners of Landfills Covered with a Protective Soil", Proceedings of Geosynthetics '93, IFAI, Roseville, MN, vol. 3, pp 1403-1412.

Laine D.L., Binley A.M. and Darilek G.T. (1997) "How to Locate Liner Leaks Under Waste", Proceedings of Geosynthetics '97, IFAI, Roseville, MN, pp 407-411.

Peggs I.D., (1993) "Practical Geoelectric Leak Surveys with Handheld, Remote, and Water Lance Probes: Concrete Basin and Waste Cell Liners", Proceedings Geosynthetics '93, IFAI, Roseville, MN, pp 1523-1532.

Peggs I.D., (1996) "Defect Identification, Leak Location, and Leak Monitoring in Geomembrane Liners", Geosynthetics: Applications, Design and Construction, Balkema, Rotterdam, pp 611-618.

CASE HISTORY OF GEOMEMBRANE DAMAGE ASSESSMENT

MICHAEL SNOW
GOLDER ASSOCIATES, USA
IAN BISHOP
GOLDER ASSOCIATES, USA
RUSSELL KEENAN
NORCAL/SAN BARNARDINO, INC., USA

ABSTRACT

This paper presents a case history of the installation, leak survey, damage assessment, and leak repair of the primary geomembrane liner in a double-lined 0.6 hectare septage impoundment at the Landers Sanitary Landfill, San Bernardino County, California. The case history outlines the importance of considering damage to geomembranes during construction and in particular during placement of soil covers. The case history also demonstrates the effectiveness of post-construction electrical leak surveys.

This case history highlights several important considerations in geomembrane design and construction: (1) construction quality control (CQA) monitoring is important during all phases of construction including during placement of soil materials; (2) geotextile cushions must be considered when soil particle sizes and loading conditions are critical; (3) specifying a minimum soil layer thickness beneath construction equipment plays an important role in protecting the geomembrane during construction and operations; and (4) leak surveys and re-surveys are effective in evaluating the performance of geomembrane liners.

INTRODUCTION

Leakage through holes in geomembranes is the primary mechanism for migration of liquids through geomembrane liners (Giroud and Bonaparte, 1989). Geomembrane holes caused by damage incurred during construction of modern geosynthetic liner systems can be a significant cause of excessive leakage. Although leakage through geomembranes can also result from defects unrelated to construction damage (i.e., pinholes, defective seams), the dimensions of construction damage defects typically exceed those resulting from other causes. Darilek and Miller (1998) reported damage of 190 mm x 76 mm caused by heavy machinery placing sand over the geomembrane. Defects with these dimensions are significant since they are typically

the dominant contributors to leakage at a site and their rate of leakage is likely to exceed acceptable leakage rates (ALRs) for a site.

In 1995, two 0.6 hectare septage drying ponds were constructed at the Landers Sanitary Landfill (LSL). The landfill is located in a remote arid area in San Bernardino County, California. The two septage ponds (East and West) were constructed with double-liner systems designed in accordance with state regulations. The double-liner system consisted of (top to bottom):

(1) 1.2 to 1.5 m of a gravelly sand protective layer with particle sizes of up to 150 mm;
(2) a 272 g/m^2 geotextile cushion;
(3) a 1.0-mm thick primary high density polyethylene (HDPE) geomembrane;
(4) a 150-mm thick sand leak detection layer;
(5) a 150-mm to 1.2-m thick gravel leak detection layer;
(6) a 272 g/m^2 geotextile cushion; and
(7) a 1.0-mm thick secondary HDPE geomembrane placed on a prepared subgrade.

A plan view and typical cross-section of the pond liner systems are presented in Figures 1 and 2.

The West pond was brought into service in November 1995 and has performed effectively with no observed leakage through the primary geomembrane. Before the East pond could be brought into service, significant leakage on the order of 400 liters per day (lpd) was measured in the leakage collection and removal (LCR) sump (see Figure 2) connected to the sand and gravel LCR layer. The leaking fluid originated from surface water precipitation resulting from heavy winter rains. The leakage jeopardized bringing the pond into service and the owner was considering completely replacing the liner system.

Geomembrane damage is often caused during installation of the liner system. The two ponds were built concurrently by the same contractor and installer, with few clues regarding the potential cause of the leakage. Construction quality assurance (CQA) services were provided by personnel with little or no experience in the installation of geosynthetic containment systems and detailed CQA documentation was not prepared. Proper CQA has been shown to result in reduced leakage rates (Bonaparte and Gross, 1990) and also provides valuable documentation regarding the quality of the installation.

LEAK SURVEY

Prior to replacing the liner system, the owner initiated a leak survey of the East pond to evaluate the extent and possible causes of the leakage. A mobile geomembrane leak location survey (MGLLS) was performed across the soil protective layer in the base of the pond. In general, electric current is passed between two metal electrodes, one inside the impoundment,

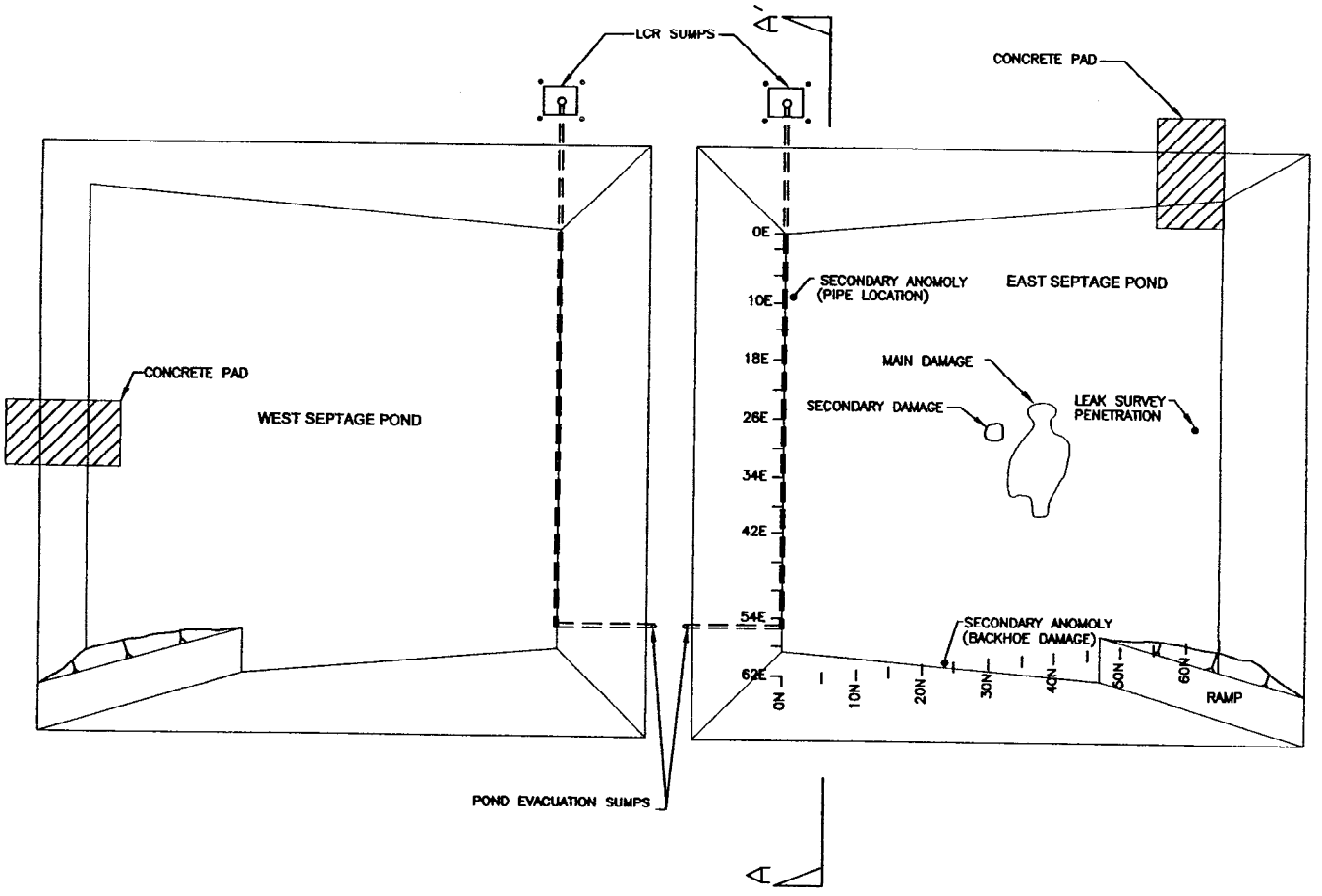

Figure 1. Plan View of Landers Sanitary Landfill Septage Ponds

one outside (Figure 3). With the synthetic liner intact, the two electrodes should be electrically isolated from each other by the liner. The resulting potential, measured as a potential difference between two non-polarizing electrodes, should be small but uniformly distributed over the liner. If the liner has a perforation(s), current will flow through the perforation(s) and the measured electrical potential will peak around the position of the perforation(s).

Data were collected using a multimeter on a 1 m grid. The results of the leak survey are presented on Figure 4. The leak survey detected a large, broad anomaly near the center of the pond as indicated by the crossover in voltage polarity on the cross-section also shown in Figure 4.

LEAK EVALUATION AND REPAIR

The main anomalous area identified during the initial leak survey was excavated over an area of approximately 8 m by 15 m using a backhoe and manual labor to remove the protective soil layer (see Figure 1). Several observations were made during the excavation:

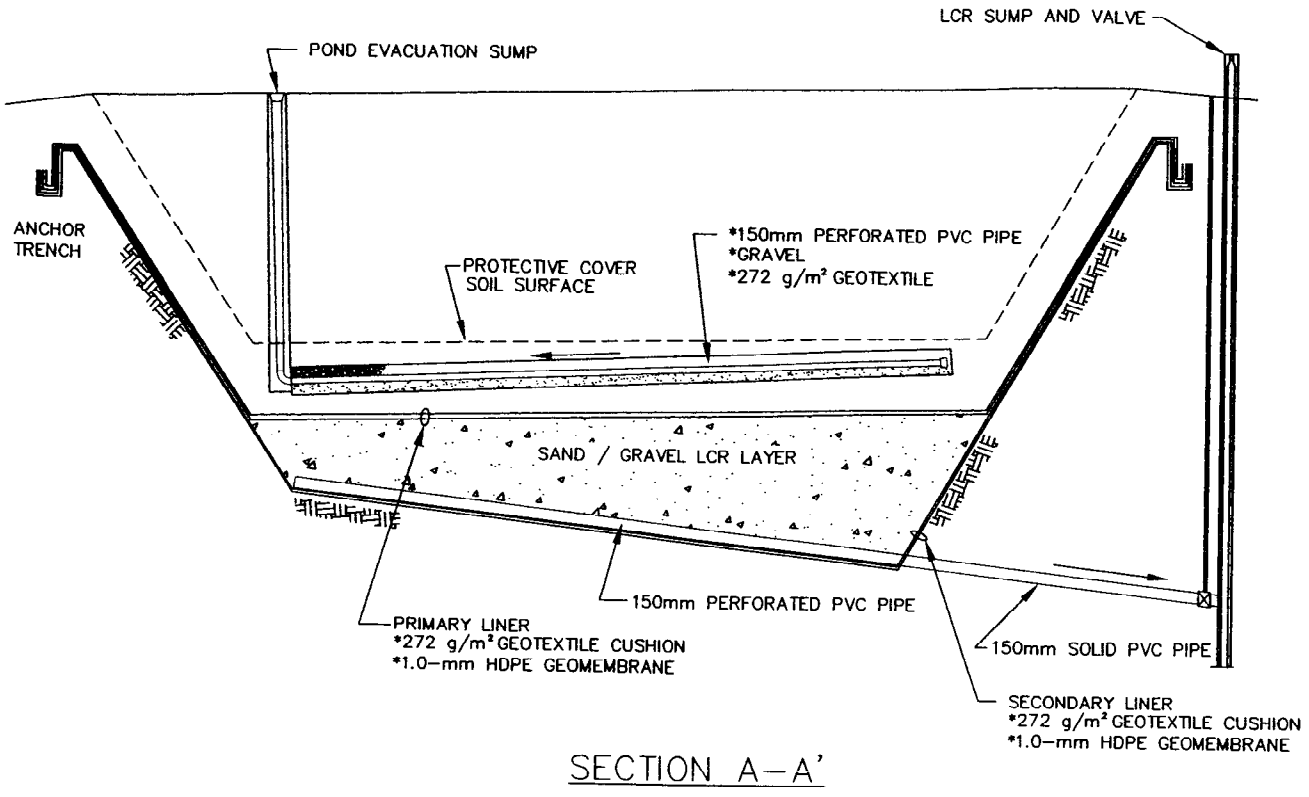

Figure 2. Typical Septage Pond North-South Cross-Section A-A'

- the geotextile cushion was either absent or had been displaced during construction causing the soil protective cover particles to come in direct contact with the primary geomembrane (see Figure 5);
- the soil in direct contact with the primary geomembrane was a very dense sand with approximately 10 to 15 percent of the particles (by weight) consisting of angular cobble and gravel particles up to 200 mm in diameter (see Figure 5);
- a 25-mm high wrinkle was observed in the primary geomembrane; and
- 13 perforations through the primary geomembrane and significant areas of other damage to the primary geomembrane, such as scratches and dimples in the primary geomembrane, were observed.

The 13 perforations were grouped into three (3) categories based on the probable cause of damage for each category. Category 1 included ten (10) perforations located along an east-west axis over a distance of approximately 2 m (see Figure 6). Each of the Category 1 perforations was in the form of a slit perpendicular to the axis. The slits ranged in width from 75 to 450 mm and were spaced at intervals of 200 mm. The nature of the Category 1 perforations was

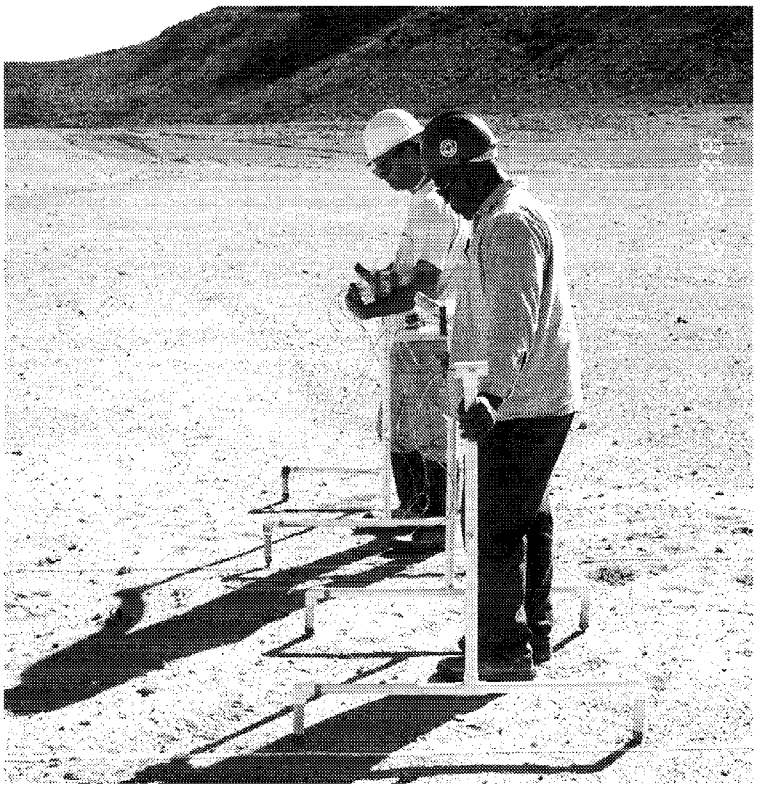

Figure 3. Electrical Leak Survey Setup

consistent with tears caused by the tracks of heavy machinery operating on a thin or nonexistent layer of protective soil cover.

Category 2 included two perforations in the form of "dimples" with diameters ranging from 125 to 175 mm (see Figure 7). Several additional dimples that damaged but did not penetrate the geomembrane were also observed with diameters up to 100 mm. The nature of the Category 2 damage was consistent with the penetration of soil particles into the geomembrane.

Significant scratches of the geomembrane were also observed in the vicinity of the perforations indicative that the soil particles were dragged along the geomembrane prior to penetration. The combination of the absent geotextile cushion, large angular soil particles, and proximity of heavy machinery to the geomembrane are believed to have contributed to the observed damage.

Category 3 included a single perforation in the form of a triangle 375 mm high by 550 mm wide (see Figure 7). The geomembrane was displaced from the apex to the base of the triangle. The nature of the Category 3 damage was consistent with the penetration caused by the blade or bucket of heavy machinery.

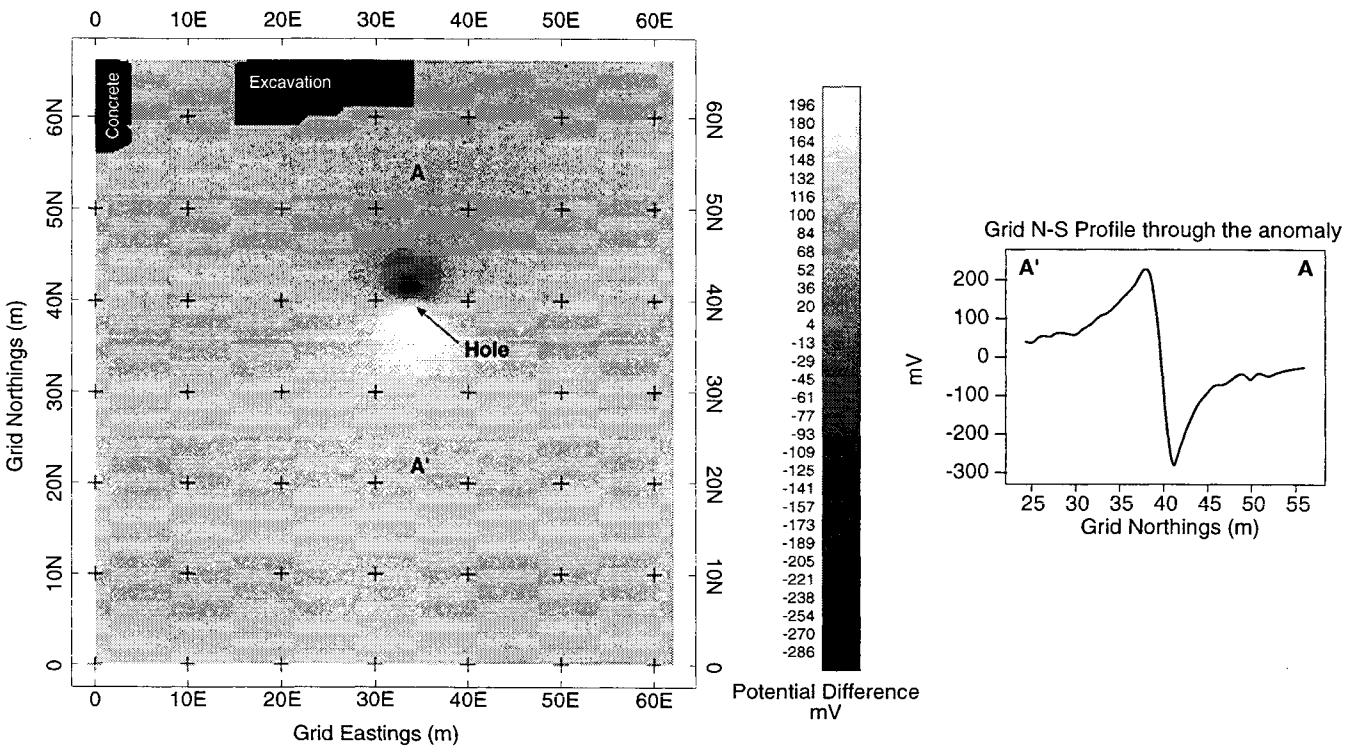

Figure 4. Results of Initial Leak Survey

The damaged area was repaired by placing a large HDPE geomembrane patch over the entire damage area, extrusion welding the patch to the primary geomembrane, and vacuum box testing the extrusion welds. The patch was covered by a 543 g/m^2 geotextile cushion and the soil protective layer material. Manual labor was used to remove large soil particles from the protective soil material as feasible. The repair work was observed by experienced CQA personnel and documented.

Following the repair work, a second leak survey of the entire pond was performed. The second leak survey was initiated because the large electrical anomaly generated by the large area of multiple perforations tends to mask or attenuate the effect of current flow through smaller holes. This is because current will tend to flow preferentially through the large area of perforations as this would be the path of least resistance. The second survey identified three additional anomalous areas (see Figure 1). Two of the areas were exhumed and one additional Category 3 perforation was observed and repaired. The second area exhumed did not uncover any damage, however, the geomembrane was penetrated by the backhoe operator during removal of the protective soil cover. Both exhumed areas were repaired in the same manner as the main

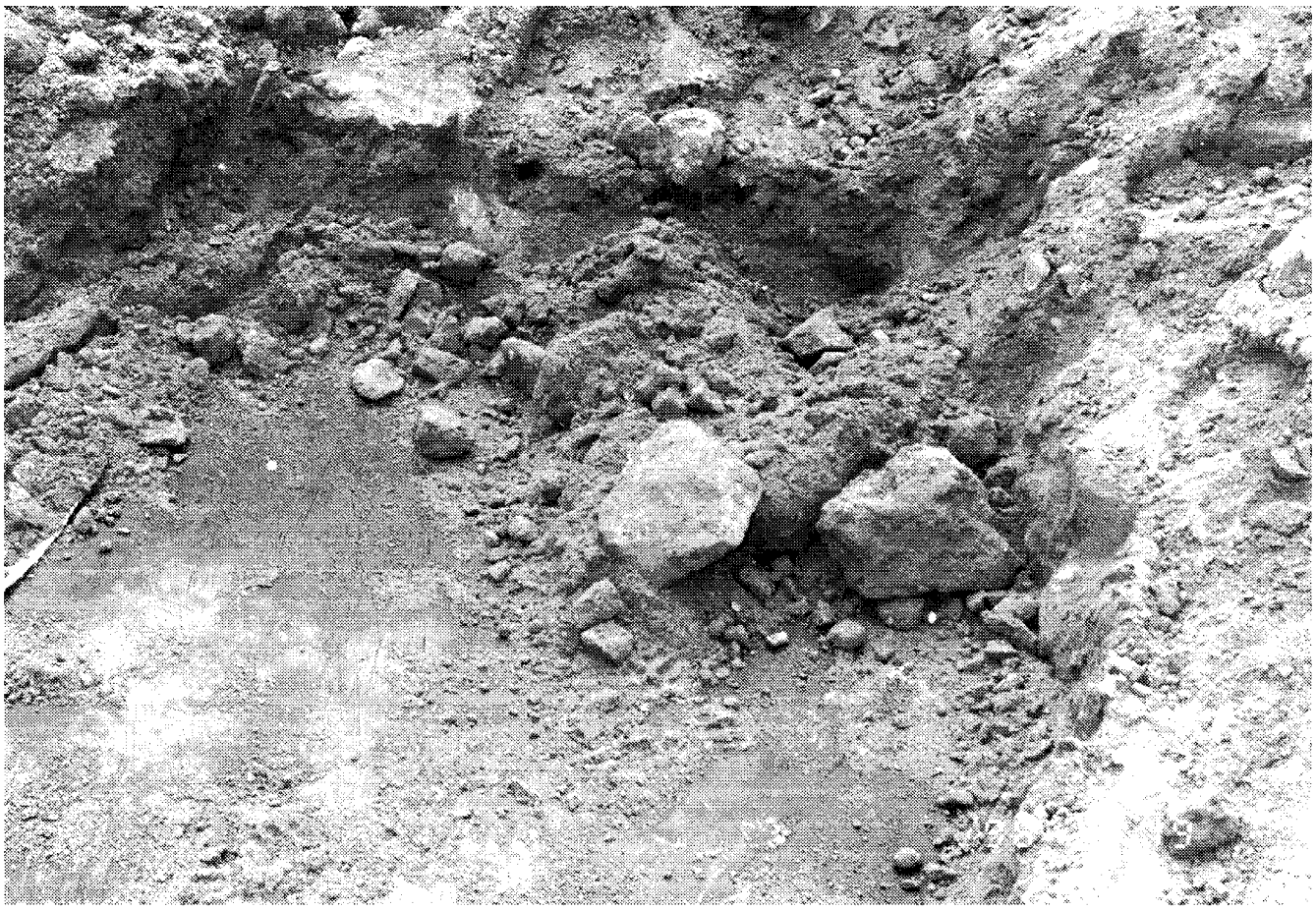

Figure 5. Missing Geotextile Cushion and Large Cobbles

damage area described before. The third area could not be exhumed at this juncture due to the presence of piping associated with the pond evacuation system (see Figure 2) and water present on the protective soil layer. The cause of the anomaly in the third area was not ascertained in this study but may have been caused by: (1) a penetration in the primary liner; or (2) the piping. Similar anomalies have been observed from electrical leak surveys in other landfills adjacent to piping.

Following completion of all evaluation and repair work, the leakage volumes were monitored regularly for a period of two weeks. Leakage volumes gradually decreased as the water trapped in the LCR layer drained into the sump. The observed leakage eventually stabilized to approximately 40 lpd. This observed leakage might be the result of a perforation present in the area of the third anomaly observed during the second leak survey or perforations beneath the median berm, which was not surveyed in this study. The reduced leakage was deemed acceptable by the regulatory agencies and allowed the pond to be brought into service. The cost to perform the leak survey and repair was less than 10 percent of the total cost needed to remove and replace the entire primary liner system.

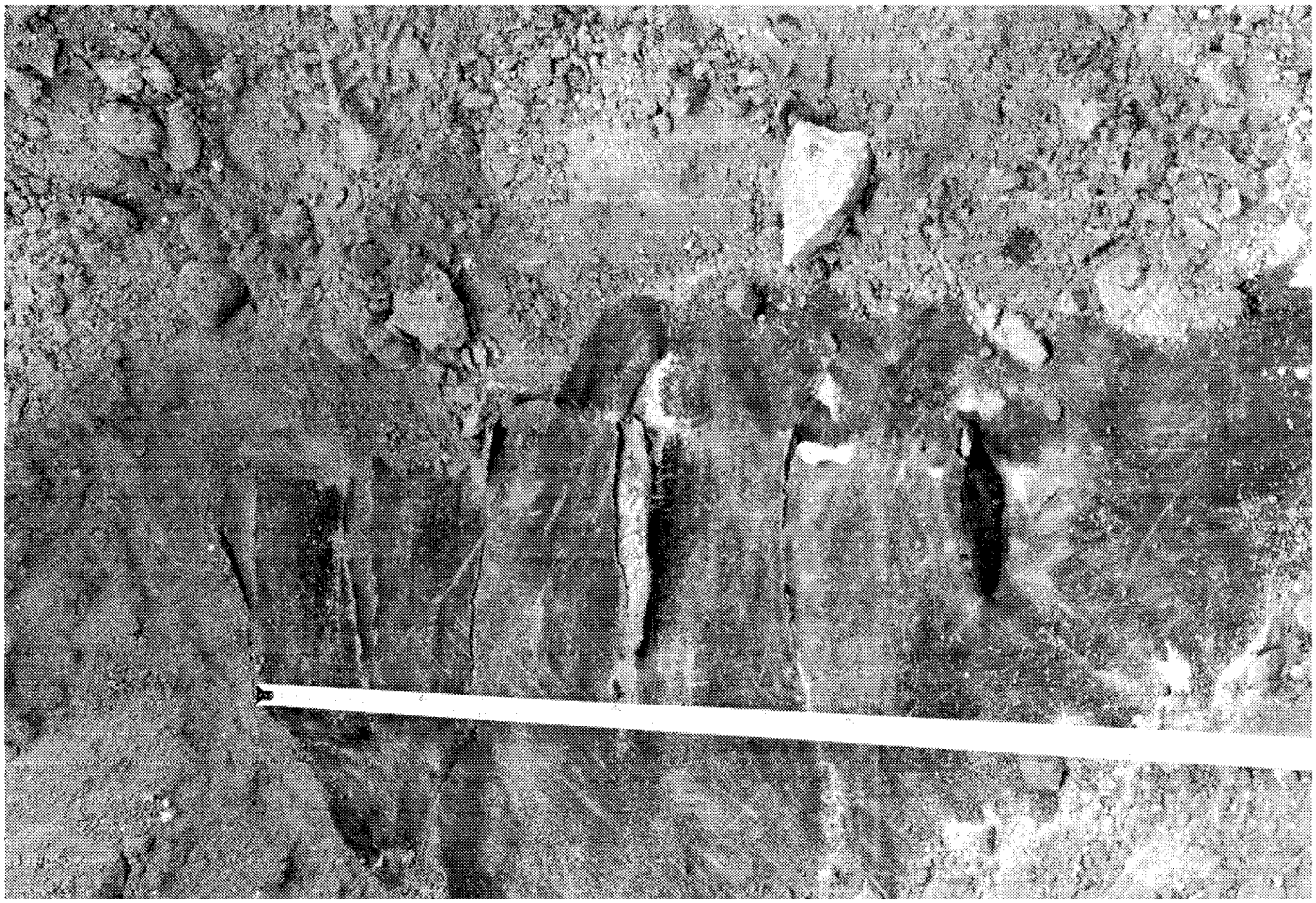

Figure 6. Category 1 Perforations

RECOMMENDATIONS

This case history highlights several important aspects of the design, construction, and CQA monitoring of geomembrane liner systems including: (1) specific details must be incorporated into the design to address the potential for construction damage; (2) CQA programs need to be vigilant during placement of protective soil covers where damage can be significant; (3) minimum requirements for construction need to be prescribed to avoid damage during protective soil placement; and (4) CQA programs should incorporate post-construction leak surveys, where practical, as an effective tool in controlling and identifying geomembrane damage during construction.

There is a need to consider the potential for construction damage during the design phase of a geomembrane liner project. Restrictions on maximum particle size of protective cover soils and use of geotextile cushions should be incorporated into all designs. Designers should consider operating stresses as well as construction stresses imposed on the liner system. In

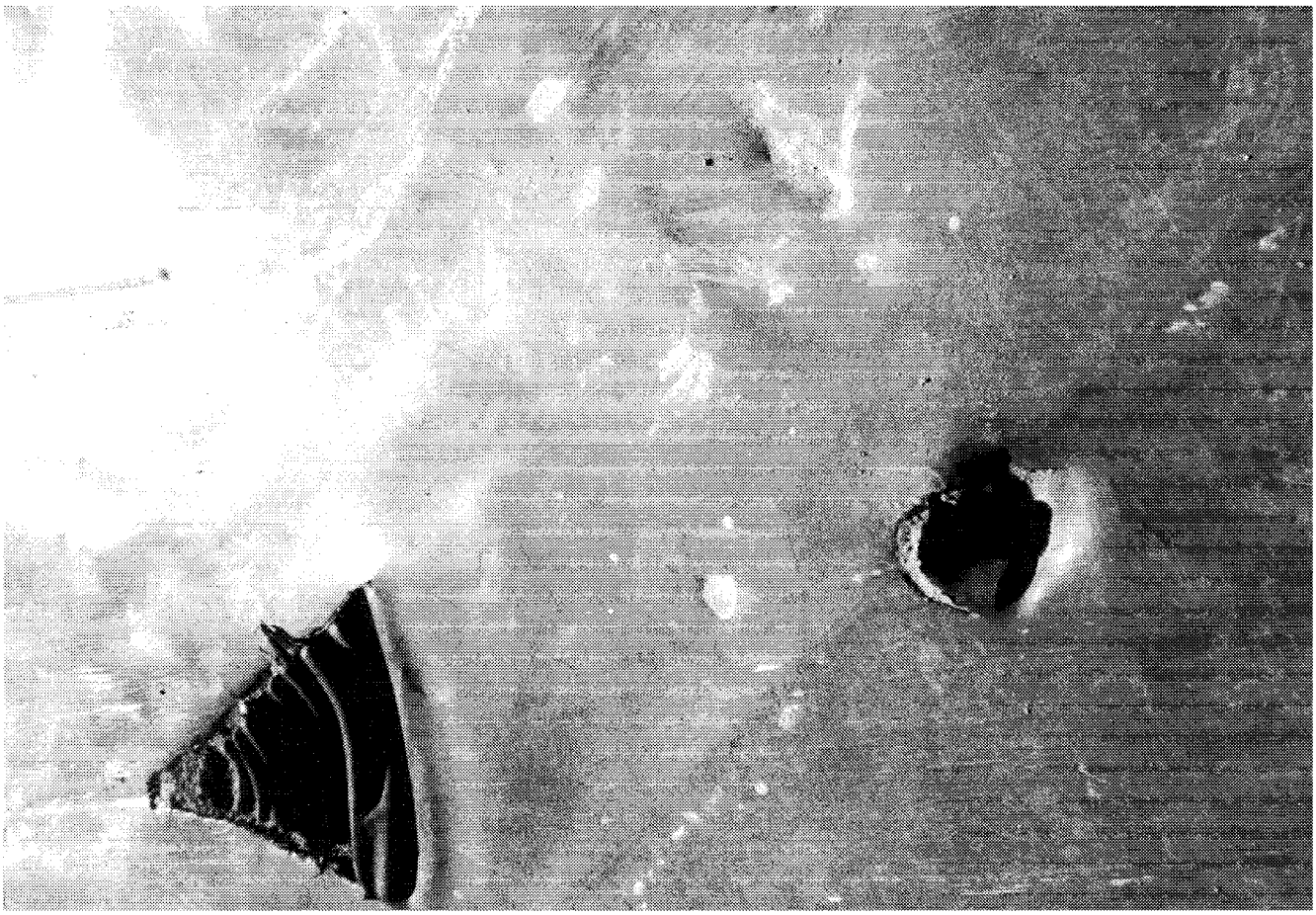

Figure 7. Category 2 and 3 Perforations

many cases, normal and shear stresses induced by heavy equipment can create the critical condition for the geomembrane liner. Construction specifications should specify the type of equipment and the minimum lift thickness to be used during placement of the protective soil cover. Minimum lift thickness specifications provide for a reduction in stresses induced in the liner by the heavy equipment but also provide for a margin of operator error. A lift thickness of 12 inches for the first lift would appear to be a minimum although thicker first lifts may be required depending on site-specific considerations and the type of equipment used. The use of nonwoven geotextile cushions is an effective means to enhance protection of the geomembrane liner. However, for this project it is questionable whether the 272 g/m^2 geotextile used would have provided adequate protection during construction given the nature of the protective soil cover materials.

CQA programs need to emphasize the monitoring of placement of the first lift of the protective soil cover placement as a full-time activity. In many cases this is regarded as a close-out activity where staffing is being reduced and attention is being focused on report preparation.

Damage created during placement of the protective soil cover is difficult to observe once the soil is placed over the geomembrane and in some cases the operator is not even aware of the damage. Full-time monitoring of this activity is critical particularly where post-construction leak surveys are not incorporated into the CQA program. Leak location surveys are a proven tool for use in the CQA program but not as a replacement for a sound CQA program. In Europe regulators demand a leak survey after installation of the protective soil cover. This provides many benefits to the overall CQA program: (1) the leak survey locates penetrations, particularly those caused during placement of the protective soil cover; (2) leak surveys make the contractor more vigilant during placement of the protective soil cover; and (3) leak surveys provide a second tier of CQA monitoring for the liner and greater reassurance to the regulators.

REFERENCES

Bonaparte, R.,and Gross, B., (1990) "Field Behavior of Double-Liner Systems", Waste Containment Systems: Construction, Regulation, and Performance, ASCE Geotechnical Special Publication No. 26, November, pp.52-83.

Giroud, J.P., and Bonaparte, R., (1989) "Leakage through Liners Constructed with Geomembranes – Part II. Composite Liners", Geotextiles and Geomembranes, vol. 8, no. 1, pp.71-111.

Darilek, G.T. and Miller, L.V., (1998) "Comparison of Dye Testing and Electrical Leak Location Testing of a Solid Waste Liner System", Proceedings, Sixth International Conference on Geosynthetics, March 25-29, pp. 273-276.

PERFORMANCE-BASED SPECIFICATION OF ELECTRICAL LEAK LOCATION SURVEYS FOR GEOMEMBRANE LINERS

G. T. DARILEK, P.E.
LEAK LOCATION SERVICES, INC., U.S.A.
D. L. LAINE
LEAK LOCATION SERVICES, INC., U.S.A.

ABSTRACT

Electrical leak location surveys can be a crucial part of the final quality control of geomembrane liner installations. The method has been offered as a commercial service since 1985 and is the only practical test method that can find holes in the liner after protective soil cover is put on the liner. During the past fourteen years the test method has been used on a wide variety of installations worldwide and is becoming a standard test method offered by several testing companies. However, merely specifying an electrical leak location survey as a requirement does not address the key elements needed to obtain a successful and meaningful leak location survey. A performance-based specification based on sound engineering practices is needed to achieve the specified degree of leak detection sensitivity and accuracy. This paper addresses the fundamental concepts of the electrical leak location detection sensitivity and provides information to allow design engineers, owners, and regulators to accurately specify electrical leak location surveys to achieve the desired results. A practical calibration test is described to determine and verify the measurement parameters needed to obtain a given leak detection sensitivity and to validate the various electrical leak location method implementations and field procedures.

INTRODUCTION

The electrical leak location method is a very powerful tool that can be used to locate leaks in geomembrane liners of landfills, ponds, and tanks. The method has several advantages over conventional test methods because the testing is accomplished after final construction, and after the liner is subjected to construction activity. In addition, this is the only effective method to locate leaks under the protective soil cover of a landfill liner. The initial development of the electrical leak location method began in 1981 and the first commercial surveys were performed in 1985. Today more than twenty companies worldwide offer various types of electrical leak location surveys. Therefore, personnel specifying electrical leak location surveys must understand the parameters that

affect the leak detection sensitivity and specify measures to verify the proper operation of the field equipment and procedures.

ELECTRICAL LEAK LOCATION METHOD

General. Figure 1 is a diagram showing the electrical leak location method. The electrical leak location method is to detect electrical paths through holes in the geomembrane liner. A voltage is connected to an electrode placed in soil or water covering the liner and to an electrode in contact with conducting material under the liner. Because the geomembrane liner is an electrical insulator, current will flow only through the leaks. This current produces localized anomalous areas of high current density near the leaks. These anomalous areas are located by making electrical potential measurements in the survey area. The data is typically recorded and plotted for analysis.

ANALYSIS

Leak Detection Sensitivity. Leak detection sensitivity is the ability to find leaks of a specified size. The detection of leaks using electrical methods is highly dependent on the proper implementation of the selected survey method, type of equipment, survey procedures, site characteristics, data interpretation, and experience of the survey personnel. The two primary controllable factors affecting leak detection sensitivity are the level of current flowing through the leak, and the distance from the leak that the leak location measurements are made. The amplitude of the leak signal is proportional to the amount of electrical current flowing through the leak. To increase the current, the voltage impressed across the liner must be increased. Also, the leak signal rapidly attenuates with distance from the leak. Therefore, increasing the impressed voltage and

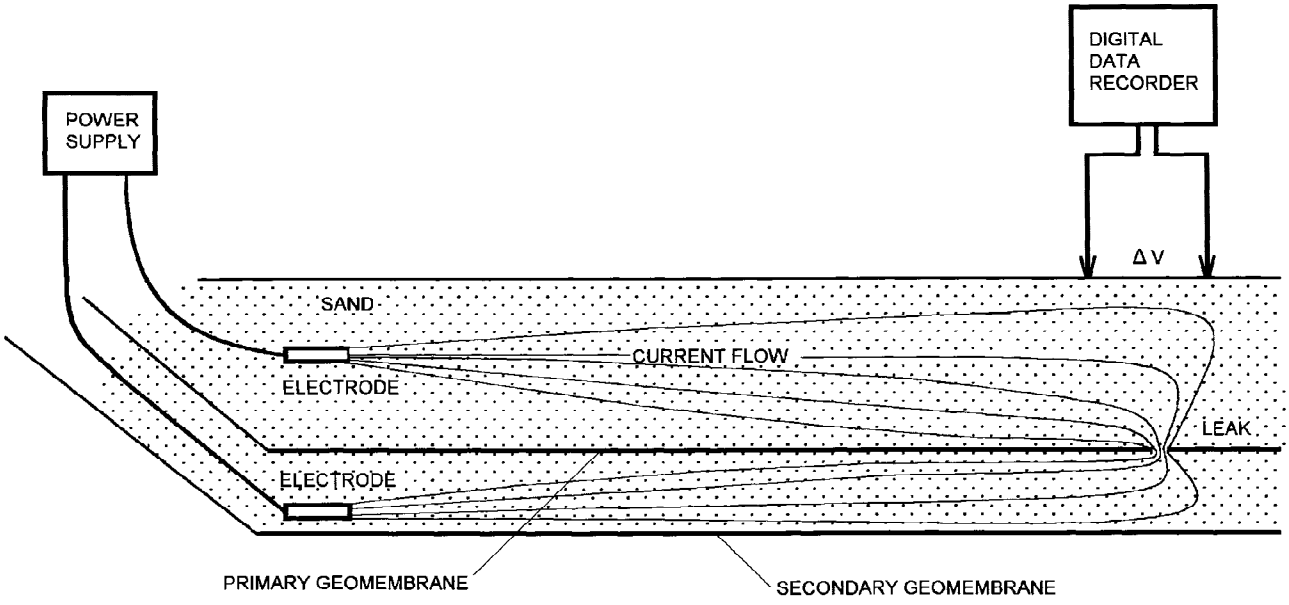

Figure 1. Diagram of the Electrical Leak Location Method

increasing the measurement density will increase the size of the leak signals to improve leak detection sensitivity. The leak detection sensitivity also depends on the electrical resistivity of the materials above and below the liner, the thickness of the soil overlying the liner, and other practical matters such as the homogeneity of the material.

Analysis of Leak Detection Sensitivity. The electrical response of a leak in a geomembrane liner was derived by Parra (1988). He derived the electrical potential for a current source in a three-layer half-space. Figure 2 shows that the very complicated result can be closely approximated by the very simple model of the potential in an infinite conducting half-space (Darilek et al., 1996). For that model the potential difference caused by current flowing from the current source is derived as:

$$\Delta V = \frac{I \rho}{2 \pi r (r + \Delta r)} \qquad (1)$$

where ΔV = voltage difference (leak signal); I = current (current flowing through the leak); ρ = resistivity of the half space (resistivity of the soil covering the liner); r = distance from the current source (distance from the leak); and Δr = radial distance between the measurement electrodes. From this equation it can be seen that the leak signal decreases essentially inversely with the square of the distance from the leak. The leak signal is also directly proportional to the current flowing through the leak. By Ohm's law, the current flowing through a leak is proportional to the voltage impressed across the leak and inversely proportional to the resistance of the leak. The resistance of a leak can be modeled as the sum of: 1) the contact resistance with the material above the leak; 2) the resistance of the material in the leak; and 3) the contact resistance with the material below the leak. For circular leaks the values for terms 1 and 3 can each be closely approximated using the equation of resistance of a plate ground (Sunde, 1969) at the surface of the earth, which is:

$$R = \frac{\rho}{4 a} \qquad (2)$$

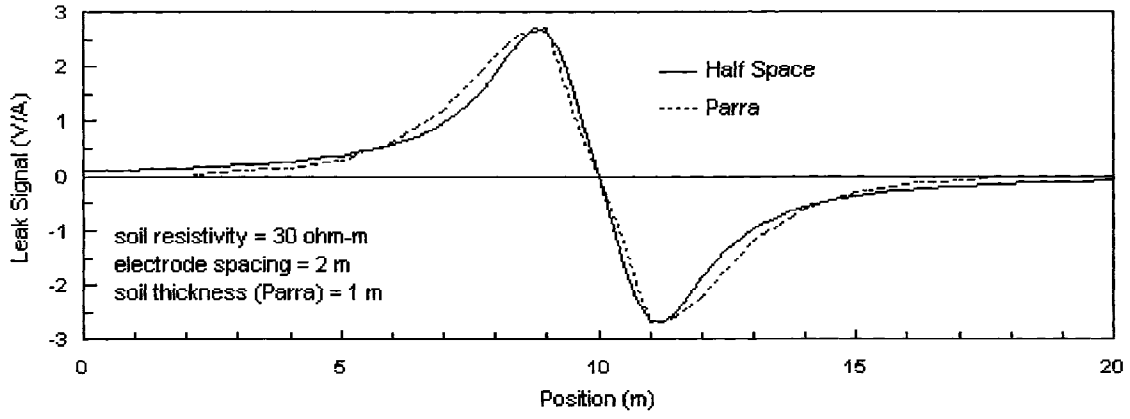

Figure 2. Comparison of Two Mathematical Models for Leak Signal

where R = resistance; and a = radius of the leak. For circular leaks, term 2 is calculated from the definition of resistance as:

$$R = \frac{\rho t}{\pi a^2} \tag{3}$$

where t = thickness of the liner. Combining these terms yields:

$$R = \rho \left(\frac{1}{2a} + \frac{t}{\pi a^2} \right) \tag{4}$$

For most leaks of practical interest, the leak radius is much greater than the thickness of the liner, so the second term in the parentheses can be ignored. From this exercise, the resistance of a leak is inversely proportional to the radius of the leak, so the leak signal will be approximately proportional to the radius of the leak. Figure 3 is a plot of the leak signal amplitude versus distance for several values of excitation current using these relationships. The curves are for a 1 mm liner, 10 mm radius leak, 30 ohm-meter soil, and a 1 m distance between the measurement electrodes. The curves show the importance of using a high voltage and making the measurements at close spacings. This analysis assumes ideal conditions of homogeneous soil, no voltage drop because of multiple leaks or other extraneous electrical paths, and no measurement noise. For rapid field data acquisition under average field conditions, measurement noise can be in the 5 to 20 millivolt range. Therefore, a valid leak signal cannot be measured for many combinations of voltage and measurement spacing previously shown in Figure 3. For these and other practical reasons, a safety factor must be used, for example by making the measurements on closer spacings. Also, because field data frequently has invalid data points, the spatial leak signal must be adequately sampled so the shape of the leak signal can be recognized as being distinct from invalid data points. However, these relationships provide important engineering guidelines for establishing or comparing leak location survey parameters.

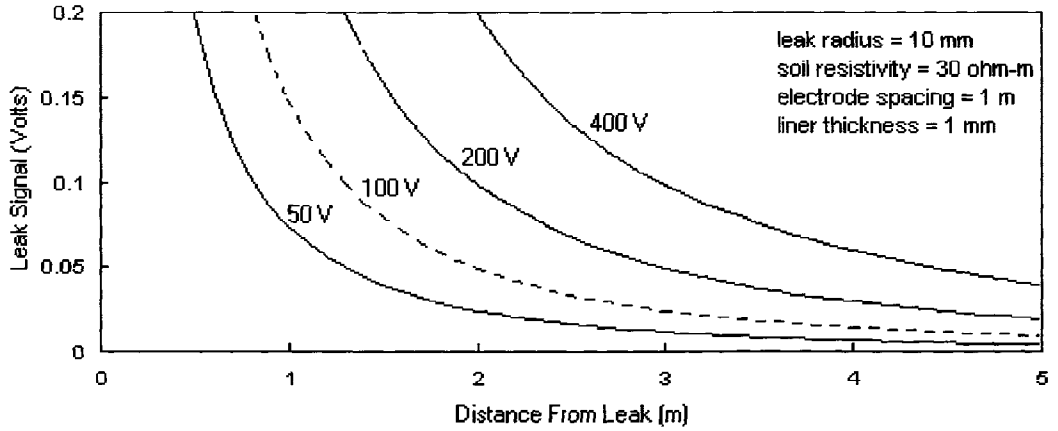

Figure 3. Leak Signal Amplitude versus Distance from Leak for Various Excitation Voltages

This analysis shows the need for establishing criteria for leak detection sensitivity. A leak survey taken with low excitation voltage, with wide measurement spacings, or without a systematic method for recording the data can produce invalid results. One approach to specify leak detection procedures is to specify all of the minimum parameters and procedures to conduct a survey. However, this approach would tend to unnecessarily stifle innovation. This specification rationale would not allow variations in the application of the method, or would be a weak specification to allow for variations. Because electrical leak location surveys are in their growth stage, such a specification method is not recommended. Instead, a performance-based specification can be used under which a minimum performance is specified, and the method used to obtain this performance can be decided by each practitioner.

PERFORMANCE-BASED SPECIFICATIONS

The most important parameter for a performance-based specification for electrical leak locations surveys is leak detection sensitivity. Sensitivity is defined as the minimum size leak that will produce a specified output signal with a specified signal-to-noise ratio. A typical leak detection sensitivity for surveys with 600 mm of soil on the liner is a 10-mm leak diameter leak, although much smaller leaks are often easily detected. Leak detection sensitivity is different from leak detection accuracy, which is the maximum error in the distance between the measured leak signal and the actual position of the leak. The leak location sensitivity can be verified by making measurements near an actual leak put into the liner. Although this method is the most valid, it requires the leak to be repaired.

As an alternate, an artificial leak can be used. An artificial leak is an electrical equivalent of a leak in a liner - an area at the liner depth where electrical current can flow to the material below the liner. An artificial leak is an electrode buried in the soil at the liner depth, connected to a length of insulated wire, the other end of which is connected to a suitable electrode in contact with the conducting material below the liner. The artificial leak should be defined in the construction quality control plan and should be specified to correspond to the leak detection sensitivity that is desired for the specific site. The most critical part of the artificial leak is the electrode buried above the liner. It can be specified to be a metal coupon of a specified size, an actual hole in a calibration cell, or even an insulated wire with a specified short length of insulation stripped off. A calibration cell can be a flat, electrically-insulating container with a top that is the approximate thickness of the geomembrane liner. A hole that corresponds to the desired leak detection sensitivity is placed in the top of the container. A suitable metal electrode connected to the insulated wire is located inside the bottom of the container. The container is filled with a sample of the actual soil that is placed on the liner.

To more closely correspond to an actual leak, a series resistor can be placed in the artificial leak circuit to simulate the resistance of the path between the leak and the power supply electrode placed below the liner. The equivalent path resistance of the medium below the liner depends on several factors, but a first order approximation can be a specified portion of the measured resistance of the circuit between the power supply electrodes placed above and below the liner.

The artificial leak then be used while collecting data along survey lines or on a grid at various distances from the artificial leak. The ends of the survey line or the edges of the grid should extend beyond the influence of the artificial leak. The data is inspected to determine the maximum distance that the leak can reliably be detected with a specified signal-to-noise ratio. The noise is the extraneous signal that is not related to a leak. One method to measure the level of the noise is to make measurements with the excitation signal disconnected. The maximum peak-to-peak value of the noise signal can be defined as being the noise level. The noise signal must be defined over a measurement interval. The measurement interval can be equal to the spatial width of the measured leak signal, or over a specified number of measurements. A leak signal with a signal-to-noise ratio of 3:1 as defined above can be reliably recognized as a valid leak signal.

The actual leak location survey must then be taken with the survey line or grid spacing no more than twice the distance from which the artificial leak can be reliably detected. A level of sampling redundancy can be specified so that if bad data points are taken, the leak detection sensitivity would not be compromised. The position of the excitation electrode can be arbitrary for the test, but production survey measurements must not be taken any farther than the distance to the excitation electrode during the tests with the artificial leak.

SUMMARY AND CONCLUSIONS

Because several implementations of electrical leak location methodologies are evolving, specifications must be written to ensure that the desired leak detection sensitivity is obtained. Rather than rigidly specifying the exact field procedures and equipment capabilities, a performance-based specification is recommended. By using a synthetic leak, measurements can be made to determine the leak detection sensitivity for measurements made at various spacings from the synthetic leak. The measurements that successfully detect the leak with a specified signal-to-noise level define the sampling interval and measurement spacings for the production survey. A similar rationale can be used for electrical leak location surveys made with only water covering the liner.

REFERENCES

Darilek, G.T., Corapcioglu, M.Y., and Yeung, A.T.,"Sealing Leaks in Geomembrane Liners Using Electrophoresis," Journal of Environmental Engineering, June, 1996.

Parra, J.O., "Electrical response of a leak in a geomembrane liner," Geophysics, Vol. 53 No. 11, November 1988.

Sunde, E.D., Earth Conduction Effects in Transmission Systems, Dover Publications, Inc., 1968, New York, 370 pages.

DISTRIBUTIONS OF LATERAL EARTH PRESSURE AND REINFORCEMENT TENSION INSIDE THE GEOSYNTHETIC REINFORCED SOIL RETAINING WALLS

WEI F. LEE

DEPARTMENT OF CIVIL ENGINEERING
UNIVERSITY OF WASHINGTON, U.S.A

ABSTRACT

Present internal stability design of the geosynthetic reinforced soil (GRS) walls is based on the limiting equilibrium concepts and requires an assumption of the lateral earth pressure distribution against the face of the reinforced section in order to obtain the tensile stresses resisted by the reinforcement. Available evidence from full-scale and model GRS walls indicates that these assumptions tend to significantly overestimate the internal stress distribution within the structure. In an effort to develop an appropriate internal stability design for GRS walls, an alternate approach to obtain the distribution of lateral earth pressure behind the wall face is presented in this paper. And it appears to improve estimates of the lateral earth pressure distribution behind the wall face and reinforcement tensions of GRS walls.

INTRODUCTION

The most common design procedure for the internal stability of geosynthetic reinforced soil (GRS) retaining walls is the U.S. Forest Service tie-back wedge technique developed by Bell and Steward (1977; see also Allen and Holtz, 1991). This method is based on the limiting equilibrium concepts and requires an assumption of the lateral earth pressure distribution against the face of the reinforced section in order to obtain the tensile stresses that must be resisted by the reinforcement. For wrapped-face GRS walls, usually classical Rankine active earth pressure conditions are assumed, while higher earth pressures are often assumed for steel strips and bar mats reinforced walls (Christopher, et al., 1990; Allen and Holtz, 1991). Available evidence from full-scale and model GRS walls indicates that these assumptions tend to significantly overestimate the internal stress distribution within the structure (Bell, et. al., 1983; Rowe and Ho, 1993; Allen et al., 1992; Christopher, 1993). These observations suggest that the assumptions of conventional lateral earth pressure theory for the tie-back wedge analyses is not appropriate for estimating the lateral earth pressure distribution of

GRS walls. To develop an appropriate internal stability design for GRS walls, an alternate approach to obtain the internal distribution of lateral earth pressure behind the wall face is needed, especially for the popular segmental block faced GRS retaining walls. This paper presents one alternate approach in the form of an analytical model that appears to yield reasonable estimates of the internal stresses of GRS walls.

In order to verify the newly developed analytical model, its results were compared with the performance of a segmental GRS retaining wall built in Algonquin, Illinois. Information on the lateral earth pressure distribution was obtained from numerical modeling results and computed using the newly developed analytical model. Feasibility of the developed analytical model is carefully examined.

NEW ANALYTICAL MODEL

An important consideration of present internal design of GRS walls is the lateral earth pressure distribution behind the face of the wall. Figure 1 shows the lateral earth pressure distribution behind the face of a conventional unreinforced retaining wall.

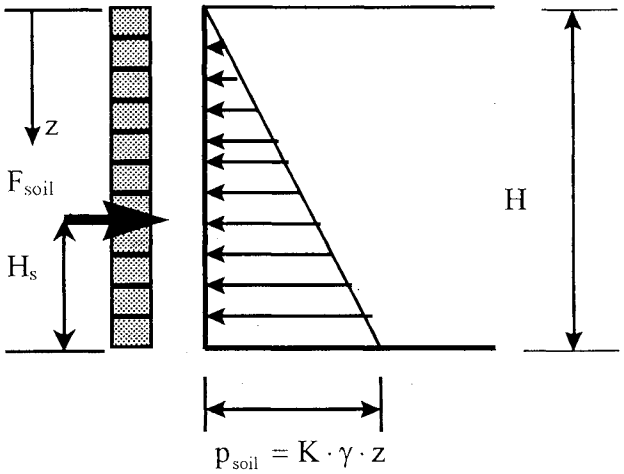

$F_{soil-*-**}$: Total earth force supported by facing blocks,
H : Height of wall,
H_s: Location of the F_{soil},
K : Lateral earth pressure coefficient, and
γ : Unit weight of soil.

Figure 1. Lateral earth pressure distribution of an unreinforced retaining wall.

Equation 1 is the general mathematical expression of the lateral earth pressure distribution of this case.

$$p_{soil} = K \cdot \gamma \cdot z \qquad (1)$$

where $K=K_0$, the lateral earth pressure coefficient at rest.
$K=K_a$, active lateral earth pressure coefficient.

When planar reinforcements such as geosynthetics are inserted into the wall backfill, the lateral earth pressure distribution will is changed because of the presence of the reinforcement tensions, as shown schematically in Figure 2.

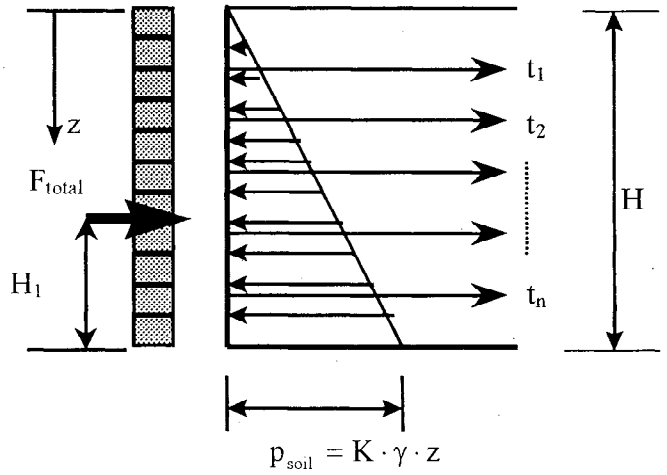

F_{total}: Total force supported by the facing,
t_n : Reinforcement tension per unit width at reinforcement layer n, and
H_1: Location of the F_{total}.

Figure 2. Lateral earth pressure distribution in a geosynthetic reinforced retaining wall.

The lateral GRS composite distribution can be determined by superposing the lateral earth pressure and the reinforcement tensions behind the wall face (Figure 3). In order to characterize the distribution of the GRS composite, a new lateral pressure coefficient, K_{comp}, is defined as the composite lateral earth pressure coefficient of the geosynthetic reinforced soil.

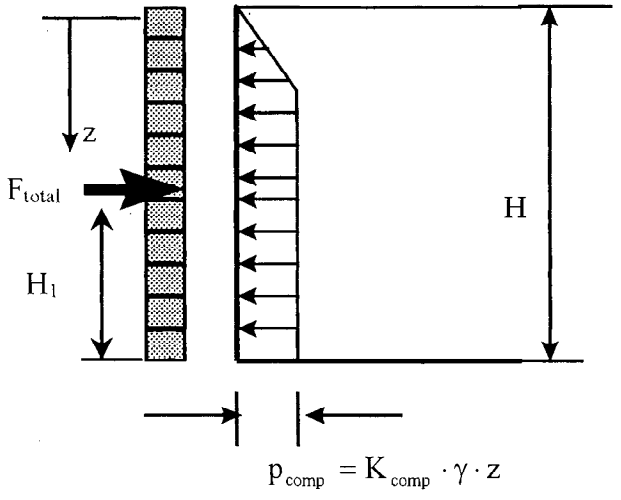

K_{comp}: Reinforced soil earth pressure coefficient.

Figure 3. Lateral composite pressure distribution of a reinforced retaining wall.

The mathematical expression of K_{comp} at any depth from the top of the backfill can be derived by comparing Figures 2 and 3 (Equation 2).

$$F_{total}(z) = F_{soil}(z) - \sum_{i=1}^{n} t_i \quad (2)$$

Where $F_{total}(z)$: Total force supported by the facing at depth z.

$F_{soil}(z)$: Total earth force supported by the facing at depth z.

$\sum_{i=1}^{n} t_i$: Total tensile forces of reinforcement at depth z.

By introducing the integral forms of the terms and recognizing that $F_{soil}(z) = \int_0^z p_{soil}(z)dA$, Equation 2 can be re-written as Equation 3.

$$F_{total}(z) = \int_0^z p_{comp}(z)dA = \int_0^z p_{soil}(z)dA - \sum_{i=1}^{n} t_i \quad (3)$$

By assuming that the retaining wall has width equal to unity (dA = dz) and performing the integration with definitions of the lateral earth pressure distributions as shown in Figures 1, 2, and 3, Equation 3 can be reduced to Equation 4.

$$F_{total}(z) = K_{comp} \cdot \gamma \cdot \frac{z^2}{2} = K_{soil} \cdot \gamma \cdot \frac{z^2}{2} - \sum_{i=1}^{n} t_i \quad (4)$$

The mathematical expression of the composite lateral earth pressure coefficient at any depth can then be obtained by rearranging Equation 4 (Equation 5).

$$K_{comp}(z) = K_{soil} - \frac{2 \cdot \sum_{i=1}^{n} t_i}{\gamma \cdot z^2} \quad (5)$$

Reinforcement tensions needed to stabilize the backfill soil at depth z can also be obtained by rearranging Equation 4 (Equation 6).

$$\sum_{1}^{n} t_i(z) = \frac{\gamma \cdot z^2}{2} \cdot (K_{soil} - K_{comp}) \quad (6)$$

CASE STUDY PART I: NUMERICAL MODEL

Direct measurements of the lateral earth pressures behind the face of the GRS retaining walls are not available at this stage because the difficulty occurs in installing appropriate instrumentation. However, reliable prediction of the GRS composite lateral earth pressures can be obtained from a well-developed numerical

model that is capable of reproducing internal strain measurements of a GRS wall. In order to verify the new analytical model presented above, a numerical GRS wall model was developed using the computer program FLAC (Itasca Consulting Group, 1993). FLAC Model Al-W9 was able to simulate the performance of one of the FHWA test walls built in Algonquin, Illinois (Bathurst, et al., 1993) with good agreement. This wall was reinforced with a flexible polyester geogrid and had modular precast concrete blocks as the face system. Figure 4 shows the cross-section and material properties of the Algonquin wall.

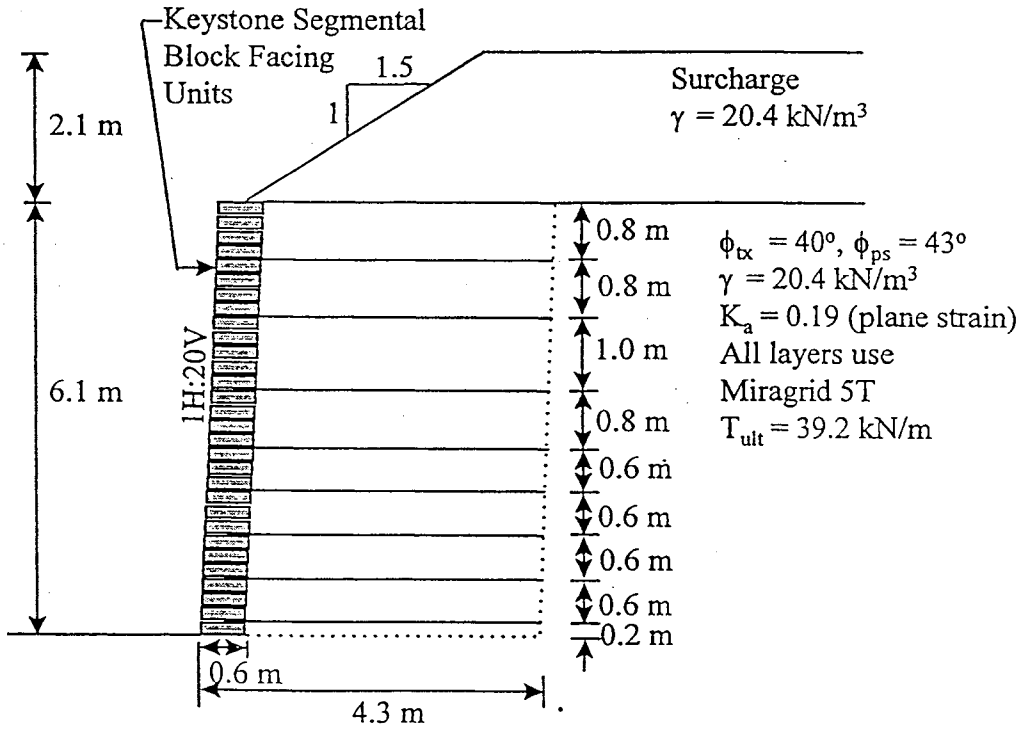

Foundation soil is 5 m of dense gravelly sand or fine to medium sand underlain by very dense sandy silt

Figure 4. Cross-section and material properties of the Algonquin wall (figure drawn by T.M. Allen).

FLAC Model Al-W9 was able to reproduce the axial strain in the reinforcement of the Algonquin wall quite well (as shown in Figure 5). The peak strain locations, the peak strain magnitudes, and the strain distributions agree well with the strain gage measurements obtained from reinforcement layers 2, 4, and 6. FLAC Model Al-W9 is confirmed to be able to provide reliable the internal stress information of the Algonquin wall.

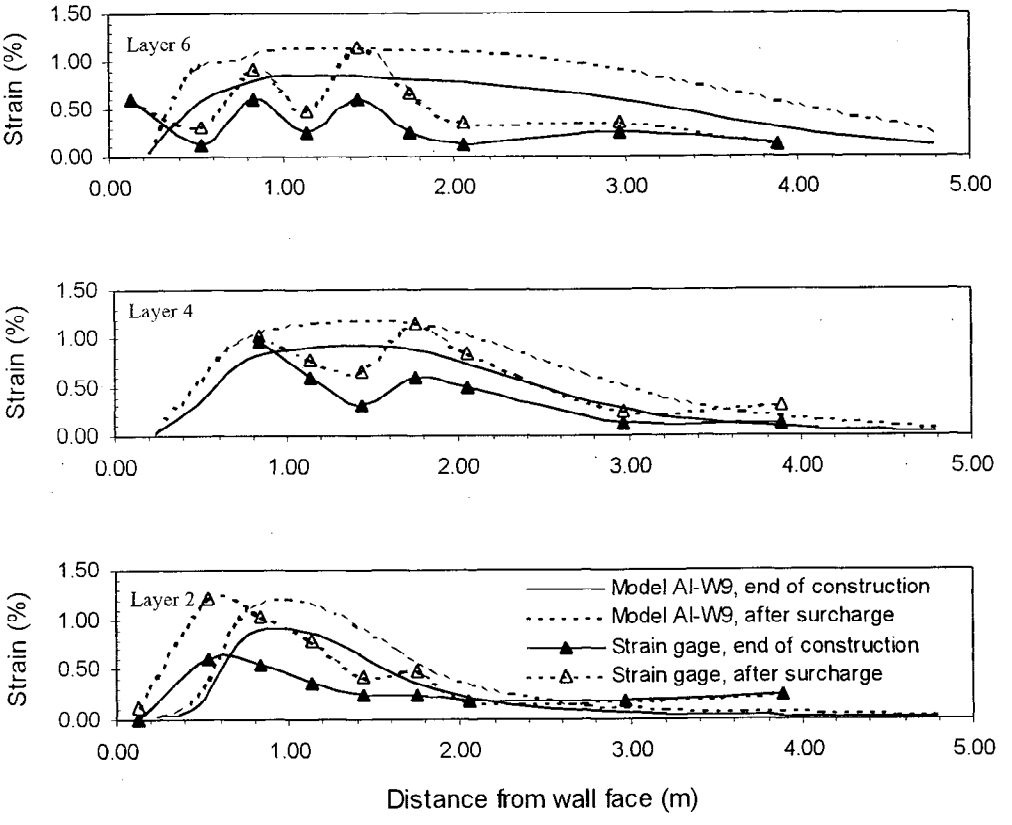

Figure 5 Predicted and measured reinforcement strain distribution for Algonquin wall.

CASE STUDY PART II: VERIFICATION OF THE NEW ANALYTICAL MODEL

To verify the new analytical model of the composite lateral earth pressures and reinforcement tensions, modeling results of the FLAC Model Al-W9 were introduced into the new analytical model to calculate the required reinforcement tensions. The calculated reinforcement tensions were then compared with the field measurements. Figure 6 shows the values of K_{comp} of the Algonquin wall versus the height of the wall both at the end of construction and after surcharge. These values were determined by reducing the numerical modeling result of FLAC Model Al-W9 using Equation 7. Typical value of K_{comp} can be determined as 0.18.

$$K_{comp}(z) = \frac{\sigma_h(z)}{\gamma \cdot z} \qquad (7)$$

where $\sigma_h(z)$ = horizontal geosynthetic reinforced earth pressure.

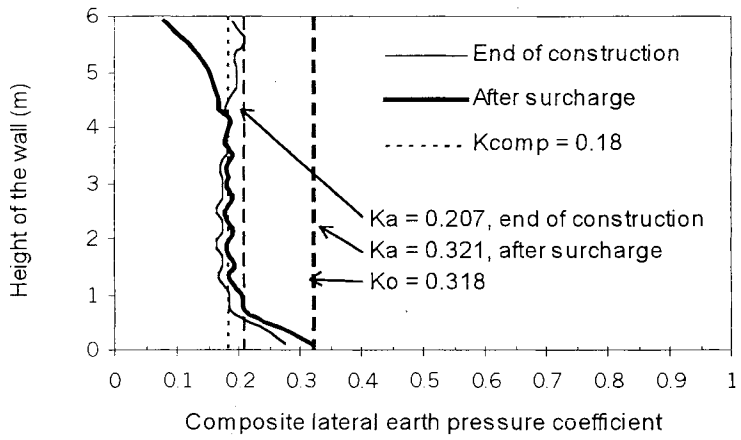

Figure 6 Composite lateral earth pressure coefficient for Algonquin wall, obtained from FLAC Model Al-W9.

Figures 7 and 8 show the predicted reinforcement tensions in comparison to the measured reinforcement tensions and reinforcement tensions calculated using the tie-back wedge method. The predicted reinforcement tensions were calculated using Equation 6 where K_{comp} = 0.18 and K_{soil} = K_a or K_0. The measured reinforcement tensions were converted from the field strain gage measurements of the reinforcement. At end of construction (Figure 7), the new analytical model was able to include the reinforcement tensions of Algonquin wall within its predictions of K_0 and K_a conditions, while the reinforcement tensions calculated using the tie-back wedge method tends to overestimate the reinforcement tensions.

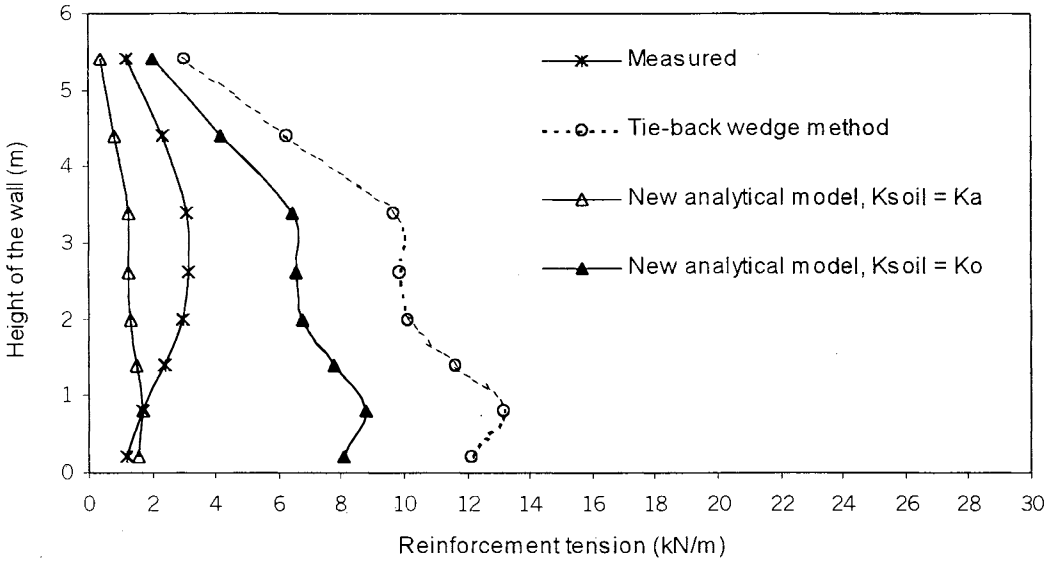

Figure 7 Predicted and measured reinforcement tension for Algonquin wall, end of construction.

As shown in Figure 8, predictions of the new analytical model (both K_0 and K_a conditions) provide a much better estimate for reinforcement tensions than the tie-back wedge method after surcharge is applied to the Algonquin wall.

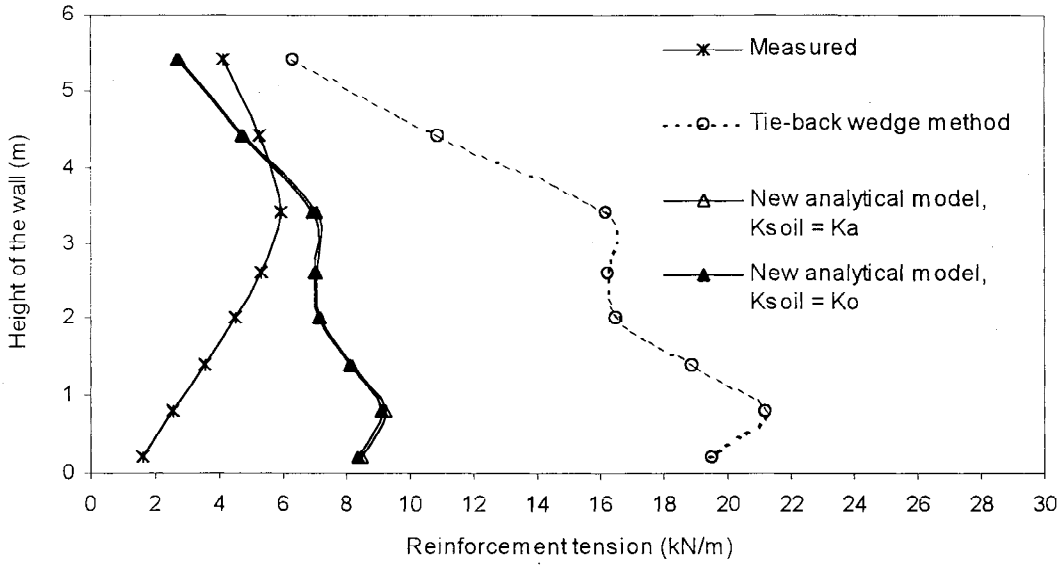

Figure 8 Predicted and measured reinforcement tension for Algonquin wall, after surcharge.

DISCUSSIONS, CONCLUSIONS, AND FUTURE WORKS

Equation 5 shows that the GRS composite lateral earth pressure distribution is a function of the height of the wall, unit weight and the lateral earth pressure coefficient of the backfill soil, and the distribution of the reinforcement tension. The reinforcement tension is a function of strength properties of reinforcement, arrangement of the reinforcement (including number of layers and length of reinforcement).

Equation 5 also indicates that the lateral geosynthetic reinforced earth pressures behind the wall face can be less than the active lateral earth pressures when the backfill reaches its active state and the reinforcements start to provide tensile forces to reinforce the backfill. Result shown in Figure 6 does confirm this observation.

Results shown in Figures 7 and 8 indicate that prediction of reinforcement tensions within the Algonquin wall can really be improved by using the new analytical model (Equation 6).

The new model tends to underestimate the reinforcement tensions of the Algonquin wall at height above 4m. Possible reason for this discrepancy is that the new model does not include the additional reinforcement tensions due to the

differential settlement between the backfill and the modular block facing. Observed modeling result of FLAC Model Al-W9 showed that increasing differential settlements occurred at upper part of the wall.

Additional research work is needed to further characterize the composite lateral earth pressure coefficient, K_{comp}. The values of K_{comp} described in this paper maybe only appropriate for analyzing reinforcement tensions of GRS walls that have similar design as the Algonquin wall. Parametric study that investigates the influence of factors such as wall height, soil properties, reinforcement properties, and reinforcement layout on the composite lateral pressures would be very helpful to determine K_{comp}.

ACKNOWLEDGMENT

The author appreciates the invaluable advises from Professor R.D. Holtz. Discussions with T.M. Allen, B.R. Christopher, and B. Race, were also helpful to the author. The author acknowledges with thanks the supports of his research by the Washington State Department of Transportation (WSDOT). However, this paper does not represent the views of WSDOT.

REFERENCES

Allen, T.M., and Holtz, R.D., (1991), "Design of Retaining Walls Reinforced With Geosynthetics," Geotechnical Special Publication No. 27, Proceedings of Geotechnical Engineering Congress 1991, Boulder, pp970~987.

Bathurst, R.J., (1998), personal communications.

Bathurst, R.J., Simac, M.R., Christopher, B.R., and Bonczkiewicz, C., (1993), "A Database of Results from a Geosynthetic Reinforced Modular Block Soil Retaining Wall," Proceeding of International Symposium of Soil Reinforcement, Paris, France, pp341-362.

Bell, J. R., Barrett, R. K., and Ruckman, A. C., (1983), "Geotextile Earth-Reinforced Retaining Wall tests: Glenwood Canyon, Colorado," Transportation Research Record 916, Washington, DC, pp. 59-69.

Boyle, S.R., (1995), "Deformation Prediction of Geosynthetic Reinforced Soil Retaining Walls", PhD. Dissertation, University of Washington, Seattle, U. S., 391p.

Boyle, S.R., Gallagher, M, and Holtz, R.D., (1996), " Influence of Strain Rate, Specimen Length and Confinement on Measured Geotextile Properties," Geosynthetics International, Vol. 3, No. 2, pp. 205-225.

Christopher, B.R., (1993), "Deformation Response and Wall Stiffness in Relation to Reinforced Soil Wall Design", Ph.D. Dissertation, Perdue University, 354p.

Christopher, B.R., Gill, S.A., Giroud, J.P., Juran, I., Mitchell, J.K., Schlosser, F. and Dunnicliff, J., (1990), "Reinforced Soil Structures Volume I. Design and Construction Guidelines", Federal Highway Administration, FHWA-RD-89-043, Washington, D.C., 283p.

Duncan, J.M., Byrne, P., Wong, K.S., and Mabry, P., (1980), "Strength, Stress-Strain and Bulk modulus Parameters for Finite Element Analyses of Stresses and Movements in Soil Masses," Geotechnical Engineering Report No. UCB/GT/80-01, University of California, Berkeley, 70p.

Holtz, R.D., and Lee, W.F., (1998), "Geosynthetic Reinforced Wall Analysis, Phase II: Use of In-Soil Geosynthetic Behavior to Predict Deformation", Report No. WA-RD 452.1, Washington State Department of Transportation, 32p.

Itasca Consulting Group, (1993), "Fast Lagrangian Analysis of Continua Version 3.3", Itasca Consulting Group, Inc., Minneapolis, MN, U. S. Vol. I, and II.

Lade, P.V., and Lee, K.L., (1976), " Engineering Properties of Soils," Report UCLA-ENG-7652, 145p.

Rowe, R. K., and Ho, S. K (1993), "Keynote Lecture: A Review of the Behavior of Reinforced Soil Walls," Earth Reinforcement Practice, Ochiai, Hayashi, and Otani, ed's, Balkema, Rotterdam, pp. 801-830.

Steward, J., Willamson, R.J., and Mohney, J., (1977), "Guidelines for Use of Fabrics in Construction and Maintenance of Low-Volume Roads", USDA, Forest Service, Portland, OR.

The Role of Contaminant Transport in Two Different Geomembrane/Geosynthetic Clay Liner Composite Liner Designs

C.B. Lake and R.K. Rowe
Department of Civil and Environmental Engineering, The University of Western Ontario, London, Ontario, Canada N6A 5B9

Abstract

Consideration is given to the relative performance of two double liner systems, viz.: 1) a geomembrane primary liner and a geomembrane/geosynthetic clay liner composite secondary liner, and 2) a geomembrane/geosynthetic clay liner composite primary liner and a geomembrane secondary liner. Contaminant transport analyses indicated that, to all practical purposes, both systems are equally effective at controlling the contaminant migration of dichloromethane into an underlying aquifer for the conditions examined. This conclusion is reached for both low design heads on the primary liner (0.01m) as well as possible situations of leachate mounds to give a subsequent head of up to 12 m on the primary liner system.

Introduction

A double liner system is sometimes incorporated as the engineered component of municipal solid waste landfills to prevent the contamination of the groundwater system under the landfill. The liner system may be composed of a primary leachate collection system (stone or geonet), a primary liner (geomembrane (GM), compacted clay liner (CCL), or geosynthetic clay liner(GCL)), a secondary leachate collection system or leak detection system and a secondary liner. Various geosynthetic separation, filtration and protection layers may also form part of the double liner system. A GM/CCL composite liner has traditionally been used in landfill applications for both the primary and secondary liner system but more recently many designers have accepted GM/GCL

composite liner systems as a viable alternative to a GM/CCL system. A GCL as part of a composite liner system allows relatively quick construction, increased air space, and possibly lower leakage rates (Harpur et al, 1993) compared to GM/CCL composite systems.

As discussed by Giroud et al. (1997), GM/CCL composite systems have traditionally been situated as part of the secondary liner system, mainly due to the fear of damaging the underlying geomembrane or leachate collection system when heavy construction equipment is used to construct the CCL as part of the primary liner system. However, Giroud et al. (1997) also noted that if light equipment was used to install the GCL, the GM/GCL composite liner system could be constructed as either the secondary liner system (Figure 1a) or the primary (Figure 1b), with relatively less concern of damaging any underlying geomembranes or leachate collection systems.

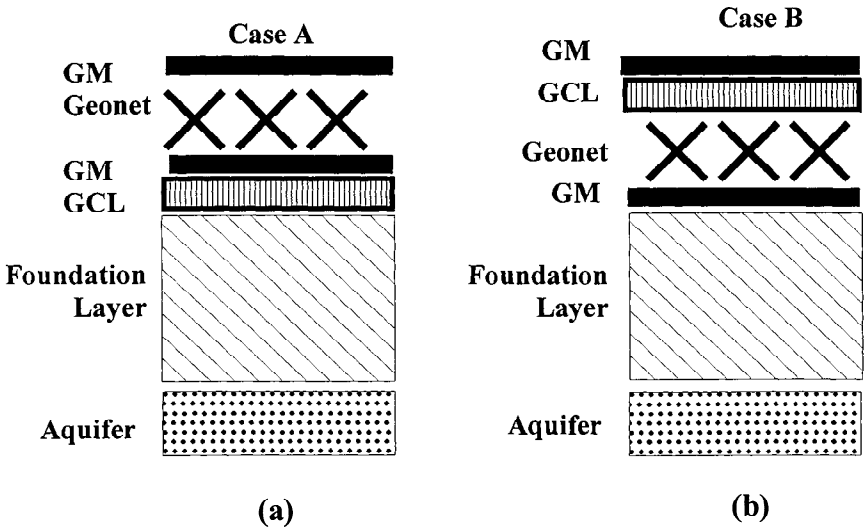

Figure 1. Schematic of Liner Systems Used To Examine Role of Contaminant Transport in Optimization of Liner Configurations

To assess which of the two configurations in Figure 1 would perform the best, Giroud et al (1997) used leakage rates through the secondary liner as the optimization criteria. The foundation layer in Figure 1 was defined as 'permeable' for the calculations. The conclusion of Giroud et al. (1997) was that Case B (Figure 1b) allowed significantly less leakage through the secondary liner

than Case A (Figure 1a) and hence was the better configuration. However, Giroud et al. (1997) acknowledged that this ranking might change if different criteria (i.e. contaminant transport) were used for the ranking. The purpose of this paper is to extend the work of Giroud et al. (1997) to examine the effect of advective – diffusive contaminant transport of a volatile organic compound on the potential performance of the same two double lined systems.

Methodology

A finite layer contaminant transport program, POLLUTE (Rowe and Booker, 1999), that has been developed to specifically consider composite systems involving a GCL was used to directly compare the two liner configurations in Figure 1: Both systems were assumed to be resting on a 3.75 m thick foundation soil underlain by a 3 m thick aquifer. For this paper, the maximum concentration impact in the aquifer for dichloromethane (DCM) was used to assess each liner system. Dichloromethane is a typical volatile organic compound found in landfill leachate and is a suspected carcinogen (Gibbons et al., 1992). The parameters used for modeling DCM in the landfill are given in Tables 1 and 2. To be conservative, no sorption of DCM was assumed for any of the liner components. The percolation rate through the cover and waste was taken to be the minimum permitted in Ontario (MOE, 1998) without special permission. It should be noted that this is a much higher percolation than would be expected in the United States due to a different philosophy to cover design in the two jurisdictions.

To examine the effect of advective-diffusive contaminant transport on the performance of the two liner configurations (Figure 1), the leakage rates calculated by Giroud et al. (1997) were used as direct inputs into the contaminant transport model (Rowe and Booker, 1999). The leakage rates through the foundation layer were assumed to be the same as those calculated by Giroud et al.

Table 1. Landfill Properties.

Parameter	Value	Reference
Length	1000m	
Mass of DCM in waste	2.3 mg/kg of waste	MOE (1998)
Initial concentration in leachate	3300 ug/L	MOE (1998)
Percolation through waste	0.15 m/a	MOE (1998)
Half-life DCM in landfill	10 a	MOE (1998)
Half-life DCM in GCL+Foundation	50 a	

Table 2. Parameters Used For Modeling Figure 1.

Geomembrane Properties	Geonet	GCL	Foundation Layer	Aquifer
Thickness: 1.5 mm	Thickness: 5 mm	Thickness: 7 mm	Thickness: 3.75m	Thickness: 3m
DCM Diffusion Coefficient: 6.9×10^{-5} m/a	DCM fully dispersed in Geonet	DCM Diffusion Coefficient: 9.4×10^{-3} m/a	DCM Diffusion Coefficient: 3×10^{-2} m^2/a	Full Mixing
Contact Conditions with Foundation Layer: Good	Hydraulic Conductivity: 10^{-1}m/s	Hydraulic Conductivity: 10^{-11} m/s	Hydraulic Conductivity: 10^{-7} m/s	Horizontal Darcy Flux: 1 m/a
Transmissivity in contact with GCL: 1×10^{-10} m^2/s			Water table 1 m above bottom of foundation layer	
	Porosity: 0.5	Porosity: 0.8	Porosity: 0.3	Porosity: 0.3

(1997) through the secondary liner. Based on the calculated leakage rates, Giroud et al. (1997) concluded that the system involving a GM/GCL composite primary and a GM secondary liner (Fig.1b) was more effective at controlling leakage through the secondary liner than a GM primary and GM/GCL secondary liner system (Fig. 1a). Table 3 shows the head levels and leakage rates calculated by Giroud et al. (1997) and the corresponding calculated contaminant impact in the underlying aquifer.

The results in Table 3 show that: 1) When comparing contaminant impacts for the two possible placements of the GM/GCL composite liner, there is no difference in DCM impact for the

Table 3. Results of POLLUTE Analyses Using Giroud et al. (1997) Leakage Rates.

Defect Diameter and Frequency	Case	Case A - GM – Primary Liner; GM/GCL Composite – Secondary Liner		Case B - GM/GCL Composite – Primary Liner; GM – Secondary Liner	
		Leakage Rates (m/s)	Maximum DCM Impact In Aquifer	Leakage Rates (m/s)	Maximum DCM Impact In Aquifer
d = 2 mm $F=2.5 \times 10^{-4}$ m^{-2} (2.5 holes/ha)	1	$h_{wp} = 0.01m$ $v_{a1}=2.09x10^{-10}$ $v_{a2}=1.01x10^{-18}$	17 ug/L occurs at 110 years	$h_{wp} = 0.01m$ $v_{a1}=1.94x10^{-15}$ $v_{a2}=2.08x10^{-24}$	17 ug/L occurs at 110 years
	2	$h_{wp} = 0.1m$ $v_{a1}=6.60x10^{-10}$ $v_{a2}=2.85x10^{-18}$	17 ug/L occurs at 110 years	$h_{wp} = 0.1m$ $v_{a1}=3.04x10^{-14}$ $v_{a2}=6.36x10^{-23}$	17 ug/L occurs at 110 years
d = 0.5 mm $F=2.5 \times 10^{-3}$ m^{-2} (25 holes/ha)	3	$h_{wp} = 0.01m$ $v_{a1}=1.31x10^{-10}$ $v_{a2}=5.02x10^{-18}$	17 ug/L occurs at 110 years	$h_{wp} = 0.01m$ $v_{a1}=1.47x10^{-14}$ $v_{a2}=4.93x10^{-23}$	17 ug/L occurs at 110 years
	4	$h_{wp} = 0.1m$ $v_{a1}=4.13x10^{-10}$ $v_{a2}=1.42x10^{-17}$	17 ug/L occurs at 110 years	$h_{wp} = 0.1m$ $v_{a1}=2.30x10^{-13}$ $v_{a2}=4.71x10^{-21}$	17 ug/L occurs at 110 years

- h_{wp} is the leachate design head on primary liner
- v_{a1} and v_{a2} are the leakage rates through the primary and secondary liner systems respectively (taken directly from Giroud et al, 1997).

parameters modeled. 2) When looking at the GM – GM/GCL or GM/GCL – GM configuration, there is no difference in DCM impact for increased flows (i.e. despite a 5 order of magnitude difference in leakage through the secondary liner, there is essentially no difference in the impact). The reason for this insensitivity is that all of the flows are very small and diffusion rather than advection (leakage) controls the impact of volatile organic compounds for liner systems shown in Figure 1. This is because the potential mass transport through the geomembrane by diffusion (see Rowe, 1998a) is much greater than the mass transport by leakage through a few holes. It is noted that in each case the impact (17ug/L) is well below the maximum acceptable concentration for drinking water (50 ug/L) for the conditions modeled. Thus with respect to DCM, there is no relative advantage to one system over the other. Since Giroud et al. (1997) showed that there was reduced leakage for the system shown in Figure 1b, it may be argued that for the low heads examined (head 0.01 m and 0.1 m), this system may be preferred for contaminants that do not

readily diffuse through a geomembrane (eg. ionic contaminants – see Rowe, 1998a) since the impact due to these contaminants may be dominated by leakage through holes in the geomembrane (assuming that the number and size of holes in both systems is similar). This leaves the question open as to whether one system is preferable to another for higher heads (>0.1 m) acting on the liner. This will be discussed in the next section.

Effect of Leachate Mounding

Various case histories have shown that the leachate head in a landfill may increase with time (Rowe, 1998a,b). The leachate head may be expected to increase the leakage rates through the liner system. To examine if these increased leakage rates have any effect on contaminant migration, the two liner configurations of Figure 1 were re-examined for the case of leachate mounding.

For modeling purposes, a hypothetical landfill was assumed to operate for a period of 20 years (with all time measured from the midpoint of this period). After closure the leachate head was controlled to design levels until at time t = 100 years (i.e. 110 years after the start of landfilling). At this time it was assumed that the efficiency of the primary leachate collection system began to decrease (e.g. due to clogging) and a leachate mound began to build up gradually over a 20 year period. The 100-year service life of the leachate collection system is based on MOE(1998). As mentioned by Rowe (1998a), the time to build a leachate mound depends on many factors, none of which will be examined for this paper. For simplicity it was assumed that 20 years were required to reach the full leachate mound height. The height of the leachate mound will depend on the difference between the percolation rate through the landfill and cover system and factors such as the amount of leakage through the liner system, seepage out of the side of the landfill, lateral migration above the liner system and/or wells installed to control the head of leachate. If the hydraulic conductivity of the leachate collection system drops below that of the

overlying waste, the amount of leachate collected will decrease and the leachate mound will build to balance the percolation of water through the cover. To simplify the problem, the leachate mound was limited to a maximum of 12 m. For the secondary liner system, the head conditions were limited to a maximum of 5 mm (i.e. the thickness of the geonet); any excess being collected by the collection system.

To provide a comparison to the work performed by Giroud et al. (1997), the same hole sizes and frequencies were used for contaminant transport modeling as well as an additional case of 40 holes per hectare (2 mm diameter) to examine the influence of QA/QC on contaminant impact in the aquifer. The calculation of leakage rates through geomembrane defects has been discussed by Giroud and Bonaparte (1989), Giroud et al., (1992) and Rowe (1998a) and will not be discussed here. The computer program LEAK (Rowe and Lake, 1997) was used to calculate the leakage through the liner systems shown in Figure 1. LEAK incorporates the analytical solutions developed by Rowe (1998a).

Results

The resulting heads, leakage rates and amount of leachate collected by the leachate collection system for the two systems shown in Figure 1 are given in Table 4 for the different hole sizes and frequencies considered.

Table 4 contains a number of items worthy of note:

- The case of a geomembrane primary liner and a GM/GCL composite secondary liner (Fig. 1a) has less leakage through the secondary liner than the case of a GM/GCL primary liner and a GM secondary liner (Fig. 1b). The relative leakage rates and amount of leakage is different to the findings of Giroud et al. (1997) because of different assumptions regarding the design head conditions on the secondary liner system and the foundation soil underlying the secondary liner. However, the difference in conclusions is of no practical significance since the leakage through the secondary liner was negligibly small for both cases.

- For Case A (d=2 mm, F= 2.5 holes/ha), the leachate mound cannot build up to the full 12m because any higher than a 5.25 m leachate head will result in a leakage rate which exceeds the assumed percolation rate through the cover (0.15 m/a – a typical value for Southern Ontario, Canada).

- The head on the secondary liners for Case B are limited by the leakage through the primary liner. Since the leakage is so small through the GM/GCL primary liner, it is assumed here that all of the fluid that makes it through this primary liner is going through the secondary liner (i.e. none is being collected by the secondary leachate collection system).

- Although the leakage through the secondary liner is greater in Case B than Case A, in both cases the leakage rates are still very small (less than 0.23 mm/a) assuming that the geomembrane remains intact.

Table 4. Calculated leakage rates for leachate mounding situation.

Defect Diameter and Frequency	Primary Leachate Collection System	Case A (Figure 1)		Case B (Figure 1)	
		Heads (m) and Leakage Rates (m/s)	Leachate Collected (m/s)	Heads (m) and Leakage Rates (m/s)	Leachate Collected (m/s)
d = 2 mm F=2.5 x 10^{-4} m^{-2} (2.5 holes/ha)	Operating	h_{wp} = 0.3 v_{a1}=1.14x10^{-9} h_{ws} = 0.005 v_{a2}=2.01x10^{-16}	q_{c1} =3.62x10^{-9} q_{c2} =2.28x10^{-4}	h_{wp} = 0.3 v_{a1}=8.44x10^{-15} h_{ws} =3.1x10^{-5} v_{a2}=8.44x10^{-15}	q_{c1} = 4.76x10^{-9} q_{c2} = 0
	Terminated	h_{wp} = 5.25 v_{a1}=4.76x10^{-9} h_{ws} = 0.005 v_{a2}=2.01x10^{-16}	q_{c1} =0 q_{c2} =9.34x10^{-4}	h_{wp} = 12.0 v_{a1}=3.31x10^{-13} h_{ws} = 1.8x10^{-3} v_{a2}=3.31x10^{-13}	q_{c1} = 4.76x10^{-9} q_{c2} = 0
d = 0.5 mm F=2.5 x 10^{-3} m^{-2} (25 holes/ha)	Operating	h_{wp} = 0.3 v_{a1}=8.04x10^{-10} h_{ws} = 0.005 v_{a2}=1.52x10^{-15}	q_{c1} =3.96x10^{-9} q_{c2} =1.61x10^{-4}	h_{wp} = 0.3 v_{a1}=6.78x10^{-14} h_{ws} =3.1x10^{-5} v_{a2}=6.78x10^{-14}	q_{c1} = 4.76x10^{-9} q_{c2} = 0
	Terminated	h_{wp} = 12.0 v_{a1}=2.18x10^{-12} h_{ws} = 0.005 v_{a2}=1.52x10^{-15}	q_{c1} =2.4x10^{-10} q_{c2} =9.04x10^{-4}	h_{wp} = 12.0 v_{a1}=2.66x10^{-12} h_{ws} = 1.8x10^{-3} v_{a2}=2.66x10^{-12}	q_{c1} = 4.76x10^{-9} q_{c2} = 0
d = 2 mm F=4.0 x 10^{-3} m^{-2} (40 holes/ha)	Operating	h_{wp} = 0.021 v_{a1}=4.76x10^{-9} h_{ws} = 0.005 v_{a2}=3.22x10^{-15}	q_{c1} =0 q_{c2} =9.52x10^{-4}	h_{wp} = 0.3 v_{a1}=1.35x10^{-13} h_{ws} =3.1x10^{-5} v_{a2}=1.35x10^{-13}	q_{c1} = 4.76x10^{-9} q_{c2} = 0
	Terminated	h_{wp} = 0.021 v_{a1}=4.12x10^{-12} h_{ws} = 0.005 v_{a2}=3.22x10^{-15}	q_{c1} =0 q_{c2} =9.52x10^{-4}	h_{wp} = 12.0 v_{a1}=5.30x10^{-12} h_{ws} = 1.8x10^{-3} v_{a2}=5.30x10^{-12}	q_{c1} = 4.76x10^{-9} q_{c2} = 0

- h_{ws} is the leachate head on the secondary liner, q_{c1} and q_{c2} are the volumes of fluid removed from the primary and secondary leachate collection systems.

When comparing the maximum concentration of DCM in the underlying aquifer for the configurations of Figure 1, Table 5 shows that regardless of the configuration of the two liner systems and regardless of the leakage rates used in this analysis, the maximum impact in the underlying aquifer is practically the same for the situations considered in this paper. What is even more interesting is that the contaminant impact is the same for Tables 3 and 5 even though in Table 5 a leachate mound of up to 12 m was assumed to develop on the primary liner. This shows that diffusion is the process controlling contaminant impact in the aquifer for the situations in Figure 1. This is because the significant diffusion and impact all occurred prior to when the full leachate mound had developed by 120 years.

Table 5. Contaminant impact in the aquifer for the cases in Table 4.

Defect Diameter and Frequency	Case A (Figure 1)	Case B (Figure 1)
	Max. DCM Impact	Max. DCM Impact
d=2 mm, F=2.5x10^{-4} m^{-2} (2.5 holes/ha)	18 ug/L at 105 years	17 ug/L at 105 years
d=0.5 mm, F=2.5x10^{-3} m^{-2} (25 holes/ha)	17 ug/L at 106 years	17 ug/L at 107 years
d=2 mm, F=4.0x10^{-3} m^{-2} (40 holes/ha)	18 ug/L at 104 years	17 ug/L at 107 years

Conclusions

It has been shown in this paper that if a GM/GCL composite liner is placed as part of the primary or secondary liner system with a GM as the other liner, there is no significant difference in DCM impact in the underlying aquifer between the two designs. This was shown for both small design heads and increased leachate heads on the primary liner assuming failure of the primary leachate collection system after 100 years. Thus for the cases considered diffusion is the process controlling contaminant impact. These conclusions may or may not be applicable for other cases, however individual cases can be readily checked using the approaches adopted in this paper.

References

Gibbons, R.D., Dolan, D., Keough, H., O'Leary, K. and O'Hara, R. (1992). A comparison of chemical constituents in leachate from industrial hazardous waste and municipal solid waste landfills. Proceedings of the 15th Annual Madison Waste Conference, pp.251-276.

Giroud, J.P., Badu-Tweneboah, K. and Bonaparte, R. (1992) Rate of leakage through a composite liner due to geomembrane defects. Geotextiles and Geomembranes, Vol. 11, No.1, p-1-12.

Giroud, J.P. and Bonaparte (1989) Leakage through liners constructed with geomembranes – PartII. Composite liners. Geotextiles and Geomembranes, Vol. 8, No. 2, pp.71-111.

Giroud, J.P., Soderman, K.L. and Badu-Tweneboah, K. (1997). Optimal Configuration of a Double Liner System Including a Geomembrane Liner and a Composite Liner. Geosynthetics International, Vol. 4, No. 3-4, pp 373-389.

Harpur, W.A., Wilson-Fahmey, R.F., and Keorner, R.M. (1993). Evaluation of the contact between geosynthetic clay liners and geomembranes in terms of transmissivity. Proceedings of the GRI Seminar on Geosynthetic Clay Liner Systems, Ed. R.M. Keorner and R.F. Wilson-Fahmey, Philadelphia, PA, Industrial Fabrics Association International, pp. 143-154.

Ontario Ministry of Environment (MOE) 1998 Landfill Standards: A guideline on the regulatory and approval requirement for new expanding landfill sites.

Rowe, R.K. (1998a) Geosynthetics and the minimization of contaminant migration through barrier systems beneath solid waste. Keynote paper presented at the 6th International Conference on Geosynthetics, Atlanta, GA, 1: pp.27-102.

Rowe, R.K. (1998b) From the past to the future of landfill engineering through case histories. Proceedings, Fourth International Conference for Case Histories in Geotechnical Engineering, St. Louis, pp. 145-166.

Rowe, R.K. and Booker, J.R. (1999) POLLUTE v.6.4 - 1-D pollutant migration through a non-homogeneous soil© 1983, 1990, 1994, 1997, 1999. Distributed by GAEA Environmental Engineering Ltd., 44 Canadian Oakes Dr., Whitby, Ontario, L1N 6W8, Fax (905) 725-9657.

Rowe, R.K. and Lake, C.B. (1997) Program LEAK – A program for calculating leakage through holes in a geomembrane in composite liners, The University of Western Ontario.©1997.

GEOTEXTILE FILTER PERFORMANCE UNDER CONDITIONS OF SEVERE VIBRATION

A. HAMEIRI

UNIVERSITY OF BRITISH COLUMBIA, CANADA

R. J. FANNIN

UNIVERSITY OF BRITISH COLUMBIA, CANADA

ABSTRACT

No existing design criteria address the case of geotextile filter performance under conditions of vibration. Yet these conditions can be present in the field, particularly for pavement edge drains, because of traffic loading and during routine construction works. In order to investigate the influence of vibration, an automatic, double acting drop-hammer was mounted on the gradient ratio test device. Loading was imposed at a frequency of 3Hz. A multiple-stage test program was developed beginning with static unidirectional flow at a hydraulic gradient of 4 and leading to a series of vibration loading to a total blow count of almost 4000. Implication of the results for uniformly graded soils are assessed, and a new design criterion then proposed for vibration loading.

KEYWORDS: design criteria, filtration, geotextile openings, gradient ratio, piping, vibration energy.

INTRODUCTION

In order to fulfill the function of filtration, a geotextile should be sufficiently permeable and yet provide soil retention. These two requirements are contradictory. The geotextile pore size opening is a key issue in design. Since the opening size can be measured directly, relatively simple relationships have been developed between the characteristic pore size of the geotextile and the particle sizes of the soil to be retained. In North America, the geotextile pore sizes are measured either by dry sieving or by hydrodynamic sieving. Dry sieving results are

characterized by the AOS value, and those from hydrodynamic sieving by the FOS value. Each is a practical measure of pore size, for which 95% of the openings are the same size or smaller.

The FHWA (Holtz et. al., 1995) suggests that, for critical/sever applications, the designer should perform a Gradient Ratio test (ASTM D 5101-96), as a performance test for evaluation of soil-geotextile compatibility in filtration applications (see Fig. 1). It uses a rigid wall permeameter with ports that allow for measurement of the head losses in the soil and the head losses across the soil/geotextile interface. The ratio of head loss across the soil/geotextile interface to the head loss across the upstream undisturbed soil is termed the Gradient Ratio (GR).

At UBC, ports 1 to 7 are used to monitor water head across the sample. Nominally, in order to calculate the GR(ASTM), (ASTM D 5101-96), the head loss in the soil/geotextile interface is measured across the geotextile and 25mm thickness of upstream soil, (ports 5 and 7), and the head loss across the soil is measured across a 50mm thickness of soil, (ports 3 and 5).

I - Inflow constant head device.
O - Outflow constant head device.
S - Soil sample.
G - Geotextile specimen, (on a support screen).
M - Manometer ports (1 to 7).
T - Cell top.
F - Collection trough.

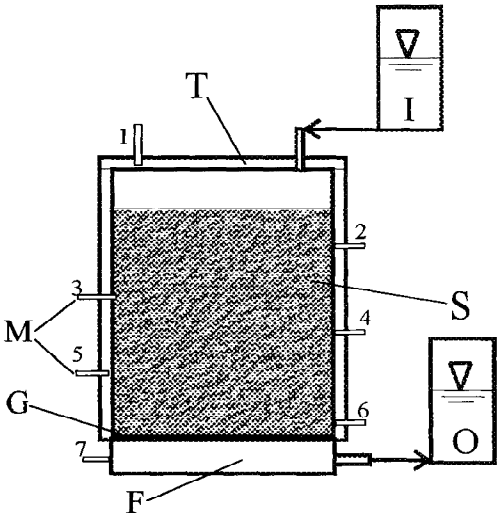

Fig. 1: The gradient ratio device: schematic drawing.

In order to increase the sensitivity of the head loss across the soil/geotextile interface layer, Fannin et al., (1994) suggested a calculation of GR(Mod.), by decreasing the thickness of the soil/geotextile interface layer to 8mm (using ports 6 and 7). This was also recognized as an important improvement to the accuracy of measurement

by Austin et al., (1997). For further information on the sample behavior, port 2 was added 13.3mm above port 3, and port 4 was added midway between ports 3 and 5.

THE CHALLENGE OF VIBRATION

Kenney and Lau (1985) explain that if the constrictions (the narrow "windows" at the junction of adjacent pores) in the pore network of the soil matrix are larger than some of the loose particles, these particles can be transported. Constrictions are variable in size and therefore small loose particles have potential transport distances which are longer than those of larger loose particles. It is believed that, under severe vibration, the constriction sizes of a dense soil increase momentarily and thus the controlling constriction of the void network also increases momentarily, which in turn results in an increase in the largest particle that can be transported. Examples of vibration in the field include the case of pavement edge drains, due both to traffic loading and construction works. Yet none of the existing design criteria address the case of a geotextile filter that might serve under conditions of vibration.

Kenney and Lau (1985) , and Lafluer (1998), have performed tests using light vibration by manually tapping the samples. The intent of their work was to induce testing conditions slightly more severe than would generally be expected under unidirectional static conditions, and therefore develop conservative design criteria for the condition of unidirectional static flow only. To extend the scope of such work to the specific case of vibration the study reported in this paper was made using an automated hammer to impose loading more severe than that expected in the field under vibration.

THE MODIFIED DEVICE AND THE MATERIALS

In a similar way to Fannin et al., (1996), an existing device (Fannin et al., 1994) was modified to allow particles passing through the geotextile to be collected during each phase of the test. Further modifications allow for a controlled energy and frequency of vibration. Energy is controlled through an air pressure regulator, and

frequency through a frequency generator, using a solenoid valve. Vibration is transmitted to the sample using a double acting belofram piston located on the cell top cover plate (see Fig. 2).

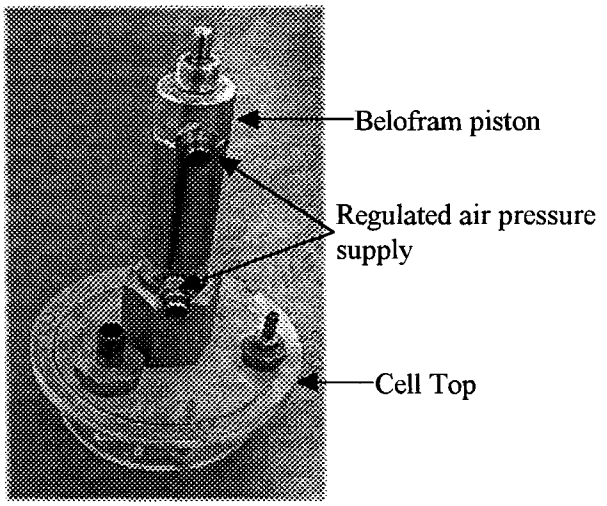

Fig. 2: The double acting drop-hammer

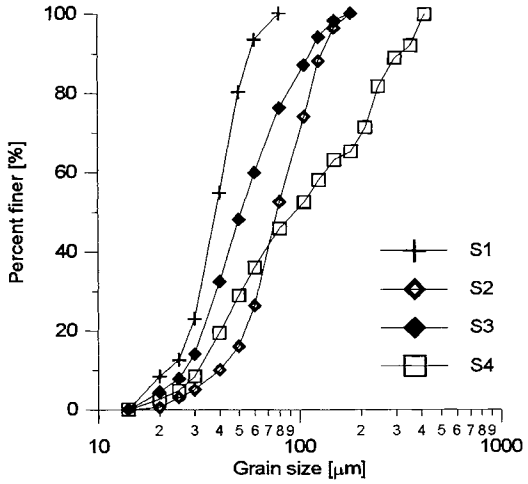

Fig. 3: Particles size distribution curves

Eight tests were performed using combinations of four narrowly graded (1<Cu<6), reconstituted saturated silty sand to sandy silt sizes of glass bead samples, see Fig. 3, and four NW needle-punched nonwoven geotextiles (see Table 1).

Table 1: Properties of the nonwoven geotextiles

Code	Thickness [mm]	Mass [g/m^2]	FOS [microns]	Permeability [cm/s]	Porosity [%]
G103	3.02	286	103	0.64	90
G122	2.50	294	122	0.59	92
G149	0.92	126	149	0.20	85
G290	1.33	216	290	0.99	82

TEST PROCESS AND MEASUREMENTS

The test process comprises a static phase for approximately 10 hours, and a dynamic phase at a frequency of 3HZ to a total of approximately 4000 blows (see Fig. 4). Both test phases are performed under a constant unidirectional hydraulic gradient of 4. Measurements taken during each phase of testing are: water head distribution in the sample, flow rate and sample length, and mass of particles passing through the geotextile (for sample preparation, static flow, and dynamic loading).

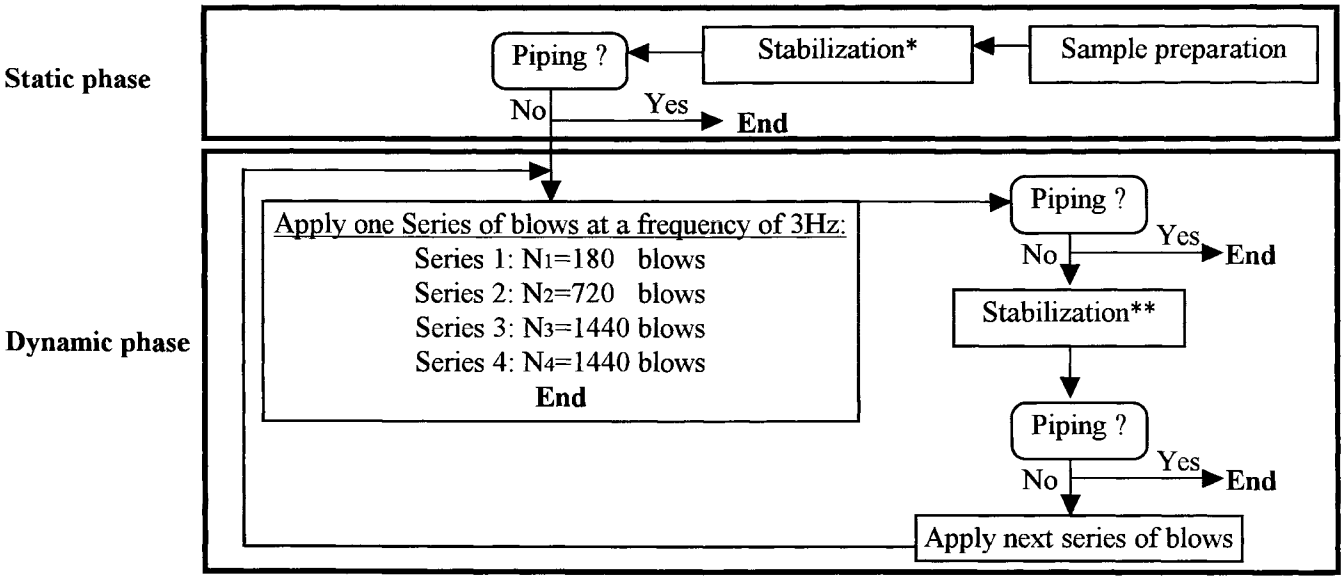

* Overnight stabilization (t≅10hrs)

** No changes observed in the water heads, and in the flow rate (t≅1.5hrs).

Fig. 4: The test process.

Valuable insight is gained in any study of soil retention criteria by conducting a grain size analysis on particles that pass through the geotextile. Therefore discrete samples were taken periodically from the collector trough and analysis made automatically with a Sedigraph X-ray unit.

RESULTS AND ANALYSIS

Results for the test combination of G122 and S3, (G122.S3), are provided in Fig. 5 and 6 to illustrate a characteristic behavior. Observation and the initial analysis of the results showed the following:

1.) **Water head distribution**: In order to check initial conditions before vibration, and the influence of the vibration, water heads along the sample observed after stabilization and before applying any vibration (N=0) are compared with those following the last series of vibration (N=3780) in Fig. 5a. In addition GR values are reported in Fig. 5b after each series of vibration. The nearly linear distribution of water head are indicative of little disturbance to sample uniformity, as shown by the corresponding GR values close to unity. The GR(mod.) is a more sensitive index of changes in particle arrangement than the GR(ASTM), as seen by the increasing value with number of blows.

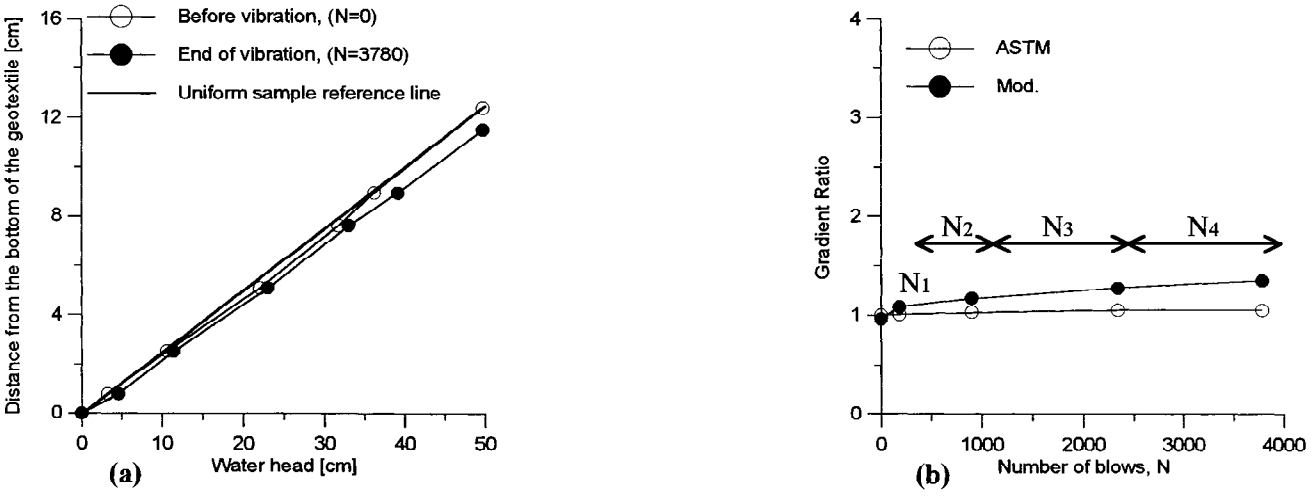

Fig. 5: The influence of vibration on: **a.)** the water head distribution. **b.)** the GR value.

2.) **Sample density:** The influence of vibration on the average density and permeability is illustrated in Fig. 6. Density increases during the first 1000 blows (see Fig. 6a), yielding a decrease in the permeability along the sample (see Fig. 6b), for the soil alone (K35) and across the soil/geotextile interface (K57 and K67).

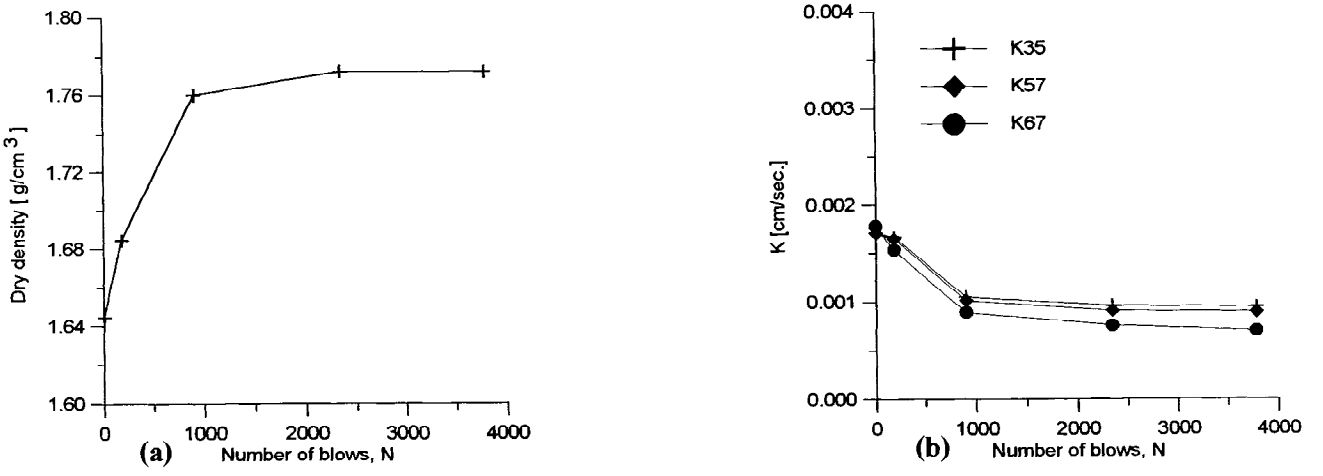

Fig. 6: Influence of vibration on the sample

3.) **Particle migration:** By observing the cumulative mass of particles passing through the geotextile during the dynamic phase only (M_D), it was possible to further identify compatibility in filtration. Two characteristic responses were found. One involves recovery from a small migration of particles (Fig. 7a), and the other a continuous loss of particles that is attributed to piping (Fig. 7b).

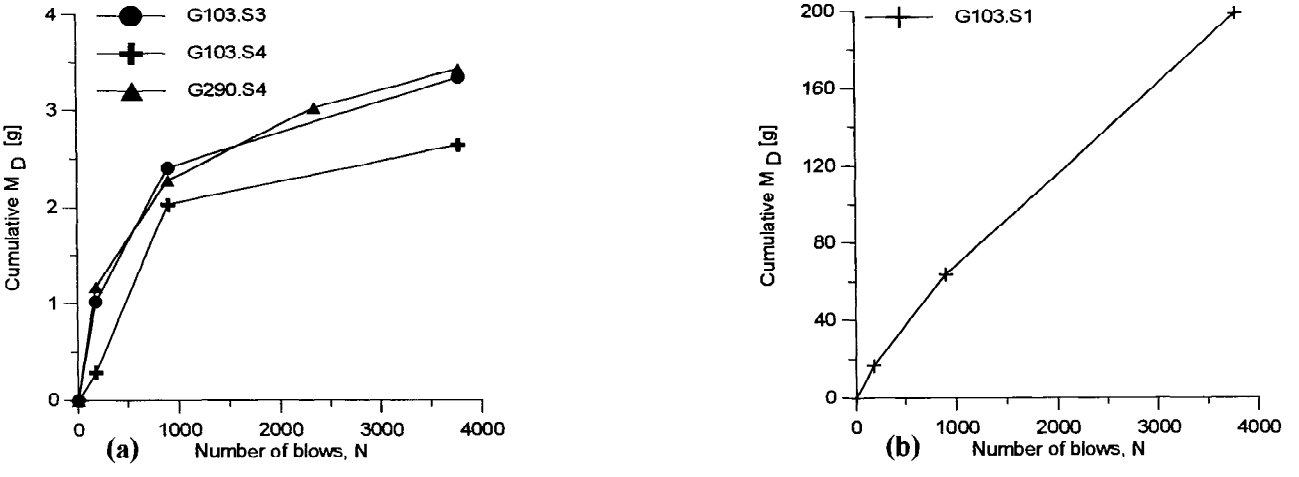

Fig. 7: Particle migration due to vibration

A Secant Piping Ratio, (SPR) is proposed to quantify the response:

$$SPR\ [\%] = \frac{\Delta M_{DF} / N_F}{\Delta M_{DI} / N_I} \times 100 \quad (1)$$

where:

$\Delta M_{DF} / N_F$ -Final slope of the cumulative M_D v. N curve, (taken here as the slope between 900 and 3780 blows).

$\Delta M_{DI} / N_I$ - Initial slope of the cumulative M_D v. N curve, (taken here as the slope between 0 and 180 blows).

4.) Retention behavior: The relationship between FOS/D85, SPR and cumulative mass of particles passing through the geotextile after both the static and dynamic phase, $M_S + M_D$, is shown in Fig. 8.

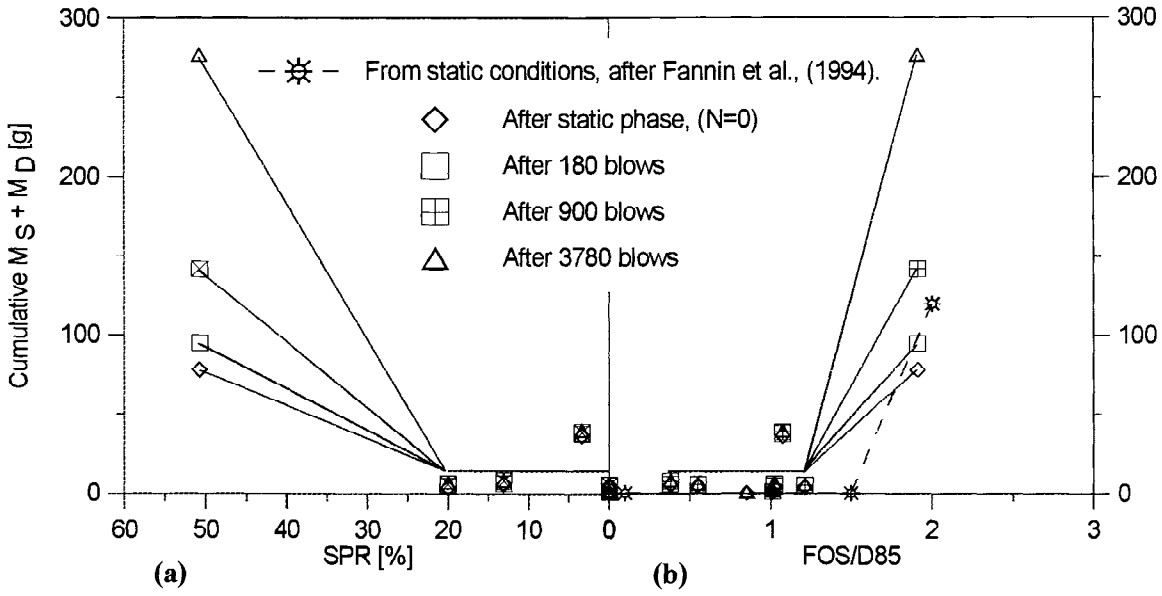

Fig. 8: Unified static and dynamic plot of the test data.

Inspection of the curves suggests:

- Dynamic Phase: Increasing the FOS/D85 above a threshold ratio of FOS/D85=1.2 yielded a notable increase in the SPR value, and in the cumulative mass of the particles passing with each series of blows. Particle size analysis showed that for the test combination yielding FOS/D85>1.2, the D95 of the migrating particles was comparable to that of the original sample gradation.

- Static phase: Results from the static phase (Fig. 8b) are in good agreement with data shown from Fannin et al., (1994), for narrowly graded soils, confirming a threshold ratio of FOS/D85=1.5 (CGS, 1992) for design in unidirectional static conditions.

CONCLUSIONS

1.) The automatic, double acting drop-hammer that was mounted on the gradient ratio test device proved effective in applying blows at a controlled frequency and energy.

2.) Vibration led to an increase in sample density, and resultant decrease in permeability, but no significant change in the water head distribution along the sample. This implies that vibration did not cause excess pore water pressure to develop or a loss of internal stability in the samples tested.

3.) As the GR(Mod.) value proved to be more sensitive than the GR(ASTM), it is suggested the standard Gradient Ratio test device (ASTM D 5101) be modified in order to better target head loss measurement across the geotextile/soil interface.

4.) Observing the cumulative mass of particles passing through the geotextile, it was possible to distinguish between two behavior patterns: one showed continuous piping and the other a small initial loss of particles. To distinguish between these two patterns, a Secant Piping Ratio (SPR) is proposed.

5.) Increasing the ratio of FOS/D85 above a threshold value leads to significant particle migration and decreases the potential for recovery during vibration. Grain size analysis reveals migration of the base soil itself and not simply a finer fraction of that soil. A relationship for onset of piping in narrowly graded soils subject to vibration loading is determined to be:

$$FOS/D85<1.2$$

6.) For conservative approach in design applications, it is recommended the MTO (1992) criterion of FOS/D85<1.0 be used for the conditions of vibration loading in narrowly-graded soils.

ACKNOWLEDGEMENT

The research is funded by the National Science and Engineering Research Council of Canada. The technical assistance of Harald Schrempp and Scott Jackson are gratefully acknowledged.

REFERENCES

- ASTM D5101-96. "Standard test method for measuring the soil-geotextile clogging potential by the gradient ratio". In 1996 Annual Book of ASTM Standards, Philadelphia, Pa.
- Austin, D.N., Mlynarek, J. and Blond, E. 1997. "Expanded Anti-Clogging Criteria For Woven Filtration Geotextiles", Geosynthetics' 97, Conference proceedings, Long Beach, California, USA, pp. 1123-1135..
- Canadian Geotechnical Society. 1992. "Canadian Foundation Engineering Manual", 3rd edition. BiTech Publishers Ltd, Richmond B.C.
- Holtz, R.D., Christopher, B.R. and Berg, R.R. 1995. "Geotextile Design and Construction Guidelines," U.S. Dept. of Transportation, Federal Highway Administration, NHI Course No. 13213, NHI.
- Fannin, R.J., Vaid, Y.P. and Shi, Y.C. 1994. "Filtration Behavior of Nonwoven Geotextiles", Canadian Geotechnical Journal, Vol. 31, pp. 555-563.
- Fannin, R.J., Vaid, Y.P., Palmeira, E.M. and Shi, Y. C. 1996. "A Modified Gradient Ratio Device", Recent Developments in Geotextile Filters and Prefabricated Drainage Geocomposites, ASTM STP 128, Shobha K. Bhatia and L David Suit, Editors, pp. 100-112.
- Kenney, T.C. and Lau, D. 1985. "Internal Stability of Granular Filters", Canadian Geotechnical Journal, Vol. 22, pp. 215-222.
- Lafleur, J. 1998. "Particles washout associated with the retention of broadly graded soils by geotextiles", Sixth International Conference on Geosynthetics, Atlanta, Georgia, USA, pp. 1001-1004.
- Ontario Ministry of Transportation. 1992. Draft engineering material report, guidelines for the design and quality control of geotextiles. Engineering Material Office, Soils and Aggregates Section, Ministry of Transportation Ontario, Downsview.

Effects of Consolidation on the Strength of the Interface between a Clay Liner and a Smooth Geomembrane

Jesús E. Gómez
Virginia Polytechnic Institute and State University, Blacksburg, Va., USA
George M. Filz
Virginia Polytechnic Institute and State University, Blacksburg, Va., USA

Abstract: Strength parameter values for design of landfill slopes with composite liners are often determined from unconsolidated undrained (UU) interface shear tests. In the field, consolidation of the clay liner under the imposed loads may substantially increase the interface strength. This increase in strength can have a beneficial impact on landfill design, especially when seismic loading controls design because it is probable that consolidation will have occurred prior to shaking by the design earthquake. For this investigation, both UU and consolidated undrained (CU) interface shear tests were performed at the interface between a high plasticity clay and a high density polyethylene (HDPE) geomembrane. The results showed that the undrained interface strength for a given normal stress depends on the water content of the clay during shear, and that this shear strength vs. water content relationship holds for both unconsolidated and consolidated interface shear. Consequently, the CU interface strength can be estimated from the results of UU interface tests if the water content of the clay after consolidation can be predicted.

1. Introduction

Refuse placement over composite liners in landfills imposes significant consolidation pressures on the soil component of such liners. It is often assumed, however, that very little consolidation occurs during the waste placement period owing to the low values of the coefficient of consolidation expected for compacted clay liners. Consequently, tests performed to measure the interface strength between clay and geomembrane components of composite liners are often carried out under unconsolidated undrained (UU) conditions achieved by shearing at a relatively rapid rate immediately after applying the normal load. However, in instances where landfill design is controlled by seismic loading from a design earthquake with a long return interval, it may be excessively conservative to use UU strength for seismic design. In such cases it is probable that clay liner consolidation would be complete prior to shaking by the design earthquake, and strengths obtained from consolidated undrained interface tests may be more appropriate.

This paper presents the results of research performed to investigate the influence of consolidation on the shear strength of the interface between a compacted clay and a smooth high-density polyethylene (HDPE) geomembrane. A series of UU and CU tests were performed in a Large Displacement Shear Box (LDSB). The following sections describe the equipment, materials, procedures, and results of the testing program.

2 The Large Displacement Shear Box (LDSB)

The LDSB is described in detail by Shallenberger and Filz (1996), and only brief descriptions of the device and testing procedures are given here. Soil samples for LDSB testing are compacted inside a 711 by 406-mm aluminum box, trimmed, and positioned in the LDSB device. A HDPE specimen with a length of 1016 mm in the direction of shear, and 406 mm across, is attached to the rigid upper assembly of the LDSB. The sample is lifted and compressed against the HDPE specimen by means of a pneumatic actuator located beneath the soil box. During shearing, the upper assembly is pulled horizontally by a screw jack driven by a stepper motor, to a maximum displacement of 305 mm.

After each test, a new surface for further interface testing on the same clay specimen is created by lowering the sidewalls of the soil box by 12.7 mm and trimming again. This procedure allows a set of five consecutive interface tests under increasing normal stresses to be performed on the specimen. A newly prepared specimen of HDPE is used for each of the tests in a set.

Important features of the LDSB are its ability to reach a continuous, monotonic displacement of up to 305 mm and minimization of end effects due to the large interface area (Shallenberger and Filz, 1996). Additionally, the effects of random variations in compaction energy and water content on test result interpretation are minimized because the same clay specimen is used throughout each set of tests.

3 Properties of the clay

The clay used for testing was obtained from a Miocene Age deposit at the Old Dominion Sanitary Landfill (ODSL) located in Henrico County, Virginia. The soils at this site have widely varying properties that have been described by Yob et al. (1995). The bulk sample obtained for this investigation is a high plasticity clay with a liquid limit of 55% and a plasticity index of 34%. The clay has a maximum dry density γ_d = 15.7 KN/m^3 and an optimum water content of 22.5% as determined from standard Proctor (ASTM D698) tests. For each set of tests, the soil was air dried, ground, mixed with distilled water to the desired water content, and then compacted using the standard Proctor energy inside the soil box. No significant change in the properties of the clay occurred as a consequence of its re-utilization, as shown by hydrometer and Atterberg limits tests performed periodically on the sample.

4 HDPE Geomembrane

The geomembrane used for the tests is a 1.5-mm Gundline HD® smooth HDPE. The geomembrane samples have a wavy pattern on one face. All the tests were performed on this side, and shearing was in the direction of extrusion. The HDPE specimens were cut to match the dimensions of the upper assembly, cleaned, stored at room temperature, and protected from direct light and dust. Before each test, the geomembrane was inspected for surface damage or any visible color change.

5 Thixotropic correction for the interface strength

The influence of thixotropy on the strength of clays has been studied by Seed and Chan (1957), Mitchell (1960), and others. According to Mitchell (1960), after the compaction effort has been removed, the clay structure tends to accommodate the lower energy level. During this process, a more flocculated structure and lower (more negative) pore pressures are generated with curing time after the compaction. Shallenberger and Filz (1996) reported a significant influence of curing time on the residual shear strength at the interface between a high plasticity clay and a HDPE geomembrane. The same phenomenon was observed during this investigation, with thixotropic strength gains being more pronounced for wetter specimens. Because of the testing sequence used with the LDSB, the time elapsed between compaction and shearing varied from test to test. Therefore, in order to permit consistent comparisons of test results, it was necessary to develop thixotropic correction factors.

Two clay samples were compacted at water contents of 1.7% and 5.1% wet of optimum. A third sample was compacted at a water content of 1.5% dry of optimum. For each of these samples, a set of interface shear tests was performed at different curing times. During curing, the samples were kept in a humid environment with no external load applied. The results are presented in Figure 1 in terms of the thixotropic strength ratio, *TSR*. The thixotropic strength ratio in soils was defined by Seed and Chan (1957) as the ratio between the strength of the aged sample and the strength measured immediately after compaction. In this paper, two thixotropic strength ratios are defined for interfaces:

$$TSR_p = \frac{\tau_p}{\tau_{p,1}} \tag{1}$$

$$TSR_r = \frac{\tau_r}{\tau_{r,1}} \tag{2}$$

where TSR_p and TSR_r are the peak and residual thixotropic strength ratios respectively, τ_p and τ_r are the measured interface peak and residual strengths respectively, and $\tau_{p,1}$ and $\tau_{r,1}$ are the interface peak and residual strengths measured one hour after compaction.

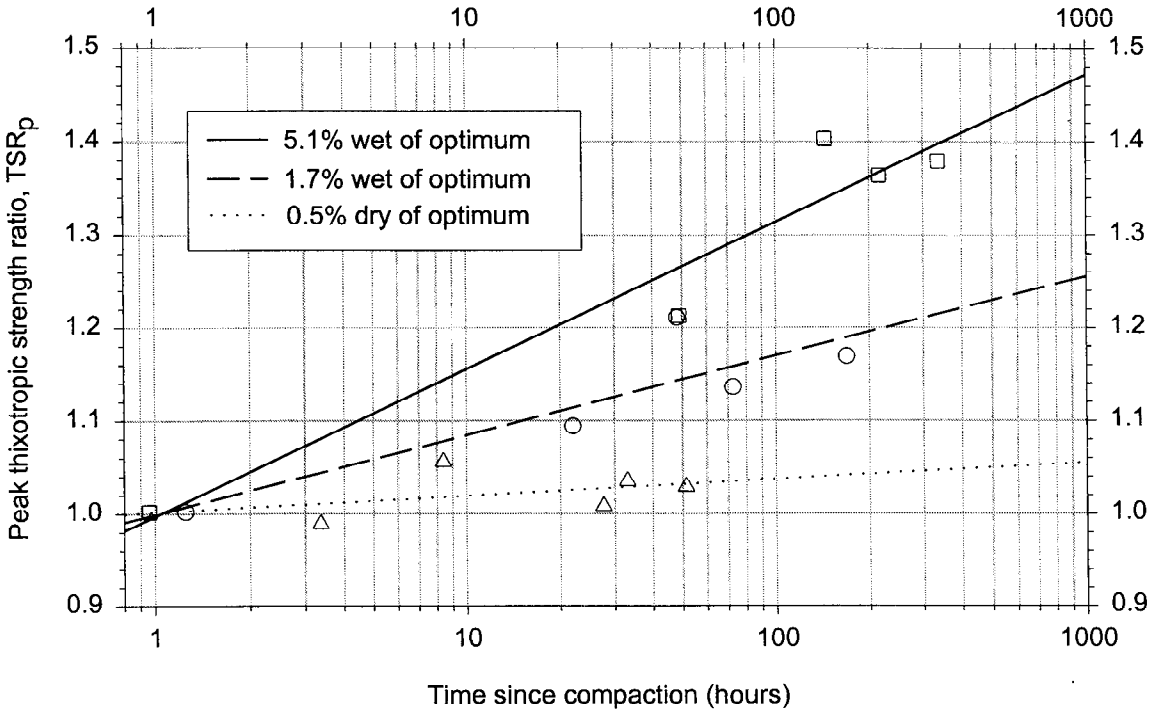

a. Variation of the peak thixotropic strength ratio with time since compaction

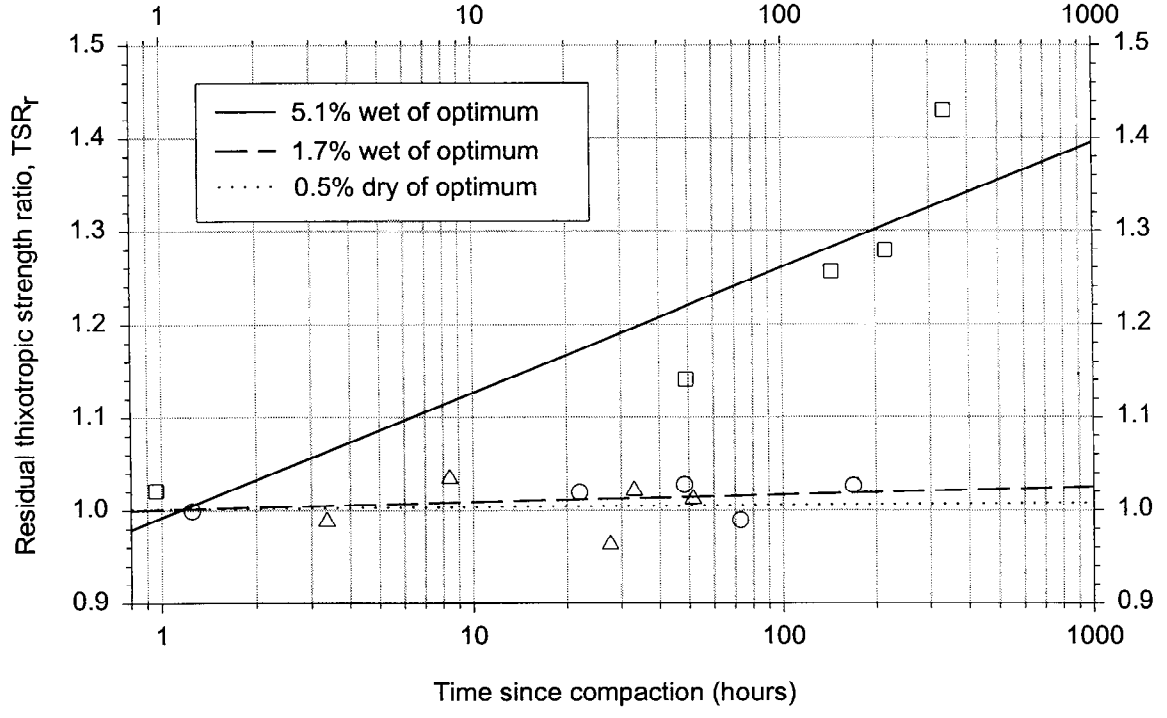

b. Variation of the residual thixotropic strength ratio with time since compaction

Figure 1. Variation of the thixotropic strength ratio with time since compaction for the ODSL clay / HDPE geomembrane interface

As can be seen in Figure 1, the sample compacted 5.1% wet of optimum showed a substantial increase in the peak and residual interface shear strengths with time. The dryer samples presented a much smaller increase in peak interface shear strength with time and no significant increase in the residual strength. The higher thixotropic ratios observed in the wetter sample are consistent with the observations by Seed and Chan (1957) of strength gain with time in compacted clays.

For the UU interface tests described in this paper, the measured interface shear strength was corrected for thixotropic effects. The measured strength was divided by the *TSR* determined from the best-fit lines in Figure 1 for the corresponding time elapsed after compaction, and the water content of the clay. The resulting strength value is referred to as the *corrected interface strength* throughout this paper.

The tests described in this section were performed to determine the influence of thixotropy on laboratory test results. The beneficial effects of thixotropy on the interface strength might not be as marked in the field due to the simultaneous changes in clay structure that occur in response to consolidation. Consolidation was not significant in the short duration, UU laboratory tests.

6 UU interface testing

Four sets of UU interface tests were performed on clay samples compacted at water contents ranging from 2.5% dry of optimum to 7.5% wet of optimum. The displacement rate during shear was kept at 2.54 mm/min in all tests. The maximum displacement attained during shear was 305 mm, which allowed a reasonable definition of the residual strength. Throughout this paper, the UU designation does not imply that the sample was sealed to prevent drainage during application of the normal and shear loads; instead, the UU designation implies rapid shearing imposed immediately after application of the normal load. Because the clay sample is large and the value of the coefficient of consolidation is low, it is believed that these loading rates produce essentially unconsolidated-undrained conditions.

Figure 2 shows the results of two of the sets of UU tests in terms of the shear stress-displacement response of the interface for normal stresses, σ, ranging from 35 to 345 kPa. The peak strength was mobilized at very small displacements ranging from 0.25 to 1.27 mm depending upon the normal stress applied. In the post-peak region, there is a rapid drop in the shear strength. In most of the tests performed, the residual strength was reached at displacements of 75 to 100 mm, for all practical purposes.

Figure 3 shows the peak and residual strength envelopes obtained from all the UU tests performed. The peak and residual strength values determined from the interface tests have been corrected for thixotropic effects according to Figure 1, as described previously. Figure 4 is a representation of the same data as is in Figure 3, but they are plotted in terms of undrained interface shear strength vs. compaction water content for different

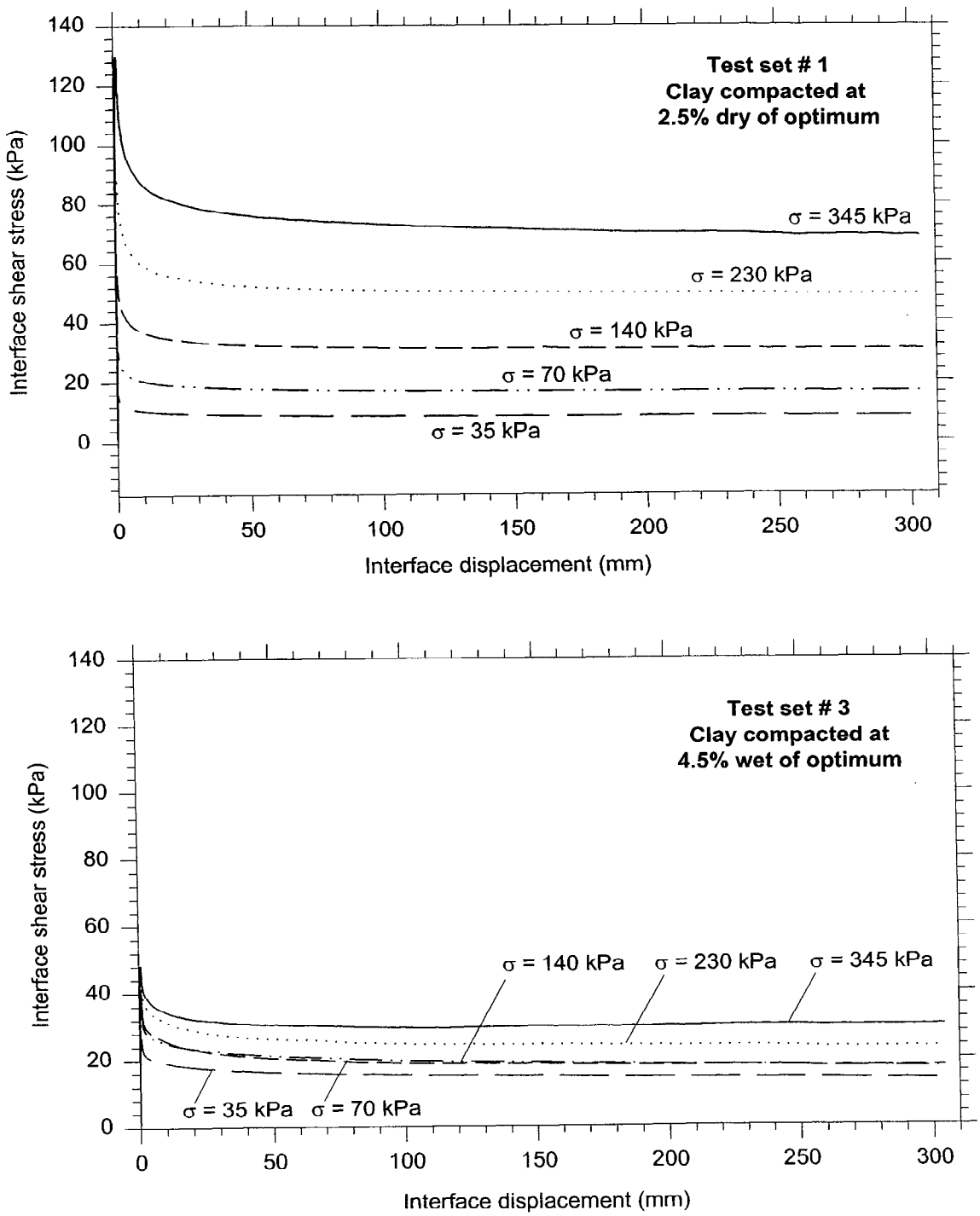

Figure 2. Results of two sets of UU tests performed at the ODSL clay / HDPE geomembrane interface

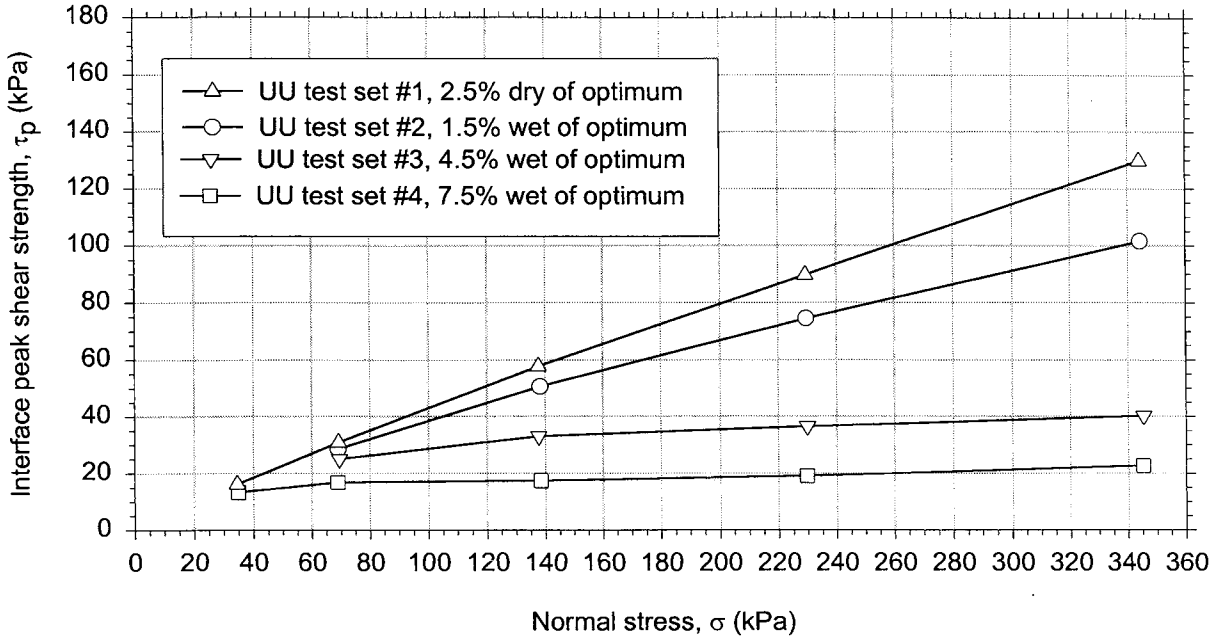

a. Peak interface shear strength envelopes

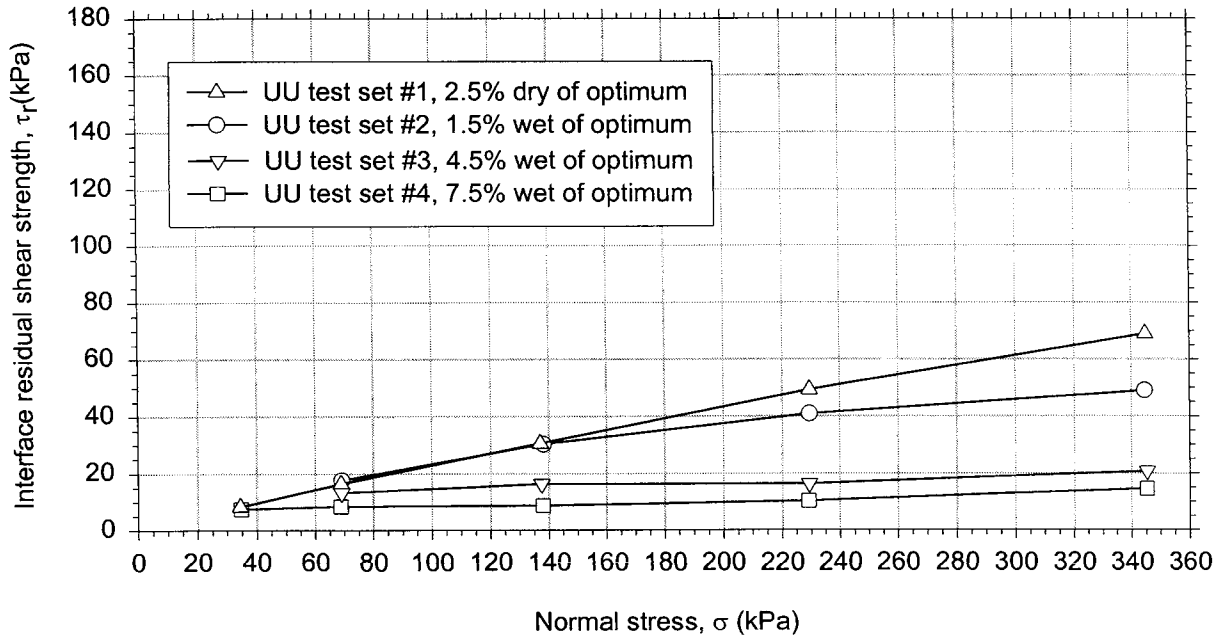

b. Residual interface shear strength envelopes

Figure 3. Interface shear strength envelopes for different compaction water contents

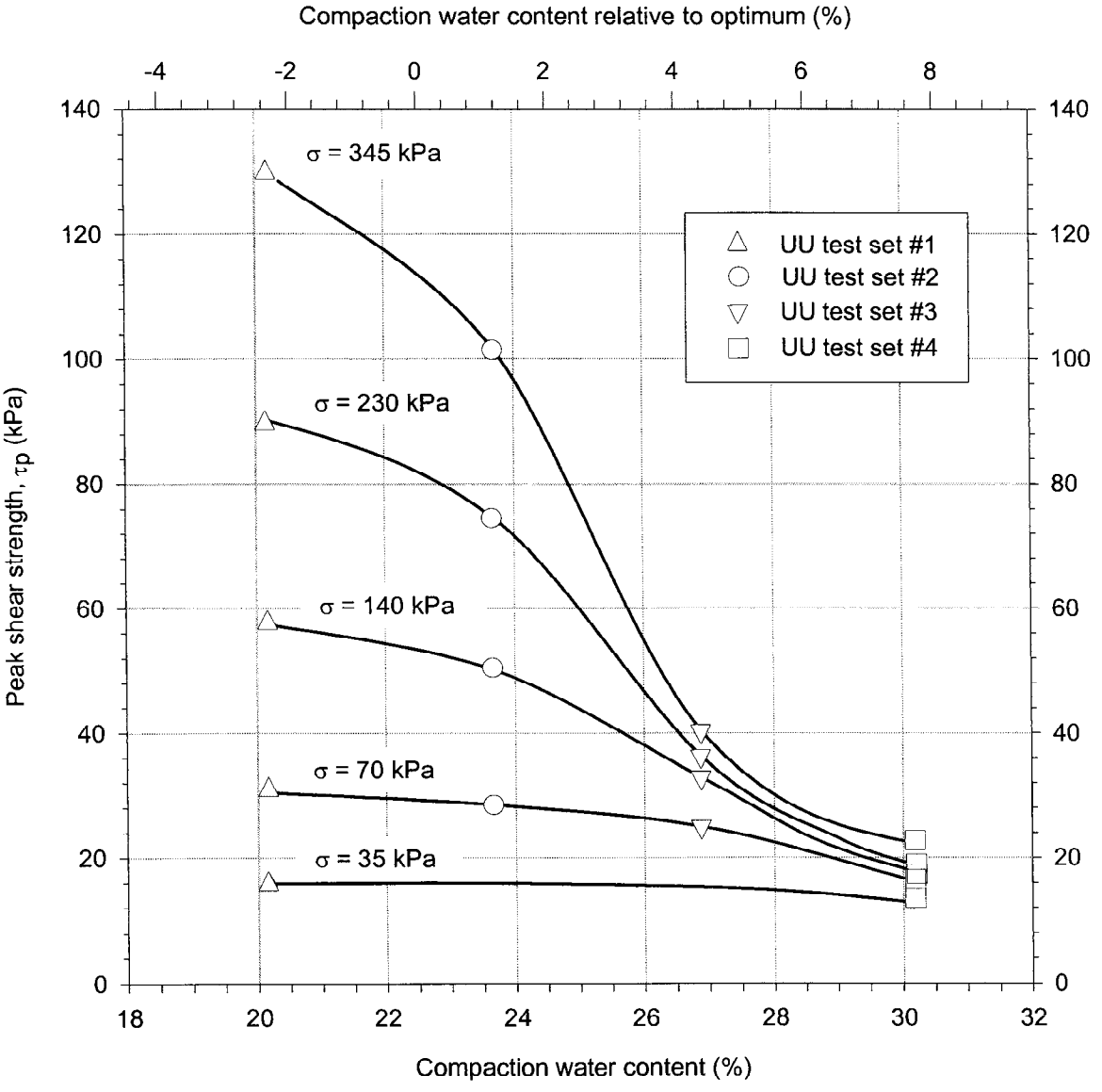

a. Peak interface shear strength

Figure 4. Variation of interface shear strength with water content at compaction

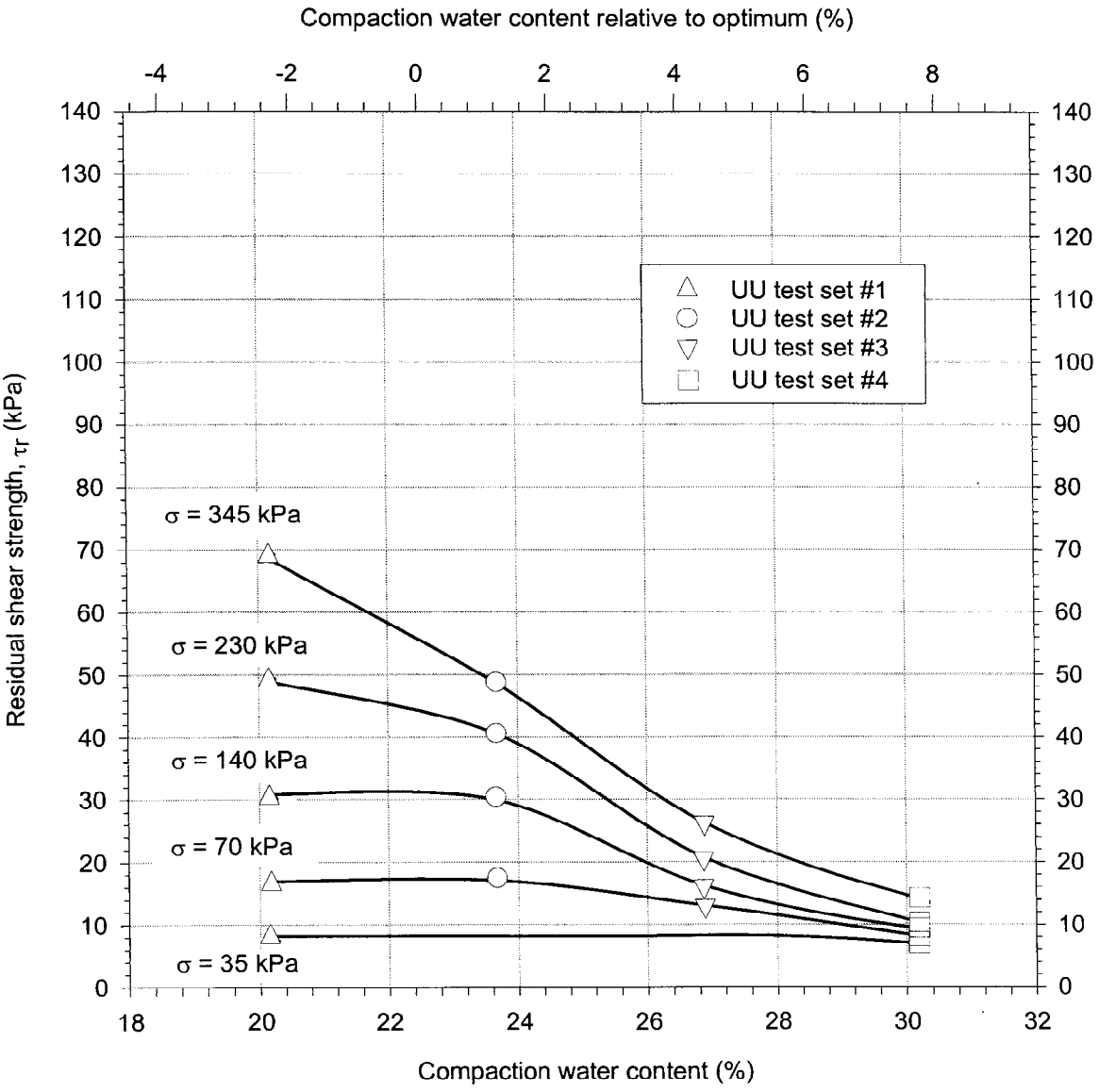

b. Residual interface shear strength

Figure 4. (concluded)

normal stresses. The undrained interface strength for a particular normal stress and compaction water content can be predicted from the trend lines in Figure 4.

7 CU interface testing

Two sets of consolidated, undrained interface tests were performed on clay samples compacted at 1.5% and 6.5% wet of optimum. Bottom drainage of the clay sample was achieved by means of a 12.7-mm thick layer of coarse sand. The normal stress was applied until primary consolidation of the clay was completed. During consolidation, a humid environment was maintained around the sample. Water content measurements were made at the interface before and after each test. After the end of primary consolidation of the clay, undrained shearing was performed at a displacement rate of 2.54 mm/min. A maximum displacement of 305 mm was attained, which allowed measurement of the interface residual strength.

Before shearing, the time under normal load required for consolidation of the clay typically ranged from 1 to 80 days. As discussed previously, the interface strength was found to increase with curing time in samples with no external loads applied. However, it is not clear that the thixotropic processes leading to an increase of interface strength can take place under load during consolidation of the clay. It may be recalled that, according to Mitchell (1960), thixotropy implies a re-arrangement of the clay structure to accommodate a lower energy level, after the compaction energy has been removed. This process of re-arrangement may be inhibited by the application of the normal stress before shear, and any thixotropic increase in strength while under normal load may be lower than indicated by the trends in Figure 1. In accordance with this reasoning, the CU test results presented here are not corrected for thixotropy.

Figure 5 shows the results of the CU interface tests in terms of the shear strength vs. the final water content measured after consolidation. For comparison, the trend lines for the UU interface strength presented in Figure 4 have also been reproduced in Figure 5. Several important observations can be made from the data in Figure 5:

- For the specimen compacted at 6.5 % wet of optimum, consolidation produced very large increases in shear strength. For example, the predicted peak UU shear strength of this specimen at a normal stress of 345 kPa is 27 kPa (point A in Figure 5a), whereas the measured CU strength at this normal stress is 90 kPa (point B in Figure 5a).
- The strength gains due to consolidation are much larger than the strength gains shown in Figure 1, which are due to thixotropy for samples that are not under load.
- Although there is some scatter in the data, the measured CU strengths are in reasonable agreement with UU strengths evaluated at the water content of the CU tests *after consolidation* (i.e. *during shear*). This is shown in Figure 6, where the measured CU strengths are compared with strength values predicted

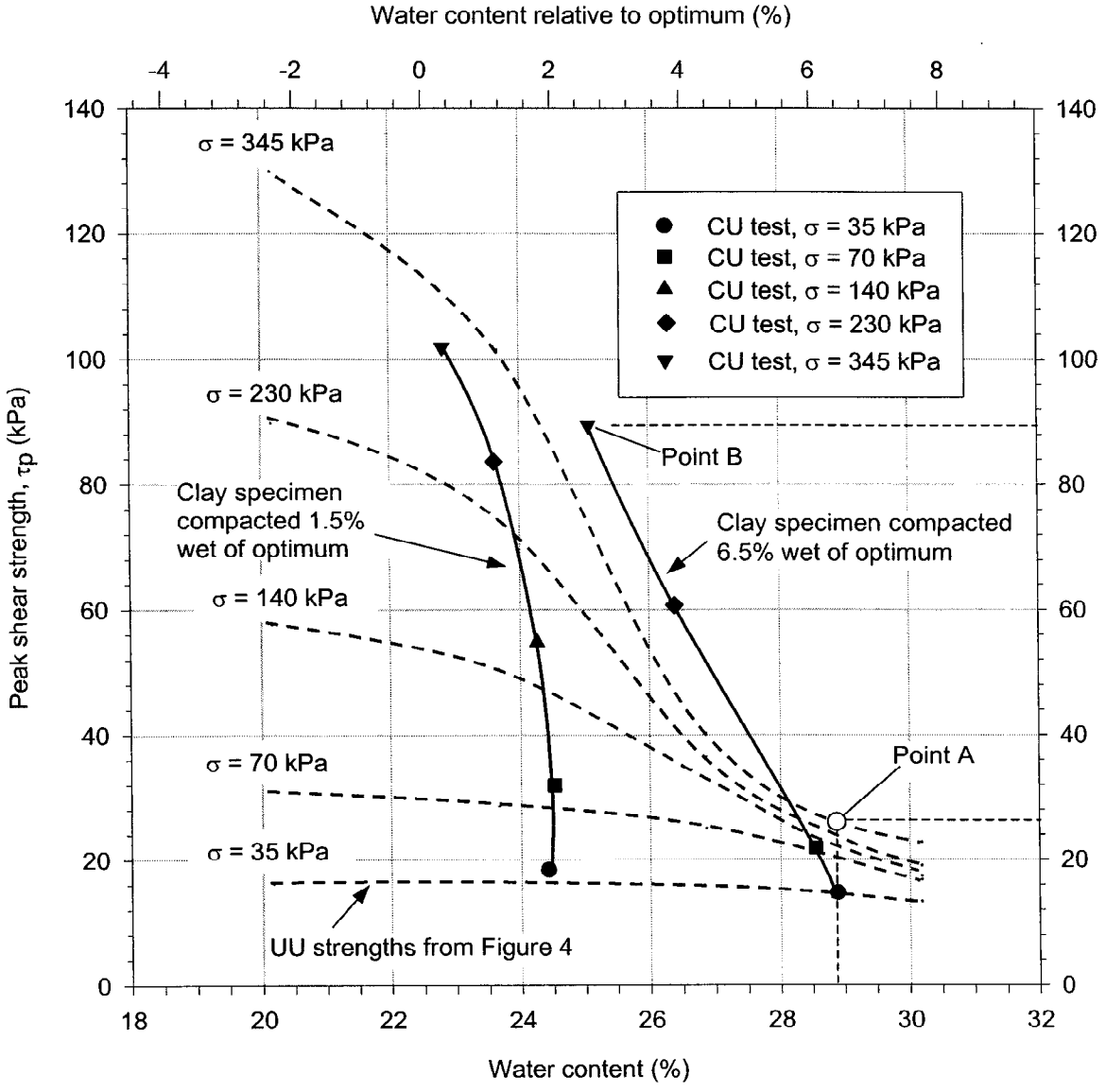

a. Peak interface shear strength

Figure 5. Comparison between interface strength values from UU tests and results of CU tests

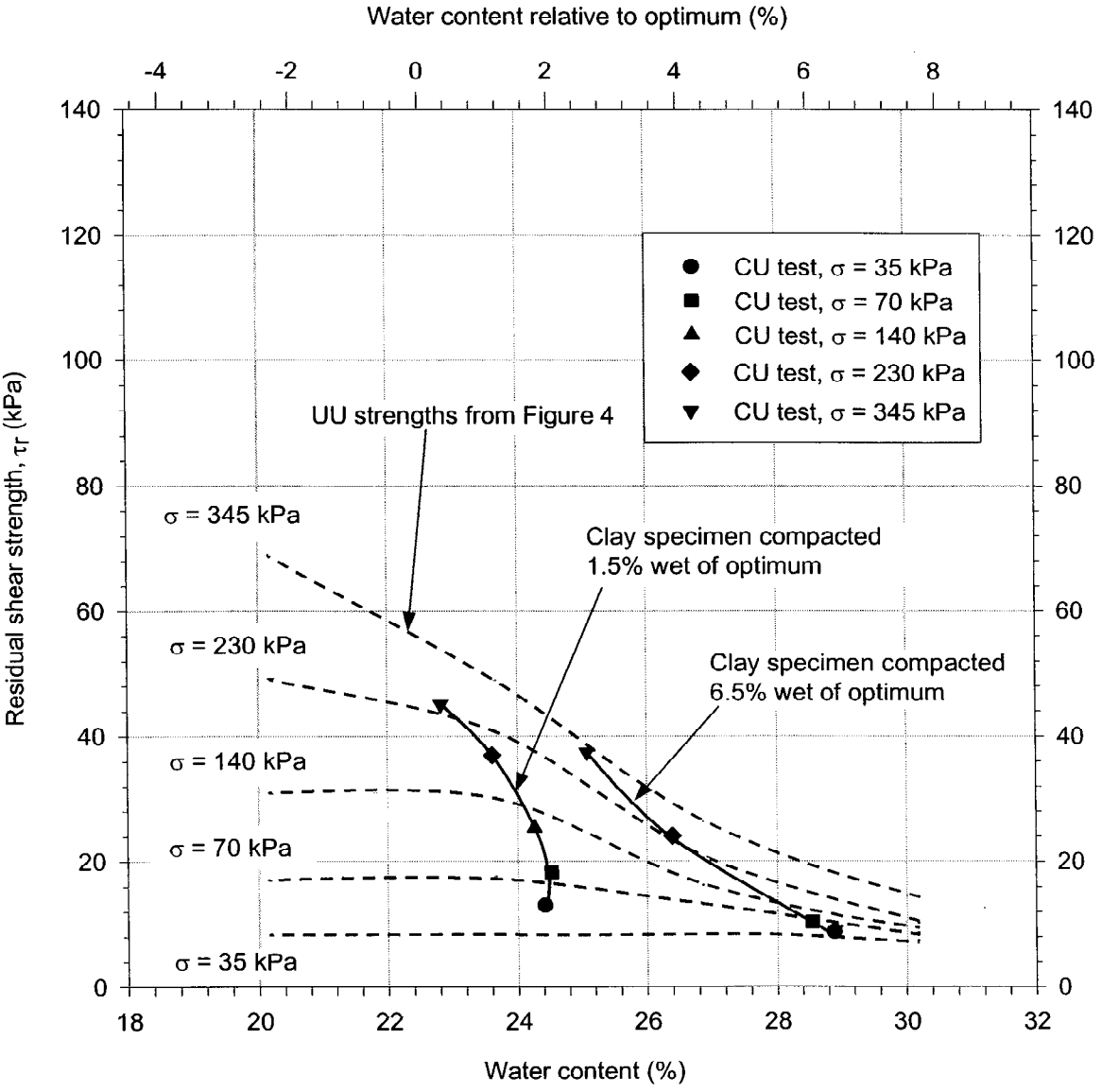

b. Residual interface shear strength

Figure 5. (concluded)

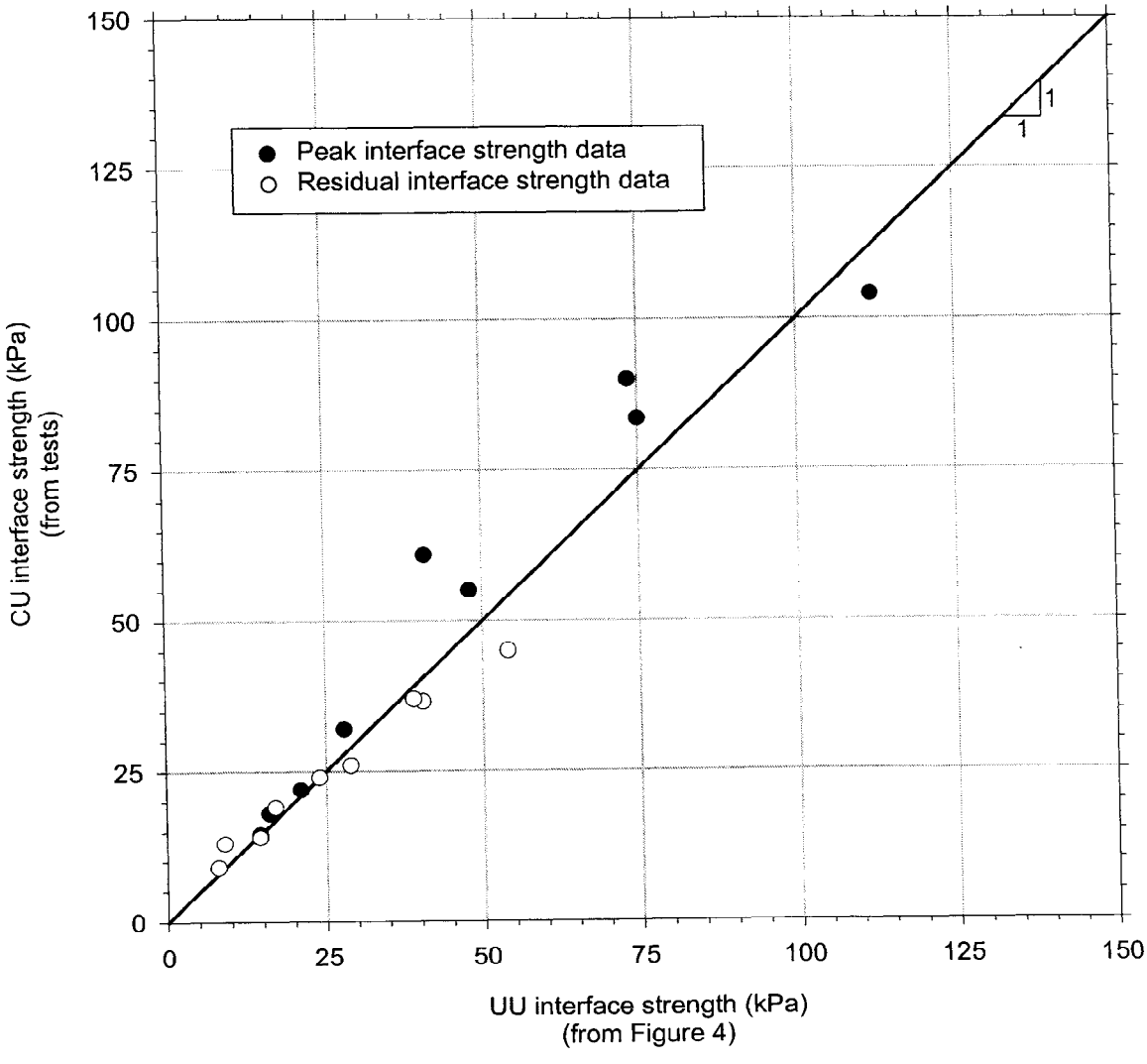

Figure 6. Comparison between CU and UU interface strength values at the same water content at shear

from the UU trend lines in Figure 4 using the water content values after consolidation from the CU tests.

From the data in Figures 5 and 6 it can be concluded that, for a given normal stress, the interface strength seems to be controlled by the water content at the interface at the time of shear, regardless of whether that water content was produced by compaction conditions or in-service consolidation. This is particularly interesting considering that other factors such as pore water pressures acting at the interface, as well as the structure and density of clay, might also be expected to control the interface shear strength.

For UU and CU tests performed at the same normal stress and water content during shear, it might be expected that the CU test would exhibit higher shear strength because any excess pore water pressures induced by the application of the normal load would have had the opportunity to dissipate prior to shearing. However, the experimental data in Figure 6 do not provide much evidence to support this. Some of the measured CU strengths are greater than the corresponding UU strengths, but the deviations from the 1:1 line are typically not very large. Possible explanations for this finding are: 1) the specimens are unsaturated so that significant pore water pressures might not be developing until the normal stresses are fairly high, 2) clay-geomembrane interface friction angles are relatively low at high normal stresses even in CU testing so that dissipation of excess pore water pressures does not produce an especially large change in shear strength in addition to the increase in shear strength associated with reduction of water content during consolidation, and 3) other factors, such as differences in clay structure, may have an influence on the measured shear strengths. Whatever the cause, the interface shear strength at the ODSL clay/geomembrane interface seems to be controlled primarily by the total normal stress and the water content during shear.

It would be useful to perform additional interface tests to determine whether this finding holds for other clay-geomembrane interfaces.

8 Determination of the CU interface strength from UU tests

The results described in the previous section suggest that the clay/geomembrane CU interface strength can be estimated from the results of UU interface tests if the water content of the clay after consolidation is known. A procedure for this is represented graphically in Figure 7, in which UU test results and consolidation test results are used to construct a CU strength envelope. For one of the normal stresses used in the UU testing, the consolidated water content is determined from consolidation test results at point A. The shear strength at that water content is obtained from the UU test results at point B. This produces a point C in the CU strength envelope at the normal stress from point A and the shear strength from point B. The procedure is repeated at other normal stresses to complete the CU envelope.

This method is reasonable for interfaces that exhibit the type of correspondence between CU and UU test results shown in Figure 6. This method would be conservative

for interfaces that exhibit greater CU strength than UU strength for specimens sheared at the same normal stress and water content.

Finally, if UU test results are already available, it is much easier to perform consolidation tests and construct the CU envelope as indicated in Figure 7 than it is to perform CU interface shear tests.

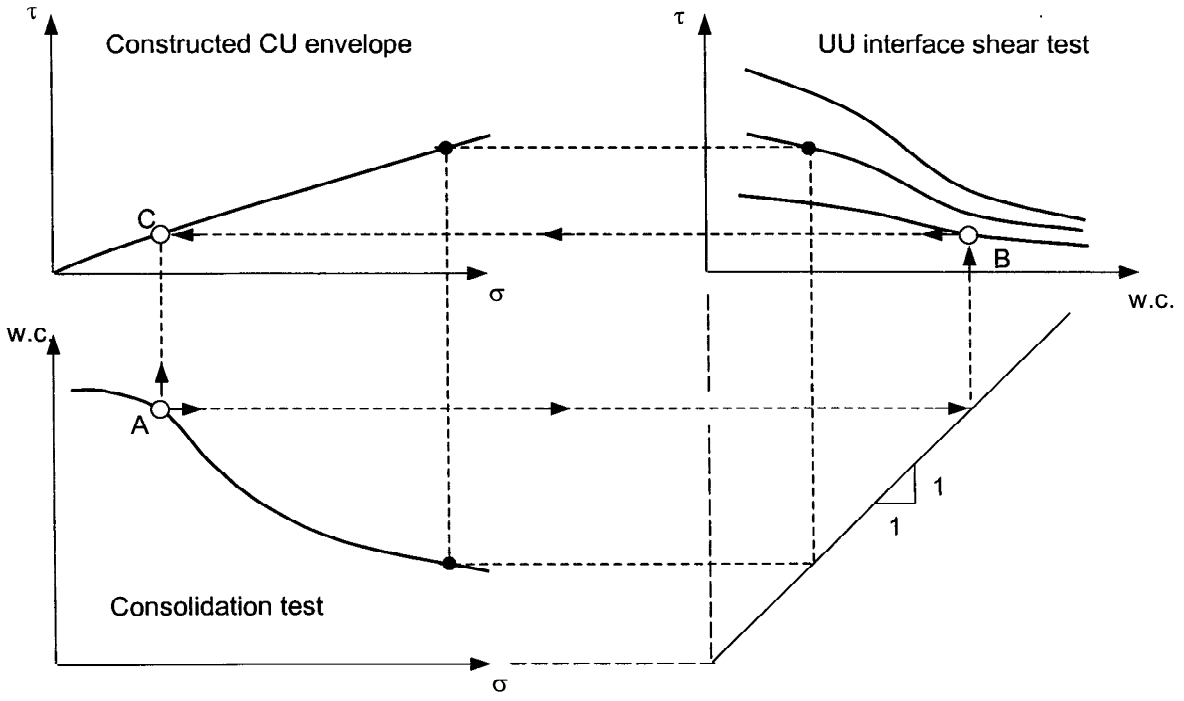

Figure 7. Tentative procedure for construction of CU interface strength envelope from results of UU interface tests and consolidation data

9 Summary and conclusions

A series of unconsolidated-undrained and consolidated-undrained interface tests performed during this investigation showed that a significant increase in the interface strength may take place during consolidation of the clay layer in a composite liner. It was found that the CU interface strength of the ODSL clay/geomembrane interface can be estimated from the results of UU interface tests if the relationship between final water content of the clay layer after consolidation and the overburden pressure is known. It would be useful to perform additional interface tests to determine whether this finding holds for other types of clay-geomembrane interfaces.

During interface testing, it was also found that thixotropy of the clay may induce a significant increase of the interface strength with time and that this effect is more pronounced at higher compaction water contents. Consideration of thixotropic strength gains may be important for interpretation of the results of testing programs in which interface tests are performed at different times after compaction of the clay specimens.

10 Acknowledgements

Thomas L. Brandon, Steve Conner, Michael Duncan, Michael J. Galli, Mark Gutberlet, James K. Mitchell, and Rob Swan contributed to the design and development of the LDSB. Will Shallenberger contributed to LDSB development, interface testing, and data interpretation. Bora Berk and Derrick A. Shelton contributed to the interface testing. Financial support for this project was provided by the Virginia Center for Innovative Technology, S&ME, Schnabel Engineering Associates, GeoSyntec, Trautwein Testing, and the National Science Foundation under Grant No. CMS-9502448. The geomembrane material was donated by Gundle/SLT Environmental, Inc. (GSE). The opinions, findings, and recommendations expressed in this material are those of the authors and do not necessarily reflect the views of the sponsors.

References

Shallenberger, W. C., and Filz, G. M. (1996). "Interface strength determination using a large displacement shear box," *Proceedings of the Second International Congress on Environmental Geotechnics*, Osaka, Japan, November 5-8, 1996. Masashi Kamon, ed., Balkema, Rotterdam, 147-152.

Yob, S. J., Spikula, D. R., Benson, C. P., and Shafer, A. L. (1995). "Geoenvironmental challenges at the Old Dominion sanitary landfill and resource management facility," *Geoenvironment 2000*, ASCE Geotechnical Special Publication 46, 641-654.

Seed, H. B., and Chan, C. K. (1957). "Thixotropic characteristics of compacted clays," *Journal of the Soil Mechanics and Foundations Division*, ASCE, 83(SM4), Proc. Paper 1427, 1-35.

Mitchell, J. K. (1960). "Fundamental aspects of thixotropy in soils," *Journal of the Soil Mechanics and Foundations Division*, ASCE, 86(SM3), 19-52.

REPEATED LOADING OF REINFORCED FINITE DEPTH GRANULAR MATERIAL

D.L. WALTERS
GRADUATE STUDENT, DEPARTMENT OF CIVIL ENGINEERING, QUEEN'S UNIVERSITY, KINGSTON, ONTARIO, CANADA, K7L 3N6

G.P. RAYMOND
PROFESSOR EMERITUS, DEPARTMENT OF CIVIL ENGINEERING, QUEEN'S UNIVERSITY, KINGSTON, ONTARIO, CANADA, K7L 3N6

ABSTRACT

Granular track supports built over compacted clay or silt subgrades are often susceptible to excessive settlement failure due to lateral spreading of the ballast, initiated by the seasonal softening of a thin upper layer of the subgrade. The inclusion of geosynthetic geogrid reinforcement within the granular support is investigated as a method of reducing the settlement of these structures. The investigation was conducted in the laboratory using a small-scale model of a track-ballast system overlying artificial subgrades of different compressibilities, including a rigid subgrade. The model was subjected to a program of repetitive loading, using a cyclic load that returned to zero at the end of each cycle. The performance of test configurations reinforced with a single layer of geosynthetic geogrid was compared with unreinforced configurations. When placed at the optimal depth, the geosynthetic geogrid reduced the rate at which accumulated plastic settlements were generated for all the subgrade conditions.

INTRODUCTION

The construction of granular track supports over clay or silt subgrades always involve some form of soil improvement to increase the strength and thereby the bearing capacity of the subgrade. The standard method is accomplished with the use of mechanized rollers. However, in some instances the subgrade soils may require the addition of chemical soil stabilizers. These stabilized subgrades often times demonstrate properties that are similar to those obtained from rigid subgrades. In poorly drained areas, the long-term performance of these subgrades will be adversely affected by periods of prolonged rainfall or the seasonal spring thaw. The moisture associated with these weather-related events may be sufficient to softening a thin upper layer of the subgrade resulting in a loss of strength. Figure 1 shows the effect of seasonal softening on the Benkelman Beam rebound values for an affected subgrade. Similarly a granular track support may now become susceptible to excessive settlement failure when subjected to repeated application of stress as each train wheel traffics the surface, since the ballast will undergo non-recoverable vertical deformations mostly due to lateral spreading of the ballast beneath the ties.

Bathurst et. al (1986), Burd (1995), Douglas (1997) and Ismail and Raymond (1995) have investigated the behaviour of geosynthetic-reinforced granular material subjected to repeated loading with the general conclusion that the inclusion of geosynthetic geogrid reinforcement within the granular support will reduce the generation of plastic settlement as well as improve the bearing capacity of the system. It has been postulated that the reinforcement provided lateral restraint of the granular material through friction, interlock and membrane action. However, those studies investigated configurations where the width of the loaded area was small in comparison with the thickness of the granular layer. This paper presents the results of small-scale models subjected to repeated loading where the width of the loaded area is greater than the thickness of the granular layer (finite depths).

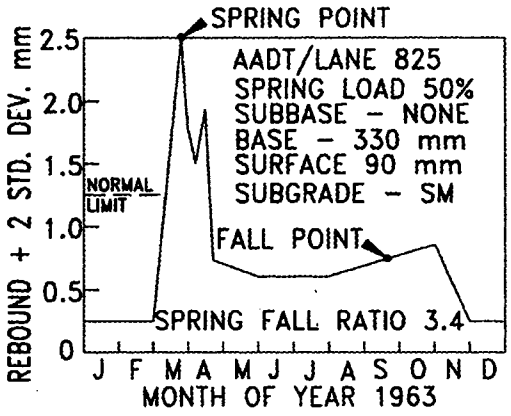

Figure 1. Seasonal effects on Benkelman Beam rebound values.

OBJECTIVE

The objectives of this study were;

1. Compare the performance of reinforced and unreinforced granular material with respect to the magnitude of the generation of plastic settlement and elastic rebound.
2. Establish an optimal depth for the placement of the geosynthetic geogrid reinforcement.
3. Investigate the effect of seasonal softening of the subgrade on the performance of the track-ballast model.
4. Examine the effect of a reducing thickness of the finite depth on the performance of the model.

SCALE MODEL

Figure 2 shows the model formulation that was based on an approximate one-tenth ($1/10^{th}$) scale for general railway engineering practice. Track with tie lengths of 2000 mm was modeled by a plane strain 200 mm wide footing. The No. 4 grading specification for ballast with an average size of 30 mm was modeled by spherical single-sized 3 mm diameter particles. The minimum depth for placing the geosynthetic geogrid below the footing was 12.5 mm, representing a ballast

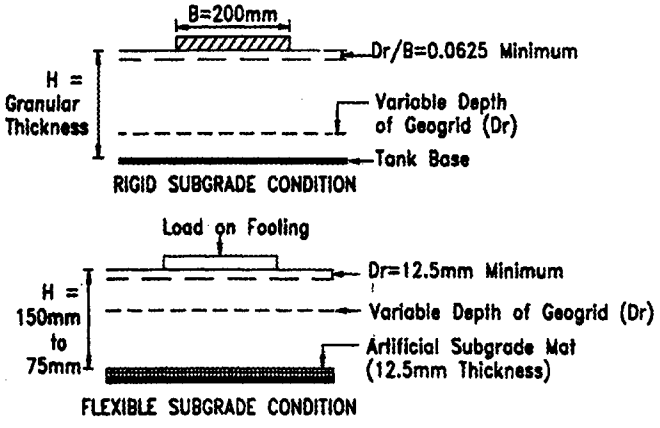

Figure 2. Model formulation.

depth of 125 mm typically required to prevent reinforcement damage from the tamper ties. Seasonal softening of the top surface of the subgrade soil that may become disturbed in-situ down to a depth of 125 mm was simulated with non-failing flexible subgrades that were 12.5 mm thick.

TESTING EQUIPMENT

Figure 3 shows the schematic layout of the testing equipment. Plane strain conditions were achieved in the testing tank that was 900 mm long, 200 mm wide and 330 mm deep. The sides of the tank were made of herculite transparent glass with a very small coefficient of friction. Single-sized 3 mm diameter rounded ceramic particles were used as the model soil. The particles had a specific gravity of 2.4 and a friction angle of 33 degrees. Soil placement in 25 mm thick layers using the funnel resulted in a placement density of 1.5 g/cm^3 (relative density of 90%). Including a range of subgrade stiffness within the test configurations simulated seasonal softening of the subgrade. The base of the tank was used to represent a rigid subgrade whereas including rubber mats of varying stiffness simulated compressible subgrades. The model footings were made from 19 mm thick aluminum plate and extended over the entire width (200 mm) of the tank. Four sets of thrust bearings, located on drill seats in the top of the footing, ensured that the load always acted vertically on the footing.

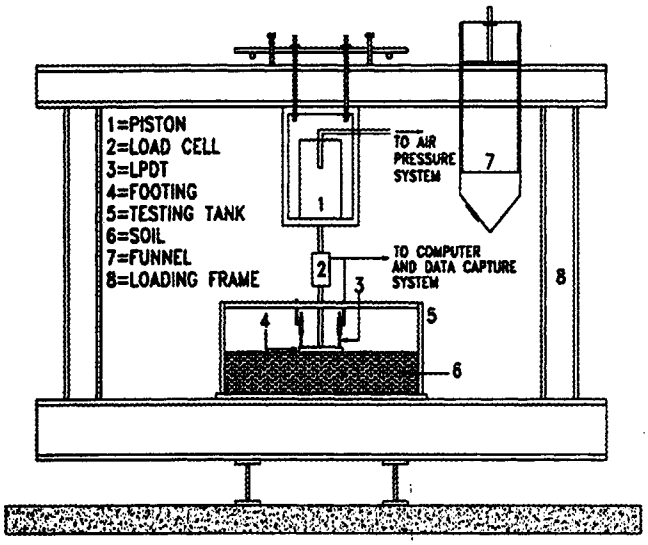

Figure 3. Testing equipment.

An air pressure activated loading piston was used to load the footing. A solenoid valve controlled by a timer regulated the frequency of the cyclic load. This timer could be stopped at any predetermined number of cycles by presetting the in-built counter. A load cell attached to the loading piston and four (4) linear position displacement transducers (LPDT), having a travel of 25 mm and repeatability of 0.002 mm, placed near each of the corners of the footing were used to monitor the load and vertical footing displacements throughout the testing program. The load cell and LPDT were connected to a computer running the data acquisition software.

SUBGRADE PROPERTIES

Reinforced and unreinforced test configurations were assembled over the artificial subgrades. A single layer of the geosynthetic geogrid was placed at varying depths below the base of the footing for the reinforced configurations. Table 1 presents a summary of the subgrade properties used in this investigation. Three (3) different subgrade compressibilities,

including the rigid subgrade, were used. The California Bearing Ratio (CBR) of each subgrade condition is also shown in Table 1.

Subgrade Type	Description	Thickness (mm)	CBR No.	General Rating
Rigid	Tank base covered with a single sheet of geotextile	0	∞	Excellent
Flexible	Closed Cell Pure Gum amber	12.5	28	Good
Very Flexible	Open Cell Neoprene Rubber	12.5	1	Very Poor

Table 1. Subgrade properties.

GEOSYNTHETIC GEOGRID PROPERTIES

The reinforcement used was a uniaxial geosynthetic geogrid manufactured from a high tenacity polyester fiber with PVC coating. The wide width tensile strength (ASTM 4595) in the machine direction was 30.5 kN/m and 17.8 kN/m in the cross-machine direction (GFR, 1995). At 5% strain these values were 10 kN/m and 4.4 kN/m respectively. The aperture size in the machine direction was 1.65 cm and 1.73 cm in the cross-machine direction. The geosynthetic geogrid was cut so that its length and width were 25.4 mm less than the length and width of the tank. This clearance was provided to ensure that no contact friction was generated between the reinforcement and the walls of the tank. The sheet of geosynthetic geogrid was reused from test to test but was replaced whenever any of the strands became visibly overstressed.

EXPERIMENTAL PROGRAM

Repeated Loading Parameters

Brown (1974) demonstrated that the effect of loading frequency between the range 0.1 Hz to 25 Hz on the magnitude of permanent deformations generated from repetitive loading of granular materials was negligible. A frequency of 0.1 Hz was decided for this program because it permitted full loading and unloading of the loading piston. The compressive repeated loading waveform was sinusoidal (nearly trapezoidal) which is typical of the loading pulse applied to railway ties under actual field conditions. The loading duration was 10^4 cycles, applying a contact cyclic stress of 40 kPa. This stress level represented approximately 50% of the ultimate bearing capacity (UBC) of the weakest unreinforced test configuration obtained during the monotonic program (Walters, 1998). On some occasions the accumulated plastic settlements exceeded the allowable 25 mm travel of the LPDT. These tests were stopped after 10^2 or 10^3 cycles, where required, to facilitate the adjustment of the LPDT thereafter continuing to 10^4 cycles.

Test Cases

Three (3) test cases were conducted for this study comprising of 25 different test configurations.

Case A

Test Case A consisted of three (3) series of tests, for the different subgrades in Table 1, using a granular thickness (H) of 150 mm, for a H/B ratio of 0.75. Within each of these series individual tests were performed with the geogrid placed at different depths. A total of three (3) different configurations comprising; no reinforcement (unrf'd), reinforcement at (Dr) 12.5 and 100 mm depth below the surface were constructed. This gave ratios of geosynthetic geogrid reinforcement depth to the footing width of Dr/B = 0.0625, 0.5 and the configuration of no reinforcement. An additional test was performed at Dr = 25 mm (Dr/B = 0.125) with the very flexible subgrade.

Case B

Test Case B also consisted of three (3) series of tests using a granular thickness (H) of 100 mm, for a H/B ratio of 0.5. Two (2) different configurations comprising; no reinforcement (unrf'd) and reinforcement at (Dr) 12.5 mm depth below the surface were constructed. An additional test was performed at Dr = 37.5 mm (Dr/B = 0.1875) with the very flexible subgrade.

Case C

Test Case C also consisted of three (3) series of tests using a granular thickness (H) of 75 mm, for a H/B ratio of 0.375. Two (2) different configurations comprising; no reinforcement (unrf'd) and reinforcement at (Dr) 12.5 mm depth below the surface were constructed. Two (2) additional tests were performed at Dr = 25 mm (Dr/B = 0.125) with the flexible subgrade and Dr = 37.5 mm (Dr/B = 0.1875) with the very flexible subgrade.

The footing was monotonically loaded to failure after the cyclic loading duration to compare the UBC obtained before and post repeated loading.

REPEATED LOADING TEST RESULTS

Repeated Load-Settlement Curves

Figures 4, 5, 6 and 7 show plots of accumulated plastic settlement on a natural scale against the logarithm of the number of load cycles from test Case A, with the geosynthetic geogrid reinforcement at various depths as well as the unreinforced configurations. The curves characterizing the accumulated plastic settlement response all trended in the same non-linear pattern. It may be seen that the magnitude of the settlement decreased with an increase in the

rigidity of the subgrade and also with the introduction of the geosynthetic geogrid.

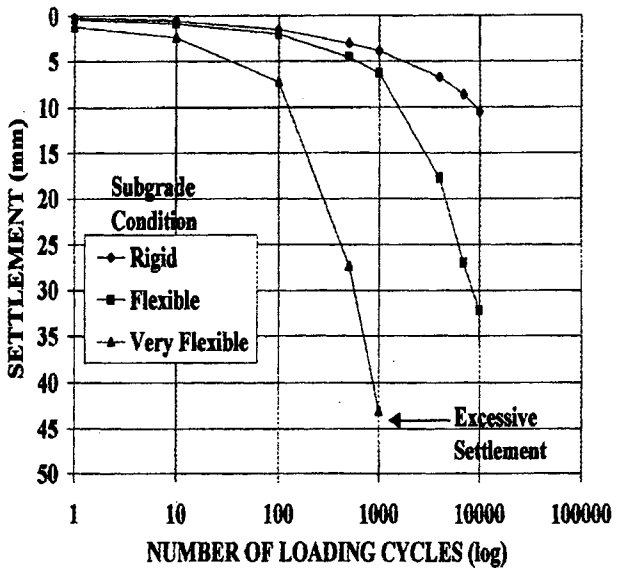

Figure 4. Accumulated plastic settlement without geosynthetic geogrid for H/B = 0.75; σ_c = 40 kPa.

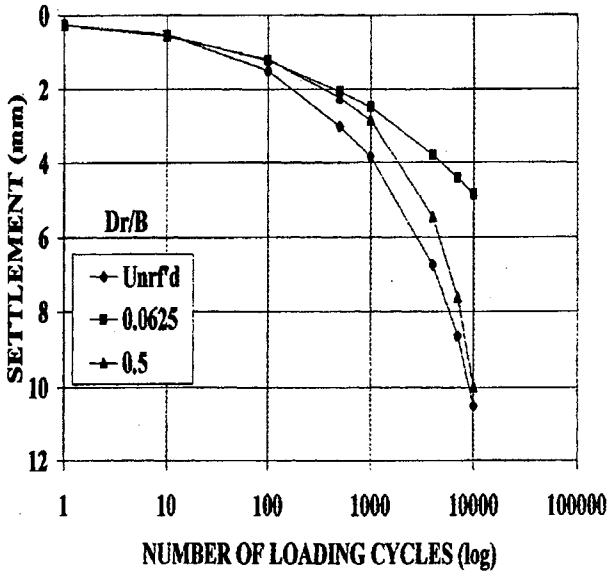

Figure 5. Accumulated plastic settlement with & without geosynthetic geogrid for H/B = 0.75 overlying the rigid subgrade; σ_c = 40 kPa.

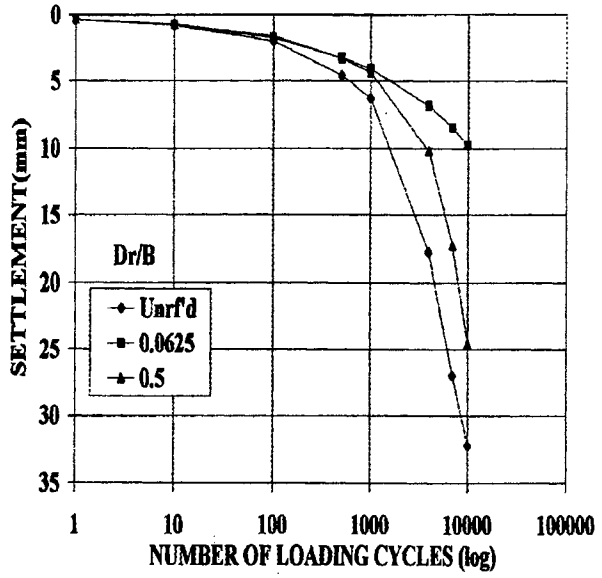

Figure 6. Accumulated plastic settlement with & without geosynthetic geogrid for H/B = 0.75 overlying the flexible subgrade (CBR = 28); σ_c = 40 kPa.

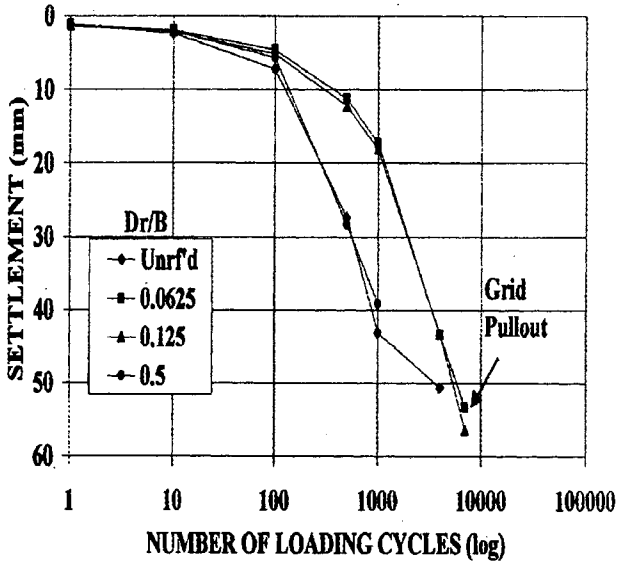

Figure 7. Accumulated plastic settlement with & without geosynthetic geogrid for H/B = 0.75 overlying the very flexible subgrade (CBR = 1); σ_c = 40 kPa.

For the test configurations shown it is seen that at low number of loading cycles (less than 10^2 cycles) the location of the geosynthetic geogrid is insignificant. However, this trend changes as the number of load cycles increases. With the geogrid placed close to the base of the footing, the accumulation of plastic settlement may be seen to decrease by about 50%, when compared with the unreinforced configurations. When placed deep in the granular layers the decrease in settlement tends to be very small. The optimum depth for placing the geosynthetic geogrid to minimize the accumulated plastic settlement was observed to be close to the base of the footing and in the range Dr/B = 0.0625 and 01875, depending on the subgrade stiffness. Considering the results from the unreinforced configurations as normal construction practice, then it may be seen that there could be significant performance benefits to be derived by the inclusion of the reinforcement within the granular track support. The placement depths (Dr) were pre-selected from a monotonic loading program (Walters, 1998) since Ismail (1994) had reported that the optimum depth for placing the geosynthetic geogrid to attain the maximum UBC when subjected to monotonic loading remained unchanged when subjected to repetitive loading.

Figure 7 shows an interesting occurrence. When the geosynthetic geogrid was placed at the minimum permissible depth (Dr/B = 0.0625) in configurations overlying the very flexible subgrade (CBR = 1), there was "grid pullout" after about 4,000 loading cycles. This placement depth (Dr/B = 0.0625) was observed to be the optimal placement depth for the geogrid for configurations overlying the rigid subgrade. It may be inferred that if the granular track support was constructed over a stabilized subgrade and the geosynthetic geogrid was placed at the optimum depth, seasonal softening of the subgrade may result in "grid pullout" and damage to the geogrid.

Elastic Unloading Rebound

Figure 8 shows the elastic unloading rebound values for test configurations without the geosynthetic geogrid reinforcement. The general trend is essentially a linear relationship between the magnitude of the elastic rebound and the logarithm of the number of loading cycles. The plot also shows that the rebound values decreased as the number of loading cycles increased. This may be due to the densification of the granular material by the application of the repeated loading. It may also be seen that the magnitude of the rebound values increased with an increase in the flexibility (compressibility) of the subgrade.

Figure 9 shows the effect of the geosynthetic geogrid on the magnitude of the elastic unloading rebound for configurations from Case A overlying the rigid subgrade. This is a typical response for all the test configurations. The linear relationship was also observed with the inclusion of the reinforcement but the magnitude of the elastic unloading rebound was only slightly affected when compared with the unreinforced configurations with the larger settlements. This shows that the geosynthetic geogrid was capable of reducing the magnitude of the plastic settlement by providing the necessary interlock and lateral restraint of the granular particles resulting in the footing behaving as if it were seated on a denser soil (geosynthetic geogrid added stiffness to the soil mass).

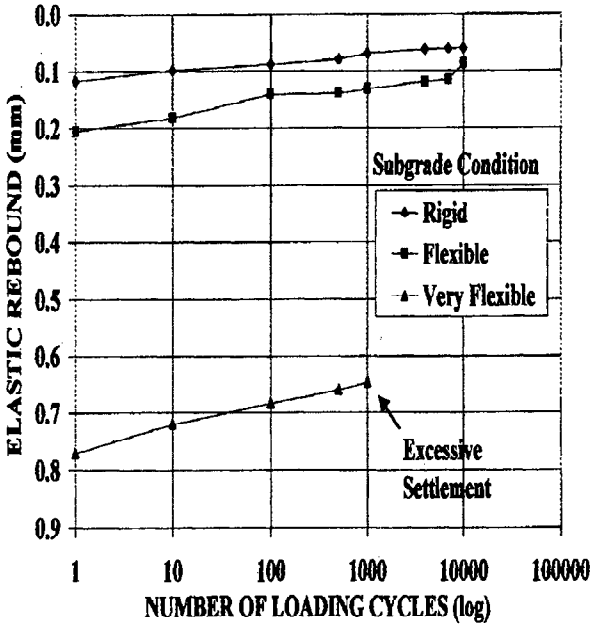

Figure 8. Elastic unloading rebound without geosynthetic geogrid for H/B = 0.75; σ_c = 40 kPa.

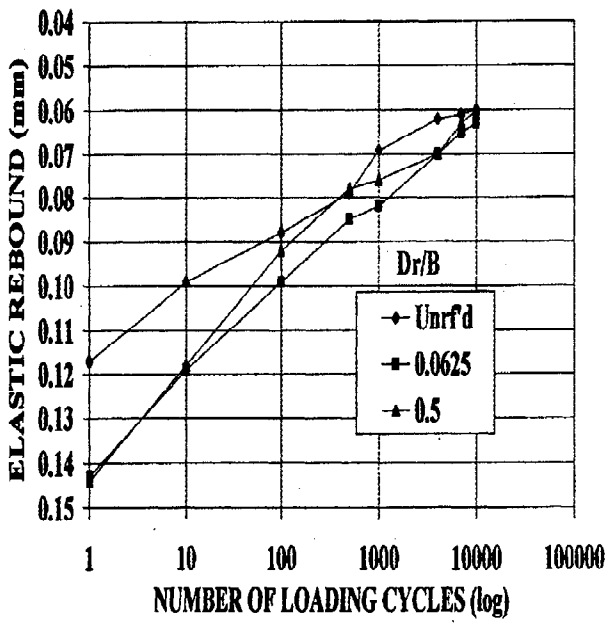

Figure 9. Elastic unloading rebound with & without geosynthetic geogrid for H/B = 0.75 overlying the rigid subgrade; σ_c = 40 kPa.

Effect of Seasonal Softening

Figures 10 shows the effect of seasonal softening on the magnitude of the accumulated plastic settlement after 10^3 applications of the cyclic stress of 40 kPa for the reinforced granular track support versus the logarithm of the CBR. The reinforcement positioned at the optimum depth of Dr/B = 0.0625 that was observed for configurations overlying the rigid subgrade. Generally, excessive settlement failure was recorded for the test configurations constructed over the very flexible subgrade (CBR = 1) before the completion of 10^4 cycles. It may be seen that increases in the compressibility from the rigid subgrade to the flexible subgrade (CBR = 28) resulted in marginal increases in the settlement of the footing. However, further increases in the compressibility of the subgrade were directly proportional to significant increases in the magnitude of the settlement. The plot also shows that when compared with the unreinforced configuration with the greatest settlement, there was dramatic performance benefit to be derived from the inclusion of the reinforcement.

Figure 11 shows the effect of seasonal softening on the elastic unloading rebound values for the reinforced track support after 10^3 loading repetitions versus the logarithm of the CBR. Again, increases in the subgrade compressibility resulted in increases in the magnitude of the rebound values. This figure shows that the compressibility of the subgrade would be the dominant factor, rather than the inclusion of the geosynthetic reinforcement, when determining the expected magnitude of the elastic unloading values.

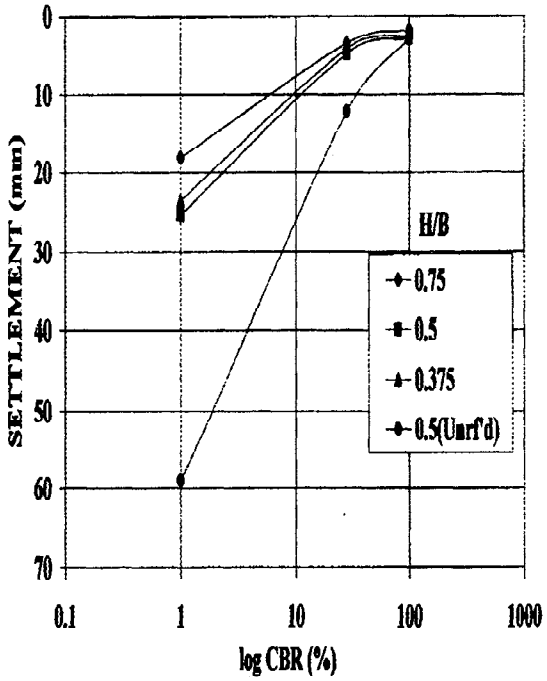

Figure 10. Effect of seasonal softening on the settlement after 10^3 loading cycles at 40 kPa for the reinforced track support.

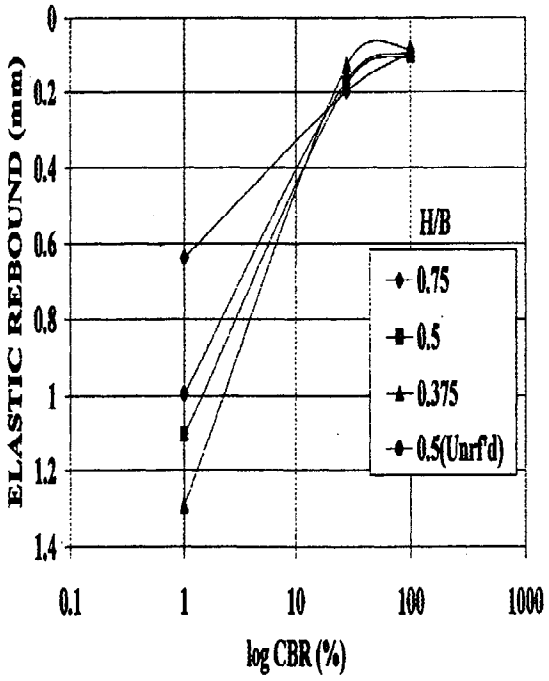

Figure 11. Effect of seasonal softening on the elastic unloading rebound after 10^3 loading cycles at 40 kPa for the reinforced track support.

Effect of Reducing Finite Depth

Figures 12 and 13 show the effect of a reducing finite depth (H) on the generation of plastic settlement and elastic rebound values for the reinforced configurations (Dr/B = 0.0625) overlying the rigid subgrade. The non-linear relationship continued to be observed between the accumulation of plastic settlement and the logarithm of the number of loading cycles. It may be seen that reductions in the H/B ratio did not produce a linear relationship between the magnitude of settlement and granular layer thickness. Among the limited cases considered in this study, the most favorable configuration occurred at H/B = 0.375 with the most unfavorable at H/B = 0.5. This observation shows that there is a composite effect between the granular layer and the subgrade where the strength and load distribution of the reinforced granular layer dominates for thick deposits but the subgrade has a greater influence for the thinner granular deposits. It is apparent that there may exist a point of minimum strength as well, occurring at H/B = 0.5.

The curves characterizing the magnitude of the elastic unloading rebound values exhibited essentially a linear relationship with the logarithm of the number of loading cycles, decreasing in value with an increase in the number of loading cycles. The rebound values observed were very small and although there was some minor scatter in the results, it may be seen that the smallest rebound values were obtained when using the thickest granular cover (H/B = 0.75).

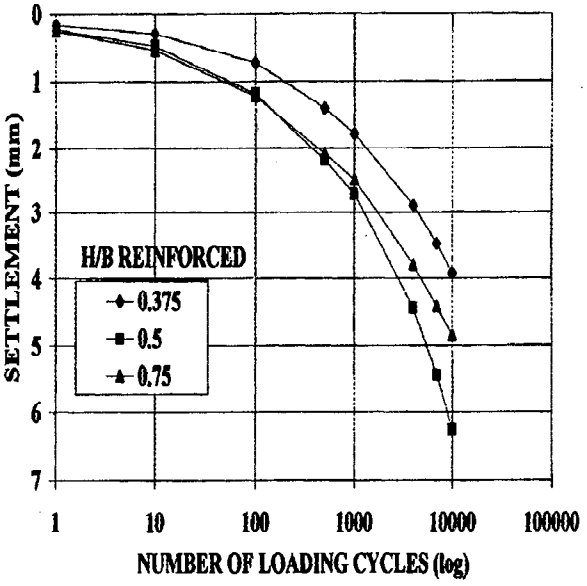

Figure 12. Effect of H/B ratio on the plastic settlement for reinforced granular soil overlying the rigid subgrade (Dr/B=0.0625); σ_c = 40 kPa.

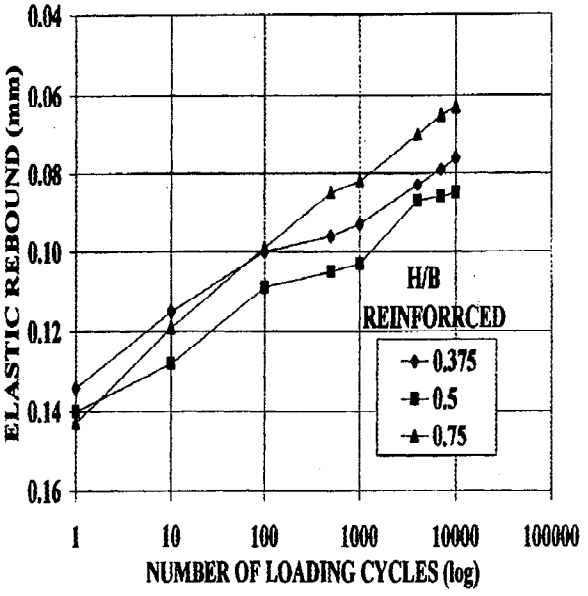

Figure 13. Effect of H/B ratio on the rebound values for reinforced granular soil overlying the rigid subgrade (Dr/B=0.0625); σ_c = 40 kPa.

Post Repeated Monotonic Test Results

Figure 14 presents a summary of the UBC before and after repeated loading for two test configurations, unreinforced and Dr/B = 0.0625, overlying the rigid subgrade. It may be seen that the UBC pattern pre and post cyclic loading was very similar for each configuration with the higher UBC values reported for the post repeated loading tests. This increase could be as a result of an increase in the shear strength of the granular material due to additional compaction and dynamic interlocking of the aggregate within the reinforcement apertures.

The test configurations overlying the compressible subgrades were not selected for this analysis because the settlement of the footing after the application of the repeated loading was relatively large when compared with the thickness of the footing. This

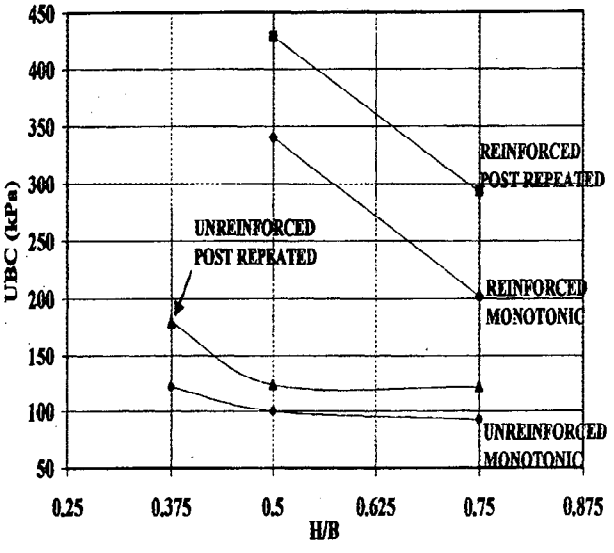

Figure 14. Summary of ultimate bearing capacity before and after repeated loading for configurations overlying the rigid subgrade.

resulted in the formation of berms at the sides of the footing that would automatically increase the UBC due to the surcharge effect.

DISCUSSION

The results of this study have shown that there was dramatic performance benefit to be derived from the inclusion of the geosynthetic geogrid reinforcement within the granular track support when compared with the normal construction practice. The geosynthetic geogrid reinforcement added stiffness to the granular track support and provided lateral restraint of the granular particles through friction and interlock within the grid apertures. The optimum depth for placing the geosynthetic geogrid in order to minimize settlement of the track support was shown to be as close as 6 to 12% of the footing width below the base of the footing. For a typical track tie of 2000 mm wide, the placement depth would then lie between about 120 to 240 mm. These placement depths are approximate multiples of the standard specified compacted lift thickness of 100 to 200mm (AREA, 1975) for granular material, and should not pose a serious concern for construction crews.

Current studies are underway to compare the performance benefits derived from using geosynthetic geogrids with that obtainable from high strength/modulus geotextiles.

RECOMMENDATIONS

The compressibility of the subgrade was shown to have a greater influence on the settlement and elastic unloading rebound values of the track than the inclusion of the geosynthetic geogrid reinforcement. Therefore, subgrade softening should be prevented or mitigated by the adherence to correct engineering internal drainage principles and maintenance practice. Additionally, since track maintenance line and level are controlled by the magnitude of the plastic settlements rather than unloading rebound values, the significance of ballast reinforcement using geosynthetic geogrid should be considered as a major improvement variable.

GEOSYNTHETIC APPLICATION IN BALLASTED TRACK CONSTRUCTION

Walls and Galbreath (1987) have reported on the application of geosynthetic geogrid in ballasted railway track rehabilitation. This case study showed that the inclusion of the geosynthetic reinforcement reduced the three (3) monthly maintenance cycle to a cycle of over three (3) years, resulting in a reduction of the maintenance costs. Several other cases where geosynthetic reinforcement have been used in railways and asphalt pavements have been documented in Geosynthetics Case Histories (Raymond and Giroud, 1993). Raymond (1993) reported of a case where a geotextile was used for a branch line upgrading in Kansas, USA. The subgrade at this site consisted of deep deposits of clay that had failed in places and there was extensive ballast fouling. The application of the geotextile demonstrated the cost savings that may be realized in the construction of the track support and future maintenance costs.

CONCLUSION

The conclusions drawn from this study are as follows;

1) The generation of permanent settlement of the footing could be reduced by about 50% with the inclusion of the geogrid, at the optimum depth, within the finite depth granular layer (Figures 5, 6, and 7).
2) The inclusion of the geogrid did not have any significant effect on the elastic unloading rebound values. The most important factor affecting these values was the compressibility of the subgrade. An increase in subgrade compressibility resulted in an increase in the elastic unloading rebound values (Figures 8 and 9).
3) Seasonal softening (compressibility) of the subgrade exerted a greater influence on the generation of plastic settlements than the inclusion of the geogrid. Increases in the subgrade compressibility were directly related to increases in the magnitude of the plastic settlements for both the reinforced and unreinforced test configurations (Figures 10 and 11).
4) Reducing the H/B ratio had a minor effect on the generation of plastic settlements and the magnitude of the elastic unloading rebound values for the reinforced track support (Figures 12 and 13).
5) Repeated loading increased the ultimate bearing capacity for similar test configurations (Figure 14).

ACKNOWLEDGEMENTS

Special thanks to the Natural Sciences and Engineering Research Council of Canada for funding made available to Dr. Raymond and to the Canadian Commonwealth Scholarship and Fellowship Program for financial support provided to Mr. Walters. The geogrid used in this study is the commercially available Stratagrid 200, manufactured by Strata Systems, Inc.

REFERENCES

American Railway Engineering Association, (1975), Manual for Railway Engineering.

Bathurst, R.J., Raymond, G.P. and Jarrett, P.M. (1986), "Performance of geogrid-reinforced ballast railroad track support", 3rd International Conference on Geotextiles, Vienna, Austria.

Brown, S.F., (1974), "Repeated loading testing of a granular material", Journal of the Geotechnical Division, ASCE, Vol. 100, No. GT 7, pp. 825-841.

Burd, H.J., (1995), "Analysis of membrane action in reinforced unpaved roads" Canadian Geotechnical Journal, Vol. 32, pp. 946-956.

Douglas, R.A., (1997) "Repeated-load behaviour of geosynthetic-built unbound roads" Canadian Geotechnical Journal, Vol. 34, pp. 197-203.

Ismail, I., (1994), "Geosynthetic reinforcement of granular layered soils", Ph.D. Thesis, Queen's University, Kingston, Ontario.

Ismail, I., and Raymond, G.P., (1995), "Geosynthetic reinforcement of unbound aggregate", Proc. 4th. Conf. of Unbound Aggregates in Roads, editor Dawson, A.R, & Jones, R.H., U.K., pp. 105 - 114.

Raymond, G.P., and Giroud, J.P., (1993) "Geosynthetics Case Histories", Available from BiTech Publishers Inc. Ltd., Vancouver, B.C., Canada.

Walls, J.C., and Galbreath, L.L., (1987) "Railroad ballast reinforcement using geogrids", Proceedings Geosynthetics Conference, Vol. 1, pp. 38-45.

Walters, D.L., (1998), "Geogrid reinforcement of finite-depth granular material subjected to monotonic and repetitive loading", Master's Thesis, Queen's University, Kingston, Ontario.